DESY–PROC–2004–01
DESY 04–123G
March 2004

ECFA DESY
Linear Collider Workshop

EXTENDED JOINT ECFA/DESY STUDY on PHYSICS and DETECTOR for a LINEAR e^+e^- COLLIDER

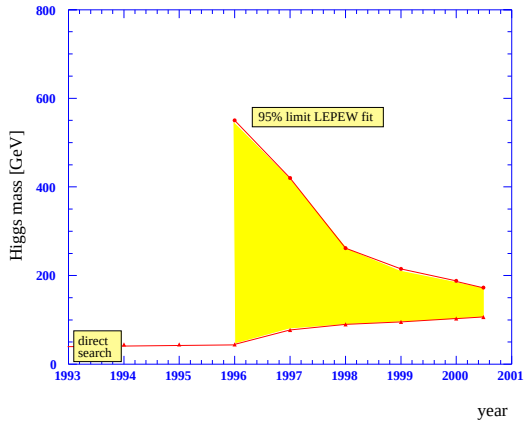

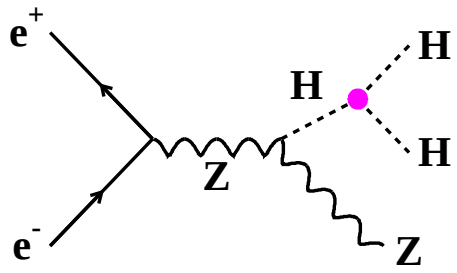

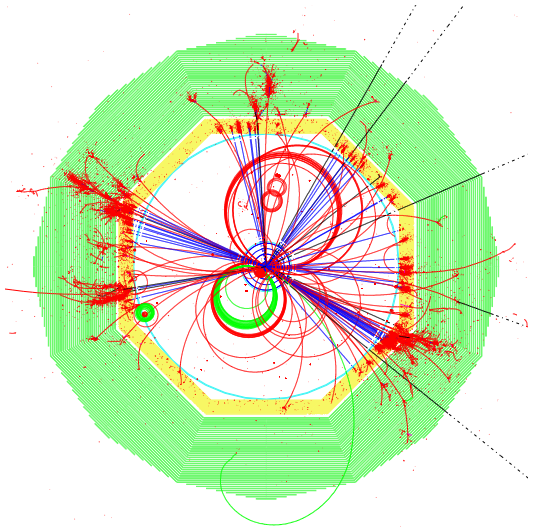

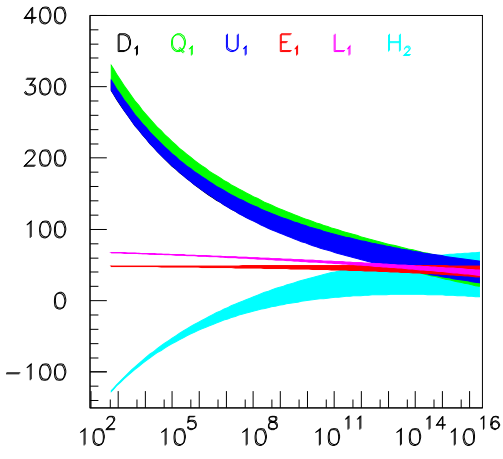

Workshops at Krakow, St.Malo, Prague, Amsterdam
September 2001 to April 2003

Authors, List of LC Notes, Proceedings of the Summary Colloquium at Amsterdam on 4 April 2003

LC Notes available at http://www-flc.desy.de/lcnotes

Edited by Ron Settles

ISSN 1435-8077, ISBN 3-935702-13-2

Authors

K. Ackermann[36], J.A. Aguilar-Saavedra[75], B.C. Allanach[12], B. Ananthanarayan[43], L. Andricek[35], D. Anipko[83], M. Antonelli[48], H.M. Araújo[102], E. Asakawa[61], S. Ask[88], D. Asner[116], J.E. Augustin[18], M. Awramik[69], D. Bardin[78], M. Ball[29], V. Barger[130], A. Bartl[2], M. Battaglia[10,90,119], H. Bauke[33], M. Baubillier[18], M. Beccaria[49], T. Behnke[25], G. Bélanger[11], A.C. Benvenuti[45], S. Berge[29], M. Berggren[18], W. Bernreuther[22], J.-D. Berst[20], A. Biernacik[72], F. Bieser[119], G.A. Blair[106], C. Blöchinger[40], J. Blümlein[26], W. de Boer[31], A. Bondar[81], E. Boos[80], F. Boudjema[11], I. Bozovic-Jelisavcic[84], J. Brau[125], A. Brandenburg[22,25], J.C. Brient[17], M. Breidenbach[128], I. Britvich[76], K. Buesser[25], P.N. Burrows[103], A. Buzulutskov[81], T. Camporesi[90], B. Canton[18], C. Carimalo[18], C.M. Carloni Calame[54], R.K. Carnegie[6], M.P. Casado[90], S.V. Chekanov[109], P. Checchia[52], S.Y. Choi[66], P. Ciafaloni[49], R. Cizeron[15], G. Claus[20], P. Cloarec[13], P. Colas[19], C. Colledani[20], D. Choudhury[90], M. Czakon[72], C. Damerell[107], W. Da Silva[18], A. Datta[10,14], S. Dawson[111], A. Delbart[19], S. DeCurtis[46], G. Degrassi[57], A. Denner[92], A. De Roeck[90], G. Deptuch[20,70], K. Desch[29], N.G. Deshpande[125], M. Diaz[9], M. Diehl[25], S. Dittmaier[36], M.S. Dixit[6], V. Djordjadze[26], A. Djouadi[14], D. Dominici[46], M. Doucet[25], H. Dreiner[24], J. Dubeau[6], M. Dubinin[80], W. Dulinski[20,21], H. Eberl[1], V. Eckardt[36],W. Edwards[119], J. Ellis[90], M. Elsing[90], M. Faisst[32], C. Fanin[52], A. Feniouk[76], A. Ferrari[89], A. Finch[100], P. Fischer[24], G. Fisk[117], J. Fleischer[23], M. Frank[31], H. Fraas[40], A. Freitas[117], R. Frey[125], T. Fritzsche[32], Y. Fujii[61], J. Fujimoto[61], E. Gabrielli[10], B. Gaissmaier[38], F. Gangemi[54], B. Gastineau[19], A. Gay[20], P. Gay[13], G. Genolini[15], A. Ghinculov[127], N. Ghodbane[25,90], D.K. Ghosh[125], Y. Giomataris[19], I.F. Ginzburg[83], J. Gluza[26,72], R. Godbole[43], P. Golonka[69], Y. Gornushkin[20], H. van der Graaf[67], J. Gronberg[120], N. de Groot[95,107], E. Gross[44], M. Gruwe[90], J. Guasch[92], J.F. Gunion[112], T. Hahn[36], T. Han[130], M. Hamann[25,29], A. van Hameren[41], K. Harder[25,29], P. Hassler[25], J. Hauschildt[25,29], R. Hawkings[90], V. Hedberg[88], S. Heinemeyer[90], C. Hensel[25], S. Hesselbach[2], J. Hewett[128], R. Heuer[29], C. Heusch[29,114], K. Hidaka[64], M. Hirsch[87], A.H. Hoang[36], W. Hollik[36], C. Hu-Guo[20], K. Huitu[10], V. A. Ilyin[80], D. Imbault[18], A. Imhof[25,29], T. Ishikawa[61], D.J. Jackson[107,105,62], S. Jadach[69], J. Jaros[128], J. Jeanjean[15], F. Jegerlehner[26], J. Jiang[109], L. Jönsson[88], L. Kalinovskaya[78], J. Kalinowski[74] M. Kalmykov[26], J. Kaminski[31], F. Kapusta[18], T. Kaneko[61], S. Kappler[31,90], K. Kato[65], A. Kaoukher[39], A. Karar[17], D. Karlen[8], H. Kawamura[26], T. Kernreiter[2], A. Kiiskinen[10], W. Kilian[25], M. Killenberg[22], M. Kincel[85], F. Kircher[19], O. Kittel[40], M. Klasen[29], G. Klemz[26], T. Klimkovich[25,29], V. Klioukhine[19,117], J.L. Kneur[14], B.A. Kniehl[29], M. Kock[25], K. Kołodziej[72], V. Korbel[25], M. Krämer[98], S. Kraml[90], F. Krauss[27,90], M. Krawczyk[74], T. Kuhl[25], J. Kuhlmann[25], J.H. Kühn[32], Y. Kurihara[61], J. Kwiecinski†,[69], P. Langacker[126], H. Lebbolo[18], B. Ledermann[31], F. LeDiberder[18], A. Leike[37], V. Lepeltier[15], V. Lishin[76], A. Lorca[26], S. Lotze[22], G. Lutz[35], T. Lux[29], F. Madricardo[29], S. Magill[109], W. Majerotto[1], V. Makarenko[4], T. Maki[10], M. Maniatis[25,29], A.V. Manohar[113], A. v.Manteuffel[25], I. Marfin[4], M. Margoni[52], T. Markiewicz[128], C. Martens[25], J.-P. Martin[7], M. Martinez[86], H.U. Martyn[22], M. Maul[88], S. Maxfield[101], M. Mazzucato[52], B. McElrath[130], B. Mele[56,57], M. Melles[92], W. Menges[25], H. Mes[6], N. Meyners[25,29], N. Meyer[25,29], D.J. Miller[90,99], D.J. Miller[102], R. Miquel[119], J. Mnich[22], K. Mönig[26], G. Montagna[54], S. Monteil[13], G. Moortgat-Pick[90,97], P. Mora de Freitas[17], V.L. Morgunov[25], M. Moretti[47], S. Moretti[90,108], G. Moultaka[14], M. Mühlleitner[92], T. Müller[31], O. Nachtmann[30], F. Nagel[30], U. Nauenberg[115], O. Nicrosini[54], H. Nieto-Chaupis[26], P. Niezurawski[74], H. Nowak[26], D. Nygren[119], V. Obraztsov[76], T. Ohl[40], K. Olive[122], W. Öller[1], A.I. Onishchenko[76], D. Orlando[17], P. Osland[68], Y. Pabot[19], M. Paganoni[50,51], A.V. Pak[83], A. Pankov[3], C. Papadopoulos[41], G. Passarino[58], N. Paver[59,60], D.V. Pavluchenko[81], S. Peñaranda[36], M. Peskin[128], S.S. Petrosyan[81], J. Peyré[16], F. Piccinini[54,90], T. Pierzchala[72], A. Pilaftsis[104], E. Piotto[90], W. Płaczek[71], M. Pohl[91], G. Polesello[54], V. Poliakov[76], V. Popov[77], W. Porod[94], P. Poulose[22], J. Pouthas,[16], A. Raspereza[25], P. Rebourgeard[19], D. Reid[67], F.M. Renard[14], F. Richard[15], R. Richter[35], S. Riemann[26], T. Riemann[26], S. Rindani[42], T. Rizzo[128], J.C. Romão[75], M. Ronan[119], A. Rosca[26], S. Rosier-Lees[11], F. Rossel[18], M. Roth[32,36], S. Roth[22], T. Robens[25], R. Rueckl[40], E. Rulikowska[70], H. Rzehak[36], K. Sachs[6], V. Saveliev[79], A. Savoy-Navarro[18], C. Schappacher[32], H.J. Schreiber[26], S. Schreiber[25], H. Schröder[39], R. Schulte[22], M. Schumacher[24], S. Schumann[27], B. Schumm[114], J. Sekaric[26], V.G. Serbo[82], R. Settles[36], L. Shekhtman,[81], Y. Shimizu[61], T. Shishkina[4], S. Shuvalov[77], M. Siemens[25], F. Simonetto[52], K. Sinram[25], M. Skrzypek[69], P. Slavich[32,36], B. Sobloher[22], S. Soeldner-Rembold[104], J. Solà[86], A. Sopczak[100], V.C. Spanos[122], M. Spira[92], A. Stahl[26], K. Stefanov[107], M. Steinhauser[25], I.W. Stewart[121], W. Struczinski[22], C. Sturm[32], Ch. de la Taille[15], O. Tarasov[26], B. Tausk[28], V.I. Telnov[81], F. Terranova[50,51], T. Teubner[101], C. Tevlin[105], M.A. Thomson[96], J. Timmermans[67],

M. Tonutti[22], E. Torrence[125], S. Trimarchi[59,60], M. Trimpl[24], R. Turchetta[107], J. Ulrici[24], P. Uwer[90], J.W.F. Valle[87], A. Vasilev[81], M. Velasco[124], O. Veretin[32], C. Verzegnassi[49,59,60], H. Videau[17], D. Vincent[18], E. Vlasov[76], A. Vologdin[80], D. Wackeroth[123], R. Walczak[105], N. Walker[25], B.F.L. Ward[110], Z. Was[69], C. Weber[1], M.M. Weber[92], G. Weiglein[97], S. Weinzierl[34], N. Wermes[24], A. Werthenbach[90], D. Wicke[90], H. Wieman[119], G. Wilson[118], M. Wing[25,95], M. Winter[20], M. Worek[72], S.M. Xella-Hansen[107], Y. Yamada[63], M. Yao[119], J. Yu[129], A.F. Zarnecki[73], P.M. Zerwas[25], R. Zimmermann[39]

†Deceased

AUSTRIA
[1]Institut für Hochenergiephysik der Österreichischen Akademie der Wissenschaften, A–1050 Vienna
[2]Institut für Theoretische Physik, Universität Wien, A–1090 Vienna

BELARUS
[3]Department of Physics, Gomel State Univeristy, Belarus–246699 Gomel
[4]Natl.Sci.Ed.Centre of Particle and HE Physics, Byelorussian State U., Belarus–220040 Minsk

BELGIUM
[5]Service de Physique des Particules Elémentaires, Univ. Libre de Bruxelles, B–1050 Bruxelles

CANADA
[6]Physics Department, Carleton University, Ottawa, ON, Canada–K1S 5B6
[7]Département de Physique, Université de Montréal, Montréal QC, Canada–H3T1J4
[8] University of Victoria, Victoria, BC, Canada–V8W 3P6

CHILE
[9]Pontificia Universidad Católica de Chile, Facultad de Física, Chile–6904411 Santiago de Chile

FINLAND
[10]Helsinki Institute of Physics, FIN–00114 University of Helsinki

FRANCE
[11]LAPP, Lab.d'Annecy le Vieux de Phys. des Particules, IN2P3-CNRS, F–74941 Annecy-Le-Vieux
[12]LAPTH, F–74941 Annecy-le-Vieux
[13]Lab. Phys. Corpusculaire de Clermont-Ferrand, U. Blaise Pascal, IN2P3-CNRS, F–63177 Aubière
[14]LPTA, Laboratoire de Physique Th/'eorique et Astroparticules, Université Montpellier II, F–34095 Montpellier
[15]LAL, IN2P3-CNRS, Université de Paris–Sud, F–91405 Orsay
[16]IPN, IN2P3 and Univ. Paris-Sud XI, F–91898 Orsay
[17]LLR École Polytechnique/IN2P3-CRNS, F–91128 Palaiseau
[18]LPNHE, IN2P3-CNRS, Université de Paris VI et VII, FR–75252 Paris
[19]DAPNIA CEA Saclay, F–91191 Gif/Yvette
[20]IReS, Inst. de Recherches Subatomiques–Hautes Energies, F–67037 Strasbourg
[21] LEPSI Lab. d électronique et de physique des systèmes instrumentaux, F–67037 Strasbourg

GERMANY
[22]RWTH Aachen, Physikzentrum, D–52056 Aachen
[23]Universität Bielefeld, Fakultät für Physik, D–33615 Bielefeld
[24]Rheinische Friedrich-Wilhelms-Universität Bonn, Physik Institut, D–53115 Bonn
[25]DESY, Deutsches Elektronen-Synchrotron, D–22603 Hamburg
[26]DESY, Deutsches Elektronen-Synchrotron, D–15738 Zeuthen
[27]Institute for Theoretical Physics, Dresden University of Technology, D–01062 Dresden
[28]Fakultät für Mathematik und Physik, Albert-Ludwigs-Universität Freiburg, D–79104 Freiburg
[29]Universität Hamburg, D–22761 Hamburg
[30]Institut für Theoretische Physik, Universität Heidelberg, D–69120 Heidelberg

[31]Institut für Experimentelle Kernphysik Universität Karlsruhe, D–76128 Karlsruhe
[32]Institut für Theoretische Teilchenphysik, Universität Karlsruhe, D–76128 Karlsruhe
[33]Institut für Theoretische Physik, Otto-von-Guericke Universitt, D–39016 Magdeburg
[34]Institut für Physik, Johannes-Gutenberg-Universität, D–55099 Mainz
[35]MPI Halbleiterlabor, D–81739 München
[36]Max-Planck-Institut für Physik, D–80805 München
[37]Fakultät für Physik, Ludwig-Maximilians-Universität, D–80799 München
[38]Physik Department der Technischen Universität München, D–85748 Garching
[39]Institut für Physik, Universität Rostock, D–18051 Rostock
[40]Lehrstuhl Theoretische Physik II, Inst.Theor.Phys.Astrophys., U. Würzburg, D–97074 Würzburg

GREECE
[41]NCSR Demokritos, GR–15310 Athens

INDIA
[42]Theory Group, Physical Research Laboratory, Navrangpura, India–Ahmedabad 380009
[43]Centre for Theoretical Studies, Indian Institute of Science India–Bangalore 560012

ISRAEL
[44]Department of Particle Physics, Weizmann Institute of Science, IL–76100 Rehovot

ITALY
[45]Dipartimento di Fisica, Università degli Studi di Bologna, I–40126 Bologna
[46]INFN Istituto Nazionale di Fisica Nucleare and Università degli Studi di Firenze, I–50125 Firenze
[47]INFN Sezione di Ferrara, I–44100 Ferrara
[48]LN, Istituto Nazionale di Fisica Nucleare INFN, I–00044 Frascati
[49]Dipartimento di Fisica, Università di Lecce, I–73100 Lecce
[50]Dipartimento di Fisica, Università degli Studi di Milano, I–20126 Milano
[51] INFN Sezione di Milano, I–20133 Milano
[52]INFN Sezione di Padova, Dipartimento di Fisica G.Galilei, I–35131 Padova
[53]INFN Gruppo Collegato di Parma, I–43100 Parma
[54]INFN Sezione di Pavia, I–27100 Pavia
[55]INFN Sezione di Pisa, San Piero a Grado, I–56010 Pisa
[56]INFN Sezione di Roma I, Dipartimento di Fisica, U. Roma I “La Sapienza”, I–00185 Roma
[57]INFN Sezione Roma III, I–00146 Roma
[58]INFN Sezione di Torino, I–10125 Torino
[59]INFN Sezione di Trieste, I–34127 Trieste
[60]Università degli Studi di Trieste, I–34127 Trieste

JAPAN
[61]KEK, National Lab. for High Energy Physics, 1-1 Oho, Tsukuba, Ibaraki, Japan 305-0801
[62]Osaka University, Osaka, 565-0871 Japan
[63]Department of Physics, Tohoku University, Sendai Japan 980-8578
[64]Department of Physics, Tokyo Gakugei University, Koganei, Tokyo Japan 184
[65]Kogakuin University, Shinjuku, Tokyo Japan 163-8677

REPUBLIC OF KOREA
[66]Department of Physics, Chonbuk National University, Jeonju City, Korea 561-756

THE NETHERLANDS
[67]NIKHEF, NL–1009 DB Amsterdam

NORWAY
[68]Department of Physics, University of Bergen, N-5007 Bergen

POLAND
[69]Institute of Nuclear Physics, PL–31342 Kraków
[70] Inst. Phys. Nucl. Tech., University of Mining and Metallurgy PL–30059 Kraków
[71]Institute of Physics, Jagiellonian University, PL–30059 Kraków
[72]Institute of Physics, University of Silesia, PL–40007 Katowice
[73] Institute of Experimental Physics, Warsaw University, PL–00 681 Warsaw
[74]Institute of Theoretical Physics, Warsaw University, PL–00 681 Warsaw

PORTUGAL
[75]Instituto Superior Técnico, Depto. de Fı́sica, P–1049-001 Lisboa

RUSSIAN FEDERATION
[76]IHEP, Institute for High Energy Physics, (Serpukhov) RU–142284 Protvino
[77]ITEP, Institute of Theoretical and Experimental Physics, RU–117259 Moscow
[78]JINR, Joint Institute for Nuclear Research, RU–141980 Dubna
[79]MEPhI, Moscow Engineering Physics Institute, RU–115 409 Moscow
[80]Skobeltsyn Institute of Nuclear Physics, Moscow State University, RU–119992 Moscow
[81]BINP Budker Institute of Nuclear Physics, RU–630090 Novosibirsk
[82]Novosibirsk State University, RU–630090 Novosibirsk
[83]Sobolev Institute of Mathematics, RU–630090 Novosibirsk

SERBIA AND MONTENEGRO
[84]VINČA Institute of Nuclear Sciences, YU–11001 Belgrade

SLOVAKIA
[85]Department of Theoretical Physics FMFI UK, Comenius University, SK-84248 Bratislava

SPAIN
[86]G.F.T and I.F.A.E., Universidad Autónoma de Barcelona, E–08193 Bellaterra
[87]AHEP Group, Instituto de Fı́sica Corpuscular CSIC, U. València, E–46071 València

SWEDEN
[88]Department of Physics, University of Lund, S–22362 Lund
[89]Uppsala University, S–75121 Uppsala

SWITZERLAND
[90]CERN, CH–1211 Genève 23
[91]DPNC Dèp. de Physique Nuclèaire et Corpusculaire, Université de Genève, CH–1211 Genève 4
[92]Paul Scherrer Institut, CH–5232 Villigen PSI
[93]Institute for Particle Physics, ETH, CH–8093 Zürich
[94]Institute for Theoretical Physics, University of Zürich, CH–8057 Zürich

UNITED KINGDOM
[95]HH Wills Physics Laboratory, University of Bristol, UK–Bristol BS8 1TL
[96]Cavendish Laboratory, University of Cambridge, UK–Cambridge CB3 0HE
[97]Institute for Particle Physics Phenomenology, University of Durham, UK–Durham DH1 3LE
[98]School of Physics, University of Edinburgh, UK–Edinburgh EH9 3JZ
[99]Department of Physics, University of Glasgow, UK–Glasgow G12 8QQ
[100]Department of Physics, Lancaster University, UK–Lancaster LA1 4YW
[101]Department of Physics, University of Liverpool, UK–Liverpool L69 3BX
[102]Department of Physics and Astronomy, University College London, UK–London WC1E 6BT
[103]Physics Department, Queen Mary, University of London, UK–London E1 4NS
[104]Department of Physics, University of Manchester, UK–Manchester M13 9PL
[105]Department of Physics, Clarendon Laboratory, University of Oxford, UK–Oxford OX1 3PU
[106]Dept. of Physics, Royal Holloway and Bedford New College, U. London, UK–Surrey TW20 OEX
[107]Particle Physics, Rutherford Appleton Laboratory, Chilton, UK–Didcot OX11 0QX
[108]School of Physics and Astronomy, University of Southampton, UK–Southampton SO17 1BJ

UNITED STATES
[109]Argonne National Laboratory, USA–Argonne IL 60439-4815
[110]Department of Physics, Baylor University, USA–Waco TX 76798
[111]Brookhaven National Laboratory, USA–Upton NY 11973-5000
[112]University of California Davis, USA–Davis CA 95616
[113]Department of Physics, UC San Diego, USA–San Diego CA 92093
[114]Institute for Particle Physics, UC Santa Cruz, USA–Santa Cruz CA 95064
[115]High Energy Physics, University of Colorado, USA–Boulder CO 80
[116]Cornell University, USA–Ithaca NY 14853-5001
[117]FNAL, Fermilab, P.O. Box 500, USA–Batavia IL 60510
[118]Department of Physics and Astronomy, University of Kansas USA–Lawrence KS 66045
[119]Lawrence Berkeley National Laboratory, USA–Berkeley CA 94720
[120]LLNL Lawrence Livermore National Laboratory, USA–Livermore CA 94551-0808
[121]Center for Theoretical Physics, MIT, USA–Cambridge MA 02139
[122]Theor.Physics Inst., School of Phys. and Astron., U. Minnesota, USA–Minneapolis MN 55455
[123]Department of Physics, SUNY at Buffalo, USA–Buffalo NY 14260-1500
[124]Department of Physics and Astronomy, Northwestern University, USA–Evanston IL 60208-3112
[125]University of Oregon, USA–Eugene OR 97403-1274
[126] Dept. of Physics and Astronomy, U. Pennsylvania, USA–Philadelphia PA 19104-6396
[127]Department of Physics, University of Rochester, USA–Rochester NY 14627
[128]SLAC, Stanford University, USA–Stanford CA 94025-7090
[129]Physics Department, University of Texas at Arlington, USA–Arlington TX 76019
[130]Physics Department, University of Wisconsin, USA–Madison WI 53706

Foreword

The appearance and numbering system of these proceedings has changed compared to earlier editions, so some history and explanation are in order. The present ECFA/DESY series of workshops was a continuation of European studies that started in 1991 on the e^+e^- physics that must follow the LEP/SLC era:

Year	Workshop venues/Proceedings
1991	Munich, Annecy, Hamburg
	DESY 92-123A&B, ed. P.M. Zerwas
1992-1993	Munich, Annecy, Hamburg
	DESY 93-123C, ed. P.M. Zerwas
1995	Annecy, Gran Sasso, Hamburg
	DESY 96-123D, ed. P.M. Zerwas
1996	Frascati, London, Munich, Hamburg
	DESY 97-123E, ed. R. Settles
1998-2000	Orsay, Lund, Frascati, Oxford, Obernai, Hamburg
	DESY 01-123, Vols. 1 to 3,
	eds. T. Behnke, S. Bertollucci, R.D. Heuer, D. Miller,
	F. Richard, R. Settles, V. Telnov, P. Zerwas
	http://www.desy.de/conferences/ecfa-desy-lc98.html
2001-2003	Cracow, St.Malo, Prague, Amsterdam
	DESY-PROC-2004-01, ed. R. Settles
	http://www.desy.de/conferences/ecfa-desy-lcext.html

From 1991 to 1995 the series evolved in a bottom-up fashion, while from 1996 onwards they were organised under the auspices of ECFA and bore the label "ECFA/DESY" in the title. The new series which has now been launched is called simply "ECFA Study of Physics and Detectors for a Linear Collider".

The e^+e^- energy covered by these studies ranges from the Z peak to $\sim$ 2 TeV. The workshops up to 1995 mapped out the physics terrain and after 1995 delved also into the detector optimisation. As the sophistication of the investigations has improved, an ever-broader understanding of the linear collider physics programme has evolved. The basic scientific motivation has remained unchanged since the beginning, so this sophistication is being built on a solid foundation.

The 1996 ECFA/DESY results were part of the "*CDR*": *Conceptual Design of a 500 GeV e^+e^- Linear Collider with Integrated X-ray Laser Facility*, DESY 1997-048/ECFA 1997-182, Vols. I and II. The 1998-2000 ECFA/DESY Study was incorporated into "*TDR*": *Technical Design Report on TESLA, the Superconducting e^+e^- Linear Collider with an Integrated X-ray Laser Laboratory*, DESY 2001-011/ECFA 2001-209, Vols. I to VI.

New Appearance for these Proceedings

Up to now the workshop proceedings appeared as the "DESY 123" series of orange books, and for the present iteration it was decided to spruce up the style. That is, to adopt Desy's standard numbering system for proceedings, to use a white cover which allows for colour pictures and a nice appearance, to take advantage of the colour plots in the articles and, finally, to try out the standard template used for EPAC, PAC, APAC, JACOW accelerator conferences which has a pleasant-to-read two-column format.

It was decided not to make a hard copy of all of the LC Notes this time since they are available on the web at http://www-flc.desy.de/lcnotes. Printing the figures in colour was then possible because the present volume of summaries at Amsterdam is relatively short. I am indebted to the proceedings secretary Maren Stein as well as Kirsten Sachs, Altmut Strate and the DESY printing office for their dedication in helping to produce this new look. Also thanks go to Steve Alpin/DESY for generating the $e^+e^- \to$ HHZ event on the cover.

This new format put a burden on the summary-session speakers of course, because they had to interact closely with their working groups for the write-up, in order to achieve a overview of all of what occurred up the end of the present series. Many thanks go to all of the workshop participants for their high-quality studies, and to the summary-session speakers who mastered the task of communicating with their working-groups to produce excellent articles. Happy reading!

Ron Settles
Munich/Hamburg, March 2004

P.S. The publication of these proceedings was delayed by about a year for various technical reasons, but mainly because the official author list (p.i) turned out to be a huge task to produce, and also turned out to be rather impressive. That author list exemplifies the global nature of our LC studies. During this one-year delay the International Technical Review Panel (ITRP) completed its mandate of deciding whether the ILC linac should be room-temperature or superconducting technology. The investigations in America, Asia and Europe have since experience rapid cohesion and progress. Thus Mark Thomson's, Jim Brau's and Nick Walker's articles on p.79, 95 and 107 respectively should be viewed as historic snapshots of the situation just before the ITRP deliberations began. All of the other reports in these proceedings are rather timeless overviews of each topic and are up-to-date except for recent papers.

Ron Settles
Munich/Hamburg, March 2005

Table of Contents

Organizing Committee

David Miller, UCL London (Chairman)
Mikhail Danilov, ITEP, Moscow
Enrique Fernandez, Barcelona
Rolf Heuer, Hamburg
Leif Jönsson, Lund
Paolo Laurelli, Frascati
Martin Leenen, DESY
Walter Majerotto, Vienna
François Richard, Orsay
Albert de Roeck, CERN
Ron Settles, MPI Munich/DESY
Valery Telnov, Novosibirsk
Janusz Zakrzewski, Warsaw
Peter Zerwas, DESY

Workshop Sessions

First Workshop, **Krakow, Poland**
14–18 September 2001
Organizer: *Marek Jezabek*

Second Workshop, **St. Malo, France**
12–15 April 2002
Organizer: *Paul Colas*

Third Workshop, **Prague, Czech Republic**
15–18 November 2002
Organizer: *Vaclav Vrba*

Fourth Workshop, **Amsterdam, Netherlands**
1–4 April 2003
Organizer: *Jan Timmermans*

Working Group	*Conveners*
Higgs Physics	*Abdelhak Djouadi, Berndt Kniehl, Marco Battaglia, Klaus Desch, Eilam Gross*
Supersymmetry	*Herbert Dreiner, Jan Kalinowski, Uli Martyn, Sylvie Rosier-Lees*
Electroweak Gauge Theories and Alternative Theories	*Ansgar Denner, Thorsten Ohl, Michael Spira, Klaus Mönig, Graham Wilson*
Top and QCD	*Werner Bernreuther, Arnd Brandenburg, Manel Martinez, Phil Burrows*
γ-γ **and e-**γ **Physics**	*Michael Krämer, Maria Krawczyk, Albert de Roeck, Stephan Maxfield, Stefan Soeldner-Rembold*
Loop Verein	*Stefan Dittmaier, Wolfgang Hollik*
Polarisation (Associated WG)	*Gudrid Moortgat-Pick*
LHC/LC Study (Associated WG)	*Georg Weiglein*
Machine-Detector Interface	*Nick Walker, Olivier Napoly, Martin Leenan, Grahame Blair, Karsten Büsser*
γ-γ **& e-**γ **Technical Questions**	*Valery Telnov, Klaus Mönig*
Software tools	*Ties Behnke*
Generators	*Stanislaw Jadach, Stavros Katsanevas, Stefano Moretti, Mario Antonelli*
Detector Studies	*Rolf Heuer, Ron Settles*
Detector Performance	*Pascal Gay, Mark Thomson, Markus Schumacher*
Detector R&D Contacts	Vertexing–*Chris Damerell* Tracking–*Ron Settles* Calorimetry–*Jean-Claude Brient, Paolo Checchia* Muons and other Detectors–*Marcello Piccolo*

List of LC Notes during the Study

(Full publications at http://www-flc.desy.de/lcnotes)

2001

DET LC-DET-2001-006 Development of a TPC with GEM readout 2001-01-15
T.Behnke, M.Hamann, M.Schumacher

DET LC-DET-2001-014 Pad readout geometries for a TPC with GEM readout for the TESLA linear collider 2001-01-16
M.Schumacher

DET LC-DET-2001-017 A CMOS based VTX detector 2001-01-26
M.Winter et al.

DET LC-DET-2001-023 A CCD-based vertex detector for TESLA 2001-02-22
C.J.S.Damerell for the LCFI collaboration

DET LC-DET-2001-027 Overview of an Electromagnetic Calorimeter for a Linear Collider based on the Shashlik technique with longitudinal segmentation 2001-01-17
CALEIDO Collaboration, A.C.Benvenuti et al.

DET LC-DET-2001-028 Lorentz angle measurements in silicon detectors 2001-01-17
W.deBoer

DET LC-DET-2001-029 Performance study of the proposed TESLA detector using a realistic track reconstruction package 2001-01-18
T.Behnke, G.Blair, I.Bozovic, M.Elsing, K.Harder, R.Hawkings, K.Moenig, D.Wicke

DET LC-DET-2001-036 Studies on a Silicon Intermediate Tracker for the TESLA Detector 2001-01-22
J.Hauschildt

DET LC-DET-2001-042 A Pixel based Vertex Tracker for the TESLA Detector 2001-02-23
M.Battaglia

DET LC-DET-2001-043 Studies of dE/dx capabilities of a TPC for the future Linear Collider TESLA 2001-01-27
M.Gruwe

DET LC-DET-2001-044 The measurement of luminosity at TESLA 2001-01-26
K.Buesser, M.Paganoni

DET LC-DET-2001-045 Mechanical Concept of the TESLA Detector 2001-02-22
N.Meyners, K.Sinram et al.

DET LC-DET-2001-046 The Hadronic Tile Calorimeter for the TESLA Detector, Design, Construction and Installation 2001-02-23
P.Hassler, M.Kock, V.Korbel, J.Kuhlmann, C.Martens, N.Meyners, V.Morgunov, S.Shuvalov, M.Siemens, K.Sinram

DET LC-DET-2001-047 The TESLA Compton Polarimeter 2001-01-26
V.Gharibyan, N.Meyners, P.Schuler

DET LC-DET-2001-048 Neutron background studies at the TESLA collider 2001-01-29
G.Wagner

DET LC-DET-2001-049 The Hadronic Tile Calorimeter for the TESLA Detector, Design, Construction and Installation 2001-02-23
P.Hassler, M.Kock, V.Korbel, J.Kuhlmann, C.Martens, N.Meyners, V.Morgunov, S.Shuvalov, M.Siemens, K.Sinram

DET LC-DET-2001-050 Upcoming R&D, Design- and Construction Studies for the HCAL Tile Calorimeter 2001-01-30
V.Korbel, V.Morgunov, V.Saveliev

DET LC-DET-2001-051 Calibration and Monitoring of the HCAL Tile Calorimeter 2001-01-30
V.Korbel, V.Morgunov

DET LC-DET-2001-052 The Optical Read Out of the HCAL Tile Calorimeter 2001-01-30
V.Korbel

DET LC-DET-2001-056 TESLA Detector Magnet Design 2001-02-05
F.Kircher, B.Gastineau, Y.Pabot, V.Klioukhine

DET LC-DET-2001-057 On the calibration of the W-Si ECAL proposed for Tesla 2001-02-05
J.C.Brient

DET LC-DET-2001-058 Si-W calorimeter performances 2001-02-05
J.C.Brient, P.Cloarec, V.Djordjadze, P.Mora de Freitas, P.Gay, F.LeDiberder, S.Monteil, D.Orlando, D.Reid, H.Videau

DET LC-DET-2001-059 Silicon diode, readout and frontend electronics of the proposed W-SI ECAL 2001-02-05
A.Karar, Ch.de la Taille

DET LC-DET-2001-061 R&D Achtivities in Aachen for a TPC with Gas Amplification by GEM Foils 2001-02-08
M.Killenberg, S.Lotze, J.Mnich, S.Roth, R.Schulte, B.Sobloher, W.Struczinski, M.Tonutti

DET LC-DET-2001-075 Study of a Silicon External Tracker : SET 2001-08-27
J.E.Augustin, M.Berggren, A.Savoy-Navarro

DET LC-DET-2001-078 Performance studies for the TESLA forward tracking system with different layouts 2001-09-13
H.Bauke

DET LC-DET-2001-080 A Lead Tungstate Detector with Integrated Light Readout for the TESLA Luminosity Calorimeter 2001-12-18
H.M.Araujo, A.Stahl, D.J.Miller

PHSM LC-PHSM-2000-026A Study of Scalar Top Quarks in the Neutralino and Chargino Decay Channel: Addendum 2001-03-15
H.Nowak, A.Sopczak

PHSM LC-PHSM-2001-003 Determination of the CP quantum numbers of the Higgs boson and test of CP invariance in the Higgs-strahlung process at a future e+ e- linear collider 2001-01-10
M.Schumacher

PHSM LC-PHSM-2001-008 Direct Determination of the CKM Matrix from Decays of W Bosons and Top Quarks at High Energy e+e- Colliders 2001-01-15
J.Letts, P.Mattig

PHSM LC-PHSM-2001-009 Precision Measurement of the W Mass with a Polarised Threshold Scan at a Linear Collider 2001-01-15
G.Wilson

PHSM LC-PHSM-2001-010 Study of the Sensitivity to Extra-Dimensions in the Photon-Graviton Channel with Polarised Beams 2001-01-15
G.Wilson

PHSM LC-PHSM-2001-016 Determination of the strong coupling constant at Giga-Z 2001-01-15
M.Winter

PHSM LC-PHSM-2001-020 Measurement of the leptoquark Yukawa couplings in e+e- collisions at TESLA 2001-01-15
A.F.Zarnecki

PHSM LC-PHSM-2001-022 A Study of Charged Current Triple Gauge Couplings at TESLA 2001-01-16
W.Menges

PHSM LC-PHSM-2001-024 Flavour tagging studies for the TESLA linear collider 2001-02-22
S.Xella-Hansen, D.J.Jackson, R.Hawkings, C.J.S.Damerell

PHSM LC-PHSM-2001-025 Higgs Production in WW-Fusion at TESLA 2001-01-25

K.Desch, N.Meyer

PHSM LC-PHSM-2001-034 Reconstruction of ZH->l+l-W+W- and ZH->qq˜W+W- Final States with Linear e+e- Collider 2001-02-02
A.Raspereza

PHSM LC-PHSM-2001-038 Strong Electroweak Symmetry Breaking Signals in WW Scattering at TESLA 2001-01-22
R.Chierici, S.Rosati, M.Kobel

PHSM LC-PHSM-2001-041 Study of e+e- -> H+H- at a 800 GeV Linear Collider 2001-01-24
M.Battaglia, A.Kueskinen, P.Poeyhoenen

PHSM LC-PHSM-2001-053 Determination of the Higgs Profile: HFITTER 2001-01-31
K.Desch, M.Battaglia

PHSM LC-PHSM-2001-054 Measurement of the Higgs Boson Mass and Cross section with a linear e^+ e^- Collider 2001-01-31
P.Garcia, W.Lohmann, A.Rasperezea

PHSM LC-PHSM-2001-055 Determination of the Higgs Boson Spin with a Linear e+e- Collider 2001-01-31
M.T.Dova, P.Garcia-Abia, W.Lohmann

PHSM LC-PHSM-2001-060 Light Higgs Production at a Photon Collider 2001-02-07
G.Jikia, S.Soeldner-Rembold

PHSM LC-PHSM-2001-072 CLIC Physics Signatures at CLIC 2001-03-27
M.Battaglia

PHSM LC-PHSM-2001-076 CLIC Study of a new Z-prime boson decaying into right-handed Majorana neutrinos at CLIC 2001-10-20
A.Ferrari

PHSM LC-PHSM-2001-077 Electroweak Precision Tests with a Future Linear Collider 2001-11-01
W.Menges

REV LC-REV-2001-074 Linear Collider Resource Book for Snowmass 2001 2001-06-06
T.Abe et al. [American Linear Collider Working Group]

TH LC-TH-2001-001 Electroweak Precision Tests with GigaZ 2001-01-02
S.Heinemeyer, G.Weiglein

TH LC-TH-2001-002 Physics Impact of GigaZ 2001-01-02
J.Erler, S.Heinemeyer, W.Hollik, G.Weiglein, P.M.Zerwas

TH LC-TH-2001-004 Polarized Beams and the Top Threshold 2001-01-10
J.Kuehn

TH LC-TH-2001-007 Fermion-Pair Production at a Linear Collider - A Sensitive Tool for New Physics Searches 2001-01-15
S.Riemann

TH LC-TH-2001-011 Pair Production of Smuons Near the Threshold in e+e-Collisions 2001-01-09
A.Freitas, D.J.Miller, P.M.Zerwas

TH LC-TH-2001-013 Dark matter and the SUSY mass scale 2001-01-15
M.Drees

TH LC-TH-2001-015 Sensitivity to sgoldstino states at the future linear e+e- and photon colliders 2001-01-16
P.Checchia, E.Piotto

TH LC-TH-2001-018 b-Quark Physics with 2 x 10^9 Z Bosons 2001-01-12
T.Mannel

TH LC-TH-2001-019 J/Psi production through resolved photon processes at e+ e- colliders 2001-01-17
R.M.Godbole, D.Indumathi

TH LC-TH-2001-021 Contact interactions and polarized beams at a Linear Collider 2001-01-16
P.Osland

TH LC-TH-2001-026 Resolving SM-like scenarios via Higgs boson production at a Photon Collider: 2HDM versus SM 2001-01-17
I.Ginzburg, M.Krawczyk, P.Osland

TH LC-TH-2001-030 Hadronic Cross sections in gamma-gammaProcesses at the next linear collider 2001-01-19
G.Pancheri, R.Godbole, A.DeRoeck

TH LC-TH-2001-031 Forwarded jets as a BFKL signature at an e+e- or egamma linear Collider 2001-01-19
G.Contreras , A.DeRoeck

TH LC-TH-2001-032 Photon Structure Function Measurements at TESLA 2001-01-19
A.DeRoeck, A.Vogt

TH LC-TH-2001-033 Measuring the spin of the Higgs boson 2001-01-19
D.J.Miller, S.Y.Choi, B.Eberle, M.M.Muehlleitner, P.M.Zerwas

TH LC-TH-2001-035 The effective fine structure constant at TESLA energies 2001-01-22
F.Jegerlehner

TH LC-TH-2001-037 Neutral MSSM Higgs boson production at e+e- colliders in the Feynman-diagrammatic approach 2001-01-22
S.Heinemeyer

TH LC-TH-2001-063 The Masses of the Neutral CP-even Higgs Bosons in the MSSM: Two-Loop Calculations in the Feynman-Diagrammatic Approach 2001-02-10
S.Heinemeyer, W.Hollik, G.Weiglein

TH LC-TH-2001-064 Decay widths of the neutral CP-even MSSM Higgs bosons in the Feynman-diagrammativc approach 2001-02-10
S.Heinemeyer, W.Hollik, G.Weiglein

TH LC-TH-2001-065 FeynHiggs and FeynHiggsFast: Programs for Higher-Order Calculations in the Neutral CP-even Higgs-Boson Sector of the MSSM 2001-02-10
S.Heinemeyer, W.Hollik, G.Weiglein

TH LC-TH-2001-066 Higgs Production and Decay in the MSSM: Status and Perspectives 2001-02-10
S.Heinemeyer, G.Weiglein

TH LC-TH-2001-067 Probing top flavor-changing neutral couplings at TESLA 2001-02-14
J.A.Aguilar-Saavedra, T.Riemann

TH LC-TH-2001-068 Production of MSSM Higgs Bosons in Photon-Photon Collisions 2001-02-14
M.Kraemer, M.M.Muehlleitner, M.Spira, P.M.Zerwas

TH LC-TH-2001-069 Higgs Radiation off Quarks in the Standard Model and supersymmetric Theories at e^+e^- Colliders 2001-02-14
S.Dittmaier, M.Kraemer, M.Spira, P.M.Zerwas

TH LC-TH-2001-071 Some results on TOP Quark decays in the MSSM 2001-03-12
J.Guasch

TH LC-TH-2001-073 Supersymmetric lepton flavour violation in a linear collider:the role of charginos 2001-03-30
M.Guchait, J.Kalinowski, P.Roy

TH LC-TH-2001-079 Compilation of SUSY particle spectra from Snowmass 2001 benchmark models 2001-11-13
N.Ghodbane, H.-U.Martyn

TOOL LC-TOOL-2001-005 BRAHMS: A Monte Carlo for a Detector at a 500/800 GeV Linear Collider 2001-01-11
T.Behnke, G.Blair et al.

TOOL LC-TOOL-2001-039 WHIZARD Manual 2001-01-22
W.Kilian

TOOL LC-TOOL-2001-040 An Optimizing Matrix Element Generator 2001-01-22
M.Moretti, T.Ohl, J.Reuter

2002

DET LC-DET-2002-001 Radiation hardness and linearity studies for a diamond luminosity calorimeter 2002-00-04
T.Behnke, M.Doucet, N.Ghodbane, A.Imhof

DET LC-DET-2002-004 A DEPFET based pixel vertex detector for the detector at TESLA 2002-04-05
P.Fischer, M.Schumacher, M.Trimpl, J.Ulrici, N.Wermes, L.Andricek, G.Lutz, R.Richter

DET LC-DET-2002-005 SIMDET - Version 4: A parametric Monte Carlo for a TESLA Detector 2002-06-03
M.Pohl, H.J.Schreiber

DET LC-DET-2002-008 A TPC for a future linear collider 2002-07-24
LC TPC group, R.Settles et al.

DET LC-DET-2002-011 A MEV Gamma Compton Polarimeter for the SLAC FFTB Undulator Test 2002-10-21
P.Schueler

DET LC-DET-2002-022 Modelling and Measurement of Charge Transfer in Multiple GEM Structures 2002-11-29
M.Killenberg, S.Lotze, J.Mnich, S.Roth, R.Schulte, B.Sobloher, W.Struczinski, M.Tonutti

PHSM LC-PHSM-2002-003 The direct method to measure the Higgs branching ratios at the future e+ e- linear collider 2002-03-20
J.-C.Brient

PHSM LC-PHSM-2002-006 CP Violation in the Production of Tau-Leptons at TESLA with Beam Polarization 2002-04-19
B.Ananthanarayan et al.

PHSM LC-PHSM-2002-007 The SM Higgs-boson production in gamma gamma -> h -> bb at the Photon Collider at TESLA 2002-12-03
P.Niezurawski, A.F.Zarnecki, M.Krawczyk

PHSM LC-PHSM-2002-008 Study of the Higgs-boson decays into WW and ZZ at the Photon Collider 2002-11-29
P.Niezurawski, A.F.Zarnecki, M.Krawczyk

REV LC-REV-2002-014 A Comparison of different Program Options at a Linear Collider 2002-11-29
K.Moenig

TH LC-TH-2002-002 Complete electroweak one-loop radiative corrections to top-pair production at TESLA - a comparison - 2002-02-12
J.Fleischer, T.Hahn, W.Hollik, T.Riemann, C.Schappacher, A.Werthenbach

TH LC-TH-2002-005 Logarithmic Fingerprints of Virtual Supersymmetry 2002-12-04
M.Beccaria, F.M.Renard, C.Verzegnassi

TH LC-TH-2002-010 Detection of heavy charged Higgs bosons at future Linear Colliders via $ auˆar u_ au Hˆ+$ production 2002-09-25
S.Moretti

TH LC-TH-2002-011 The process $eˆ-eˆ+o gamma gamma, Zgamma, ZZ$ in SM and MSSM 2002-11-28
G.J.Gounaris, J.Layssac, F.M.Renard

TH LC-TH-2002-012 Triple gauge couplings in polarised e-e+ -> W-W+ and their measurement using optimal observables 2002-11-29
M.Diehl, O.Nachtmann, F.Nagel

TH LC-TH-2002-013 Precision Analysis of the Lightest MSSM Higgs Boson at Future Colliders 2002-12-04
J.Ellis, S.Heinemeyer, K.Olive, G.Weiglein

TH LC-TH-2002-015 Towards High-Precision Predictions for the MSSM Higgs Sector 2002-12-04
G.Degrassi, S.Heinemeyer, W.Hollik, P.Slavich, G.Weiglein

TH LC-TH-2002-016 The Higgs-Boson Masses of the Complex MSSM: A Complete One-Loop Calculation 2002-12-04
M.Frank, S.Heinemeyer, W.Hollik, G.Weiglein

TH LC-TH-2002-017 A high energy determination of Yukawa couplings in SUSY models 2002-12-17
M.Beccaria, F.M.Renard, C.Verzegnassi

TH LC-TH-2002-018 MSSM Higgs-Boson Production at the LC: Dominant Corrections to the WW-Fusion channel 2002-12-04
T.Hahn, S.Heinemeyer, G.Weiglein

TH LC-TH-2002-019 Very Heavy MSSM Higgs-Boson Production at the LC 2002-12-04
T.Hahn, S.Heinemeyer, G.Weiglein

TH LC-TH-2002-020 Transverse Polarization Signatures of Extra Dimensions at Linear Colliders 2002-12-03
T.Rizzo

TH LC-TH-2002-021 Leading Electroweak Two-Loop Corrections to Precision Observables in the MSSM 2002-12-04
S.Heinemeyer, G.Weiglein

TOOL LC-TOOL-2002-007 CompAZ: parametrization of the photon collider luminosity spectra 2002-07-22
A.F.Zarnecki

TOOL LC-TOOL-2002-009 HERWIG: an event generator for e^+e^- Linear Colliders 2002-09-25
S.Moretti

2003

DET LC-DET-2003-009 Comparison of simulated analog versus digital energy measurement in a finely-segmented hadron calorimeter 2003-02-18
S.Magill

DET LC-DET-2003-013 A Silicon Envelope for the TPC 2003-06-03
L.E.Augustin, M.Baubillier, M.Berggren, B.Canton, C.Carimalo, W.DaSilva, D.Imbault, F.Kapusta, H.Lebbolo, F.Rossel, A.Savoy-Navarro, D.Vincent

DET LC-DET-2003-014 LCcal an R&D project for the barrel Electromagnetic Calorimeter 2003-05-13
P.Checchia

DET LC-DET-2003-025 Cooling of a W-Si calorimeter 2003-06-05
J.Badier

DET LC-DET-2003-044 Undulator based Production of Polarised Positrons: A Proposal for the SLAC FFTB 2003-06-20
E-166 collaboration, G.Alexander et.al.

DET LC-DET-2003-054 Beam energy measurement at linear colliders using spin precession 2003-07-15
V.I.Telnov

DET LC-DET-2003-059 Interaction region for gamma-gamma, gamma-electron collisions at linear colliders 2003-07-15
V.I.Telnov

DET LC-DET-2003-060 A CCD-based Vertex Detector for the Future Linear Collider 2003-06-30
C.Damerell, K.Stefanov

DET LC-DET-2003-080 Position Sensing from Charge Dispersion in Micro-Pattern Gas Detectors with a Resistive Anode 2003-07-29
M.S.Dixit, J.Dubeau, J.-P.Martin, K.Sachs

DET LC-DET-2003-092 Method for calibration of the tile HCAL with silicon photomultiplier as a photodetector (proposal) 2003-10-05
V.Popov

M LC-M-2003-045 Improved TESLA Optics and Beam Induced Backgrounds Update 2003-07-03
K.Buesser, O.Napoly

M LC-M-2003-058 Electron (positron) beam polarization by Compton scattering on circularly polarized laser photons 2003-07-15
G.L.Kotkin, V.G.Serbo, V.I.Telnov

M LC-M-2003-062 Is a laser "wire" a non-invasive method? 2003-07-15
V.I.Telnov

PHSM LC-PHSM-2003-001 Selection and reconstruction of top quarks in the all-hadronic decay at a linear collider 2003-01-10
S.Chekanov, V.Morgunov

PHSM LC-PHSM-2003-002 Physics Benefits of Positron and Transverse Polarisation at a Linear Electron Positron Collider 2003-01-31
K.Desch

PHSM LC-PHSM-2003-003 Measureing the Higgs Boson Parity at a Linear Collider using the Tau Impact Parameter and tau->rho nu Decay 2003-02-06
K.Desch, Z.Was, M.Worek

PHSM LC-PHSM-2003-004 Measurement of the HZgamma coupling at the future linear e+e- collider 2003-02-17
M.Dubinin, H.J.Schreiber, A.Vologdin

PHSM LC-PHSM-2003-016 Measuring the Luminosity of a $gamma gamma$ Collider with $gamma gamma ightarrow ellˆ+ ellˆ- gamma$ Events 2003-05-09
V.Makarenko, K.Moenig, T.Shishkina

PHSM LC-PHSM-2003-018 Polarization in Sfermion Decays: Determining tan(beta) and Trilinear Couplings 2003-06-16
E.Boos et al.

PHSM LC-PHSM-2003-019 Sfermion Precision Measurements at a Linear Collider 2003-06-16
A.Freitas et al.

PHSM LC-PHSM-2003-032 The Gain to Polarimetry and A(LR) Measurements from a Polarised Positron Beam in TESLA 2003-06-23
G.Alexander, E.Reinherz-Aronis

PHSM LC-PHSM-2003-048 Multi-Jet Higgsstrahlung Analysis 2003-06-19
M.T.Ronan

PHSM LC-PHSM-2003-049 Transverse spin effects in H/A -> tau tau; tau -> X nu, Monte Carlo approach 2003-07-09
M.Worek

PHSM LC-PHSM-2003-050 Higgs CP from H/A -> tau tau decay 2003-07-09
M.Worek

PHSM LC-PHSM-2003-051 Pair production of charged Higgs bosons in e+e- collisions at CLIC 2003-07-10
A.Ferrari

PHSM LC-PHSM-2003-055 The Snowmass Points and Slopes 2003-07-25
N.Ghodbane, H.-U.Martyn

PHSM LC-PHSM-2003-057 Measurement of gamma-gamma and gamma-electron luminosities at photon colliders 2003-07-15
A.V.Pak, D.V.Pavluchenko, S.S.Petrosyan, V.G.Serbo, V.I.Telnov

PHSM LC-PHSM-2003-061 Update on flavour tagging studies for the Future Linear Collider using the Brahms simulation 2003-07-04
S.M.Xella-Hansen, M.Wing, D.J.Jackson, N.deGroot, C.J.S.Damerell

PHSM LC-PHSM-2003-064 Determining tan(beta) with Neutral and Charged Higgs Bosons 2003-06-23
J.Gunion, T.Han, J.Jiang, A.Sopczak

PHSM LC-PHSM-2003-066 Measuring Resonance Parameters of Heavy Higgs Bosons at TESLA 2003-08-12
N.Meyer

PHSM LC-PHSM-2003-068 Probing the CP nature of the Higgs boson at linear colliders with tau spin correlations; the case of mixed scalar--pseudoscalar couplings 2003-07-29
K.Desch, A.Imho, Z.Was and M.Worek

PHSM LC-PHSM-2003-071 Study of Sleptons - Supersymmetry Scenario SPS 1 2003-08-15
H.-U.Martyn

PHSM LC-PHSM-2003-072 A Study of Charged Current Triple Gauge Couplings at e/gamma collider 2003-06-27
K.Moenig, J.Sekaric

PHSM LC-PHSM-2003-074 Smuon Production at TESLA 2003-08-26
H.N.Chaupis

PHSM LC-PHSM-2003-075 A Scalar Top Study with c-Quark Tagging at a Linear e+e- Collider 2003-07-11
A.Finch, H.Nowak, A.Sopczak

PHSM LC-PHSM-2003-076 Identification of New Physics with Fermion-Pair Production at a Linear Collider 2003-09-01
S.Riemann (to be submitted)

PHSM LC-PHSM-2003-084 Measurement of the Two Photon Decay Width at the TESLA Photon Collider 2003-09-07
A.Rosca, K.Moenig

PHSM LC-PHSM-2003-085 Anomalous quartic boson couplings via gamma-gamma->WW and gamma-gamma->WWZ at the TESLA kinematics 2003-10-08
I.Marfin, V.Mossolov, T.Shishkina

PHSM LC-PHSM-2003-086 Light Higgs-boson production at the Photon Collider at TESLA with an improved background analysis 2003-10-06
P.Niezurawski, A.F.Zarnecki, M.Krawczyk

PHSM LC-PHSM-2003-087 Measurement of the MSSM Higgs-bosons production in gamma gamma -> A,H -> b bbar at the Photon Collider at TESLA 2003-10-06
P.Niezurawski, A.F.Zarnecki, M.Krawczyk

PHSM LC-PHSM-2003-088 Measurement of the Higgs-boson CP properties using decays into WW and ZZ at the Photon Collider 2003-10-03
P.Niezurawski, A.F.Zarnecki, M.Krawczyk

PHSM LC-PHSM-2003-096 Investigations of invisible decays of the Higgs boson at a future e+e- linear collider 2003-11-05
M.Schumacher

PHSM LC-PHSM-2003-100 The Unintegrated Gluon Density in the Photon and Heavy Quark Production 2003-12-02
M.Hansson, H.Jung, L.Jnsson

REV LC-REV-2003-056 Critical Issues in Linear Colliders 2003-07-15
V.I.Telnov

TH LC-TH-2003-005 The Higgs Boson Production Cross Section as a Precision Observable? 2003-02-17
S.Dawson, S.Heinemeyer

TH LC-TH-2003-006 Singlino-dominated Neutralinos in Extended Supersymmetric Models 2003-02-24
S.Hesselbach, F.Franke

TH LC-TH-2003-007 Electroweak radiative corrections to e+ e- -> nu nubar H 2003-02-26
A.Denner, S.Dittmaier, M.Roth, M.M.Weber

TH LC-TH-2003-008 Electroweak radiative corrections to single Higgs-boson production in e+ e- annihilation 2003-03-18
A.Denner, S.Dittmaier, M.Roth, M.M.Weber

TH LC-TH-2003-011 Large extra dimension effects in Higgs boson production at linear colliders and Higgs factories 2003-04-09
A.Datta, E.Gabrielli, B.Mele

TH LC-TH-2003-012 Electroweak radiative corrections to single Higgs-boson production in e- e+ annihilation 2003-02-26
A.Denner, S.Dittmaier, M.Roth, M.M.Weber

TH LC-TH-2003-017 Theoretical uncertainties in sparticle mass predictions from computational tools 2003-06-10
B.Allanach, S.Kraml, W.Porod

TH LC-TH-2003-020 Reconstruction of Fundamental SUSY Parameters 2003-06-16
P.M.Zerwas et al.

TH LC-TH-2003-021 The Reconstruction of Supersymmetric Theories at High-Energy Scales 2003-06-16
G.A.Blair, W.Porod, P.M.Zerwas

TH LC-TH-2003-022 The Snowmass Points and Slopes: Benchmarks for SUSY Searches 2003-06-16
B.C.Allanach et al.

TH LC-TH-2003-023 Analysis of the Neutralino System in Supersymmetric Theories: Addendum 2003-06-16
S.Y.Choi, J.Kalinowski, G.Moortgat-Pick, P.M.Zerwas

TH LC-TH-2003-024 Analysis of the Neutralino System in Supersymmetric Theories 2003-06-16
S.Y.Choi, J.Kalinowski, G.Moortgat-Pick, P.M.Zerwas

TH LC-TH-2003-026 Testing neutrino mixing at future collider experiments 2003-06-19
W.Porod, M.Hirsch, J.C.Romao, J.W.F.Valle

TH LC-TH-2003-027 Tau-sleptons and tau-sneutrino in the MSSM with complex parameters 2003-06-19
A.Bartl, K.Hidaka, T.Kernreiter, W.Porod

TH LC-TH-2003-028 A CP sensitive asymmetry in the three-body decay stop_1 -> b tau-sneutrino tau+ 2003-06-19

A.Bartl, T.Kernreiter, W.Porod

TH LC-TH-2003-029 Probing neutrino properties with charged scalar lepton decays 2003-06-19
M.Hirsch, W.Porod, J.C.Romao, J.W.F.Valle

TH LC-TH-2003-030 Large lepton flavor violating signals in supersymmetric particle decays at future e+ e- colliders 2003-06-20
W.Porod, W.Majerotto

TH LC-TH-2003-031 Selectron pair production at e- e- and e+ e- colliders with polarized beams 2003-06-20
C.Bloechinger, H.Fraas, G.Moortgat-Pick, W.Porod

TH LC-TH-2003-033 Electroweak radiative corrections to sfermion decays 2003-06-23
J.Guasch, W.Hollik, J.Sol‘a

TH LC-TH-2003-034 The Higgs Sector of the Next-to-Minimal Supersymmetric Standard Model 2003-06-16
D.J.Miller, R.Nevzorov, P.M.Zerwas

TH LC-TH-2003-035 Effects of Genuine Dimension Six Higgs Operators 2003-06-16
V.Barger, T.Han, P.Langacker, B.McElrath, P.M.Zerwas

TH LC-TH-2003-036 Identifying the Higgs Spin and Parity in Decays to Z Pairs 2003-06-16
S.Y.Choi, D.J.Miller, M.M.Muehlleitner, P.M.Zerwas

TH LC-TH-2003-037 Two-Higgs-Doublet Models with CP violation 2003-06-14
I.F.Ginzburg, M.Krawczyk, P.Osland

TH LC-TH-2003-038 CP-violation in the neutralino system 2003-06-27
J.Kalinowski

TH LC-TH-2003-039 CP Phases, LFV, RpV & all that 2003-06-27
A.Bartl, K.Hidaka, M.Hirsch, J.Kalinowski, T.Kernreiter, W.Majerotto, W.Porod, J.C.Romao, J.W.F.Valle

TH LC-TH-2003-040 Slepton flavour violation at colliders 2003-06-27
J.Kalinowski

TH LC-TH-2003-041 Impact of SUSY CP Phases on Stop and Sbottom Decays in the MSSM 2003-06-18
A.Bartl, S.Hesselbach, K.Hidaka, T.Kernreiter, W.Porod

TH LC-TH-2003-043 Some results on distinction of Higgs boson models 2003-06-23
J.Guasch, W.Hollik, S.Penaranda

TH LC-TH-2003-046 Discriminating graviton exchange effects from other new physics scenarios in e^+e^- collisions 2003-06-13
P.Osland, A.A.Pankov, N.Paver

TH LC-TH-2003-047 Slepton LSP Decays: Trilinear versus Bilinear R-parity Breaking 2003-06-23
A.Bartl, M.Hirsch, T.Kernreiter, W.Porod, J.W.F.Valle

TH LC-TH-2003-052 Physics Impact of a Precise Determination of the Top Quark Mass at a e+ e- Linear Collider 2003-07-22
S.Heinemeyer, S.Kraml, W.Porod, G.Weiglein

TH LC-TH-2003-063 Associated production of single sneutrino and fermion pairs at polarised photon colliders 2003-07-25
D.K.Ghosh, S.Moretti

TH LC-TH-2003-065 CP asymmetries in $ e^+e^- o ildechi^0_i ildechi^0_j$ 2003-08-06
A.Bartl, H.Fraas, O.Kittel, W.Majerotto

TH LC-TH-2003-067 A Future Linear Collider with Polarised Beams:Searches for New Physics 2003-06-23
G.Moortgat-Pick

TH LC-TH-2003-069 Electroweak radiative corrections to e+e-->t anti-t H 2003-07-16
A.Denner, S.Dittmaier, M.Roth, M.M.Weber

TH LC-TH-2003-070 Higgs production in the 1 TeV domain: logarithmic Sudakov expansion and $ aeta$ measurement analysis 2003-07-22
S.Trimarchi

TH LC-TH-2003-073 Higgs pair production in association with a vector bosons at e+e- colliders in theories of higher dimensional gravity 2003-07-29
N.G.Deshpande, D.K.Ghosh

TH LC-TH-2003-077 Complete Two Loop Bosonic Contributions to the Muon Lifetime in the Standard Model 2003-07-14
M.Awramik, M.Czakon

TH LC-TH-2003-078 Complete Two Loop Electroweak Contributions to the Muon Lifetime in the Standard Model 2003-07-14
M.Awramik, M.Czakon

TH LC-TH-2003-079 Bosonic Corrections to Delta_r at the Two Loop Level 2003-07-14
M.Awramik, M.Czakon, A.Onishchenko, O.Veretin

TH LC-TH-2003-082 Massive two-loop Bhabha scattering -- the factorizable subset 2003-09-15
J.Fleischer, T.Riemann, O.V.Tarasov, A.Werthenbach

TH LC-TH-2003-083 O(alpha) electroweak corrections to the processes e+e- to tau-tau+,c c-bar, b b-bar, t t-bar: a comparison 2003-08-12
T.Hahn, W.Hollik, A.Lorca, T.Riemann, A.Werthenbach

TH LC-TH-2003-089 Identifying an SM-like Higgs particle at future colliders 2003-10-06
I.F.Ginzburg, M.Krawczyk, P.Osland

TH LC-TH-2003-090 CJK- Improved LO Parton Distributions in the Real Photon and Their Experimental Uncertainties 2003-10-06
F.Cornet, P.Jankowski, M.Krawczyk

TH LC-TH-2003-091 Electro-weak Fits at CLIC 2003-07-09
S.DeCurtis

TH LC-TH-2003-093 Probing triple gauge couplings with transverse beam polarisation in e+e- -> W+W- 2003-09-11
M.Diehl, O.Nachtmann, F.Nagel

TH LC-TH-2003-094 One-loop corrections to the process e+e- to t bar-t including hard bremsstrahlung 2003-10-13
J.Fleischer, J.Fujimoto, T.Ishikawa, A.Leike, T.Riemann, Y.Shimizu, A.Werthenbach

TH LC-TH-2003-095 Tree and one-loop level tests of the minimal LR-symmetric model 2003-07-15
M.Czakon, J.Gluza, Hejczyk

TH LC-TH-2003-097 CP Violation in the 3 Jet and 4 Jet Decays of the Z-Boson at GigaZ 2003-08-12
O.Nachtmann, C.Schwanenberger

TH LC-TH-2003-098 Study of selectron properties in the e~ e~ -> e- X_1^0 e- X_2^0 decay channel 2003-11-20
J.A.Aguilar-Saavedra

TH LC-TH-2003-099 CP violation at a linear collider with transverse polarization 2003-10-31
B.Ananthanarayan, S.D.Rindani

TOOL LC-TOOL-2003-010 Detector Simulation with MOKKA and Geant4: Present and Future 2003-03-13
P.M.deFreitas

TOOL LC-TOOL-2003-015 Java Physics Generator and Analysis Modules 2003-06-03
M.T.Ronan

TOOL LC-TOOL-2003-042 SPheno, a program for calculating supersymmetric spectra, SUSY particle decays and SUSY particle production at e+ e- colliders 2003-06-19
P.Werner

TOOL LC-TOOL-2003-053 LCIO - A persistency framework for linear collider simulation studies 2003-07-17
F.Gaede, T.Behnke, N.Gra, T.Johnson

TOOL LC-TOOL-2003-081 MC-TESTER: a universal tool for comparisons of Monte Carlo predictions for particle decays in high energy physics 2003-07-10
P.Golonka, T.Pierzchala, Z.Was

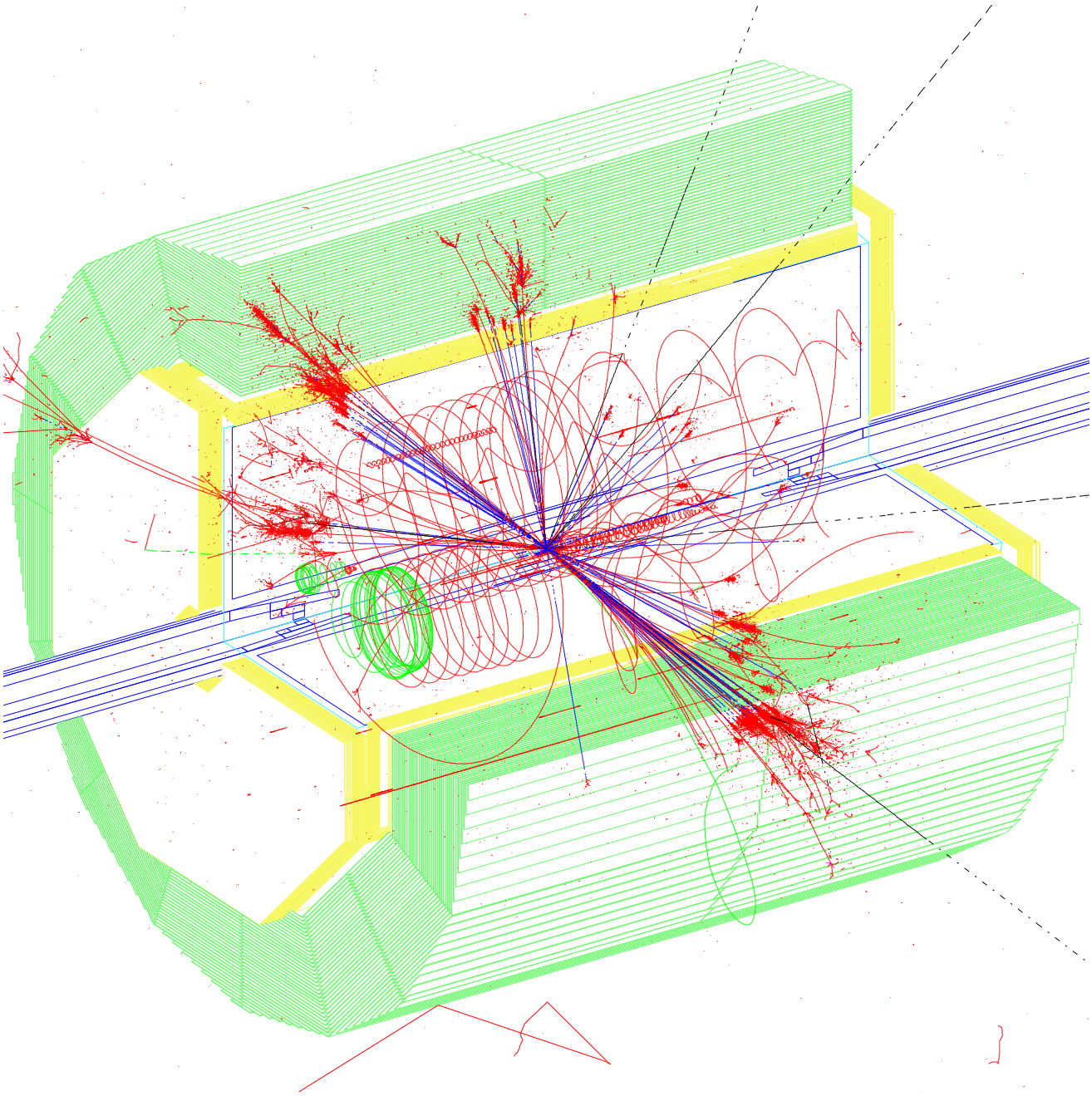

The same $e^+e^- \to$ HHZ event as on title page. Blue lines connect the vertex to the photons in the ECAL and the black lines show the neutrino directions. All of the remaining deposites are raw data.

.

TOP QUARK PHYSICS and QCD: PROGRESS since the TESLA TDR*

A. Brandenburg, Institut für Theoretische Physik, RWTH Aachen, D-52056 Aachen, Germany
and DESY Theory Group, D-22607 Hamburg, Germany†

Abstract

I review progress on investigations concerning top quark physics and QCD at a future linear e^+e^- collider that has been achieved since the presentation of the TESLA technical design report [1] in spring 2001. I concentrate on studies that have been presented during the workshop series of the Extended Joint ECFA/DESY Study on Physics and Detectors for a Linear Electron-Positron Collider.

INTRODUCTION

Since the presentation of the TESLA technical design report [1] in spring 2001, important progress has been achieved and reported in the top quark/QCD working group of the Extended Joint ECFA/DESY Study on Physics and Detectors for a Linear Electron-Positron Collider. The common aim of these studies is to improve theoretical predictions and perform more realistic simulations in order to obtain an accurate understanding of top quark interactions and QCD phenomena at a linear collider. A basic issue is a precision determination of two fundamental parameters of the Standard Model, namely the top quark mass m_t and the strong coupling constant α_s. These parameters as well as the top quark width can be extracted from a scan of the $t\bar{t}$ threshold cross section with high accuracy, and I will report on the progress of the simulation of such a scan and of the refinements in the theoretical computation of the threshold cross section. Before that, I will summarize a recent study on the importance of a very precise measurement of m_t. Further topics covered here include new studies on top quark production and decay in the continuum and a summary of QCD-related studies. I concentrate on work reported at the ECFA/DESY workshops. A summary of top quark and QCD studies presented at the last International Linear Collider Workshop (LCWS02) is given in [2].

* Much of the work reported in this talk was done by members of the Top and QCD working group of the Extended ECFA/DESY Study: W. Bernreuther (RWTH Aachen), G.A. Blair (London U.), E. Boos (Moscow State U.), P.N. Burrows (London U.), M.P. Casado (CERN), S.V. Chekanov (Argonne), S. Dittmaier (MPI München), M. Dubinin (Moscow U.), J. Fleischer (Bielefeld U.), A. Gay (IRES Strasbourg), T. Hahn (MPI München), S. Heinemeyer (München U.), A.H. Hoang (MPI München), W. Hollik (MPI München), K. Kolodziej (Silesia U.), S. Kraml (CERN), F. Krauss (CERN), J.H. Kühn (Karlsruhe U.), J. Kwiecinski (Inst. of Nucl. Phys. Krakow), A. Lorca (DESY Zeuthen), M. Maniatis (Hamburg U.), A.V. Manohar (UC San Diego), M. Martinez (Barcelona U.), R. Miquel (LBL Berkeley), V.L. Morgunov (DESY), W. Porod (Zürich U.), T. Riemann (DESY Zeuthen), M. Roth (Karlsruhe U.), T. Robens (Heidelberg U.), C. Schappacher (Karlsruhe U.), I.W. Stewart (MIT), C. Sturm (Karlsruhe U.), T. Teubner (CERN), P. Uwer (Karlsruhe U.), G. Weiglein (IPPP Durham), A. Werthenbach (CERN), M. Winter (IRES Strasbourg), P.M. Zerwas (DESY Hamburg). I also would like to thank B.A. Kniehl, A.A. Penin and M. Steinhauser for discussions.

† arnd.brandenburg@desy.de

WHY DO WE WANT TO KNOW M_T VERY PRECISELY?

The physics impact of a very precise measurement of the top quark mass with $\delta m_t \lesssim 100$ MeV has been recently studied in detail [3]. An accurate knowledge of m_t strongly affects tests of the Standard Model (SM) and its extensions using electroweak precision observables. This is demonstrated in Fig. 1, where the prospective experimental errors of M_W and $\sin^2\theta_{\rm eff}$ at the LHC/LC and the GigaZ option of the LC are compared to theoretical predictions within the SM and the Minimal Supersymmetric extension of the SM (MSSM). Since these observables receive radiative corrections $\sim m_t^2$, an improvement from δm_t= 2 GeV (a value to be obtained at the LHC) to δm_t= 100 MeV leads to a significant reduction of the allowed parameter space both in the SM (about factor of 10) and in the MSSM (about a factor of 2). This will be very important in the effort to constrain new interactions in using electroweak precision observables. A precise knowledge of m_t also improves the

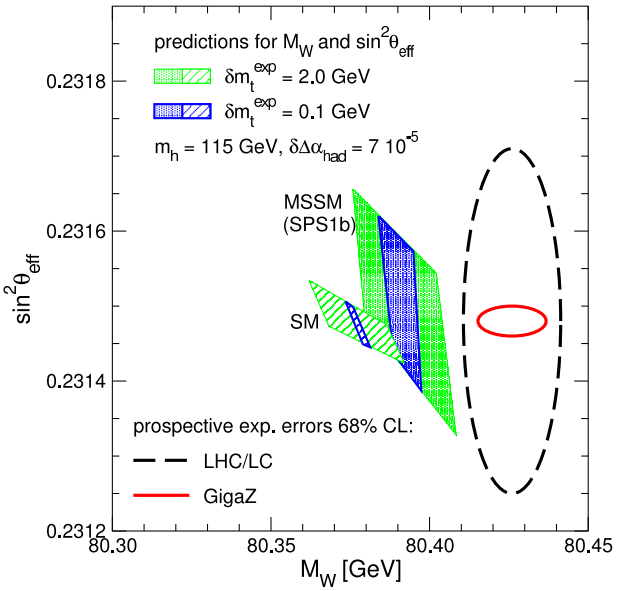

Figure 1: The predictions for M_W and $\sin^2\theta_{\rm eff}$ in the SM and the MSSM (SPS1b). Figure taken from [3].

indirect determination of the top quark Yukawa coupling from electroweak precision observables. Further, if one wants to obtain constraints on the MSSM by comparing a precise measurement of the Higgs boson mass with the theoretical predictions of m_h in this model, a precise value of m_t is mandatory due to the strong dependence ($\sim m_t^4$) of m_h on the top quark mass. For further details and other

applications of a precision measurement of m_t, see [3].

TOP QUARK PAIR PRODUCTION CLOSE TO THRESHOLD

Update of $t\bar{t}$ threshold scan simulation

Recently, an updated $t\bar{t}$ threshold scan simulation has been performed [4]. It comprises several new features as compared to previous studies. First, three observables have been considered: the total cross section, the position of the peak of the top quark momentum distribution, and the forward-backward asymmetry. Second, a multiparameter fit with up to four parameters (m_t, α_s, Γ_t and the top quark Yukawa coupling λ_t) has been performed. Finally, apart from experimental systematic errors an estimate of the theoretical error in the cross section prediction has been included in the fits. An integrated luminosity of $\mathcal{L} = 300\,\mathrm{fb}^{-1}$ was distributed equally among 10 scan points, where one of them was placed well below threshold in order to determine directly the background. A theoretical error on the total cross section of $\Delta\sigma/\sigma = 3\%$ was assumed in the simulation (see below for a discussion). The results may thus give a good impression about the final experimental accuracy of the determination of the parameters. The expected scan results are shown in Fig. 2. From a two

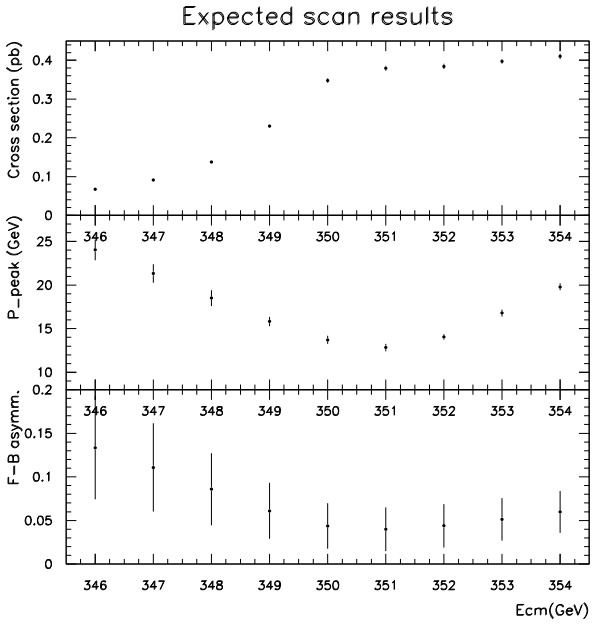

Figure 2: Expected scan result for the cross section, the peak of the top quark momentum distribution and the forward-backward charge asymmetry. Figure taken from [4].

parameter fit for α_s and m_t the following estimates of their errors were obtained:

$$\Delta m_t^{1S} = 16\,\mathrm{MeV}, \qquad \Delta\alpha_s = 0.0012. \qquad (1)$$

Here, m_t^{1S} denotes the $1S$ mass of the top quark, the usage of which stabilises the location of the threshold with respect to higher order corrections and reduces the correlations between this mass and α_s. The correlation plot between m_t and α_s is shown in Fig. 3. The correlation coefficient is $\rho = 0.33$. While the cross section has the highest sensitivity on both m_t and α_s, the additional measurement of the peak of the momentum distribution reduces the errors and the correlation substantially.

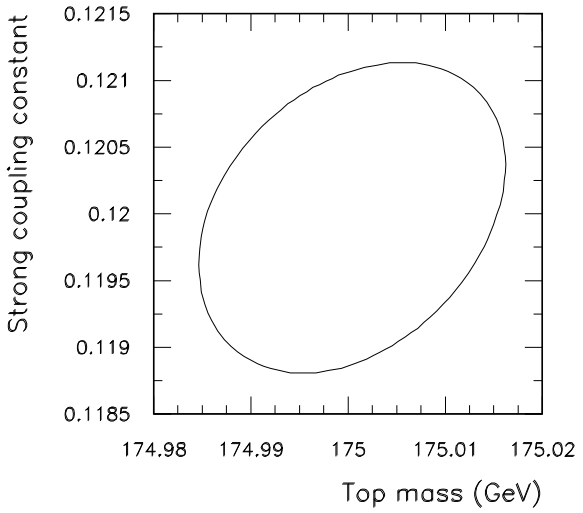

Figure 3: $\Delta\chi^2 = 1$ contour as a function of m_t^{1S} and $\alpha_s(M_Z)$. Figure taken from [4].

The size of the top quark width Γ_t determines how pronounced the $1S$ resonance is. A three-parameter fit for m_t, α_s and Γ_t gives:

$$\Delta m_t^{1S} = 19\,\mathrm{MeV},\ \Delta\alpha_s = 0.0012,\ \Delta\Gamma_t = 32\,\mathrm{MeV}. \quad (2)$$

This means that the top quark width can be determined with 2% accuracy, which is a factor of about 9 better than reported in earlier studies. This improvement is due to assuming a higher integrated luminosity, a better selection efficiency for $t\bar{t}$ events, a sharper TESLA beam spectrum and a better scanning strategy when using the $1S$ mass.

The sensitivity of a threshold scan to the top quark Yukawa coupling λ_t through a modification of the $t\bar{t}$ potential is not very large: if one performs a four-parameter fit with an external constraint on $\alpha_s(M_Z)$, the results are (for $M_H = 120$ GeV):

$$\Delta m_t^{1S} = 31\,\mathrm{MeV}, \quad \Delta\alpha_s = 0.001\ (\mathrm{constr.}),$$
$$\Delta\Gamma_t = 34\,\mathrm{MeV}, \quad \frac{\Delta\lambda_t}{\lambda_t} = {}^{+0.35}_{-0.65}\,. \qquad (3)$$

Thus, constraining the top quark Yukawa coupling from a threshold scan is a challenging task. A better method is provided by analysing the associated Higgs production process $e^+e^- \to t\bar{t}H$ [5].

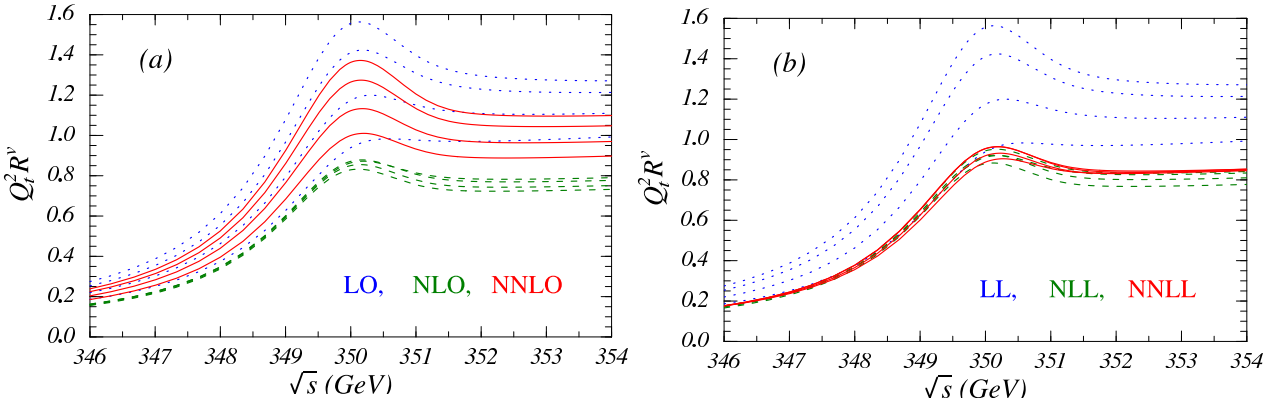

Figure 4: Results for the vector current R-ratio with fixed m_t^{1S} mass for fixed order and renormalization group improved predictions. The dotted, dashed, and solid curves in a) are LO, NLO, and NNLO, and in b) are LL, NLL, and NNLL order. For each order four curves are plotted for velocity renormalization scales $\nu = 0.1,\ 0.125,\ 0.2$ and 0.4. Figure taken from [10] (an update with very small changes was given in [12]).

The very accurate measurement of m_t^{1S} is certainly impressive; however, in order to use the top mass as an input for precision tests of the SM, we have to convert the $1S$ mass to the $\overline{\rm MS}$ mass. The current theoretical uncertainty in the perturbative relation between these two masses is of the order of 100 MeV [6].

Theoretical developments

The status of $t\bar{t}$ threshold cross section calculations in spring 2001 was as follows: Several groups had calculated the cross section at NNLO (for a synopsis of these results and further references, see [6]). The corrections turned out to be large, and the threshold location was found to be unstable under perturbative corrections when the top quark pole mass was used in the calculation. Further, a strong correlation between α_s and m_t limited the experimental precision of m_t to about 300 MeV. The usage of threshold masses [7, 8, 9] reduced this correlation and stabilized the position of the threshold significantly. However, the height of the cross section still suffered from large perturbative corrections of the order of 20 to 30 %, even when expressed in terms of a top quark threshold mass. In order to improve the prediction of the threshold cross section, the impact of a summation of QCD logarithms of ratios of the scales m_t, $m_t v$, and $m_t v^2$ was computed in [10, 11]. A comparison of the fixed order results and the renormalization group improved results is shown in Fig. 4. The remaining theoretical uncertainty of the cross section was estimated in [10] to be $\pm 3\%$. This number was obtained by varying the dimensionless velocity subtraction scale that separates hard, soft and ultrasoft momenta and by estimating the size of the one yet unknown NNLL contribution from the running at the production current. Very recently, the NNLL non-mixing contributions to the running of the production current have been determined [13]. It remains to be seen whether the $\pm 3\%$ estimate will withstand future refinements of the cross section calculations. For testing the convergence of the alternative fixed order (LO, NLO, NNLO, ...) perturbation series the computation of the NNNLO contributions is mandatory. Important progress has been recently achieved in this direction [14].

Electoweak effects have not yet been consistently included either at NNLL order or NNLO.

TOP QUARK PRODUCTION AND DECAY IN THE CONTINUUM

Mass determination from continuum production

In [15] the possibility of measuring the top quark mass in the continuum was investigated. The process $e^+e^- \to t\bar{t} \to 6$ jets was simulated including the QCD background. Top quarks were reconstructed by grouping the 6 jets into pairs of three-jet groups. Only three-jet groups which are produced back-to-back are accepted. The three-jet invariant mass distribution (see Fig. 5) then shows a prominent peak, the position of which is interpreted as the top quark mass. The statistical uncertainty of the peak position is 100 MeV for an integrated luminosity of 300 fb^{-1} at $\sqrt{s} = 500$ GeV. Experimental systematic errors have not yet been studied. Further, it is not clear yet how to relate this 'kinematic mass' to the pole mass or other top quark mass definitions. The method was recently extended to semileptonic top decays [16].

Anomalous top quark couplings

A new analysis was started to evaluate the sensitivity of $e^+e^- \to t\bar{t}$ to anomalous top quark couplings [17]. The plan is to use PANDORA/PYTHIA and SIMDET in the simulation and try to find observables that optimize the sensitivity.

New theoretical studies and tools

In the following I briefly discuss further studies on top quark production and decay in the continuum that have been presented during the workshop series.

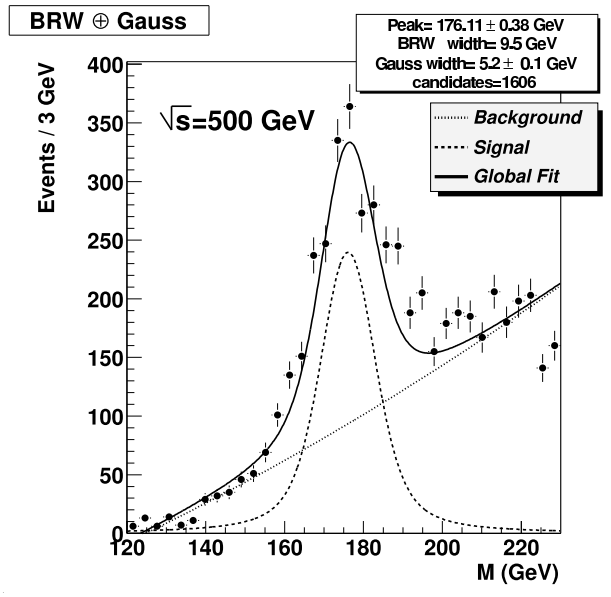

Figure 5: The invariant-mass distribution for three-jet clusters in $e^+e^- \to 6$ jets. Figure taken from [15].

- Several calculations of the electroweak one-loop radiative corrections to the process $e^+e^- \to t\bar{t}$ have been compared in detail [18]. The numerical agreement is excellent (see also Table 4 in [19]). The package `topfit` containing these corrections is publicly available [20].

- New tree level Monte Carlo generators (`AMEGIC++` [21], `eett6f` [22] and `LUSIFER` [23]) for the processes $e^+e^- \to 6$ fermions have been written (for details, see [19]). These programs allow to study in particular the non-resonant background to $t\bar{t}$ production and decay.

- In [24], the production of single top quarks in $e^+e^-, e^-e^-, e\gamma$ and $\gamma\gamma$ collisions was studied at tree level. By comparing all possible reactions, the best option turned out to be collisions of circular polarized photons with left-handed electrons. The cross section at $\sqrt{s} = 500$ GeV is $\sigma(\gamma_+ e^-_L \to \bar{t}b\nu) \sim 100$ fb, and this process is very sensitive to V_{tb} as well as to possible anomalous couplings. If one aims at an experimental precision of 1% for V_{tb}, the inclusion of higher order corrections is mandatory. The QCD corrections to this process have been computed very recently [25] and are of the order of 5%.

- The SUSY-QCD corrections to the production and decay of *polarized* top quarks in e^+e^- collisions have been computed in [26]. While the decay width and lepton energy spectrum can be modified at the percent level, top polarization observables are hardly affected by these corrections.

QCD STUDIES

Measurement of α_s

The primary goal of QCD studies at a linear collider is to measure the strong coupling constant α_s as precisely as possible. The aim is to reduce the current accuracy $\Delta\alpha_s(M_Z) = 0.003$ to a value of $\Delta\alpha_s(M_Z) = 0.001$ or smaller. In the context of QCD, such an accuracy is important, since *all* predictions of perturbative QCD are directly affected, in particular multi-jet cross sections at higher orders. Furthermore, an extrapolation of $\alpha_s(Q)$ to very high energy scales which is performed to test the hypothesis of Grand Unification needs precise initial conditions, and the uncertainty on α_s is currently the limiting factor of such tests. This is illustrated in Fig. 6, where the running of the inverse coupling constants is shown. The narrow error band on $1/\alpha_3$ in Fig. 6b corresponds to $\Delta\alpha_s(M_Z) = 0.001$. The techniques for a determination of $\alpha_s(M_Z)$ at TESLA have been described in detail in the TDR. In a recent study [28], the prospects of a measurement of α_s from GigaZ analyses have been investigated. The factor of ~ 100 in the size of the data sample as compared to LEP data together with the expected better performance of the detector give rise to the expectation that systematic errors may shrink by a factor of 3 to 5. This would mean that the experimental accuracy on α_s could be brought down to $(5-7) \times 10^{-4}$, the most sensitive observable being the inclusive ratio $\Gamma_Z^{\rm hadron}/\Gamma_Z^{\rm lepton}$. No theoretical errors are included in this analysis. At present, the theoretical uncertainty of α_s-determinations from $\Gamma_Z^{\rm hadron}/\Gamma_Z^{\rm lepton}$ is estimated to be of the same size as the current experimental accuracy [29]. In view of the prospective accuracy from a GigaZ run, there is an ongoing effort to compute more and more terms of the perturbation series for $\Gamma_Z^{\rm hadron}/\Gamma_Z^{\rm lepton}$ and related quantities like $R(s)$ and $\Gamma_\tau^{\rm hadron}/\Gamma_\tau^{\rm lepton}$. The most recent step in this direction has been the calculation of a gauge-invariant subset of the order α_s^4 contributions, namely the terms of order $\alpha_s^4 n_f^2$, where n_f is the number of fermion flavours [30].

The bottleneck of determinations of $\alpha_s(M_Z)$ from event shapes (like thrust distribution, jet rates etc.) is currently the insufficient theoretical precision of perturbative QCD calculations. Currently most shape variables are known to next-to-leading order accuracy, while for some observables resummed calculations are available. However, enormous progress towards the calculation of $e^+e^- \to 3$ jets to NNLO ($\mathcal{O}(\alpha_s^3)$) has been achieved within the last few years [31]. It is estimated that once these calculations are accomplished, the current theoretical uncertainty (obtained by a variation of the QCD renormalisation scale) of $\Delta\alpha_s(M_Z) \simeq 0.006$ will shrink by a factor of 3 to 5.

Saturation model for $\gamma\gamma$ and $\gamma^*\gamma^*$ processes

In [32] a saturation model has been constructed to describe the total cross section for $\gamma\gamma$ and $\gamma^*\gamma^*$ collisions at high energies. The $\gamma^*\gamma^*$ total cross section is assumed

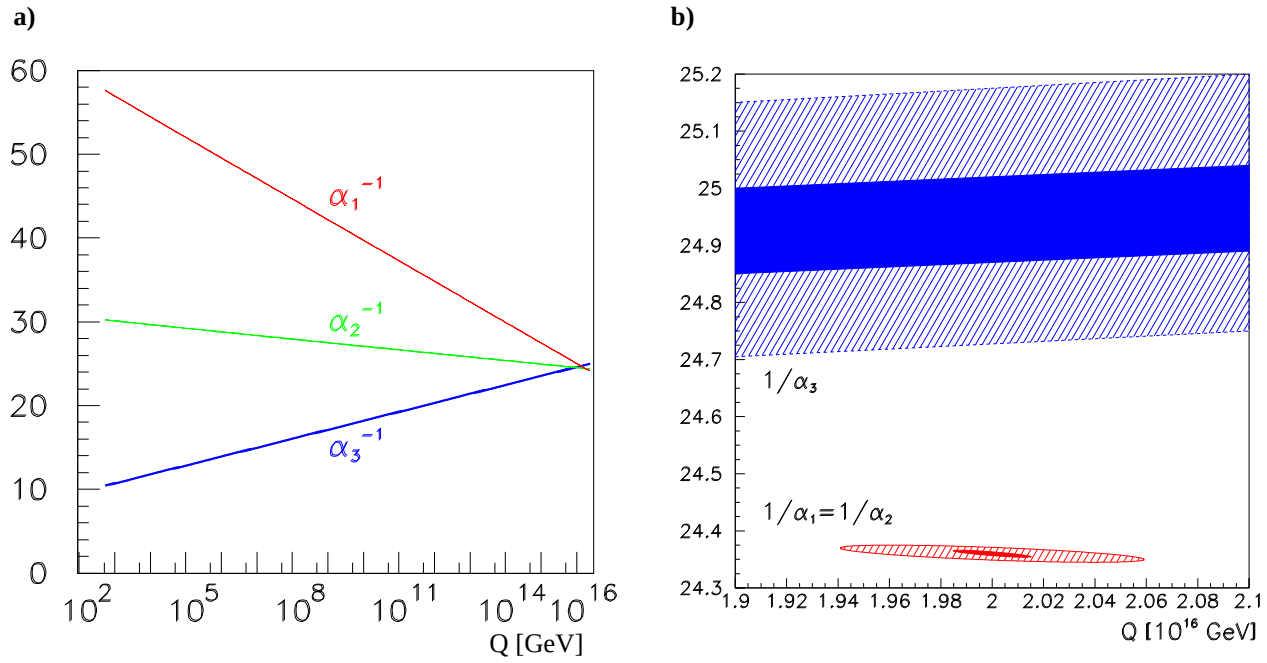

Figure 6: *a) Running of the inverse gauge couplings. b) Determination of M_U, α_U^{-1}; the unification point U is defined by the meeting point of α_1 with α_2. The wide error bands are based on present data, the narrow bands demonstrate the improvement expected by future GigaZ analyses. Figure taken from [27].*

to be dominated by interactions of two colour dipoles into which the photons can fluctuate, the novel feature being that the saturation property of the dipole-dipole cross section is incorporated. This allows to describe the variation of the energy dependence of the cross section when the virtualities of the photons change. The model fits the available two-photon data reasonably well, except for b-quark production. Predicitions for TESLA energies have been formulated.

Odderon contribution to exclusive pion-photoproduction

In [33] the nonperturbative odderon contributions to the processes $e^+e^-, \gamma\gamma \to \pi^0\pi^0$ have been studied. The cross sections are very sensitive, both in the e^+e^- and the $\gamma\gamma$ mode, to the coupling strength of the odderon, while the Regge trajectory parameters are harder to determine.

CONCLUSIONS

Without doubt a future high-energy, high luminosity e^+e^- linear collider like TESLA will be an excellent facility to study in detail the physics of top quarks and strong interaction phenomena. In particular, a $t\bar{t}$ threshold scan will provide a measurement of m_t with unmatched precision, with important implications for searches for physics beyond the Standard Model. Important progress has been achieved recently to predict the threshold cross section precisely and to evaluate the experimental sensitivity to m_t and other SM parameters. However, future improvements are necessary and possible: For example, the experimental uncertainty with which a threshold mass like m_t^{1S} can be extracted is expected to be much smaller than the current theoretical uncertainty that relates this parameter to the $\overline{\rm MS}$ mass. An ongoing challenging task is the refinement of the theoretical understanding of the threshold cross section. Furthermore, it would be desirable to include a realistic luminosity spectrum $d\mathcal{L}/dE$ in the threshold scan simulation. Another important task is a simulation of a determination of top quark form factors at the detector level.

Challenging issues in perturbative QCD are the calculation of event shape variables at NNLO and a further improvement of the theoretical predictions of inclusive quantities like $\Gamma_Z^{\rm hadron}/\Gamma_Z^{\rm lepton}$. Progress in these areas would contribute significantly to the aim of determining $\alpha_s(M_Z)$ with an accuracy of a percent or better.

REFERENCES

[1] J.A. Aguilar-Saavedra et al., "TESLA technical design report part III: Physics at an e^+e^- linear collider", hep-ph/0106315, see http://tesla.desy.de/tdr/ .

[2] Y. Sumino, Talk presented at LCWS02, Jeju Island, Korea, August 2002, hep-ph/0302086.

[3] S. Heinemeyer, S. Kraml, W. Porod and G. Weiglein, LC-TH-2003-052, hep-ph/0306181.

[4] M. Martinez and R. Miquel, Eur. Phys. Jour. **C 27** (2003) 49 [hep-ph/0207315].

[5] K. Desch, these proceedings.

[6] A.H. Hoang et al., Eur. Phys. J. direct C **3** (2000) 1 [hep-ph/0001286].

[7] M. Beneke, Phys. Lett. B **434** (1998) 115 [hep-ph/9804241].

[8] A.H. Hoang and T. Teubner, Phys. Rev. D **60** (1999) 114027 [hep-ph/9904468].

[9] I.I. Bigi, M. Shifman, N. Uraltsev and A. Vainshtein, Phys. Rev. D **56** (1997) 4017 [hep-ph/9704245].

[10] A.H. Hoang, A.V. Manohar, I.W. Stewart and T. Teubner, Phys. Rev. Lett. **86** (2001) 1951 [hep-ph/0011254] and Phys. Rev. D **65** (2002) 014014 [hep-ph/0107144].

[11] A. Pineda, Phys. Rev. D **65** (2002) 074007 [hep-ph/0109117] and Phys. Rev. D **66** (2002) 054022 [hep-ph/0110216].

[12] A.H. Hoang and I.W. Stewart, Phys. Rev. D **67** (2003) 114020 [hep-ph/0209340].

[13] A.H. Hoang, hep-ph/0307376.

[14] B.A. Kniehl, A.A. Penin, V.A. Smirnov and M. Steinhauser, Nucl. Phys. B **635** (2002) 357 [hep-ph/0203166];
A.A. Penin and M. Steinhauser, Phys. Lett. B **538** (2002) 335 [hep-ph/0204290];
B.A. Kniehl, A.A. Penin, V.A. Smirnov and M. Steinhauser, Phys. Rev. Lett. **90** (2003) 212001 [hep-ph/0210161];
Y. Kiyo and Y. Sumino, Phys.Rev. D **67** (2003) 071501 [hep-ph/0211299].

[15] S.V. Chekanov, V.L. Morgunov, LC-PHSM-2003-001 [hep-ex/0301014].

[16] S.V. Chekanov, V.L. Morgunov, "Top quark at a linear collider", talk presented in the Top and QCD working group session at the Fourth ECFA/DESY Workshop of the Extended Joint ECFA/DESY Study on Physics and Detectors for a Linear Electron-Positron Collider , Amsterdam, The Netherlands, 1.-4. April 2003.

[17] M.P. Casado, talks presented in the Top and QCD working group session at the First and Second Workshop of the Extended Joint ECFA/DESY Study on Physics and Detectors for a Linear Electron-Positron Collider, Krakow, Poland, 14.-18. September 2001 and St. Malo, France, 12.-15. April 2002.

[18] J. Fleischer, T. Hahn, W. Hollik, T. Riemann, C. Schappacher and A. Werthenbach, LC-TH-2002-002, hep-ph/0202109;
J. Fleischer, J. Fujimoto, T. Ishikawa, A. Leike, T. Riemann, Y. Shimizu and A. Werthenbach, KEK Proceedings 2002-11 (2002) (Y. Kurihara, ed.) 153 [hep-ph/0203220];
T. Hahn, W. Hollik, A. Lorca, T. Riemann and A. Werthenbach, hep-ph/0307132.

[19] S. Dittmaier, these proceedings.

[20] See http://www-zeuthen.desy.de/∼riemann/.

[21] F. Krauss, R. Kuhn and G. Soff, JHEP **0202** (2002) 044 [hep-ph/0109036];
A. Schalicke, F. Krauss, R. Kuhn and G. Soff, JHEP **0212** (2002) 013 [hep-ph/0203259].

[22] K. Kolodziej, Eur. Phys. J. C **23** (2002) 471 [hep-ph/0110063].

[23] S. Dittmaier and M. Roth, Nucl. Phys. B **642** (2002) 307 [hep-ph/0206070].

[24] E. Boos, M. Dubinin, A. Pukhov, M. Sachwitz and H.J. Schreiber, Eur. Phys. J. C **21** (2001) 81 [hep-ph/0104279].

[25] J.H. Kühn, C. Sturm, P. Uwer, hep-ph/0303233.

[26] A. Brandenburg and M. Maniatis, Phys. Lett. B **545** (2002) 139 [hep-ph/0207154] and Phys. Lett. B **558** (2003) 79 [hep-ph/0301142].

[27] G.A. Blair, W. Porod, P.M. Zerwas, Eur. Phys. J. C **27** (2003) 263, LC-TH-2003-021 [hep-ph/0210058].

[28] M. Winter, "Determination of the strong coupling constant at GigaZ", LC-PHSM-2001-016.

[29] S. Bethke, J. Phys. G **26** (2000) R27 [hep-ex/0004021].

[30] P.A. Baikov, K.G. Chetyrkin, J.H. Kühn, Phys. Rev. Lett. **88** (2002) 012001 [hep-ph/0108197].

[31] L.W. Garland, T. Gehrmann, E.W.N. Glover, A. Koukoutsakis and E. Remiddi, Nucl. Phys. B **626** (2002) 107 [hep-ph/0112081] and Nucl. Phys. B **642** (2002) 227 [hep-ph/0206067];
S. Moch, P. Uwer, S. Weinzierl, Phys. Rev. D **66** (2002) 114001 [hep-ph/0207043];
S. Weinzierl, JHEP 0303 (2003) 062 [hep-ph/0302180] and hep-ph/0306248.

[32] N. Timneanu, J. Kwiecinski, L. Motyka, Eur. Phys. J. C **23** (2002) 513 [hep-ph/0110409].

[33] T. Robens, hep-ph/0302048 and talk presented in the Top and QCD working group session at the Fourth ECFA/DESY Workshop of the Extended Joint ECFA/DESY Study on Physics and Detectors for a Linear Electron-Positron Collider, Amsterdam, The Netherlands, 1.-4. April 2003.

THEORETICAL TOOLS for a FUTURE e^+e^- LINEAR COLLIDER*

S. Dittmaier, Max-Planck-Institut für Physik (Werner-Heisenberg-Institut), Munich, Germany†

Abstract

Recent progress in the calculation of radiative corrections and in Monte Carlo event generation, relevant for a future e^+e^- linear collider, is reviewed.

INTRODUCTION

Precision measurements at LEP, SLC, and the Tevatron rendered the last decade the era of high-precision physics. A future e^+e^- linear collider (LC), such as TESLA [1], the NLC [2], or the GLC (former JLC) [3], does not only offer an even greater physics potential, but in turn represents a great challenge for theorists to understand phenomena at the experimentally achievable level of precision.

For instance, returning again to the Z-boson resonance in the "GigaZ" mode of TESLA (where about 10^9 Z bosons can be produced within 50–100 days of running) allows for a repetition of the LEP1/SLC physics program with roughly an order of magnitude higher precision (see also Ref. [4]). Specifically, the uncertainty in the effective weak mixing angle could be reduced from 1.7×10^{-4} to 1.3×10^{-5}. For a theoretical description of the Z resonance at this level of accuracy full two-loop calculations of the observables as well as the knowledge of leading higher-order effects are clearly necessary. A scan over the W-pair production threshold could provide a sensitivity to the W-boson mass of about $7\,\mathrm{MeV}$, which should be compared with the present error of $34\,\mathrm{MeV}$, resulting from the kinematical reconstruction of W bosons. The present approach of approximating the radiative corrections to $e^+e^- \to WW \to 4$ fermions by an expansion about the double resonance is not applicable (or at least not reliable) in the threshold region where singly- or non-resonant contributions become important. The only solution seems to be the full treatment of the complete four-fermion production processes at the one-loop level, including higher-order improvements.

At energies exceeding the reach of LEP2, many new processes will be accessible, such as top-quark pair production, Higgs production (if the Higgs boson exists), or reactions with new-physics particles, as e.g. predicted by SUSY models. Most of these heavy particles are unstable, so that their production eventually leads to many-particle final states. For example, the production of $t\bar{t}$ pairs or of a Higgs-boson with an intermediate or large mass ($M_H > 2M_W$) leads to six-fermion final states. To exploit the potential of a LC, predictions for such reactions should be based on full transition matrix elements and improved by radiative corrections as much as possible. The higher level of accuracy at a future LC does, however, not only call for proper event generators for many-particle final states. "True" event generators, i.e. including parton showering and hadronization, have to be improved as well.

In this brief article the main progress on precision calculations and event generators that has been achieved in the "Loopverein" and "Generators" working groups of the Extended ECFA/DESY Study since the appearance of the TESLA TDR [1] is reviewed. More studies on the physics potential of a LC in view of electroweak and strong interactions, top-quark physics, Higgs physics, and new physics searches, in particular supersymmetry, are summarized in Ref. [5].

HIGH-PRECISION OBSERVABLES AND MULTI-LOOP CALCULATIONS

Precision calculations for μ decay

The precision measurement of the muon lifetime, or equivalently of the Fermi constant G_μ, sets an important constraint on the SM parameters,

$$G_\mu = \frac{\pi\alpha(0)}{\sqrt{2}M_W^2 s_w^2}\,(1+\Delta r), \qquad (1)$$

* The work reported in this article is based on the progress reached since Spring 2001 by the "Loopverein" and "Monte Carlo event generators" working groups of the extended ECFA/DESY Study; particular thanks goes to the working-group members M. Antonelli (Frascati), M. Awramik (Cracow), D. Bardin (Dubna), G. Bélanger (Annecy), A. Biernacik (Katowice), J. Blümlein (DESY Zeuthen), F. Boudjema (Annecy), A. Brandenburg (Aachen), C. M. Carloni Calame (Pavia), P. Ciafaloni (Lecce), M. Czakon (Katowice), A. Denner (PSI Villigen), M. Diaz (Catolica), M. Faisst (Karlsruhe), J. Fleischer (Bielefeld), J. Fujimoto (KEK), A. Freitas (FNAL), F. Gangemi (Pavia), A. Ghinculov (Rochester), P. Golonka (Cracow), J. Guasch (PSI Villigen), T. Hahn (MPI Munich), A. van Hameren (Athens), S. Heinemeyer (LMU Munich), W. Hollik (MPI Munich), V. A. Ilyin (Moscow), T. Ishikawa (KEK), S. Jadach (Cracow), F. Jegerlehner (DESY Zeuthen), L. Kalinovskaya (Dubna), M. Kalmykov (DESY Zeuthen), T. Kaneko (KEK), K. Kato (Tokyo), H. Kawamura (DESY Zeuthen), W. Kilian (DESY Hamburg), K. Kołodziej (Katowice), M. Krämer (Edinburgh), F. A. Krauss (CERN), J. Kühn (Karlsruhe), Y. Kurihara (KEK), M. Maniatis (Hamburg), K. Mönig (DESY Zeuthen), G. Montagna (Pavia), M. Moretti (Ferrara), S. Moretti (Southampton), O. Nicrosini (Pavia), A. Leike (LMU Munich), A. Lorca (Granada), T. Ohl (Würzburg), W. Öller (Vienna), A. I. Onishchenko (Moscow), C. Papadopoulos (Athens), G. Passarino (Torino), M. Peskin (SLAC), F. Piccinini (CERN/Pavia), T. Pierzchala (Karlsruhe), W. Płaczek (Cracow), T. Riemann (DESY Zeuthen), M. Ronan (Berkeley), M. Roth (Karlsruhe), C. Schappacher (Karlsruhe), S. Schumann (Dresden), Y. Shimizu (KEK), M. Skrzypek (Cracow), M. Spira (PSI Villigen), O. Tarasov (DESY Zeuthen), B. Tausk (Freiburg), O. Veretin (Karlsruhe), C. Verzegnassi (Trieste), D. Wackeroth (Buffalo), B. F. L. Ward (Knoxville), Z. Was (Cracow), C. Weber (Vienna), M. Weber (PSI Villigen), G. Weiglein (Durham), S. Weinzierl (Parma), A. Werthenbach (CERN), M. Wing (Bristol), M. Worek (Katowice), P. Zerwas (DESY Hamburg).

† Stefan.Dittmaier@mppmu.mpg.de

where $s_{\rm w}^2 = 1 - c_{\rm w}^2 = 1 - M_{\rm W}^2/M_{\rm Z}^2$ and the quantity Δr comprises the radiative corrections to muon decay (apart from the photonic corrections in the Fermi model). In the past it has become common practice to implicitly solve this relation for the W-boson mass $M_{\rm W}$, thus yielding a precise prediction for $M_{\rm W}$ that can be compared with the directly measured value. Recently the full prediction at the two-loop level has been completed. In detail, first the contributions from closed fermion loops and from bosonic loops involving Higgs-boson exchange were calculated in Ref. [6] by making use of the FEYNARTS package [7] and the program TWOCALC [8] both written in MATHEMATICA. The algebraic reduction leads to two-loop master integrals which are evaluated by semi-analytical methods. The full bosonic corrections have been calculated in Refs. [9] and [10]; Ref. [9] includes also a recalculation of the fermion-loop correction. In the former calculation the diagrams were generated with the C++ library DIAGEN (by Czakon) and evaluated using semi-analytical methods. In the latter case the graphs were generated with the package DIANA [11] and evaluated by asymptotic expansions. The results of Refs. [6, 9, 10] are in good numerical agreement [12].[1] The two-loop fermionic corrections influence the $M_{\rm W}$ prediction at the level of $\sim 50\,\mathrm{MeV}$, where the bulk of this effect is due to universal, top-mass enhanced corrections to the ρ-parameter, which are proportional to $m_{\rm t}^4$ or $m_{\rm t}^2$. The non-universal two-loop fermionic corrections have an impact of up to $4\,\mathrm{MeV}$, the two-loop bosonic corrections of only $1-2\,\mathrm{MeV}$.

The predictions at the two-loop level have been further improved by universal higher-order corrections to the ρ-parameter. The corrections of $\mathcal{O}(G_\mu^2 m_{\rm t}^4 \alpha_{\rm s})$ and $\mathcal{O}(G_\mu^3 m_{\rm t}^6)$ have been calculated for arbitrary $M_{\rm H}$ in Ref. [13] (for other universal corrections to $\Delta\rho$ and Δr see references therein) and were found to change $M_{\rm W}$ at the level of $5\,\mathrm{MeV}$ and $0.5\,\mathrm{MeV}$, respectively. The Feynman diagrams were generated using QGRAF [14] and asymptotically expanded with the program EXP [15]; the resulting massive three-loop tadpole integrals were evaluated with MATAD [16].

Figure 1 compares the prediction for $M_{\rm W}$, including the above-mentioned two-loop and leading three-loop effects, with the experimental value. Note that the shown parametric uncertainty is much larger than the estimated theoretical uncertainty, which is about $3-4\,\mathrm{MeV}$ [17, 18]. Comparing this estimate with the aimed precision of $7\,\mathrm{MeV}$ in the $M_{\rm W}$ determination at a future LC, the prediction of the W-boson mass from muon decay is in rather good shape.

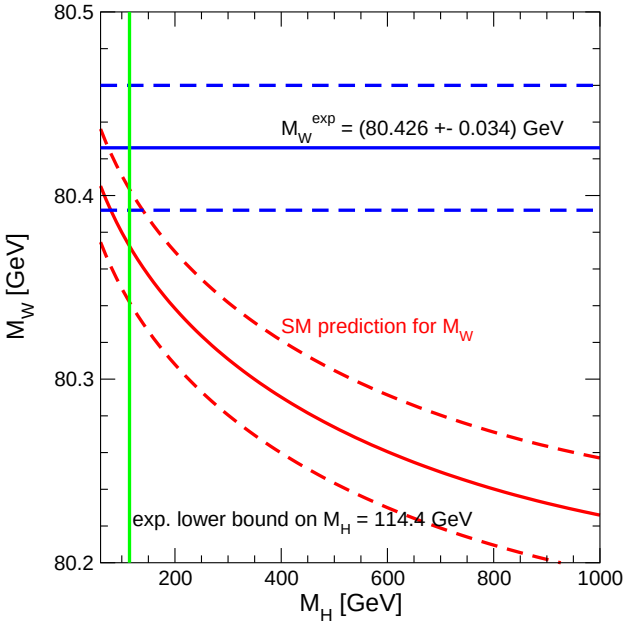

Figure 1: Theoretical prediction of the W-boson mass with the parametric error from uncertainties in the top-quark mass and the running electromagnetic coupling, in comparison with the experimental value $M_{\rm W}^{\rm exp}$ (plot shown in Ref. [17])

Precision observables on the Z resonance

In order to describe the Z-boson resonance at LEP1 within satisfactory precision it was possible to parametrize the cross section near the resonance in such a way [19] that a Born-like form with generalized "effective" couplings is convoluted with QED structure functions modeling initial-state radiation (ISR). From these effective Z-boson–fermion couplings so-called "pseudo-observables" were derived, such as various asymmetries, the hadronic Z-peak cross section, partial Z-decay widths, etc. Following the formal tree-level parametrization of the couplings, an "effective weak mixing angle", usually given as $\sin^2\theta_{f,\rm eff}$, was derived for each fermion. Among these parameters the leptonic variable $\sin^2\theta_{\rm lep,eff}$ plays a particularly important role, since it is measured with the high accuracy of 1.7×10^{-4} and is very sensitive to the Higgs-boson mass. The state-of-the-art in the precision calculations of the pseudo-observables, which is implemented in the programs ZFITTER and TOPAZ0 (see Ref. [20] and references therein), did not change very much since the release of the TESLA TDR [1]. For instance, the estimated theoretical uncertainty in $\sin^2\theta_{\rm lep,eff}$ is still $\sim 6 \times 10^{-5}$. A critical overview about high-precision physics at the Z pole, in particular focusing on the theoretical uncertainties, can be found in Ref. [21] (see also Ref. [4]).

Whether the pseudo-observable approach will also be sufficient for Z-boson physics at the high-luminosity GigaZ option remains to be investigated carefully. In any case, tremendous theoretical progress will be needed to match the aimed GigaZ precision on the theoretical side. For example, the expected experimental accuracy in $\sin^2\theta_{\rm lep,eff}$ is about 1.3×10^{-5}, i.e. about a factor 4 below the present theoretical uncertainty. A full control of observables at the two-loop level, improved by leading higher-order effects, seems to be indispensable.

[1] The results of Ref. [6] for $M_{\rm W}$ have been corrected at the level of $\sim 1\,\mathrm{MeV}$ recently.

Recent results from the 2-loop frontier

Although there are no complete next-to-next-to-leading (NNLO) predictions for $2 \to 2$ scattering reactions and $1 \to 3$ decays (with one truly massive leg) available yet, enormous progress was reached in this direction in recent years.

Complete virtual two-loop amplitudes for (massless) Bhabha scattering [22], light-by-light scattering [23], and $\mathrm{e^+e^-} \to 3$ jets [24] have been worked out, using a large variety of special techniques, which have been summarized in Ref. [25]. A survey of similar results relevant for hadron-collider physics can also be found there. Apart from this two-loop progress on massless particle scattering, also a first step has been made towards massive Bhabha scattering in Ref. [26].

Full NNLO calculations have to include real double-parton bremsstrahlung as well as interference contributions of one-parton bremsstrahlung and one-loop diagrams. The major complication in these parts concerns the proper extraction of the infrared (soft and collinear) singularities. The general form of multiple singular particle emission has been worked out in Ref. [27], which can serve as a basis for the extraction of the singularities. The actual separation of the singularities can be performed either by applying phase-space cuts ("slicing approach") or by subtracting an auxiliary cross section with the same singular structure as the original integrand ("subtraction approach"). In Ref. [28] subtraction terms have been constructed for the leading colour contribution to $\mathrm{e^+e^-} \to 2$ jets in NNLO. However, suitable general subtraction terms as well as their integrated counterparts that have to be added again are not yet available.

Electroweak radiative corrections at high energies

Electroweak corrections far above the electroweak scale, e.g. in the TeV range, are dominated by soft and collinear gauge-boson exchange, leading to corrections of the form $\alpha^N \ln^M(s/M_\mathrm{W}^2)$ with $M \le 2N$. The leading terms ($M = 2N$) are called Sudakov logarithms. At the one-loop ($N = 1$) and two-loop ($N = 2$) level the leading and subleading corrections to a $2 \to 2$ process at $\sqrt{s} \sim 1\,\mathrm{TeV}$ typically amount to [29]

$$\begin{aligned}
\delta_\mathrm{LL}^{1-\mathrm{loop}} &\sim -\frac{\alpha}{\pi s_\mathrm{w}^2} \ln^2\Big(\frac{s}{M_\mathrm{W}^2}\Big) \simeq -26\%, \\
\delta_\mathrm{NLL}^{1-\mathrm{loop}} &\sim +\frac{3\alpha}{\pi s_\mathrm{w}^2} \ln\Big(\frac{s}{M_\mathrm{W}^2}\Big) \simeq 16\%, \\
\delta_\mathrm{LL}^{2-\mathrm{loop}} &\sim +\frac{\alpha^2}{2\pi^2 s_\mathrm{w}^4} \ln^4\Big(\frac{s}{M_\mathrm{W}^2}\Big) \simeq 3.5\%, \\
\delta_\mathrm{NLL}^{2-\mathrm{loop}} &\sim -\frac{3\alpha^2}{\pi^2 s_\mathrm{w}^4} \ln^3\Big(\frac{s}{M_\mathrm{W}^2}\Big) \simeq -4.2\%, \qquad (2)
\end{aligned}$$

revealing that these corrections become significant in the high-energy phase of a future LC. In contrast to QED and QCD, where the Sudakov logarithms cancel in the sum of virtual and real corrections, these terms need not compensate in the electroweak SM for two reasons. The weak charges of quarks, leptons, and electroweak gauge bosons are open, not confined, i.e. there is (in contrast to QCD) no need to average or to sum over gauge multiplets in the initial or final states of processes. Even for final states that are inclusive with respect to the weak charges Sudakov logarithms do not completely cancel owing to the definite weak charges in the initial state [30]. Moreover, the large W- and Z-boson masses make an experimental discrimination of real W- or Z-boson production possible, in contrast to unobservable soft-photon or gluon emission.

In recent years several calculations of these high-energy logarithms have been carried out in the Sudakov regime, where all kinematical invariants $(p_i p_j)$ of different particle momenta p_i, p_j are much larger than all particle masses.[2] A complete analysis of all leading and subleading logarithms at the one-loop level can be found in Ref. [31]. Diagrammatic calculations of the leading two-loop Sudakov logarithms have been carried out in Refs. [29, 32]. Diagrammatic results on the so-called "angular-dependent" subleading logarithms have been presented in Ref. [29]. All these explicit results are compatible with proposed resummations [33, 34] that are based on a symmetric SU(2)×U(1) theory at high energies matched with QED at the electroweak scale. In this ansatz, improved matrix elements $\mathcal{M}$ result from lowest-order matrix elements $\mathcal{M}_0$ upon dressing them with (operator-valued) exponentials,

$$\mathcal{M} \sim \mathcal{M}_0 \otimes \exp(\delta_\mathrm{ew}) \otimes \exp(\delta_\mathrm{em}). \qquad (3)$$

Explicit expressions for the electroweak and electromagnetic corrections δ_ew and δ_em, which do not commute with each other, can, for instance, be found in Ref. [29]. For $2 \to 2$ neutral-current processes of four massless fermions, even subsubleading logarithmic corrections have been derived and resummed [34] using an infrared evolution equation that follows the pattern of QCD.

In supersymmetric models the form of radiative corrections at high energies has also been worked out for a broad class of processes [35]. Based on one-loop results their exponentiation has been proposed.

Higher-order initial-state radiation

Photon radiation off initial-state electrons and positrons leads to large radiative corrections of the form $\alpha^N \ln^N(m_\mathrm{e}^2/s)$. These logarithmic corrections are universal and governed by the DGLAP evolution equations. The solution of these equations for the electron-photon system yields so-called structure functions, generically denoted by $\Gamma(x)$ below, which can be used via convolution to improve hard scattering cross sections $\hat{\sigma}(p_{\mathrm{e}^+}, p_{\mathrm{e}^-})$ by

[2] Note that this regime does not cover the case of forward scattering of particles, which is also of interest in several cases.

photon emission effects,

$$\sigma(p_{e^+}, p_{e^-}) = \int_0^1 \mathrm{d}x_+ \, \Gamma(x_+) \int_0^1 \mathrm{d}x_- \, \Gamma(x_-) \times \hat{\sigma}(x_+ p_{e^+}, x_- p_{e^-}). \quad (4)$$

While the soft-photon part of the structure functions ($x \to 1$) can be resummed, resulting in an exponential form, the contributions of hard photons have to be calculated order by order in perturbation theory. In Ref. [36] the structure functions are summarized up to $\mathcal{O}(\alpha^3)$. Ref. [37] describes a new calculation of the (non-singlet) contributions up to $\mathcal{O}(\alpha^5)$ and of the small-x terms $[\alpha \ln^2(x)]^N$ to all orders (for previous calculations see papers cited in Ref. [37]).

RADIATIVE CORRECTIONS TO $2 \to 3, 4, \ldots$ PROCESSES

W-pair production and four-fermion final states

The theoretical treatment and the presently gained level in accuracy in the description of W-pair-mediated $4f$ production were triggered by LEP2, as it is reviewed in Refs. [36, 38]. The W bosons are treated as resonances in the full $4f$ processes, $e^+e^- \to 4f\,(+\gamma)$. Radiative corrections are split into universal and non-universal corrections. The former comprise leading-logarithmic corrections from ISR, higher-order corrections included by using appropriate effective couplings, and the Coulomb singularity. These corrections can be combined with the full lowest-order matrix elements easily. The remaining corrections are called non-universal, since they depend on the process under investigation. For LEP2 accuracy, it was sufficient to include these corrections by the leading term of an expansion about the two W poles, defining the so-called double-pole approximation (DPA). Different versions of such a DPA have been used in the literature [39, 40, 41]. Although several Monte Carlo programs exist that include universal corrections, only two event generators, YFSWW [40] and RACOONWW [41, 42], include non-universal corrections.

In the DPA approach, the W-pair cross section can be predicted within $\sim 0.5\%(0.7\%)$ in the energy range between $180\,\mathrm{GeV}$ ($170\,\mathrm{GeV}$) and $\sim 500\,\mathrm{GeV}$, which was sufficient for the LEP2 accuracy of $\sim 1\%$ for energies $170{-}209\,\mathrm{GeV}$. At threshold ($\sqrt{s} \lesssim 170\,\mathrm{GeV}$), the present state-of-the-art prediction results from an improved Born approximation based on leading universal corrections only, because the DPA is not reliable there, and thus possesses an intrinsic uncertainty of about 2%. In Figure 2 this uncertainty is compared with the sensitivity of the W-pair production cross section to the W-boson mass and some assumed experimental data points of a threshold scan. The figure demonstrates the necessary theoretical improvements. At energies beyond $500\,\mathrm{GeV}$ effects beyond $\mathcal{O}(\alpha)$, such as the above-mentioned Sudakov logarithms at higher orders, become important and have to be included in predictions at per-cent accuracy.

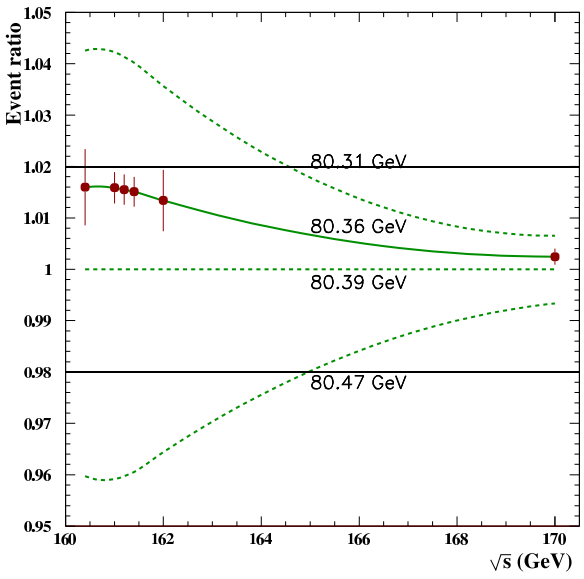

Figure 2: Sensitivity of the W-pair production cross section to the W-boson mass and some assumed experimental data points, compared with the theoretical uncertainty of $\sim 2\%$ (taken from Ref. [1])

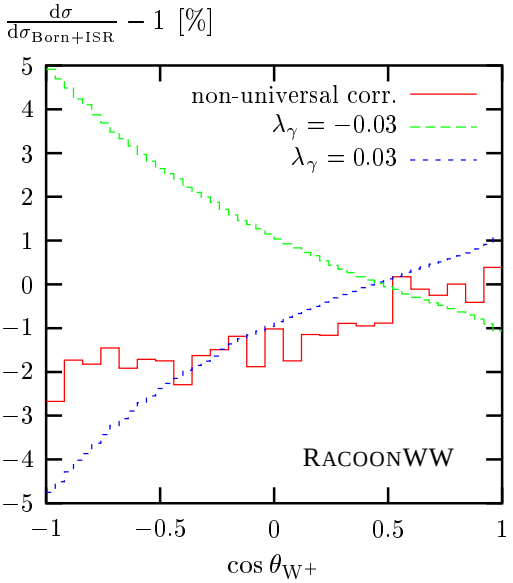

Figure 3: Influence of the anomalous triple gauge-boson coupling λ_γ and of non-universal corrections in the W^+-production-angle distribution at $\sqrt{s} = 200\,\mathrm{GeV}$ for the process $e^+e^- \to u\bar{d}\mu^-\bar{\nu}_\mu$ (taken from Ref. [45])

At LEP2, the W-boson mass is determined by the reconstruction of the W bosons from their decay products with a final accuracy of about $30\,\mathrm{MeV}$. In Ref. [43] the theoretical uncertainty is estimated to be of the order of $\sim 5\,\mathrm{MeV}$, which is comparable to the estimated [44] accuracy of $\sim 10\,\mathrm{MeV}$ at a future LC. Theoretical improvements are, thus, desirable.

The main sensitivity of all observables to anomalous couplings in the triple-gauge-boson vertices is provided by the W-pair production angle distribution. Figure 3 shows the impact of an anomalous coupling $\lambda_\gamma = \pm 0.03$, the size of which is of the order of the LEP2 sensitivity, together with the impact of non-universal corrections on the spectrum. The theoretical uncertainty in constraining the parameter combination $\lambda = \lambda_\gamma = \lambda_\mathrm{Z}$ was estimated to be about 0.005 [46] for the LEP2 analysis. Since a future LC is more sensitive to anomalous couplings than LEP2 by more than an order of magnitude, a further reduction of the uncertainties by missing radiative corrections is necessary. However, a thorough estimate of the theoretical uncertainty in the determination of anomalous couplings at higher scattering energies ($\sqrt{s} \gtrsim 500\,\mathrm{GeV}$), where the experimental sensitivity to non-standard couplings increases, is not yet available.

The above discussion illustrates the necessity of a full one-loop calculation for the $\mathrm{e^+e^-} \to 4f$ process and of further improvements by leading higher-order corrections.

Single-W production

The single-W production process $\mathrm{e^+e^-} \to \mathrm{e}\nu_\mathrm{e}\mathrm{W} \to \mathrm{e}\nu_\mathrm{e} + 2f$ plays a particularly important role among the $4f$ production processes at high scattering energies. The process is predominantly initiated by $\mathrm{e}\gamma^*$ collision (see Figure 4) where the photon is radiated off the electron (or positron) by the Weizsäcker–Williams mechanism, i.e. with a very small off-shellness q_γ^2. Consequently the cross section rises logarithmically with the scattering energy and is of the same size as the W-pair production cross section at about $\sqrt{s} = 500\,\mathrm{GeV}$; for higher energies single-W dominates over W-pair production.

Theoretically the dominance of photon exchange at low q_γ^2 poses several complications. Technically, $q_\gamma^2 \to 0$ means that the electrons (or positrons) are produced in the forward direction and that the electron mass has to be taken into account in order to describe the cross section there. Moreover, the mere application of s-dependent leading-logarithmic structure functions does not describe the leading photon-radiation effects properly, since ISR and final-state radiation (FSR) show sizeable interferences for forward scattering. Thus, the improvement of lowest-order calculations by leading radiation effects is more complicated than for s-channel-like processes. Finally, the running of the electromagnetic coupling $\alpha(q_\gamma^2)$ has to be evaluated in the region of small momentum transfer ($q_\gamma^2 < 0$) where the fit [47] of this quantity to the hadronic vacuum polarisation should be used.

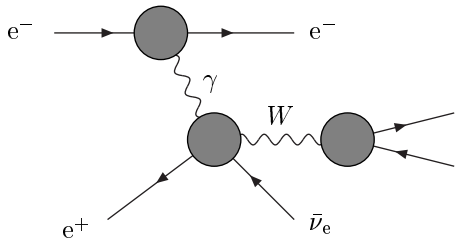

Figure 4: Generic diagram for the dominant contributions to single-W production, $\mathrm{e^+e^-} \to \mathrm{e^-}\nu_\mathrm{e}\mathrm{W} \to \mathrm{e^-}\nu_\mathrm{e} + 2f$

The Monte Carlo generator KORALW [48] has recently been updated to include the ISR-FSR interference effects as well as the proper running of $\alpha(q_\gamma^2)$. Therefore, this program now has reached a level of accuracy similar to the other state-of-the-art programs for single-W production: GRC4F [49], NEXTCALIBUR [50], SWAP [51], WPHACT [52], and WTO [53]. More detailed descriptions of these codes can be found in Ref. [38]. It should be kept in mind that none of these calculations includes non-universal electroweak corrections, leading to a theoretical uncertainty of about $\sim 5\%$ in cross-section predictions. Although the final solution for a high-energy LC certainly requires a full $\mathcal{O}(\alpha)$ calculation of the $4f$-production process, a first step of improvement could be done by a careful expansion about the propagator poles of the photon and W boson. The electroweak $\mathcal{O}(\alpha)$ corrections to the process $\mathrm{e}\gamma \to \nu_\mathrm{e}\mathrm{W}$, which are known [54], represent a basic building block in this calculation.

Technical progress on radiative corrections to multi-particle production processes

One-loop integrals become more and more cumbersome if the number N of external legs in diagrams increases. For $N > 4$, however, not all external momenta are linearly independent because of the four-dimensionality of space-time. As known for a long time [55], this fact opens the possibility to relate integrals with $N > 4$ to integrals with $N \leq 4$. In recent years, various techniques for actual evaluations of one-loop integrals with $N = 5, 6$ have been worked out [56, 57] (see also references therein for older methods and results). The major complication in the treatment of $2 \to 3$ processes at one loop concerns the numerical evaluation of tensor 5-point integrals; in particular, the occurrence of inverse Gram determinants in the usual Passarino–Veltman reduction to scalar integrals leads to numerical instabilities at the phase-space boundary. A possible solution to this problem was worked out in Ref. [57] where the known direct reduction [55] of scalar 5-point to 4-point integrals was generalized to tensor integrals, thereby avoiding the occurrence of leading Gram determinants completely.

In the evaluation of real corrections, such as bremsstrahlung, a proper and numerically stable separation of infrared (soft and collinear) divergences represents one of

the main problems. In the phase-space slicing approach (see Ref. [58] and references therein) already mentioned above, the singular regions are excluded from the "regular" phase-space integration by small cuts on energies, angles, or invariant masses. Using factorization properties, the integration over the singular regions can be done in the limit of infinitesimally small cut parameters. The necessary fine-tuning of cut parameters is avoided in so-called subtraction methods (see Refs. [59, 60, 61] and references therein), where a specially tuned auxiliary function is subtracted from the singular integrand in such a way that the resulting integral is regular. The auxiliary function has to be chosen simple enough, so that the singular regions can be integrated over analytically. In Ref. [59] the so-called "dipole subtraction approach" has been worked out for massless QCD. The technique admits a convenient construction of such auxiliary functions for arbitrary one-parton emission processes, without the need of any further complicated analytical integrations. The dipole subtraction formalism was subsequently worked out for photon emission off massive fermions in Ref. [60] and for QCD with massive quarks in Ref. [61].

Results on $2 \to 3$ processes at one-loop order – $\mathrm{e^+e^-} \to \nu\bar{\nu}\mathrm{H}, \mathrm{t\bar{t}H}$

Recently some one-loop calculations of electroweak radiative corrections have been presented for $2 \to 3$ processes that are interesting at a future LC: $\mathrm{e^+e^-} \to \nu\bar{\nu}\mathrm{H}$ [63, 64] and $\mathrm{e^+e^-} \to \mathrm{t\bar{t}H}$ [65, 66, 67]. The results of Refs. [63, 66] were obtained with the GRACE-LOOP [68] system (see below). In Refs. [64, 65, 67] the technique [57] for treating tensor 5-point integrals was employed. While Refs. [63, 65, 66] make use of the slicing approach for treating soft-photon emission, the results of Refs. [64, 67] have been obtained by dipole subtraction and checked by phase-space slicing for soft and collinear bremsstrahlung.

In $\mathrm{e^+e^-}$ annihilation there are two main production mechanisms for the SM Higgs boson. In the Higgs-strahlung process, $\mathrm{e^+e^-} \to \mathrm{ZH}$, a virtual Z boson decays into a Z boson and a Higgs boson. The corresponding cross section rises sharply at threshold ($\sqrt{s} \gtrsim M_\mathrm{Z} + M_\mathrm{H}$) to a maximum at a few tens of GeV above $M_\mathrm{Z} + M_\mathrm{H}$ and then falls off as s^{-1}, where $\sqrt{s}$ is the CM energy of the $\mathrm{e^+e^-}$ system. In the W-boson-fusion process, $\mathrm{e^+e^-} \to \nu_\mathrm{e}\bar{\nu}_\mathrm{e}\mathrm{H}$, the incoming $\mathrm{e^+}$ and $\mathrm{e^-}$ each emit a virtual W boson which fuse into a Higgs boson. The cross section of the W-boson-fusion process grows as $\ln s$ and thus is the dominant production mechanism for $\sqrt{s} \gg M_\mathrm{H}$. At the one-loop level, first the contributions of fermion and sfermion loops in the Minimal Supersymmetric Standard Model (MSSM) have been evaluated in Ref. [62]. A complete calculation of the $\mathcal{O}(\alpha)$ electroweak corrections to $\mathrm{e^+e^-} \to \nu\bar{\nu}\mathrm{H}$ in the SM has subsequently been performed in Refs. [63, 64].[3] Some results of Refs. [63, 64] are compared in Table 1. The agreement of the correction is within 0.2% or better w.r.t. the lowest-order cross sections.

[3] Analytical results for the one-loop corrections have been obtained in Ref. [69] as MAPLE output, but a numerical evaluation of these results is not yet available.

Table 1: Comparison of lowest-order cross sections for $\mathrm{e^+e^-} \to \nu\bar{\nu}\mathrm{H}$, ($\sigma_\mathrm{tree}$), of one-loop-corrected cross section (σ), and of relative corrections ($\delta = \sigma/\sigma_\mathrm{tree} - 1$) between Refs. [63, 64] at $\sqrt{s} = 500\,\mathrm{GeV}$ (input parameters of Ref. [63])

$M_\mathrm{H}[\mathrm{GeV}]$	$\sigma_\mathrm{tree}[\mathrm{fb}]$	$\sigma[\mathrm{fb}]$	$\delta[\%]$	Ref.
150	61.074(7)	60.99(7)	-0.2	[63]
	61.076(5)	60.80(2)	$-0.44(3)$	[64]
200	37.294(4)	37.16(4)	-0.4	[63]
	37.293(3)	37.09(2)	$-0.56(4)$	[64]
250	21.135(2)	20.63(2)	-2.5	[63]
	21.134(1)	20.60(1)	$-2.53(3)$	[64]
300	10.758(1)	10.30(1)	-4.2	[63]
	10.7552(7)	10.282(4)	$-4.40(3)$	[64]

Table 2: Comparison of lowest-order cross sections for $\mathrm{e^+e^-} \to \mathrm{t\bar{t}H}$, ($\sigma_\mathrm{tree}$), of one-loop-corrected cross section (σ), and of relative corrections ($\delta = \sigma/\sigma_\mathrm{tree} - 1$) between Refs. [66, 67] for $M_\mathrm{H} = 120\,\mathrm{GeV}$ (input parameters of Ref. [66], results taken from Ref. [67])

$\sqrt{s}[\mathrm{GeV}]$	$\sigma_\mathrm{tree}[\mathrm{fb}]$	$\sigma[\mathrm{fb}]$	$\delta[\%]$	Ref.
600	1.7293(3)	1.738(2)	0.5	[66]
	1.7292(2)	1.7368(6)	0.44(3)	[67]
800	2.2724(5)	2.362(4)	3.9	[66]
	2.2723(3)	2.3599(6)	3.86(2)	[67]
1000	1.9273(5)	2.027(4)	5.2	[66]
	1.9271(3)	2.0252(5)	5.09(2)	[67]

The Yukawa coupling of the top quark could be measured at a future LC with high energy and luminosity at the level of $\sim 5\%$ [1] by analyzing the process $\mathrm{e^+e^-} \to \mathrm{t\bar{t}H}$. A thorough prediction for this process, thus, has to control QCD and electroweak corrections. Table 2 summarizes some results on the electroweak $\mathcal{O}(\alpha)$ corrections of Refs. [66, 67]. The agreement within $\sim 0.1\%$ also holds for other energies and Higgs-boson masses. The results of the previous calculation [65] roughly agree with the ones of Refs. [66, 67] at intermediate values of $\sqrt{s}$ and M_H, but are at variance at high energies (TeV range) and close to threshold (large M_H).

EVENT GENERATORS FOR MULTI-PARTICLE FINAL STATES

Multi-purpose generators at parton level

The large variety of different final states for multi-particle production renders multi-purpose Monte Carlo event generators rather important, i.e. generators that deliver an event generator for a user-specified (as much as possible) general final state based on full lowest-order amplitudes. As results, these tools yield lowest-order predictions for observables, or more generally Monte Carlos samples of events, that are improved by universal radiative corrections, such as initial-state radiation at the leading-logarithmic level or beamstrahlung effects. Most of the multi-purpose generators are also interfaced to parton-shower and hadronization programs. The generality renders these programs, however, rather complex devices and, at present, they are far from representing tools for high-precision physics, because non-universal radiative corrections are not taken into account in predictions.

The following multi-purpose generators for multi-parton production, including program packages for the matrix-element evaluation, are available:

- AMEGIC [70]: Helicity amplitudes are automatically generated by the program for the SM, the MSSM, and some new-physics models. Various interfaces (ISR, PDFs, beam spectra, ISAJET, etc.) are supported. The phase-space generation was successfully tested for up to six particles in the final state.

- GRACE [71]: The amplitudes are delivered by a built-in package, which can also handle SUSY processes. The phase-space integration is done by BASES [72]. Tree-level calculations have been performed for up to (selected) six-fermion final states. The extension of the system to include one-loop corrections, the GRACE-LOOP [68] program, is under construction.

- MADEVENT [73] + MADGRAPH [74]: The MADGRAPH algorithm can generate tree-level matrix elements for any SM process (fully supporting particle masses), but a practical limitation is 9,999 diagrams. In addition, MADGRAPH creates MADEVENT, an event generator for the requested process.

- PHEGAS [75] + HELAC [76]: The HELAC program delivers amplitudes for all SM processes (including all masses). The phase-space integration done by PHEGAS has been tested for selected final states with up to seven particles.

- WHIZARD [77] + COMPHEP [78] / MADGRAPH [74] / O'MEGA [79]: Matrix elements are generated by an automatic interface to (older versions of) COMPHEP, MADGRAPH, and (the up-to-date version of) O'MEGA. Phase-space generation has been tested for most $2 \to 6$ and some $2 \to 8$ processes; unweighed events are supported, and a large variety of interfaces (ISR, beamstrahlung, PYTHIA, PDFs, etc.) exists. The inclusion of MSSM amplitudes (O'MEGA) and improved phase-space generation ($2 \to 6$) are work in progress.

All but the GRACE program make use of the multi-channel approach for the phase-space integration. More details can be found in the original references.

Tuned comparisons of different generators, both at parton and detector level, are extremely important, but become more and more laborious owing to the large variety of multi-particle final states. Some progress to a facilitation and automization of comparisons are made by MC-tester project [80] and Java interfaces [81].

Event generators and results for $\mathrm{e^+e^-} \to 6f$

Particular progress was reached in recent years in the description of six-fermion production processes. Apart from the multi-purpose generators listed in the previous section, also dedicated Monte Carlo programs and generators have been developed for this class of processes:

- SIXFAP [82]: Matrix elements are provided for all $6f$ final states (with finite fermion masses), including all electroweak diagrams. The generalization to QCD diagrams and the extension of the phase-space integration for all final states is in progress.

- EETT6F [83]: Only processes relevant for $\mathrm{t\bar{t}}$ production are supported (a new version includes $\mathrm{e^\pm}$ in the final state and QCD diagrams); finite fermion masses are possible.

- LUSIFER [84]: All $6f$ final states are possible, including QCD diagrams with up to four quarks; representative results for all these final states have been presented. External fermions are massless. An unweighting algorithm and an interface to PYTHIA are available.

Table 3 summarizes a brief comparison of results for some processes $\mathrm{e^+e^-} \to 6f$ relevant for $\mathrm{t\bar{t}}$ production for massless external fermions. The results reveal good agreement between the various programs, where minor differences are presumably due to the different treatments of the bottom-quark Yukawa coupling, which is neglected in some cases.

A tuned comparison of results obtained with LUSIFER and WHIZARD for a large survey of $6f$ final states has been presented in Ref. [84].

"True" Monte Carlo event generators

The event generators described above work at parton level (partially improved by parton showers), i.e. the final-state particles cannot be directly identified with particles in a detector. For detector simulations, these parton-level generators have to be interfaced with parton shower and hadronization programs. To facilitate this interface, the

Table 3: Comparison of lowest-order predictions for some processes $e^+e^- \to t\bar{t} \to 6$ fermions at $\sqrt{s} = 500\,\mathrm{GeV}$ in approximation of massless fermions (input parameters and cuts of Ref. [84])

$\sigma_{\mathrm{full}}[\mathrm{fb}]$	AMEGIC++	EETT6F	LUSIFER	PHEGAS	SIXFAP	WHIZARD
$\nu_e e^+ e^- \bar{\nu}_e b\bar{b}$	5.879(8)	5.862(6)	5.853(7)	5.866(9)	5.854(3)	5.875(3)
$\nu_e e^+ \mu^- \bar{\nu}_\mu b\bar{b}$	5.827(4)	5.815(5)	5.819(5)	5.822(7)	5.815(2)	5.827(3)
$\nu_\mu \mu^+ \mu^- \bar{\nu}_\mu b\bar{b}$	5.809(5)	5.807(3)	5.809(5)	5.809(5)	5.804(2)	5.810(3)
$\nu_\mu \mu^+ \tau^- \bar{\nu}_\tau b\bar{b}$	5.800(3)	5.797(5)	5.800(4)	5.798(4)	5.798(2)	5.796(3)
$\nu_\mu \mu^+ d\bar{u} b\bar{b}$	17.209(9)	17.213(23)	17.171(24)	17.204(18)		
without QCD:	17.097(8)	17.106(15)	17.095(11)	17.107(18)	17.096(4)	17.103(8)

"Les Houches accord" [85] has been designed, a set of FORTRAN common blocks for the transfer of event configurations from parton level generators to showering and hadronization event generators. Alternatively so-called "true" event generators could be used, which fully include hadronization. The following well-known "true" MC generators represent general-purpose tools for investigating not only e^+e^- collisions, but also lepton–hadron and hadron–hadron scattering: HERWIG [86], ISAJET [87], and PYTHIA [88]. The programs are supported and extended continuously; recent upgrades and new features relevant for LC physics are:

- implementation of all $2 \to 2$ scattering processes of the MSSM in lowest order;
- associated Higgs production ($Q\bar{Q}^{(\prime)}H$) in the SM and MSSM in lowest order (the case of charged Higgs bosons is not yet available in ISAJET and PYTHIA);
- R-parity-violation SUSY in HERWIG;
- MSSM with complex parameters (cMSSM) in PYTHIA;
- inclusion of spin correlations and matrix elements for 3- and 4-body decays in HERWIG;
- introduction of real corrections based on matrix elements for several e^+e^- processes in HERWIG and PYTHIA (see e.g. Ref. [89]).

Among other work in progress, the implementation of NLO QCD corrections in "true" generators is one of the most pressing issues. In particular, the matching of parton showers with matrix-element calculations at NLO has to be performed carefully; first results look very promising [90].

Finally, it should be mentioned that the present FORTRAN versions of HERWIG and PYTHIA will be replaced by C++ programs in the future [91].

RADIATIVE CORRECTIONS IN SUPERSYMMETRIC THEORIES

In order to avoid too much overlap with the reports of the Higgs and SUSY groups, this section is mainly restricted to the topics that have been presented in the Loopverein working group. More details and references on the subject can be found in Ref. [5].

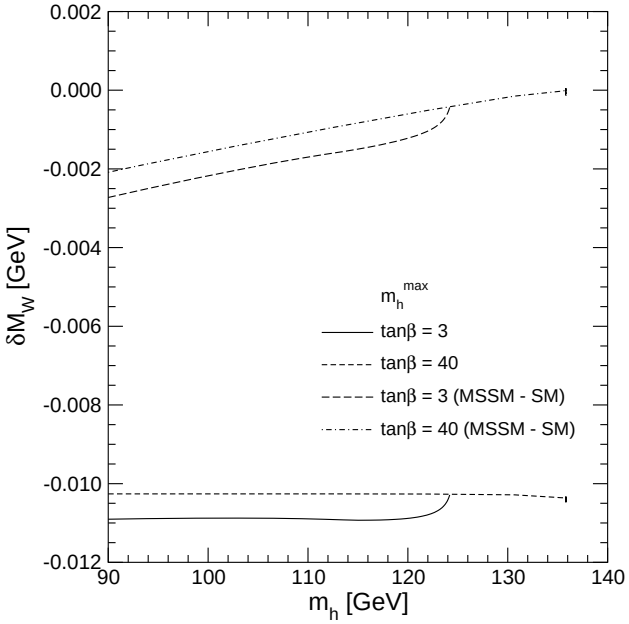

Figure 5: Effect of the SUSY $\mathcal{O}(\alpha_t^2)$ corrections on the prediction of M_W in the MSSM (taken from Ref. [93])

SUSY corrections to precision observables

The confrontation of high-precision data with theoretical predictions is, of course, also very interesting in extensions of the SM. The one-loop corrections of the MSSM to muon decay and to the pseudo-observables of the Z resonance have been known for many years, but not many corrections beyond one loop exist. Recently the known universal corrections of $\mathcal{O}(\alpha\alpha_s)$ [92] to the ρ-parameter have been supplemented by the terms of $\mathcal{O}(\alpha_t^2)$, $\mathcal{O}(\alpha_t\alpha_b)$ and $\mathcal{O}(\alpha_b^2)$ in Ref. [93], where $\alpha_{t/b} = h_{t/b}^2/(4\pi)$ with $h_{t/b}$ denoting the top/bottom Yukawa coupling. Figure 5 illustrates the effect of the $\mathcal{O}(\alpha_t^2)$ corrections on the prediction of the W-boson mass in the MSSM. The genuine MSSM $\mathcal{O}(\alpha_t^2)$ effects modify M_W at the level of $2-3\,\mathrm{MeV}$.

Mass spectra in the MSSM

In theories with unbroken supersymmetry the fermions and bosons within the same multiplet have a common mass. In realistic theories, such as the MSSM, SUSY is broken, and this statement is not valid anymore. However, the masses of fermions or bosons within multiplets are not all independent, i.e. there are non-trivial relations among mass parameters. Since the mass spectra of SUSY theories bear a lot of information on the mechanism of SUSY breaking, precision analyses of these spectra can serve as a window to grand unification.

SUSY demands (at least) two Higgs doublets to give the up- and down-type fermions masses. Thus, the MSSM predicts the existence of two charged ($\mathrm{H}^\pm$), two neutral scalar ($\mathrm{h}^0, \mathrm{H}^0$), and one neutral pseudo-scalar (A^0) Higgs bosons. In lowest order, the Higgs masses $M_{\mathrm{H}^\pm}$, M_h, and M_H can be calculated as functions of the A^0-boson mass M_A, the ratio of Higgs-field vacuum expectation values, $\tan\beta = v_2/v_1$, and the gauge-boson masses; in particular, the mass M_h of the lightest Higgs boson is constrained to be smaller than M_Z at tree level. Beyond lowest order, also the remaining MSSM parameters are involved in the mass relations, and M_h can reach values up to about $135\,\mathrm{GeV}$. The status of precision calculations of the neutral Higgs-boson masses has been recently reviewed in Ref. [94]. All available corrections[4] are implemented in the program FEYNHIGGS [96]. The predictions are based on full one-loop calculations and on the leading effects in two-loop order, i.e. the corrections of the order $\mathcal{O}(\alpha_\mathrm{s}\alpha_\mathrm{t})$, $\mathcal{O}(\alpha_\mathrm{t}^2)$ and $\mathcal{O}(\alpha_\mathrm{s}\alpha_\mathrm{b})$ (see Ref. [94] and references therein). Recently the corrections of $\mathcal{O}(\alpha_\mathrm{t}\alpha_\mathrm{b})$ and $\mathcal{O}(\alpha_\mathrm{b}^2)$ have become available [97]. The current theoretical uncertainty in the Higgs-mass predictions is about $3\,\mathrm{GeV}$ [94], but a further reduction to $\lesssim 0.5\,\mathrm{GeV}$ should be reached to match the accuracy needed for a LC. In this context a proper definition of $\tan\beta$ in higher perturbative orders is crucial, since different renormalization schemes (see, e.g., Ref. [98]) for $\tan\beta$ lead to rather different relations between $\tan\beta$ and physical observables such as the Higgs-boson masses.

In the sector of charginos and neutralinos of the MSSM only three out of the six mass parameters are independent. In Refs. [99, 100] the three masses $m_{\tilde{\chi}^0_{2,3,4}}$ of the heavier neutralinos have been expressed in terms of the mass $m_{\tilde{\chi}^0_1}$ of the lightest neutralino and of the masses $m_{\tilde{\chi}^+_{1,2}}$ of the two charginos, including the complete one-loop corrections, which depend also on the other MSSM parameters. The corrections modify the calculated masses by up to several GeV. The on-shell renormalization in the chargino-neutralino sector is described in Refs. [99, 100, 101] in detail.

The relations among sfermion masses, together with the corresponding on-shell renormalization, are worked out in Refs. [101, 102]. For each generation, one of the four squark masses and one of the three slepton masses can be calculated from the other sfermion masses (and the other MSSM parameters entering at one loop). The one-loop corrections can amount to about 5%.

Higgs-boson and SUSY-particle decays in the MSSM

Analyses of particle decays are of great importance for the reconstruction of coupling structures and, thus, of interaction Lagrangians. The rich particle content of SUSY theories leads to a large variety of decay cascades, which depend in detail on the chosen scenario. A discussion of phenomenological implications and of radiative corrections to SUSY-particle decays can be found in Ref. [5] and Ref. [103], respectively.

The decay widths of Higgs bosons in the MSSM received much attention in recent years, so that the predictions are well elaborate. Precise predictions can be obtained with the programs FEYNHIGGSDECAY (based on Ref. [104]) and HDECAY [105]. Recently the electroweak $\mathcal{O}(\alpha)$ corrections to the decay of the CP-odd A^0 boson into sfermion pairs have been calculated in Ref. [106]. For the Higgs decay $\phi \to \mathrm{b\bar{b}}$ ($\phi = \mathrm{h}^0, \mathrm{H}^0, \mathrm{A}^0$), which is of particular importance for light Higgs bosons, the resummation of the leading SUSY-QCD effects and the related theoretical uncertainty have been discussed in Ref. [107] (for previous work on $\phi \to \mathrm{b\bar{b}}$ see references therein).

Apart from considering integrated decay rates, it is interesting to inspect distributions of decay products, which is important for the determination of the spin and parity of the decaying particle. This task requires the development of appropriate Monte Carlo tools. For the $\phi \to \tau^+\tau^-$ decay, for instance, the TAUOLA program was extended to include τ-spin correlations in Ref. [108].

SUSY-particle production

The direct production of SUSY particles, if they exist, is among the most interesting issues at future colliders. In order to determine the properties (mass, spin, decay widths, couplings) of these new particles, precise measurements and predictions of the corresponding cross sections at the same level of accuracy are necessary, i.e. radiative corrections have to be taken into account.

The electroweak radiative corrections to the production of sfermions, $\mathrm{e^+e^-} \to \tilde{f}\bar{\tilde{f}}$, and charginos, $\mathrm{e^+e^-} \to \tilde{\chi}^+\tilde{\chi}^-$, were worked out in Refs. [109] and [110], respectively. Since in these calculations the sfermions and charginos are assumed to be stable, the results are relevant for energies a few decay widths above the production threshold. For a threshold scan the decay of the sfermions as well as non-resonant coherent background effects have to be included; in Ref. [111] off-shell effects in sfermion-pair production have been investigated at tree level (improved

[4] It should be mentioned that the full effective potential has been presented in Ref. [95] at the two-loop level. However, the precise relation of these results with the parameters defined in the on-shell renormalization scheme used in MSSM parameter analyses has not been worked out so far.

by universal Coulomb-like corrections). Theoretically the whole issue is very similar to a description of the process $e^+e^- \to WW \to 4f$ which is discussed above.

The SUSY multiplet structure, in particular, predicts that the strengths of the gauge-boson–fermion and gauge-boson–sfermion interactions, which are equal owing to the gauge principle, coincide with the gaugino–sfermion–fermion Yukawa coupling. In order to test this relation in SUSY QCD the processes $e^+e^- \to q\bar{q}g, \tilde{q}\bar{\tilde{q}}g, \tilde{q}\bar{q}\tilde{g}, q\bar{\tilde{q}}\tilde{g}$ should be studied. In Ref. [112] the QCD and SUSY-QCD corrections to these processes were calculated.

More details on radiative corrections to SUSY particle production and decays can be found in Ref. [103] (and references therein).

Renormalization of the MSSM beyond one loop

Beyond one loop the calculation of radiative corrections within SUSY theories is highly non-trivial, because there is no regularization scheme that respects gauge invariance and supersymmetry at the same time. For instance, conventional dimensional regularization breaks supersymmetry, while dimensional reduction, which respects supersymmetry, is known to be not fully consistent. In this situation, a mathematically convincing way to perform renormalization is provided by *algebraic renormalization*. In this framework the symmetry identities and a proof of renormalizability for the MSSM have been established in Ref. [113]. These results can serve as a basis for the construction of all symmetry-restoring counterterms in the MSSM.

OTHER DEVELOPMENTS

Automization of loop calculations and maintenance of computer codes

Once the necessary techniques and theoretical subtleties of a perturbative calculation are settled, to carry out the actual calculation is an algorithmic matter. Thus, an automization of such calculations is highly desirable, in order to facilitate related calculations. Various program packages have been presented in the literature for automatized tree-level, one-loop, and multi-loop calculations. A comprehensive overview was, for instance, given in Ref. [114]; in the following we have to restrict ourselves to a selection of topics, where the emphasis is put on recent developments.

The generation of Feynman graphs and amplitudes is a combinatorial problem that can be attacked with computer algebra. The program packages FEYNARTS [7] (which has been extended [115] for the MSSM), QGRAF [14], DIANA [11] (based on QGRAF) are specifically designed for this task; also the GRACE-LOOP [68] system automatically generates Feynman diagrams and loop amplitudes. Moreover, the task of calculating virtual one-loop and the corresponding real-emission corrections to $2 \to 2$ scattering reactions is by now well understood. Such calculations are widely automated in the packages FORMCALC, combined with LOOPTOOLS [116], and GRACE-LOOP [68].

As an illustrating example, Table 4 provides some results on the differential cross section for $e^+e^- \to t\bar{t}$ in lowest order as well as including electroweak $\mathcal{O}(\alpha)$ corrections. The program FA+FC was obtained from the output of the FEYNARTS and FORMCALC packages and makes use of the LOOPTOOLS library for the numerical evaluation. The TOPFIT program [117, 118] was developed from an algebraic reduction of Feynman graphs (delivered from DIANA) within FORM; for the numerics LOOPTOOLS is partially employed. More detailed comparisons between FA+FC and TOPFIT, including also other fermion flavours, can be found in Refs. [117, 119]. The GRACE-LOOP result is completely independent of the two others. The agreement between these results reflects the enormous progress achieved in recent years in the automization of one-loop calculations.

The GRACE-LOOP system has recently been used in the calculation of the electroweak corrections to the $2 \to 3$ processes $e^+e^- \to \nu\bar{\nu}H, t\bar{t}H$ [63, 66], which are discussed above.

Clearly the calculation of radiative corrections is a very laborious task, leading to rather complex and lengthy computer codes, which should be carefully documented. The SANC project [120] (former CALCPHEP [121]) aims at providing theoretical support of this kind for future accelerator experiments, using the principle of knowledge storing. This approach is rather different from the strategy of automization described above, which aims at generating completely new programs. The SANC program contains another independent calculation of the $\mathcal{O}(\alpha)$ corrections to $e^+e^- \to t\bar{t}$, the results of which are also included in Table 4.

Numerical approaches to loop calculations

Most of the various techniques of performing loop calculations share the common feature that the integration over the loop momenta is performed analytically. This procedure leads to complications at one loop if five or more external legs are involved, since both speed and stability of programs become more and more jeopardized. At the two-loop level, already the evaluation of self-energy and vertex corrections can lead to extremely complicated higher transcendental functions that are hard to evaluate numerically.

An idea to avoid these complications is provided by a more or less purely numerical evaluation of loop corrections. There are two main difficulties in this approach. Firstly, the appearing ultraviolet and infrared divergences have to be treated and canceled carefully. Secondly, even finite loop integrals require a singularity handling of the integrand near so-called particle poles, where Feynman's $i\epsilon$ prescription is used as regularization.

In Ref. [122] a method for a purely numerical evaluation of loop integrals is proposed. Each integral is parametrized with Feynman parameters and subsequently rewritten with

Table 4: Differential cross sections for $e^+e^- \to t\bar{t}$ for selected scattering angles at $\sqrt{s} = 500\,\mathrm{GeV}$; input parameters are defined in Ref. [117], the soft-photon cut parameter $\omega/\sqrt{s}$ is set to 10^{-5}.

$\cos\theta$	program	$\left(\frac{d\sigma}{d\cos\theta}\right)_{\mathrm{Born}}$ [pb]	$\left(\frac{d\sigma}{d\cos\theta}\right)_{\mathrm{Born+virt+soft}}$ [pb]	$\left(\frac{d\sigma}{d\cos\theta}\right)_{\mathrm{Born+virt+real}}$ [pb]
-0.9	FA + FC	0.108839194076039	-0.00205485893415	
	GRACE-LOOP	0.108839194076	-0.002054859	0.13206(12)
	SANC	0.10883919407522	-0.00205485893360	
	TOPFIT	0.108839194076039	-0.00205485893466	0.13229
0.0	FA+FC	0.225470464033559	-0.04321416793299	
	GRACE-LOOP	0.225470464033	-0.043214168	0.23513(14)
	SANC	0.22547046403258	-0.04321416793300	
	TOPFIT	0.225470464033559	-0.04321416793192	0.23476
$+0.9$	FA+FC	0.491143715767761	-0.16747885864057	
	GRACE-LOOP	0.491143715767	-0.16747886	0.47709(21)
	SANC	0.49114371576694	-0.16747885864510	
	TOPFIT	0.491143715767761	-0.16747885863793	0.47768

partial integrations. The final expression consists of a quite simple part containing the singular terms and another more complicated looking part that can be integrated numerically. The actual application of the method to a physical process is still work in progress.

Another idea was proposed in Ref. [123] and applied to event-shape variables in $e^+e^- \to 3$ jets in NLO. In this approach virtual and real corrections are added before integration. In their sum, no soft singularities, or more generally singularities that cancel between virtual and real corrections, appear from the beginning. Nevertheless the problem of a stable treatment of particle poles in loop amplitudes still remains. In Ref. [123] a solution via contour deformations in complex integration domains is described, but how this procedure can be generalized is not yet clear.

CONCLUSIONS

In spite of the complexity of higher-order calculations for high-energy elementary particle reactions, there has been continuous progress in the development of new techniques and in making precise predictions for physics at future colliders. However, to be prepared for a future e^+e^- linear collider with high energy and luminosity, such as TESLA, an enormous amount of work is still ahead of us. Full two-loop predictions for $e^+e^- \to 2$ fermion scattering reactions, such as the Bhabha process, or full one-loop calculations for $e^+e^- \to 4$ fermions are more than technical challenges. At this level of accuracy, field-theoretical issues such as renormalization, the treatment of unstable particles, etc., demand a higher level of understanding. Of course, both loop calculations as well as the descriptions of multi-particle production processes with Monte Carlo techniques require and will profit from further improving computing devices.

It is certainly out of question that the list of challenges and interesting issues could be continued at will. The way to a future LC will also be highly exciting in precision physics.

REFERENCES

[1] J. A. Aguilar-Saavedra *et al.*, TESLA Technical Design Report Part III: Physics at an e^+e^- Linear Collider [hep-ph/0106315].

[2] T. Abe *et al.* [American Linear Collider Working Group Collaboration], in *Proc. of the APS/DPF/DPB Summer Study on the Future of Particle Physics (Snowmass 2001)* ed. R. Davidson and C. Quigg, SLAC-R-570, *Resource book for Snowmass 2001* [hep-ex/0106055, hep-ex/0106056, hep-ex/0106057, hep-ex/0106058].

[3] K. Abe *et al.* [ACFA Linear Collider Working Group Collaboration], ACFA Linear Collider Working Group report, [hep-ph/0109166].

[4] U. Baur *et al.*, in *Proc. of the APS/DPF/DPB Summer Study on the Future of Particle Physics (Snowmass 2001)* ed. N. Graf, hep-ph/0111314 and hep-ph/0202001.

[5] A. Brandenburg, K. Desch, J. Kalinowski, and K. Mönig, these proceedings.

[6] A. Freitas, W. Hollik, W. Walter and G. Weiglein, Phys. Lett. B **495** (2000) 338 [hep-ph/0007091] and Nucl. Phys. B **632** (2002) 189 [hep-ph/0202131].

[7] J. Küblbeck, M. Böhm and A. Denner, Comput. Phys. Commun. **60** (1990) 165;
T. Hahn, Comput. Phys. Commun. **140** (2001) 418 [hep-ph/0012260].

[8] G. Weiglein, R. Scharf and M. Böhm, Nucl. Phys. B **416** (1994) 606 [hep-ph/9310358].

[9] M. Awramik and M. Czakon, Phys. Rev. Lett. **89** (2002) 241801 [hep-ph/0208113] and hep-ph/0305248.

[10] A. Onishchenko and O. Veretin, Phys. Lett. B **551** (2003) 111 [hep-ph/0209010].

[11] M. Tentyukov and J. Fleischer, Comput. Phys. Commun. **132** (2000) 124 [hep-ph/9904258].

[12] M. Awramik, M. Czakon, A. Onishchenko and O. Veretin, hep-ph/0209084, to appear in Phys. Rev. D.

[13] M. Faisst, J. H. Kühn, T. Seidensticker and O. Veretin, hep-ph/0302275.

[14] P. Nogueira, J. Comput. Phys. **105** (1993) 279.

[15] R. Harlander, T. Seidensticker and M. Steinhauser, Phys. Lett. B **426** (1998) 125 [hep-ph/9712228];
T. Seidensticker, hep-ph/9905298.

[16] M. Steinhauser, Comput. Phys. Commun. **134** (2001) 335 [hep-ph/0009029].

[17] G. Weiglein, talk given at the *International Europhysics Conference on High Energy Physics EPS*, Aachen, Germany, 2003.

[18] W. Hollik, in proceedings of the Zeuthen workshop *Electroweak Precision Data and the Higgs Mass*, Zeuthen, 2003, eds. S. Dittmaier and K. Mönig, DESY-PROC-2003-01 and MPP-2003-50.

[19] F.A. Berends *et al.*, in *Z Physics at LEP 1*, eds. G. Altarelli, R. Kleiss and C. Verzegnassi (CERN 89-08, Geneva, 1989), Vol. 1, p. 89;
W. Beenakker, F. A. Berends and S. C. van der Marck, Z. Phys. C **46** (1990) 687;
A. Borrelli, M. Consoli, L. Maiani and R. Sisto, Nucl. Phys. B **333** (1990) 357.

[20] D. Y. Bardin and G. Passarino, hep-ph/9803425;
G. Montagna, O. Nicrosini, F. Piccinini and G. Passarino, Comput. Phys. Commun. **117** (1999) 278 [hep-ph/9804211];
D. Y. Bardin, M. Grünewald and G. Passarino, hep-ph/9902452;
D. Y. Bardin *et al.*, Comput. Phys. Commun. **133** (2001) 229 [hep-ph/9908433].

[21] Contributions of W. Hollik, W. van Neerven, and G. Passarino to the proceedings of the Zeuthen workshop *Electroweak Precision Data and the Higgs Mass*, Zeuthen, 2003, eds. S. Dittmaier and K. Mönig, DESY-PROC-2003-01 and MPP-2003-50.

[22] Z. Bern, L. J. Dixon and A. Ghinculov, Phys. Rev. D **63** (2001) 053007 [hep-ph/0010075];
E. W. Glover, J. B. Tausk and J. J. Van der Bij, Phys. Lett. B **516** (2001) 33 [hep-ph/0106052].

[23] Z. Bern *et al.*, JHEP **0111** (2001) 031 [hep-ph/0109079].

[24] L. W. Garland *et al.*, Nucl. Phys. B **627** (2002) 107 [hep-ph/0112081] and Nucl. Phys. B **642** (2002) 227 [hep-ph/0206067];
S. Moch, P. Uwer and S. Weinzierl, Phys. Rev. D **66** (2002) 114001 [hep-ph/0207043].

[25] T. Gehrmann, Nucl. Phys. Proc. Suppl. **116** (2003) 13 [hep-ph/0210157].

[26] J. Fleischer, T. Riemann, O. V. Tarasov and A. Werthenbach, Nucl. Phys. Proc. Suppl. **116** (2003) 43 [LC-TH-2003-082, hep-ph/0211167].

[27] D. A. Kosower, Phys. Rev. D **67** (2003) 116003 [hep-ph/0212097].

[28] S. Weinzierl, JHEP **0303** (2003) 062 [hep-ph/0302180].

[29] A. Denner, M. Melles and S. Pozzorini, Nucl. Phys. B **662** (2003) 299 [hep-ph/0301241].

[30] M. Ciafaloni, P. Ciafaloni and D. Comelli, Phys. Lett. B **501** (2001) 216 [hep-ph/0007096].

[31] A. Denner and S. Pozzorini, Eur. Phys. J. C **18** (2001) 461 [hep-ph/0010201] and Eur. Phys. J. C **21** (2001) 63 [hep-ph/0104127].

[32] W. Beenakker and A. Werthenbach, Phys. Lett. B **489** (2000) 148 [hep-ph/0005316] and Nucl. Phys. B **630** (2002) 3 [hep-ph/0112030];
M. Melles, Phys. Lett. B **495** (2000) 81 [hep-ph/0006077];
M. Hori, H. Kawamura and J. Kodaira, Phys. Lett. B **491** (2000) 275 [hep-ph/0007329].

[33] V. S. Fadin, L. N. Lipatov, A. D. Martin and M. Melles, Phys. Rev. D **61** (2000) 094002 [hep-ph/9910338];
J. H. Kühn, A. A. Penin and V. A. Smirnov, Eur. Phys. J. C **17** (2000) 97 [hep-ph/9912503];
M. Melles, Phys. Rept. **375** (2003) 219 [hep-ph/0104232] and Eur. Phys. J. C **24** (2002) 193 [hep-ph/0108221];

[34] J. H. Kühn, S. Moch, A. A. Penin and V. A. Smirnov, Nucl. Phys. B **616** (2001) 286 [Erratum-ibid. B **648** (2003) 455] [hep-ph/0106298].

[35] M. Beccaria *et al.*, Phys. Rev. D **64** (2001) 053016 [hep-ph/0104245]; Phys. Rev. D **65** (2002) 093007 [hep-ph/0112273]; LC-TH-2002-005 [hep-ph/0203254]; hep-ph/0212167; LC-TH-2002-017 [hep-ph/0212247]; hep-ph/0304110 and Nucl. Phys. B **663** (2003) 394 [hep-ph/0304175].

[36] W. Beenakker *et al.*, in *Physics at LEP2*, eds. G. Altarelli, T. Sjöstrand and F. Zwirner (CERN 96-01, Geneva, 1996), Vol. 1, p. 79 [hep-ph/9602351].

[37] J. Blümlein and H. Kawamura, Acta Phys. Polon. B **33** (2002) 3719 [hep-ph/0207259].

[38] M. W. Grünewald *et al.*, in *Reports of the Working Groups on Precision Calculations for LEP2 Physics*, eds. S. Jadach, G. Passarino and R. Pittau (CERN 2000-009, Geneva, 2000), p. 1 [hep-ph/0005309].

[39] W. Beenakker, F. A. Berends and A. P. Chapovsky, Nucl. Phys. B **548**, 3 (1999) [hep-ph/9811481];
Y. Kurihara, M. Kuroda and D. Schildknecht, Nucl. Phys. B **565** (2000) 49 [hep-ph/9908486] and Phys. Lett. B **509** (2001) 87 [hep-ph/0104201].

[40] S. Jadach *et al.*, Phys. Rev. D **61** (2000) 113010 [hep-ph/9907436]; Phys. Rev. D **65** (2002) 093010 [hep-ph/0007012]; Comput. Phys. Commun. **140** (2001) 432 [hep-ph/0103163] and Comput. Phys. Commun. **140** (2001) 475 [hep-ph/0104049].

[41] A. Denner, S. Dittmaier, M. Roth and D. Wackeroth, Phys. Lett. B **475** (2000) 127 [hep-ph/9912261]; LC-TH-2000-014 [hep-ph/9912447]; Nucl. Phys. B **587** (2000) 67 [hep-ph/0006307]; hep-ph/0101257 and hep-ph/0209330.

[42] A. Denner, S. Dittmaier, M. Roth and D. Wackeroth, Nucl. Phys. B **560** (1999) 33 [hep-ph/9904472] and Eur. Phys. J. C **20** (2001) 201 [hep-ph/0104057].

[43] S. Jadach *et al.*, Phys. Lett. B **523** (2001) 117 [hep-ph/0109072].

[44] K. Mönig and A. Tonazzo, talk given by K. Mönig at the *2nd ECFA/DESY Study on Physics and Detectors for a Linear Electron–Positron Collider*, Padova, Italy, 2000.

[45] A. Denner, S. Dittmaier, M. Roth and D. Wackeroth, hep-ph/0110402.

[46] R. Brunelière *et al.*, Phys. Lett. B **533** (2002) 75 [hep-ph/0201304].

[47] F. Jegerlehner, LC-TH-2001-035 [hep-ph/0105283].

[48] S. Jadach *et al.*, Comput. Phys. Commun. **119** (1999) 272 [hep-ph/9906277] and Eur. Phys. J. C **27** (2003) 19 [hep-ph/0209268].

[49] J. Fujimoto *et al.*, hep-ph/9603394 and Comput. Phys. Commun. **100** (1997) 128 [hep-ph/9605312].

[50] F. A. Berends, C. G. Papadopoulos and R. Pittau, hep-ph/0002249 and Comput. Phys. Commun. **136** (2001) 148 [hep-ph/0011031].

[51] G. Montagna *el al.*, Eur. Phys. J. C **20** (2001) 217 [hep-ph/0005121].

[52] E. Accomando and A. Ballestrero, Comput. Phys. Commun. **99** (1997) 270 [hep-ph/9607317];
E. Accomando, A. Ballestrero and E. Maina, Phys. Lett. B **479** (2000) 209 [hep-ph/9911489] and Comput. Phys. Commun. **150** (2003) 166 [hep-ph/0204052].

[53] G. Passarino, Comput. Phys. Commun. **97** (1996) 261 [hep-ph/9602302]; hep-ph/9810416 and Nucl. Phys. B **578** (2000) 3 [hep-ph/0001212].

[54] A. Denner and S. Dittmaier, Nucl. Phys. B **398** (1993) 239; M. Böhm and S. Dittmaier, Nucl. Phys. B **409** (1993) 3.

[55] D. B. Melrose, *Nuovo Cimento* **XL A** (1965) 181.

[56] J. Fleischer, F. Jegerlehner and O. V. Tarasov, Nucl. Phys. B **566** (2000) 423 [hep-ph/9907327];
T. Binoth, J. P. Guillet and G. Heinrich, Nucl. Phys. B **572** (2000) 361 [hep-ph/9911342];
F. Tramontano, Phys. Rev. D **67** (2003) 114005 [hep-ph/0211390];
T. Binoth, G. Heinrich and N. Kauer, Nucl. Phys. B **654** (2003) 277 [hep-ph/0210023].

[57] A. Denner and S. Dittmaier, Nucl. Phys. B **658** (2003) 175 [hep-ph/0212259].

[58] B. W. Harris and J. F. Owens, Phys. Rev. D **65** (2002) 094032 [hep-ph/0102128].

[59] S. Catani and M. H. Seymour, Nucl. Phys. B **485** (1997) 291 [Erratum-ibid. B **510** (1997) 291] [hep-ph/9605323].

[60] S. Dittmaier, Nucl. Phys. B **565** (2000) 69 [hep-ph/9904440].

[61] L. Phaf and S. Weinzierl, JHEP **0104**, 006 (2001) [hep-ph/0102207];
S. Catani, S. Dittmaier, M. H. Seymour and Z. Trócsányi, Nucl. Phys. B **627** (2002) 189 [hep-ph/0201036].

[62] H. Eberl, W. Majerotto and V. C. Spanos, Phys. Lett. B **538** (2002) 353 [hep-ph/0204280] and Nucl. Phys. B **657** (2003) 378 [hep-ph/0210038];
T. Hahn, S. Heinemeyer and G. Weiglein, Nucl. Phys. B **652** (2003) 229 [LC-TH-2002-018, hep-ph/0211204] and Nucl. Phys. Proc. Suppl. **116** (2003) 336 [LC-TH-2002-019, hep-ph/0211384].

[63] G. Bélanger *et al.*, Phys. Lett. B **559** (2003) 252 [hep-ph/0212261].

[64] A. Denner, S. Dittmaier, M. Roth and M. M. Weber, Phys. Lett. B **560** (2003) 196 [LC-TH-2003-008, hep-ph/0301189] and Nucl. Phys. B **660** (2003) 289 [LC-TH-2003-007, hep-ph/0302198].

[65] Y. You *et al.*, hep-ph/0306036.

[66] G. Bélanger *et al.*, hep-ph/0307029.

[67] A. Denner, S. Dittmaier, M. Roth and M. M. Weber, LC-TH-2003-069 [hep-ph/0307193], to appear in Phys. Lett. **B**.

[68] J. Fujimoto *el al.*, Acta Phys. Polon. B **28** (1997) 945.

[69] F. Jegerlehner and O. Tarasov, hep-ph/0212004.

[70] F. Krauss, R. Kuhn and G. Soff, JHEP **0202** (2002) 044 [hep-ph/0109036];
A. Schalicke, F. Krauss, R. Kuhn and G. Soff, JHEP **0212** (2002) 013 [hep-ph/0203259].

[71] T. Ishikawa *et al.*, [Minami-Tateya Collaboration], KEK-92-19;
H. Tanaka *et al.*, [Minami-Tateya Collaboration], Nucl. Instrum. Meth. A **389** (1997) 295;
F. Yuasa *et al.*, Prog. Theor. Phys. Suppl. **138** (2000) 18 [hep-ph/0007053].

[72] S. Kawabata, Comput. Phys. Commun. **88** (1995) 309.

[73] F. Maltoni and T. Stelzer, JHEP **0302** (2003) 027 [hep-ph/0208156].

[74] T. Stelzer and W. F. Long, Comput. Phys. Commun. **81** (1994) 357 [hep-ph/9401258];
H. Murayama, I. Watanabe and K. Hagiwara, KEK-91-11.

[75] C. G. Papadopoulos, Comput. Phys. Commun. **137** (2001) 247 [hep-ph/0007335].

[76] A. Kanaki and C. G. Papadopoulos, Comput. Phys. Commun. **132** (2000) 306 [hep-ph/0002082].

[77] W. Kilian, LC-TOOL-2001-039.

[78] A. Pukhov *et al.*, hep-ph/9908288.

[79] M. Moretti, T. Ohl and J. Reuter, LC-TOOL-2001-040, hep-ph/0102195.

[80] P. Golonka, T. Pierzchala and Z. Was, hep-ph/0210252.

[81] M. T. Ronan, LC-TOOL-2003-015 [physics/0306019].

[82] G. Montagna, M. Moretti, O. Nicrosini and F. Piccinini, Eur. Phys. J. C **2** (1998) 483 [hep-ph/9705333];
F. Gangemi *et al.*, Eur. Phys. J. C **9** (1999) 31 [hep-ph/9811437] and Nucl. Phys. B **559** (1999) 3 [hep-ph/9905271];
F. Gangemi, hep-ph/0002142.

[83] K. Kołodziej, Eur. Phys. J. C **23** (2002) 471 [hep-ph/0110063] and Comput. Phys. Commun. **151** (2003) 339 [hep-ph/0210199];
A. Biernacik and K. Kołodziej, Nucl. Phys. Proc. Suppl. **116** (2003) 33 [hep-ph/0210405].

[84] S. Dittmaier and M. Roth, Nucl. Phys. B **642** (2002) 307 [hep-ph/0206070].

[85] E. Boos *et al.*, hep-ph/0109068.

[86] S. Moretti, LC-TOOL-2002-009 [hep-ph/0209209];
G. Corcella *et al.*, hep-ph/0210213.

[87] H. Baer, F. E. Paige, S. D. Protopopescu and X. Tata, hep-ph/0001086.

[88] T. Sjöstrand, L. Lönnblad and S. Mrenna, hep-ph/0108264.

[89] J. Andre, hep-ph/9706325;
J. Andre and T. Sjöstrand, Phys. Rev. D **57** (1998) 5767 [hep-ph/9708390];
S. Moretti, hep-ph/0008197;
G. Corcella, E. K. Irish and M. H. Seymour, hep-ph/0012319.

[90] S. Frixione and B. R. Webber, JHEP **0206** (2002) 029 [hep-ph/0204244];
S. Frixione, P. Nason and B. R. Webber, JHEP **0308** (2003) 007 [hep-ph/0305252].

[91] M. Bertini, L. Lönnblad and T. Sjöstrand, Comput. Phys. Commun. **134** (2001) 365 [hep-ph/0006152];
S. Gieseke, hep-ph/0210294.

[92] A. Djouadi *et al.*, Phys. Rev. Lett. **78** (1997) 3626 [hep-ph/9612363] and Phys. Rev. D **57** (1998) 4179 [hep-ph/9710438].

[93] S. Heinemeyer and G. Weiglein, JHEP **0210** (2002) 072 [LC-TH-2002-021, hep-ph/0209305].

[94] G. Degrassi *et al.*, Eur. Phys. J. C **28** (2003) 133 [LC-TH-2002-015, hep-ph/0212020].

[95] S. P. Martin, Phys. Rev. D **66** (2002) 096001 [hep-ph/0206136] and Phys. Rev. D **67** (2003) 095012 [hep-ph/0211366].

[96] S. Heinemeyer, W. Hollik and G. Weiglein, Comput. Phys. Commun. **124** (2000) 76 [hep-ph/9812320]; Eur. Phys. J. C **9** (1999) 343 [hep-ph/9812472] and LC-TH-2001-065;
M. Frank, S. Heinemeyer, W. Hollik and G. Weiglein, hep-ph/0202166.

[97] A. Dedes, G. Degrassi and P. Slavich, hep-ph/0305127.

[98] A. Freitas and D. Stöckinger, Phys. Rev. D **66** (2002) 095014 [hep-ph/0205281].

[99] H. Eberl, M. Kincel, W. Majerotto and Y. Yamada, Phys. Rev. D **64** (2001) 115013 [hep-ph/0104109];
W. Öller, H. Eberl, W. Majerotto and C. Weber, hep-ph/0304006.

[100] T. Fritzsche and W. Hollik, Eur. Phys. J. C **24** (2002) 619 [hep-ph/0203159].

[101] J. Guasch, W. Hollik and J. Sola, Phys. Lett. B **510** (2001) 211 [hep-ph/0101086] and JHEP **0210** (2002) 040 [hep-ph/0207364].

[102] W. Hollik and H. Rzehak, hep-ph/0305328.

[103] W. Majerotto, hep-ph/0209137.

[104] S. Heinemeyer, W. Hollik and G. Weiglein, Eur. Phys. J. C **16** (2000) 139 [hep-ph/0003022].

[105] A. Djouadi, J. Kalinowski and M. Spira, Comput. Phys. Commun. **108** (1998) 56 [hep-ph/9704448].

[106] C. Weber, H. Eberl and W. Majerotto, hep-ph/0210354 and hep-ph/0305250.

[107] J. Guasch, P. Häfliger and M. Spira, hep-ph/0305101.

[108] Z. Was and M. Worek, Acta Phys. Polon. B **33** (2002) 1875 [hep-ph/0202007];
K. Desch, A. Imhof, Z. Was and M. Worek, hep-ph/0307331.

[109] A. Freitas and A. von Manteuffel, hep-ph/0211105.

[110] T. Blank and W. Hollik, LC-TH-2000-054 [hep-ph/0011092];
M. A. Diaz and D. A. Ross, JHEP **0106** (2001) 001 [hep-ph/0103309] and hep-ph/0205257.

[111] A. Freitas, D. J. Miller and P. M. Zerwas, Eur. Phys. J. C **21** (2001) 361 [hep-ph/0106198] and LC-TH-2001-011.

[112] A. Brandenburg, M. Maniatis and M. M. Weber, hep-ph/0207278.

[113] W. Hollik *et al.*, Nucl. Phys. B **639** (2002) 3 [hep-ph/0204350].

[114] R. Harlander and M. Steinhauser, Prog. Part. Nucl. Phys. **43** (1999) 167 [hep-ph/9812357].

[115] T. Hahn and C. Schappacher, Comput. Phys. Commun. **143** (2002) 54 [hep-ph/0105349].

[116] T. Hahn and M. Perez-Victoria, Comput. Phys. Commun. **118** (1999) 153 [hep-ph/9807565];
T. Hahn, Nucl. Phys. Proc. Suppl. **89** (2000) 231 [hep-ph/0005029].

[117] J. Fleischer *et al.*, LC-TH-2002-002 [hep-ph/0202109].

[118] J. Fleischer, A. Leike, T. Riemann and A. Werthenbach, hep-ph/0302259.

[119] T. Hahn, W. Hollik, A. Lorca, T. Riemann and A. Werthenbach, LC-TH-2003-083 [hep-ph/0307132].

[120] A. Andonov *el al.*, hep-ph/0209297.

[121] A. Andonov *el al.*, hep-ph/0202112 and hep-ph/0207156.

[122] G. Passarino, Nucl. Phys. B **619** (2001) 257 [hep-ph/0108252];
G. Passarino and S. Uccirati, Nucl. Phys. B **629** (2002) 97 [hep-ph/0112004];
A. Ferroglia, M. Passera, G. Passarino and S. Uccirati, Nucl. Phys. B **650** (2003) 162 [hep-ph/0209219].

[123] D. E. Soper, Phys. Rev. D **64** (2001) 034018 [hep-ph/0103262];
M. Krämer and D. E. Soper, Phys. Rev. D **66** (2002) 054017 [hep-ph/0204113].

ELECTROWEAK GAUGE THEORIES and ALTERNATIVE THEORIES

K. Mönig*, DESY Zeuthen, Germany

Abstract

The measurement of Standard Model processes tests the validity of the model at a given scale and is simultaneously sensitive to new physics through loop effects or interference with the Standard Model amplitudes. A variety of studies has been done to see what a linear collider in the energy range $m_{\mathrm{Z}} < \sqrt{s} < 1\,\mathrm{TeV}$ can offer. The work that has been done within the ECFA/DESY study on linear colliders is reviewed, especially what was not included in the TESLA TDR.

INTRODUCTION

It is a common belief that the Standard Model of electroweak interactions is not the final theory valid up to very high scales. Nevertheless the model is able to describe all experimental data up to now with a typical precision around one per mille [1]. At a linear $\mathrm{e^+e^-}$ collider that can run at centre of mass energies, $\sqrt{s}$, between the Z-pole and around $1\,\mathrm{TeV}$ one expects to see finally deviations from the Standard Model predictions. These deviations in precision measurements occur typically for two reasons. If the new physics occurs in loop diagrams their effect is usually suppressed by a loop factor $\alpha/4\pi$ and very high precision is required to see it. If the new physics occurs already on the Born level but at very high masses, the effects are suppressed by a propagator factor $\frac{s}{(s-m^2_{NP})+im_{NP}\Gamma}$ so that it is important to work at the highest possible energies. Both effects have already been used successfully in the past. PEP, PETRA and TRISTAN have been able to measure the fermion couplings to the Z although they were running at energies roughly a factor two below the resonance pole [2]. Ten years ago LEP could predict the mass of the top from its loop effects [3], exactly where it was found at the TEVATRON later [4]. Today we are able to limit the Higgs mass to roughly $200\,\mathrm{GeV}$ from loop effects at LEP, SLD and the TEVATRON (figure 1) or to set limits of about $500\,\mathrm{GeV}$ on the mass of a hypothetical Z' boson from two fermion production at LEP II (figure 2) [5]. In the same way we expect that in ten years from now a linear collider will estimate, depending on the physics scenario nature has chosen, model parameters in a supersymmetric theory from high statistics running at the Z resonance or the mass of a techni-ρ resonance from W-pair production at high energies [6].

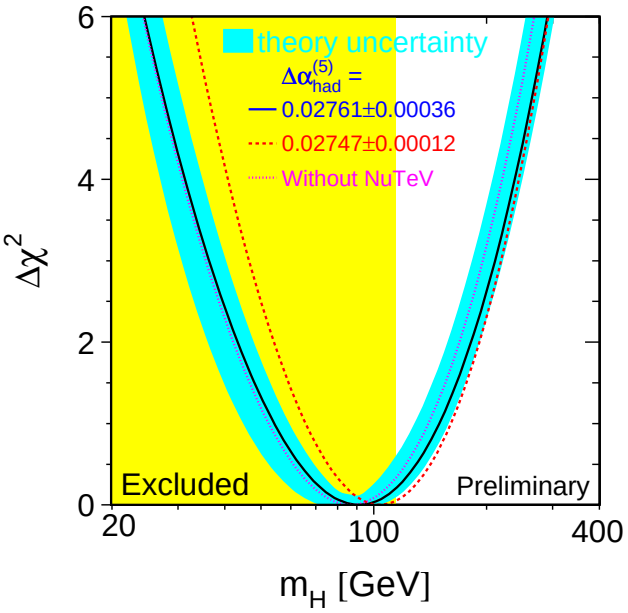

Figure 1: Prediction of the Higgs mass from the electroweak precision data.

There are several types of reactions to test the Standard Model or to investigate alternative theories. With two fermion or four fermion production on the Z-pole or close to the W-pair production threshold one can improve on the measurements done at LEP and SLD by an order of magnitude. Two fermion production at high energies is sensitive to contact interactions in general or more specific to heavy Z'-bosons or models with extra space dimensions. Four or six fermion production at high energy has a large contribution from multi gauge boson production which is sensitive to gauge boson couplings. This is especially interesting if no elementary Higgs boson exists and the electroweak symmetry is broken by a new strong interaction at a high scale.

In the following sections the results of the "Electroweak Gauge Theories and Alternative Theories" group of the

* The work reported in this talk was done by the members of the "Electroweak Gauge Theories and Alternative Theories" working group of the Extended ECFA/DESY Study; B. Ananthanarayan (Bangalore), D. Anipko (Nowosibirsk), D. Bardin (Dubna), I. Bozovic (VINCA Belgrade), A. Datta (Helsinki), A. Denner (PSI Villingen), M. Diehl (DESY Hamburg), S. Dittmaier (MPI Munich), J. Fleischer (Uni Bielefeld), I. Ginzburg (Nowosibirsk), J. Gluza (DESY Zeuthen), T. Hahn (MPI Munich), S. Heinemeyer (LMU Munich), J. Hewett (SLAC), W. Kilian (DESY Hamburg), A. Leike (LMU Munich), A. Lorca (DESY Zeuthen), V. Makarenko (NC PHEP Minsk), I. Marfin (NC PHEP Minsk), M. Maul (Lund), W. Menges (DESY Hamburg), O. Nachtmann (Uni Heidelberg), F. Nagel (Uni Heidelberg), T. Ohl (Uni Würzburg), P. Osland (Bergen), A. Pankov (Gomel), N. Paver (Trieste), F. Piccinini (Pavia), W. Placzek (Krakow), P. Poulose (RWTH Aachen), F. Richard (Orsay), S. Riemann (DESY Zeuthen), T. Riemann (DESY Zeuthen), S. Rindani (Ahmedabad), T. Rizzo (SLAC), M. Ronan (LBL Berkeley), M. Roth (Karlsruhe), M. Schumacher (Uni Bonn), J. Sekaric (DESY Zeuthen), T. Shishkina (NC PHEP Minsk), M. Spira (PSI Villingen), A. Stahl (DESY Zeuthen), D. Wackerroth (Buffalo), A. Werthenbach (CERN), G. Weiglein (Durham), G. Wilson (Kansas)

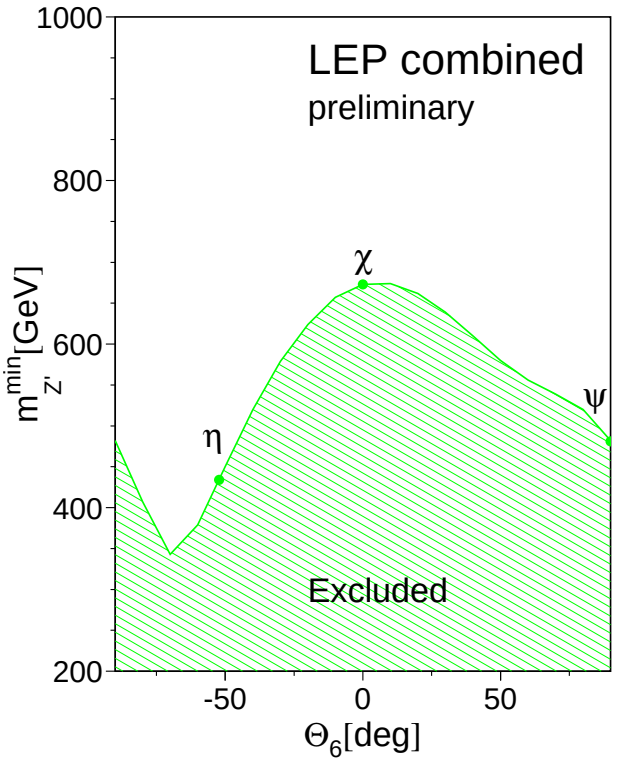

Figure 2: Exclusion of Z' within E(6) models from LEP.

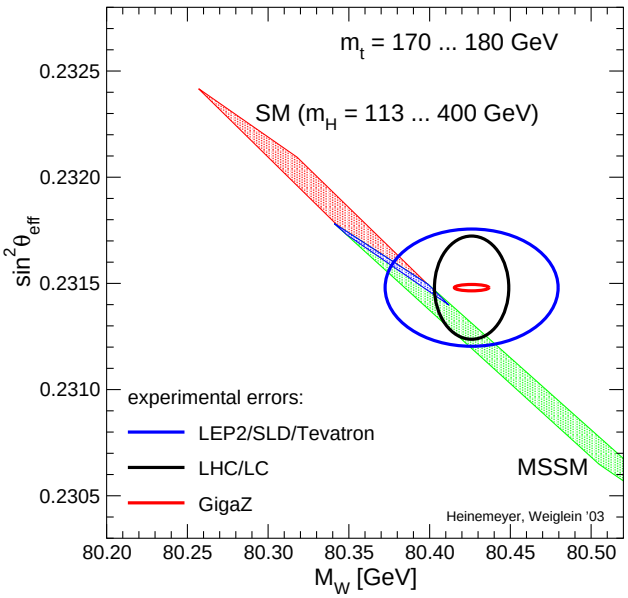

Figure 3: Expected precision for m_{W} and $\sin^2\theta^l_{eff}$ at Giga-Z compared to the present situation and to the LHC expectation. LHC/LC denotes LC high energy running only.

ECFA/DESY linear collider study will be discussed with particular emphasis on the progress since the TESLA TDR [6] in March 2001.

An essential ingredient for all precision measurements are accurate Standard Model calculations which are needed to one or two loop precision. Quite some progress has been made in the last years and many more calculations are still under way. This work is summarised in a special contribution to these proceedings [7].

THE GIGA-Z SCENARIO

The main physics goals of the Giga-Z scenario are a measurement of the effective leptonic weak mixing angle with a precision of $\Delta \sin^2\theta^l_{eff} = 0.000013$ from the left-right asymmetry, which would be an improvement of a factor 13 from LEP/SLD and a measurement of the W-mass with an experimental accuracy of $\Delta m_{\mathrm{W}} = 6\,\mathrm{MeV}$, improving the present LEP/TEVATRON result by a factor six [6]. While the $\sin^2\theta^l_{eff}$ measurement has no competition at any other machine the LHC has the goal to measure the W-mass with a precision of $15\,\mathrm{MeV}$ [8]. The anticipated Giga-Z accuracy is shown in figure 3 [9] compared to the present and LHC precision and to the predictions of the Standard Model and the MSSM.

The experimental requirements for this measurement are a luminosity of $\mathcal{L} \approx 5 \cdot 10^{33}\mathrm{cm}^{-2}\mathrm{s}^{-1}$ at $\sqrt{s} \sim m_{\mathrm{Z}}$ which allows to record 10^9 Z-decays in less than a year, electron and positron polarisation to measure polarisation mainly from data, a beam energy measurement of $\Delta\sqrt{s} = 1\,\mathrm{MeV}$ relative to m_{Z} close to the Z-peak and an extrapolation from m_{Z} to $2m_{\mathrm{W}}$ with $\Delta\sqrt{s}/\sqrt{s} < 5 \cdot 10^{-5}$ and control of the beamstrahlung on the few % level. If also the Z-partial width measurements are to be improved, an absolute measurement of the luminosity with a precision of $\Delta\mathcal{L}/\mathcal{L} = 10^{-4}$ is needed [10, 11, 12].

Excellent polarimeters are needed for relative measurements like time dependencies or the polarisation difference between positive and negative helicities of the beam particles. Detailed design studies for polarimetry, beam energy measurement, measurement of the beamstrahlung and of the luminosity are currently under way [13, 14].

Significant progress was achieved on the theoretical side. The largest parametric uncertainty for the measurement of $\sin^2\theta^l_{eff}$ is the uncertainty in the hadronic contribution to the running of the fine structure constant up to the Z-mass, $\alpha(m_{\mathrm{Z}}^2)$. Not to be limited too much by the knowledge of $\alpha(m_{\mathrm{Z}}^2)$ the hadronic cross section $\sigma(\mathrm{e^+e^-} \to \mathrm{q\bar{q}})$ needs to be known with 1% precision up to the Υ region [15]. CMD II basically achieved this goal in the ρ region [16, 17], however there are some discrepancies with the τ spectral functions [18, 19]. In the region $2\,\mathrm{GeV} < \sqrt{s} < 5\,\mathrm{GeV}$ BES II improved the data recently from 20% to 7% accuracy [20] and further progress is possible. In addition precise results from radiative return experiments at DAΦNE, CESR and the b-factories can be expected in the near future.

Significant progress has been achieved also in the prediction of the W-mass. The calculation of m_{W} from the Fermi constant and m_{Z} is now complete to second order plus the m_{t} dependent 3-loop corrections [7]. This results in an uncertainty in the m_{W} prediction of around $3 - 4\,\mathrm{MeV}$. For $\sin^2\theta^l_{eff}$ some 2-loop contributions are still missing and the theoretical uncertainty is estimated to

be $\Delta \sin^2 \theta^l_{eff} = 0.00006$ much larger than the experimental goal [21]. Also some other complicated calculations that are necessary for Giga-Z are not yet done and there is still a long way to go.

$e^+e^- \to f\bar{f}$ AT HIGH ENERGY

The most general parameterisation for new physics at high scales are contact interactions. For very large masses of the exchange particles the propagator goes like

$$\left|\frac{1}{s-M^2}\right| \approx \left|\frac{1}{t-M^2}\right| \approx \frac{1}{M^2}$$

so that the new interaction can be parameterised in a contact term $\frac{1}{\Lambda^2}$ which is equal to $\frac{g^2}{16\pi M^2}$ in gauge theories.

Since the experimental sensitivity to the contact term comes mostly from the interference with the Standard Model amplitude the helicity structure is important. TDR studies at $\sqrt{s} = 800\,\mathrm{GeV}$ gave typical limits around $50\,\mathrm{TeV}$ for $e^+e^- \to \mu^+\mu^-$ and $e^+e^- \to b\bar{b}$. The LHC reaches similar limits, however mainly for the coupling between leptons and light quarks. Figure 4 shows the linear collider reach in Λ for $e^+e^- \to \mu^+\mu^-$, $\sqrt{s} = 500\,\mathrm{GeV}$ and $\mathcal{P}_e = 0.8$ as a function of the integrated luminosity [22]. In a recent study the sensitivity of Bhabha and Moller scattering to contact interactions has been studied [23]. It was found that the limits can be improved by typically 20% compared to muons. Due to the lower luminosity in e^-e^- running compared to e^+e^- the sensitivities in Bhabha and Moller scattering are about the same.

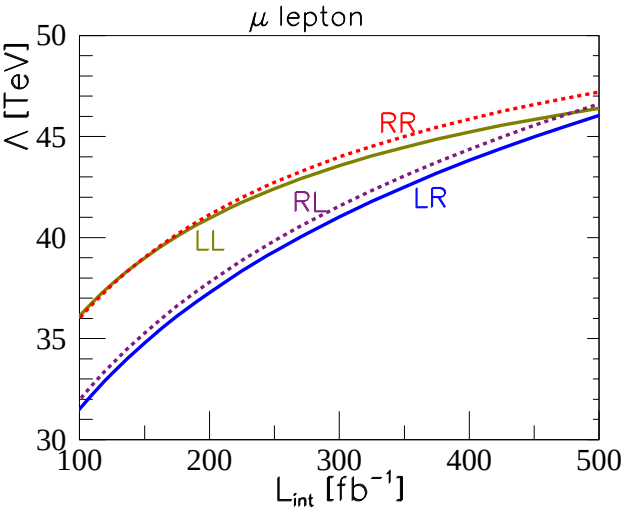

Figure 4: Contact interaction reach of the linear collider for $e^+e^- \to \mu^+\mu^-$, $\sqrt{s} = 500\,\mathrm{GeV}$ and $\mathcal{P}_e = 0.8$ as a function of the integrated luminosity.

Models with Z'

There are two approaches to study models with a Z' at a linear collider. In a model dependent study one assumes that one knows the model so that the Z'-mass is the only free parameter. In this case all couplings are fixed and any deviation of a measurement from the Standard Model value translates directly into a value of the Z'-mass. All final states can be used in this case. As for the contact terms there is a large difference between the models since the main sensitivity comes from the interference term. Figure 5 compares the reachable Z' masses for different models at the linear collider and the LHC [24]. On average the reachable masses are similar for both machines and around $4\,\mathrm{TeV}$.

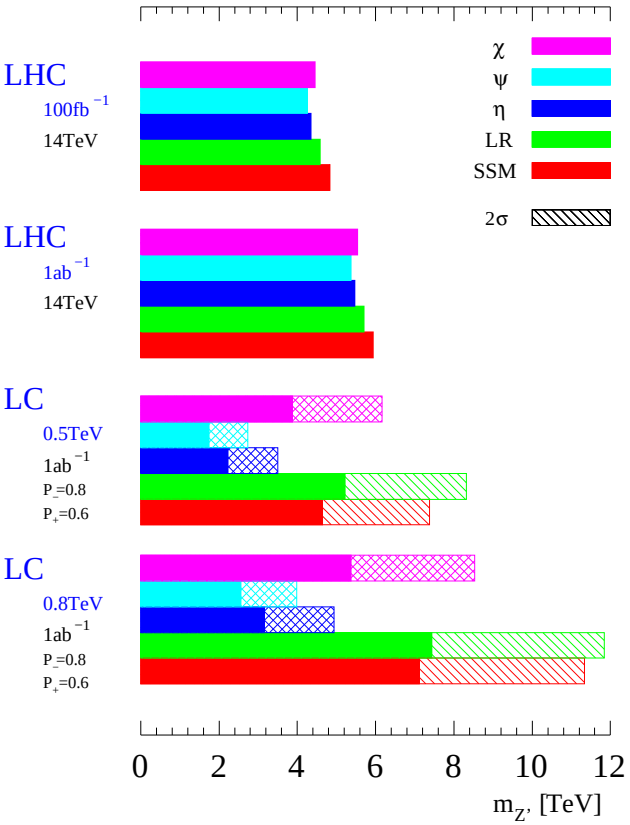

Figure 5: Mass reach for a Z' in different models for LHC and LC. The solid bars correspond to a 5σ discovery, while the dashed ones correspond to a 2σ exclusion.

In a model independent approach the Z' mass and the Z' couplings are considered simultaneously as free parameters. Any observable is given as the product of initial state and final state couplings, so that a Z' remains invisible in e^+e^- if it does not couple to leptons. For this reason hadronic events can be used only when non-zero Z'-lepton couplings are already established. At a given centre of mass energy a linear collider is sensitive to the normalised couplings

$$a_f^N = a'_f \sqrt{\frac{s}{m^2_{Z'} - s}}$$
$$v_f^N = v'_f \sqrt{\frac{s}{m^2_{Z'} - s}}$$

which can be measured for leptons in a model independent way using cross sections and asymmetries. A Z' model is then defined as a line in the $a_f^N - v_f^N$ plane where the exact position is given by the Z' mass. Figure 6 shows the sensitivity of the linear collider assuming for the central value a χ-model with $m_{Z'} = 6\,\mathrm{TeV}$, which is outside the LHC sensitivity [24]. Also shown is the prediction for several E(6) models, where χ, ψ, η stands for different mixing angles between the gauge bosons from the $\mathrm{U}(1)_\chi$ and $\mathrm{U}(1)_\psi$ gauge group [25]. The different models can be clearly separated with high luminosity.

In the ideal case the LHC finds a Z' and measures its mass so the linear collider can measure the couplings. Figure 7 shows the LC sensitivity in this case for different models and different assumptions on $\sqrt{s}$ and $m_{Z'}$ [6]. In general the couplings can be measured with a precision of a few percent.

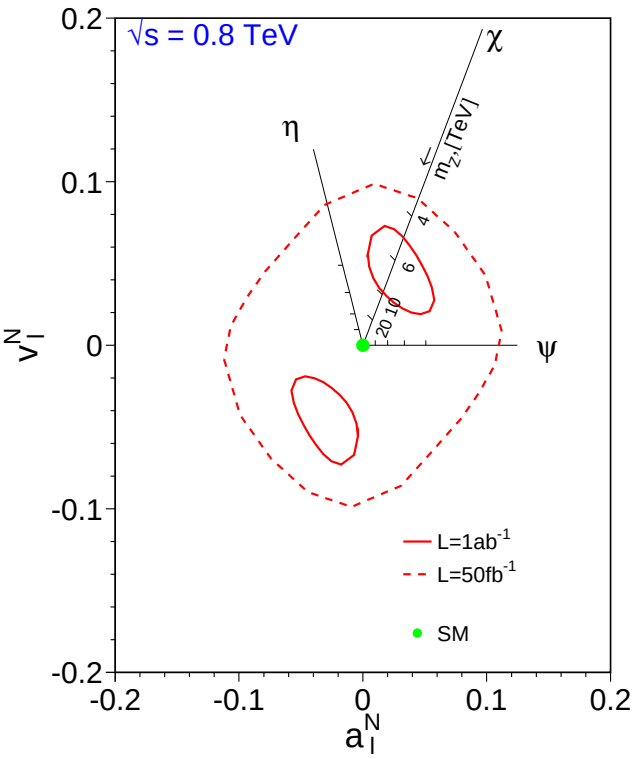

Figure 6: Measurement of normalised Z' couplings at TESLA. The χ-model with $m_{Z'} = 6\,\mathrm{TeV}$ is assumed for the central value.

For the left-right symmetric model an analysis on the one loop level has been performed [26]. In this model the quadratic top mass dependence of $\Delta\rho$ is suppressed by a term $\frac{M_{W_1}^2}{M_{W_2}^2 - M_{W_1}^2}$ where W_1 is the observed W-boson and $M_{W_2} > 500\,\mathrm{GeV}$. The successful prediction of m_t at LEP would be therefore a pure accident and the heavy Higgs and right handed neutrino masses need to be fine tuned to fit the LEP/SLD precision data.

Another study analysed the sensitivity to Z–Z' mixing one can get from the Z-data and the W mass [27]. As an

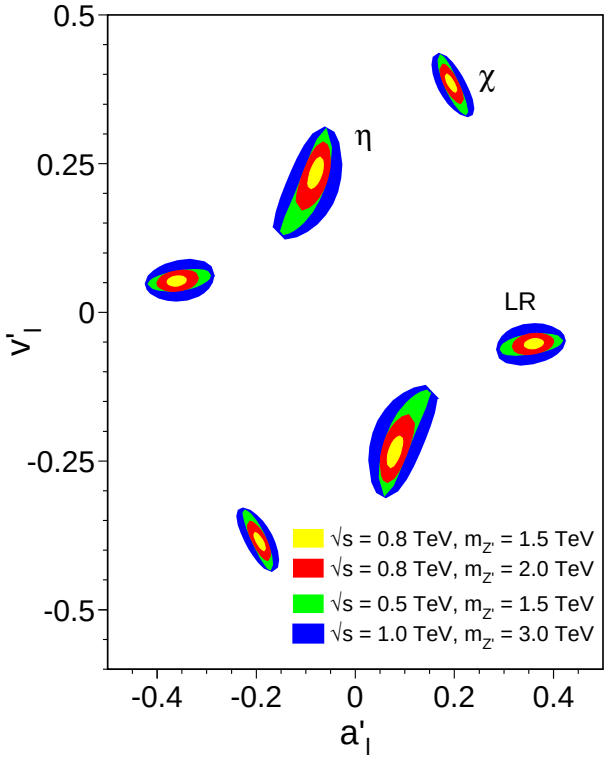

Figure 7: Measurement of the Z' couplings at a linear collider for different Z' masses and centre of mass energies.

example figure 8 shows the current measurements and the Giga-Z expectation compared to several Z' models assuming that a 115 GeV Higgs has been found. It can be seen that apart from $\sin^2\theta^l_{eff}$ and m_W an accurate measurement of the leptonic decay width of the Z, Γ_l, is useful as well.

Extra space dimensions

The linear collider and the LHC are sensitive to the presence of extra space dimensions via effects from Kaluza Klein tower graviton (G^*) exchange. In the TDR it has been shown that there are visible effects from $\mathrm{e^+e^-} \to \gamma G^*$ and $\mathrm{e^+e^-} \to G^* \to \mathrm{f\bar{f}}$ for an extra dimension scale of $M_H < 8\,\mathrm{TeV}$ and $\sqrt{s} = 800\,\mathrm{GeV}$. The reach of LHC is similar. Recently the emphasis has been put on the question how one can distinguish an extra dimensions signal from a Z' in case a deviation from the Standard Model is seen. Here one can use the fact that the Graviton is a tensor particle.

If one defines the moments $\langle P_n \rangle = \int dz \frac{1}{\sigma}\frac{d\sigma}{dz} P_n(z)$, where the P_n are the Legendre polynomials and $z = \cos\theta$ is the cosine of the polar angle, one can show that for vector or scalar particle s-channel exchange $\langle P_n \rangle = 0$ for $n > 2$ while for tensor particle exchange $\langle P_{3,4} \rangle \neq 0$ [28]. A unique identification of tensor particle exchange can be achieved up to around 5 TeV with $\sqrt{s} = 800\,\mathrm{GeV}$, $\mathcal{L} = 1\ \mathrm{ab}^{-1}$ and electron (positron) polarisation of 80% (60%). Similar results can be obtained with specially constructed asymmetries [29].

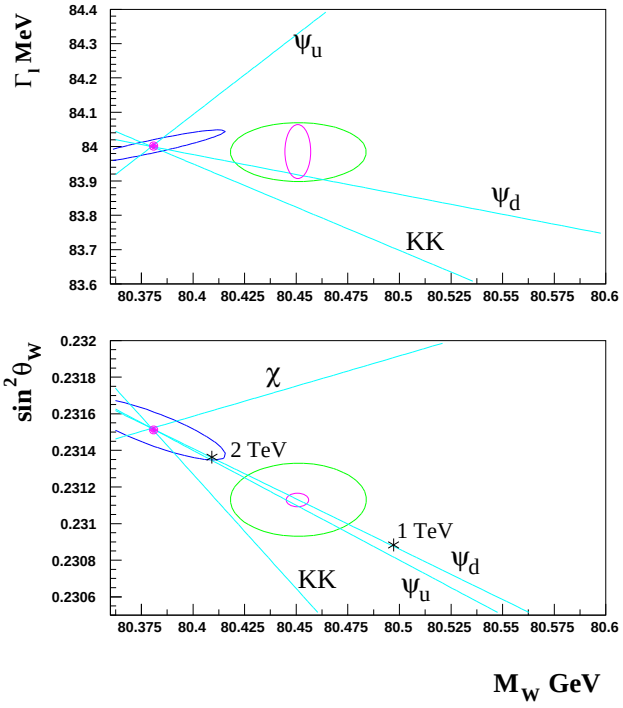

Figure 8: Predictions of several models with a Z' compared to the present and predicted Giga-Z precision data. The ellipse around the crossing point indicates the uncertainty from the present day error on m_t and $\alpha(m_Z)$.

If transverse beam polarisation is available for both beams one can measure the azimuthal asymmetry as a function of the polar angle [30]. Figure 9 shows this asymmetry for leptons b- and c-quarks for the Standard Model and for $M_H = 1.5\,\mathrm{TeV}$. Using this asymmetry extra dimensions can be excluded up to $M_H < 10(22)\,\mathrm{TeV}$ for $\sqrt{s} = 0.5(1)\,\mathrm{TeV}$, which is the highest reach at a next generation collider. For vector and scalar particle exchange the azimuthal asymmetry is symmetric in $\cos\theta$, while it is asymmetric if also tensor particle exchange is present. This allows to distinguish extra dimensions from Z' exchange up to $M_H < 10\sqrt{s}$.

CP violation in τ production

In the Standard Model the CP-violating dipole moment of the τ lepton is extremely small ($\sim 10^{-34}\,\mathrm{e\,cm}$). However for example in models with Majorana neutrinos or in CP violating two Higgs doublet models these moments can be of order $10^{-19}\,\mathrm{e\,cm}$.

It has been studied how well the electric and weak dipole moment can be measured in τ pair production at TESLA using spin correlations and polarised beams [31]. For this analysis $\tau \to \pi\nu$ and $\tau \to \rho\nu$ decays have been used and CP-odd vector correlations between the two τs have been constructed. At $\sqrt{s} = 800\,\mathrm{GeV}$ the real parts of the weak and the electromagnetic dipole moment can be measured with a precision of $3 - 4 \cdot 10^{-19}\,\mathrm{e\,cm}$ which touches the interesting region. For the imaginary parts the precision is about three orders of magnitude worse.

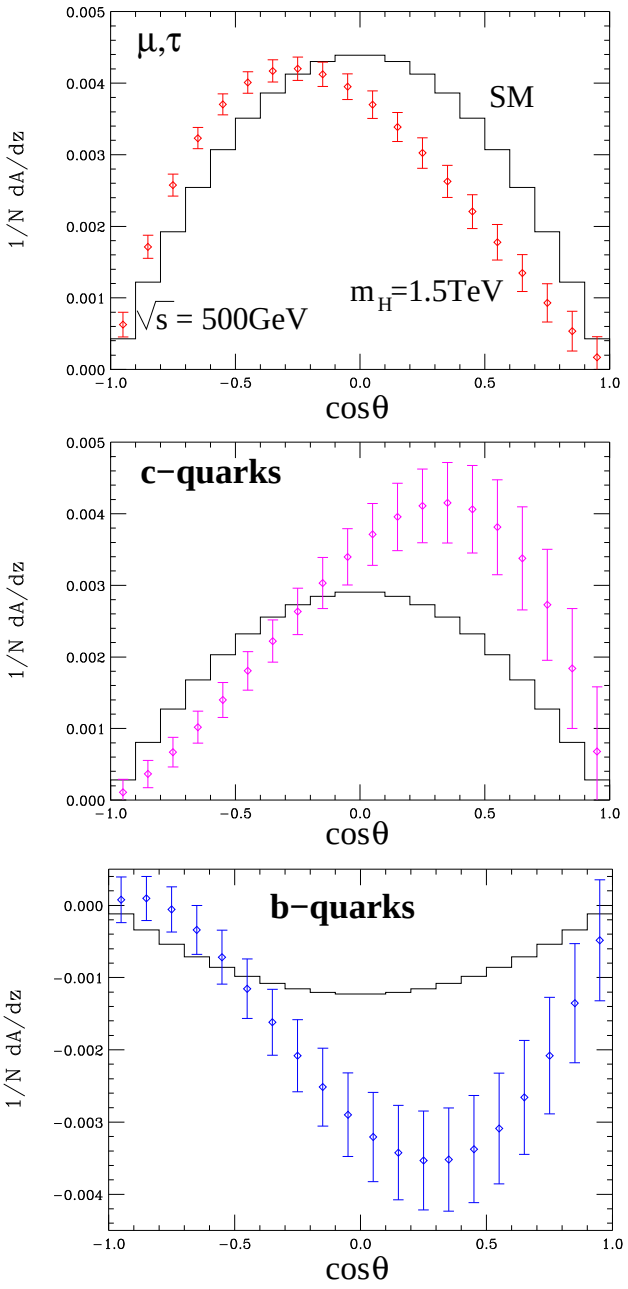

Figure 9: Azimuthal asymmetry with transverse beam polarisation as a function of the polar angle for leptons b- and c-quarks for the Standard Model and for $M_H = 1.5\,\mathrm{TeV}$.

GAUGE BOSON PRODUCTION

High precision measurements of gauge boson production are interesting in several aspects. The interactions amongst gauge bosons are directly given by the structure of the gauge group. The longitudinal gauge bosons are connected to the mechanism of electroweak symmetry breaking so that their interactions can teach us about this mechanism in case no elementary Higgs boson exists. In a strongly in-

teracting theory the longitudinal components of the gauge bosons are expected to have similar interactions at very high energies as the pions in QCD at low energy.

In a weakly interacting theory including an elementary Higgs boson gauge boson self-interactions should receive loop corrections of $\mathcal{O}(\frac{g^2}{16\pi^2}) \sim 3 \cdot 10^{-3}$. If the experimental precision is larger than this number gauge boson interactions should be able to test the Standard Model in the same way as $\sin^2\theta^l_{eff}$ and m_{W} do it now.

For the TDR a detailed study including full detector simulation has been done for $\mathrm{e^+e^-} \to \mathrm{W^+W^-}$ [32]. It has been found than the C, P conserving couplings can be measured with a precision of $3-15\cdot10^{-4}$ at $\sqrt{s} = 500\,\mathrm{GeV}$ and around a factor two better at $\sqrt{s} = 800\,\mathrm{GeV}$. This is much better than the expected effects from radiative corrections so that W-pair production will become a new precision observable. In a strongly interacting scenario this precision translates into a new physics scale of $\Lambda > 10\,\mathrm{TeV}$ which is also significantly above the $\Lambda \leq 3\,\mathrm{TeV}$ limit from unitarity. The C or P violating couplings can be measured roughly one order of magnitude worse than the C, P conserving ones.

Recently a study using optimal observables has been done [33]. This work is on parton level only up to now, but it has shown that the imaginary parts of the couplings can be measured simultaneously with the real parts with about the same precision and without degrading the precision of the real parts. Only one combination of couplings $(\mathrm{Im}(g_1^R+\kappa_R))$ cannot be measured with longitudinal beam polarisation. If transverse beam polarisation is available this coupling can be measured. In this case, however, the precision of the other coupling is degraded by roughly a factor of two [34].

Also the measurement of the triple gauge couplings at a photon collider in $\gamma\gamma \to WW$ and $e\gamma \to W\nu$ has been studied, using hadronic W decays only. The study of $e\gamma \to W\nu$ is reasonably complete [35], while in $\gamma\gamma \to WW$ the azimuthal decay angle, ϕ, which is sensitive to the interference of the different helicity amplitudes is still missing [36]. Both reactions can be selected cleanly with an overall efficiency around 80%. Figure 10 shows the polar angle distribution for $e\gamma \to W\nu$ and the background after cuts on the visible energy and the invariant mass. In the real $e\gamma$ mode, where only one beam is converted, only some background in the extreme forward and backward regions is left from $e\gamma \to Ze$ and from $\gamma\gamma$ induced hadron production which can easily be rejected by an angular cut. In the parasitic mode, where the $e\gamma$ luminosity during $\gamma\gamma$ running is used, some additional background from $\gamma\gamma \to WW$ where one W decays leptonically is left.

The cross sections in these two channels are much larger than in $\mathrm{e^+e^-}$. However there are no large gauge cancellations so that the final precision is comparable in all cases. Figure 11 compares the expected precision for κ_γ and λ_γ at the different machines. For $\gamma\gamma$ and $e\gamma$ a 0.1% error on the luminosity is assumed. It should be noted that κ_γ is very sensitive to the luminosity error and to uncertainties

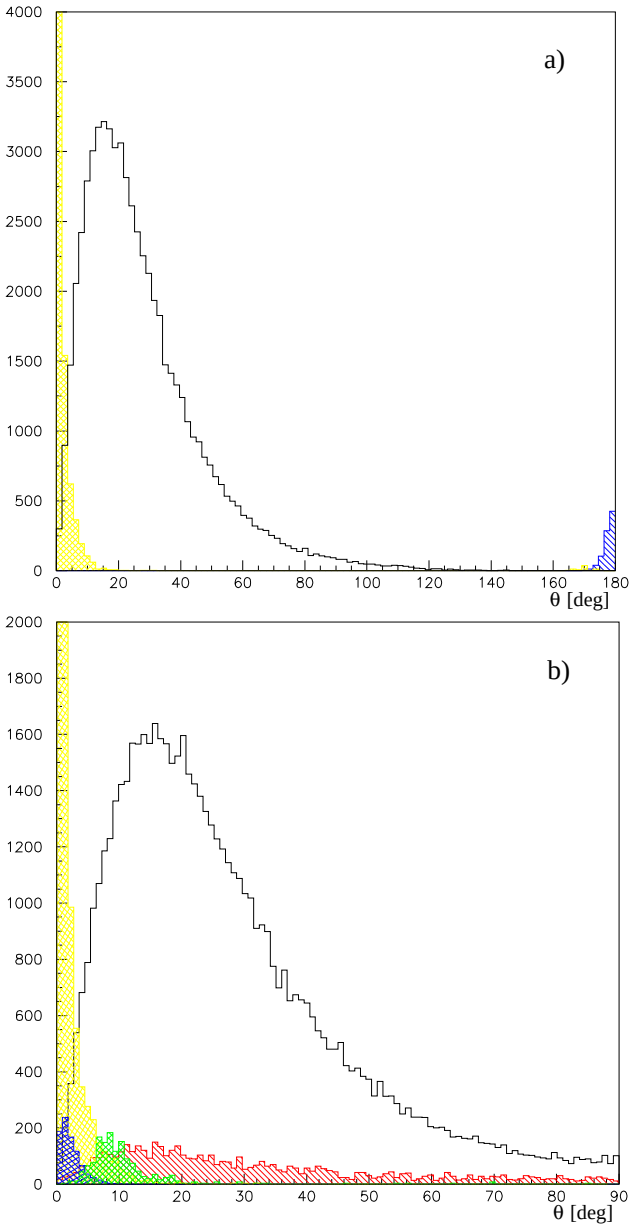

Figure 10: Signal and background for $e\gamma \to W\nu$ in the real $e\gamma$ mode (a) and from the parasitic $\gamma\gamma$ running (b). The white area represents the signal. In a) the hatched contribution on the left is from $\gamma\gamma$ induced processes and the one on the right from $e\gamma \to eZ$. The additional cross-hatched (green) contribution in b) is from $\gamma\gamma \to q\bar{q}$ and the singly hatched (red) from $\gamma\gamma \to WW$.

in the polarisation while λ_γ is basically insensitive to these effects. For $e\gamma$ the improvement using the ϕ angle in the fit is a factor seven for λ_γ, a similar factor can be expected for $\gamma\gamma$ as well. In summary κ_γ will be measured significantly worse in $e\gamma$ and $\gamma\gamma$ than in $\mathrm{e^+e^-}$, however still good enough for cross checks in case deviations from the Standard Model are found. For λ_γ the photon collider could give the best result.

In an alternative study the leptonic W decays in $e\gamma \to$

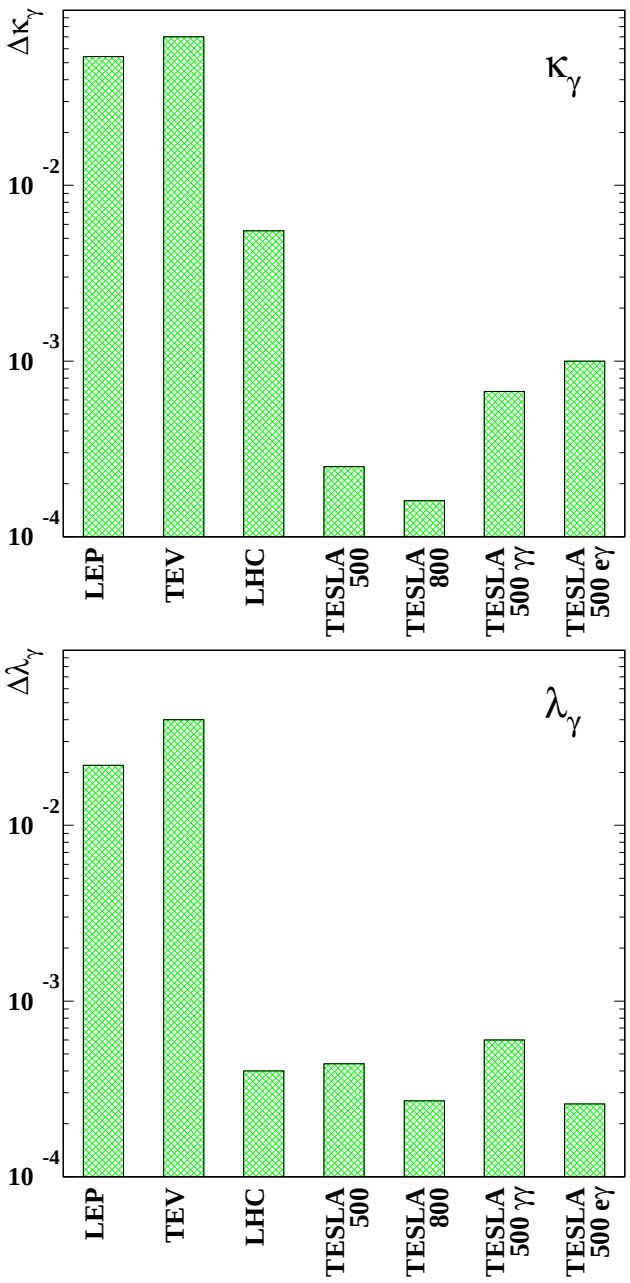

Figure 11: The expected precision for κ_γ and λ_γ at different machines.

$W\nu$ have been considered [37]. In these events only a single lepton is seen in the detector. The couplings have been measured from the cross section in an optimised phase space region where background and the variable photon energy has been taken into account. Assuming no error on the normalisation, the error in κ_γ is similar for the two analyses taking the lower leptonic branching ratio of the W into account. For λ_γ the error in the leptonic analysis is significantly larger because of the missing information due to the second missing neutrino.

It is known since long that $\mathrm{e^+e^-} \to \mathrm{W^+W^-}$ is sensitive to technicolour vector resonances in the same way as the ρ is seen in $\mathrm{e^+e^-} \to \pi^+\pi^-$ [38]. It has been shown now, that $\gamma\gamma \to \mathrm{W^+W^-}$ is sensitive to rescattering effects from a scalar or a tensor resonance [39]. Figure 12 compares the cross section for longitudinal gauge boson production in the central region for the Standard Model and for a tensor resonance with a mass of $2.5\,\mathrm{TeV}$. An experimental study, whether these effects are measurable at TESLA, is planned.

These studies underline the importance to measure the gauge couplings in several different channels. For example a vector resonance would result in anomalous gauges couplings in $\mathrm{e^+e^-}$ while in $\gamma\gamma$ and $e\gamma$ one might still measure the Standard Model values.

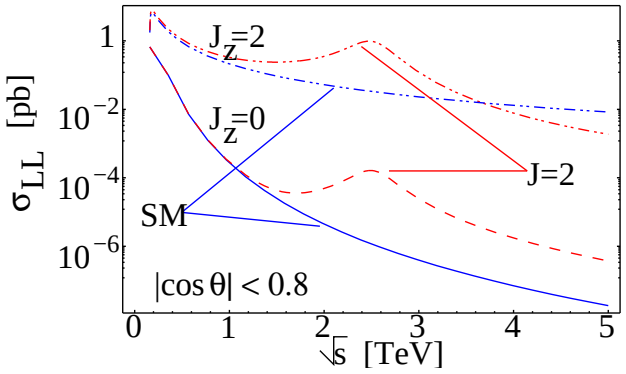

Figure 12: Cross section for longitudinal W-pair production in $\gamma\gamma$ scattering for the Standard Model and in presence of a tensor resonance with $2.5\,\mathrm{TeV}$ mass. J_z denotes the spin of the $\gamma\gamma$ system.

The reaction $\gamma\gamma \to \mathrm{W^+W^-}$ is also the ideal place to test for anomalous $\gamma\gamma\mathrm{W^+W^-}$ quartic couplings. These couplings have been first studied in $\mathrm{e^+e^-} \to \mathrm{W^+W^-}\gamma$ and limits of the coupling parameters of $\mathcal{O}(1)$ at $\sqrt{s} = 500\,\mathrm{GeV}$ have been found [40, 41]. The cross section dependence of $\gamma\gamma \to \mathrm{W^+W^-}$ on these couplings has been studied and limits on these couplings have been derived [42]. Figure 13 shows the cross section dependence on these couplings for $\sqrt{s} = 1\,\mathrm{TeV}$. Without systematic uncertainties limits between 10^{-4} and 10^{-2} can be achieved. This is about three orders of magnitude better than the $\mathrm{e^+e^-}$ result.

CONCLUSIONS

It has been shown that electroweak precision tests contribute significantly to the physics of a linear collider. Precision measurements on the Z pole can test model parameters inside or beyond the Standard Model. Two-fermion production at high energy tests a wide class of models like those containing additional Z' bosons or extra space dimensions. The limits are often comparable or better than those at the LHC. W-pair production provides new precision observables on the same level as $\sin^2\theta^l_{eff}$ or m_W. If no light Higgs exists, gauge boson production offers a window to strong electroweak symmetry breaking.

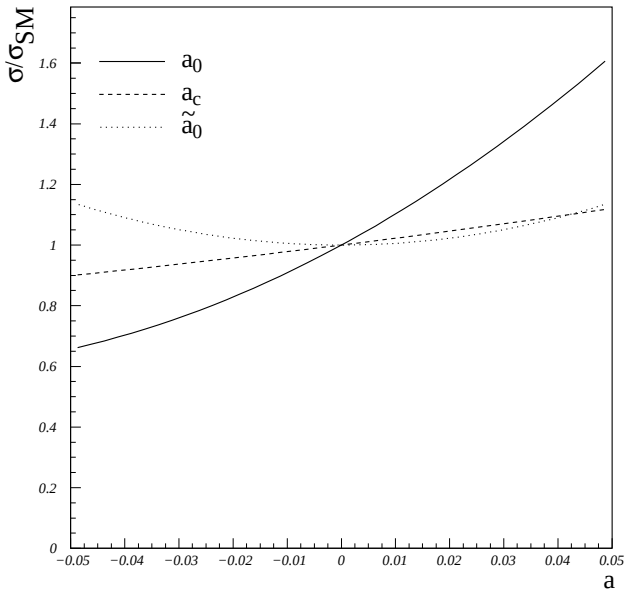

Figure 13: Dependence of $\sigma(\gamma\gamma \to \mathrm{W^+W^-})$ for $\sqrt{s} = 1$ TeV on the $\gamma\gamma\mathrm{W^+W^-}$ couplings. The exact definition of the couplings can be found in [41, 42].

In summary it is the combination of the direct studies of the probable extensions of the Standard Model, like Higgs and SUSY, with the potential of the precision tests that makes the Linear Collider a unique tool to understand the physics of electroweak symmetry breaking.

REFERENCES

[1] J. Erler, P. Langacker in K. Hagiwara et al., Phys. Rev. D 66, 010001 (2002).

[2] K. Fujii, Nucl. Phys. Proc. Suppl. **16** (1990) 92.

[3] The LEP Collaboratons and the LEP Electroweak Working Group, CERN-PPE/93-157.

[4] CDF Collaboration, F. Abe et al., Phys. Rev. Lett. 74, 2626 (1995);
D0 Collaboration, S. Abachi et al., Phys. Rev. Letters 74 2632 (1995) .

[5] The LEP collaborations, CERN-EP/2002-091, hep-ex/0212036.

[6] J. A. Aguilar-Saavedra *et al.*, *TESLA Technical Design Report Part III: Physics at an* $\mathrm{e^+e^-}$ *Linear Collider*, DESY-01-011C, hep-ph/0106315.

[7] S. Dittmaier, these proceedings and hep-ph/0308079.

[8] S. Haywood et al. *Electroweak Physics*, CERN-2000-004, 117, hep-ph/0003275.

[9] S. Heinemeyer and G. Weiglein, JHEP **0210** (2002) 072 [arXiv:hep-ph/0209305].

[10] R. Hawkings, K. Mönig, EPJdirect **C8** (1999) 1.

[11] M. Winter, *Determination of the strong coupling constant at GigaZ*, LC-PHSM-2001-016.

[12] G.W. Wilson, *Precision Measurement of the W Mass with a Polarised Threshold Scan at a Linear Collider*, LC-PHSM-2001-009.

[13] D. Cinabro, E. Torrence, M. Woods, *Status of Linear Collider Beam Instrumentation Design*, http://www.slac.stanford.edu/xorg/lcd/ipbi/notes/white.pdf.

[14] The forward Calorimeter Group, DESY-PRC R&D 02/01.

[15] F. Jegerlehner, hep-ph/0105283.

[16] R. R. Akhmetshin *et al.* [CMD-2 Collaboration], Phys. Lett. B **527**, 161 (2002) [arXiv:hep-ex/0112031].

[17] R. R. Akhmetshin *et al.* [the CMD-2 Collaboration], arXiv:hep-ex/0308008.

[18] M. Davier, S. Eidelman, A. Hocker and Z. Zhang, Eur. Phys. J. C **27** (2003) 497 [arXiv:hep-ph/0208177].

[19] M. Davier, S. Eidelman, A. Hocker and Z. Zhang, arXiv:hep-ph/0308213.

[20] J. Z. Bai *et al.* [BES Collaboration], Phys. Rev. Lett. **88**, 101802 (2002) [arXiv:hep-ex/0102003].

[21] U. Baur et al., in *Proc. of the APS/DPF/DPB Summer Study on the Future of Particle Physics (Snowmass 2001)* ed. N. Graf, eConf **C010630** (2001) P122 [arXiv:hep-ph/0111314].

[22] A.A. Babich, P. Osland, A.A. Pankov and N. Paver, Phys. Lett. B **518** (2001) 128 [hep-ph/0107159].

[23] A. A. Pankov and N. Paver, Eur. Phys. J. C **29** (2003) 313 [arXiv:hep-ph/0209058].

[24] S. Riemann, *Identification of New Physics with Fermion-Pair Production at a Linear Collider*, LC-PHSM-2003-076.

[25] G. C. Cho, K. Hagiwara and Y. Umeda, Nucl. Phys. B **531** (1998) 65 [Erratum-ibid. B **555** (1999) 651] [arXiv:hep-ph/9805448].

[26] M. Czakon, J. Gluza and J. Hejczyk, Nucl. Phys. B **642** (2002) 157 [arXiv:hep-ph/0205303];
M. Czakon, J. Gluza, F. Jegerlehner and M. Zralek, Eur. Phys. J. C **13** (2000) 275 [arXiv:hep-ph/9909242];
M. Czakon, M. Zralek and J. Gluza, Nucl. Phys. B **573** (2000) 57 [arXiv:hep-ph/9906356].

[27] F. Richard, arXiv:hep-ph/0303107.

[28] T. G. Rizzo, JHEP **0210** (2002) 013 [arXiv:hep-ph/0208027].

[29] P. Osland, A. A. Pankov and N. Paver, Phys. Rev. D **68** (2003) 015007 [arXiv:hep-ph/0304123].

[30] T. G. Rizzo, JHEP **0302** (2003) 008 [arXiv:hep-ph/0211374].

[31] B. Ananthanarayan, S. D. Rindani and A. Stahl, Eur. Phys. J. C **27** (2003) 33 [arXiv:hep-ph/0204233].

[32] W. Menges, *A Study of Charged Current Triple Gauge Couplings at TESLA*, LC-PHSM-2001-022.

[33] M. Diehl, O. Nachtmann and F. Nagel, Eur. Phys. J. C **27** (2003) 375 [arXiv:hep-ph/0209229].

[34] M. Diehl, O. Nachtmann and F. Nagel, arXiv:hep-ph/0306247.

[35] K. Mönig, J. Sekaric, *A Study of Charged Current Triple Gauge Couplings at an* $e\gamma$ *- collider*, LC-PHSM-2003-072

[36] I. Bozovic-Jelisavcic, K. Mönig and J. Sekaric, arXiv:hep-ph/0210308.

[37] D. Anipko, I. Ginzburg, A. Pak, Proc. Suppl. of ACAT'2002 Workshop (Moscow, Russia; June, 2002), Nucl. Instr. and Meth. **A502** (2003), 752.

[38] T. L. Barklow, hep-ph/0112286.

[39] P. Poulose and L. M. Sehgal, Phys. Lett. B **552** (2003) 57 [arXiv:hep-ph/0211179].

[40] W. J. Stirling and A. Werthenbach, Eur. Phys. J. C **14** (2000) 103 [arXiv:hep-ph/9903315].

[41] A. Denner, S. Dittmaier, M. Roth and D. Wackeroth, Eur. Phys. J. C **20** (2001) 201 [arXiv:hep-ph/0104057].

[42] I. Marfin, V. Mossolov, T. Shishkina, *Anomalous quartic boson couplings via $\gamma\gamma \to WW$ and $\gamma\gamma \to WWZ$ at the TESLA kinematics*, LC-PHSM-2003-085.

...

...

SUPERSYMMETRY WORKING GROUP: SUMMARY REPORT*

J. Kalinowski†, Institute of Theoretical Physics, Warsaw University, Warsaw, Poland

Abstract

This report summarizes the progress in SUSY studies performed during the Extended ECFA/DESY Workshop since the TESLA TDR [1]. Based on accurate future measurements of masses of SUSY particles and the determination of the couplings and mixing properties of sfermions and gauginos, we discuss how the low-energy Lagrangian parameters can be determined. In a 'bottom-up' approach, by extrapolating to higher energies, we demonstrate how model assumptions on SUSY breaking can be tested. To this end precise knowledge of the SUSY spectrum and the soft SUSY breaking parameters is necessary to reveal the underlying supersymmetric theory.

INTRODUCTION

An e^+e^- linear collider in the 500 - 1000 GeV energy range (LC) is widely considered as the next high-energy physics machine [2]. One of the many arguments for its construction is the possibility of exploring supersymmetry (SUSY). Of the many motivations for the supersymmetric extension of the Standard Model, perhaps the most important, next to the connection to gravity, is the ability to stabilize the electroweak scale. If the electroweak scale is not fine-tuned, the superpartner masses (at least some of them) need to be in the TeV range. In such a case the Large Hadron Collider (LHC) will certainly see SUSY. Many different channels, in particular from squark and gluino decays will be explored and many interesting quantities measured. In specific scenarios characterized by a handful of free parameters some of the elements of supersymmetry can be reconstructed [3]. However, to prove SUSY one has to scrutinize its characteristic features in as model-independent a way as possible. We will have to:

- measure masses of new particles, their decay widths, production cross sections, mixing angles etc.,
- verify that they are superpartners, *i.e.* measure their spin and parity, gauge quantum numbers and couplings,
- reconstruct the low-energy SUSY breaking parameters without assuming a specific scenario,
- and ultimately unravel the SUSY breaking mechanism and shed light on physics at the high (GUT?, Planck?) scale.

In answering all the above points an e^+e^- LC would be an indispensable tool. Therefore the concurrent running of the LHC and the LC is very much welcome [4]. First, the LC will provide independent checks of the LHC findings. Second, thanks to the LC unique features: clean environment, tunable collision energy, high luminosity, polarized incoming beams, and additional e^-e^-, $e\gamma$ and $\gamma\gamma$ modes, it will offer precise measurements of masses, couplings, quantum numbers, mixing angles, CP phases etc. Last, but not least, it will provide additional experimental input to the LHC analyses, like the mass of the lightest supersymmetry particle (LSP). Coherent analyses of data from the LHC *and* LC would thus allow for a better, model independent reconstruction of low-energy SUSY parameters, and connect low-scale phenomenology with the high-scale physics. The interplay between LHC and LC is investigated in detail in the LHC/LC Study Group [5].

During the Extended ECFA/DESY Workshop[1] the discovery potential of TESLA [1] - design of the superconducting LC - for SUSY particles has been further studied. In particular, it has been demonstrated that the expected high luminosity ($\mathcal{L} \sim 300$ fb^{-1} per year) and availability of polarized electron (up tp 80%) and positron (up to 60%) beams makes precision experiments possible. The virtues of polarized beams are investigated in the POWER Study Group [7]. Here we will summarize in some detail how accurate measurements of the masses of SUSY particles and the determination of the couplings and mixing properties of sleptons, charginos, neutralinos and scalar top quarks can be performed.

* Much of the work reported in this talk was done by members of the SUSY Working Group of the Extended ECFA/DESY Study: B.C.Allanach[a], M.Ball[b], A.Bartl[c], S.Berge[b], G.Blair[d], C.Blöchinger[e], E.Boos[f], A.Brandenburg[g], P.Checchia[h], S.Y.Choi[i] A.Datta[j], K.Desch[b], A.Djouadi[j], H.Dreiner[λ] (co-convener), H.Eberl[k], A.Finch[ζ], H.Fraas[e], A.Freitas[l], T.Fritzsche[m], B.Gaissmaier[n], N.Ghodbane[b], D.K.Ghosh[o], J.Guasch[p], S.Heinemeyer[r], C.Hensel[g], S.Hesselbach[c], K.Hidaka[s], M.Hirsch[t], W.Hollik[u], T.Kernreiter[c], M.Kincel[v], O.Kittel[e], M.Klasen[b], S.Kraml[w], J.L.Kneur[j], W.Majerotto[k], M.Maniatis[g], A.v.Manteuffel[g], H.U.Martyn[x] (co-convener), M.Melles [p], D.J.Miller[w], K.Mönig[y], G.Moortgat-Pick[z], S.Moretti[α], G.Moultaka[j], M.Mühlleitner[p], U.Nauenberg[β], H.Nieto-Chaupis[y], H.Nowak[y], V.Öller[k], E.Piotto[w], G.Polesello[κ], W.Porod[γ], F.Richard[ρ], J.C.Romão[δ], S.Rosier-Lees[μ] (co-convener), H.Rzehak[u], A.Stahl[y], J.Solà[ϵ], A.Sopczak[ζ], C.Tevlin[η], J.W.F.Valle[t], C.Verzegnassi[ν], R.Walczak[η], C.Weber[k], M.M.Weber[p], G.Weiglein[z], Y.Yamada[θ], P.M.Zerwas[g] ([a] LAPTH Annecy, [b] U.Hamburg, [c] U.Vienna, [d] U.London, [e] U.Würzburg, [f] Moscow State U., [g] DESY Hamburg, [h] U.Padova, [i] Chonbuk National U., [j] U.Montpellier II, [k] ÖAW Vienna, [l] Fermilab, [m] U.Karlsruhe, [n] TU Munich, [o] Oregon U. Eugene, [p] PSI Villigen, [r] LMU Munich, [s] Gakugei U. Tokyo, [t] U.València, [u] MPI Munich, [v] Comenius U. Bratislava, [w] CERN, [x] RWTH Aachen, [y] DESY Zeuthen, [z] U.Durham, [α] U.Southampton, [β] U.Colorado Boulder, [γ] U.Zürich, [δ] IST Lisboa, [ϵ] U.Barcelona, [ζ] U.Lancaster, [η] U.Oxford, [θ] Tohoku U. Sendai, [κ] INFN Pavia, [λ] U.Bonn, [μ] LAPP Annecy, [ν] U.Trieste, [ρ] LAL Orsay.)

† Supported by by the KBN Grant 2 P03B 040 24 (2003-2005).

[1] The SUSY WG group was very active: the members have given 14 talks in Cracow, 15 in St. Malo, 11 in Prague and 15 in Amsterdam, and the transparencies can be found in [6].

We will start the discussion with the Minimal Supersymmetric Standard Model considered as an effective low energy model with a) minimal particle content, b) R-parity conservation, c) most general soft supersymmetry breaking terms. Since the mechanism of SUSY breaking is unknown, several Snowmass benchmark scenarios, so-called 'Snowmass Points and Slopes' (SPS) [8], with distinct signatures have been studied. Although each benchmark scenario is characterized by a few parameters specified at high energies (for example at the GUT scale), most of the phenomenological analyses have been performed strictly on low-energy supersymmetry.

A word of caution is in order here. The deduction of low-energy parameters from high-scale assumptions (and vice-versa) inevitably involves theoretical errors coming from the level of approximation used, neglected higher order terms etc. The SPS benchmarks, while motivated in terms of specific SUSY-breaking scenarios (like the mSUGRA scenario), have explicitly been defined in terms of the low-energy MSSM parameters. Therefore it is not necessary in the SPS benchmarks to refer to any particular program for calculating the SUSY spectrum from high-energy parameters. Studies during the Workshop [10, 11] showed large differences between various calculations of the MSSM spectrum. Recent analysis [11] of the most advanced modern codes for the MSSM spectra: ISAJET 7.64, SOFTSUSY 1.71 [12], SPHENO 2.0 [13] and SUSPECT 2.101 [14], shows that the typical relative uncertainty in mSUGRA and mGMSB scenarios in generic (i.e. not tricky) regions of parameter space is about $2-5\%$. In some cases, in particular in focus point, high $\tan\beta$ and mAMSB scenarios, the relative uncertainty is larger, about $5-10\%$. For the focus point and high $\tan\beta$ scenarios, sparticle masses are particularly sensitive to the values of the Yukawa couplings (especially the top Yukawa for the focus point, and the bottom Yukawa for the high $\tan\beta$ regime). Slightly different treatments of top and bottom masses can lead to large differences in mass predictions. In the mAMSB scenario larger differences between various programs are due to a different implementation of GUT-scale boundary conditions. Nevertheless, even in these particular cases, comparison with previous versions of the codes [10] (where SUSYGEN3.00 [15], PYTHIA6.2 [16] and the mSUGRA Post-LEP benchmarks [17] have also been investigated) shows a significant improvement. Differences in the results between the codes (which may be interpreted as very conservative upper bounds on current theoretical uncertainties [11] as some programs are more advanced than others) should be reduced by future higher–order theoretical calculations.

After extensive discussion of experimentation and extraction of SUSY parameters in the MSSM, we will go to 'beyond the MSSM' scenarios by considering R-parity violating couplings and/or extended gaugino sector. Finally, in a 'bottom-up' approach, by extrapolating to higher energies the SUSY parameters determined at the electroweak scale with certain errors, we demonstrate how model assumptions on SUSY breaking can be tested. It will be seen that precise knowledge of the SUSY spectrum and the soft SUSY breaking parameters is necessary to reveal the underlying supersymmetric theory.

SFERMIONS

Sfermions $\tilde{f}_L$, $\tilde{f}_R$ are spin-zero superpartners of the SM chiral fermions f_L, f_R. The sfermion mass matrix has the form

$$\mathcal{M}^2_{\tilde{f}} = \begin{pmatrix} m^2_{\tilde{f}_L} & a^*_{\tilde{f}} m_f \\ a_{\tilde{f}} m_f & m^2_{\tilde{f}_R} \end{pmatrix} \quad (1)$$

$$m^2_{\tilde{f}_i} = M^2_{\tilde{F}_i} + m^2_Z \cos 2\beta\,(I^3_{f_i} - Q_f \sin^2\theta_W) + m^2_f$$

$$a_{\tilde{f}} = A_{\tilde{f}} - \mu^*(\tan\beta)^{-2I^3_f}$$

where $M^2_{\tilde{F}_L,\tilde{F}_R}$, $A_{\tilde{f}}$ are soft SUSY breaking parameters (which can be 3×3 matrices in the flavor space), and μ is the higgs/higgsino mass term. Both $A_{\tilde{f}} = |A_{\tilde{f}}|e^{i\varphi_{A_{\tilde{f}}}}$ and $\mu = |\mu|e^{i\varphi_\mu}$ can be complex. The mixing between L and R states is important when the off-diagonal term is comparable to the splitting of diagonal ones $\Delta_{\tilde{f}} = m^2_{\tilde{f}_L} - m^2_{\tilde{f}_R}$, *i.e.* $|\Delta_{\tilde{f}}| \leq |a_{\tilde{f}} m_f|$. For $\tilde{e}$ and $\tilde{\mu}$ the $L-R$ mixing is therefore usually neglected.

Neglecting inter-generation mixing, the masses of physical sfermions $\tilde{f}_{1,2}$

$$\tilde{f}_1 = \tilde{f}_L e^{i\varphi_{\tilde{f}}}\cos\theta_{\tilde{f}} + \tilde{f}_R \sin\theta_{\tilde{f}}$$
$$\tilde{f}_2 = -\tilde{f}_L \sin\theta_{\tilde{f}} + \tilde{f}_R e^{-i\varphi_{\tilde{f}}}\cos\theta_{\tilde{f}} \quad (2)$$

and the mixing angle $\theta_{\tilde{f}}$ and the phase $\varphi_{\tilde{f}}$ are given by

$$m^2_{\tilde{f}^\pm_{1,2}} = (m^2_{\tilde{f}_L} + m^2_{\tilde{f}_R} \mp [\Delta^2_{\tilde{f}} + 4|a_{\tilde{f}} m_f|^2]^{1/2})/2$$
$$\tan\theta_{\tilde{f}} = (m^2_{\tilde{f}_1} - m^2_{\tilde{f}_L})/|a_{\tilde{f}} m_f|$$
$$\varphi_{\tilde{f}} = arg(A_{\tilde{f}} - \mu^*(\tan\beta)^{-2I^3_f}) \quad (3)$$

Thus reconstructing the sfermion sector requires $m^2_{\tilde{f}_L}$, $m^2_{\tilde{f}_R}$, $a_{\tilde{f}}$ to be decoded from measurements of sfermion masses, cross sections, decay widths etc. [18].

With the anticipated experimental precision, however, higher order corrections will have to be taken into account. A current summary of theoretical progress in this direction can be found in Ref.[19]. Complete one-loop calculations have been performed for $\tilde{\mu}\tilde{\mu}$ and $\tilde{e}\tilde{e}$ production [20] and for sfermion masses and their decays [21]. For a relatively light SUSY spectrum and a high–energy LC ($M_{\rm SUSY} \ll \sqrt{s} \lesssim$ 2 – 3 TeV), the simple one–loop approximation may turn out to be inadequate and resummation of higher–order effects might be necessary to obtain good theoretical predictions [22].

Study of selectrons/smuons

At e^+e^- collisions charged sleptons are produced in pairs via the s-channel γ/Z exchange; for the first generation there is additional t-channel neutralino exchange.

Different states and their quantum numbers can be disentangled by a proper choice of the beam energy and polarization.

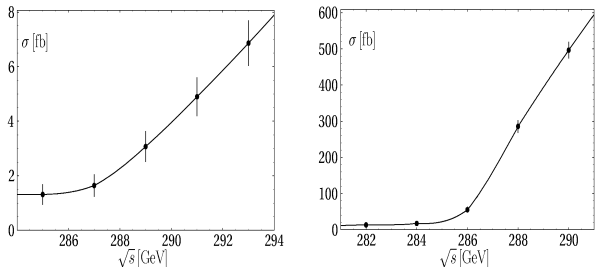

Figure 1: Cross sections at threshold for the reactions $e^+_L e^-_R \to \tilde{e}^+_R \tilde{e}^-_R$ (left) and $e^-_R e^-_R \to \tilde{e}^+_R \tilde{e}^-_R$ (right) in the SPS#1a scenario, including background [20]. Error bars correspond to a luminosity of 10 fb^{-1} (left) and 1 fb^{-1} (right) per point.

Slepton masses can be measured in threshold scans or in continuum. At threshold: $\tilde{\mu}^+_L \tilde{\mu}^-_L$, $\tilde{\mu}^+_R \tilde{\mu}^-_R$, $\tilde{e}^+_L \tilde{e}^-_L$ and $\tilde{e}^+_R \tilde{e}^-_R$ pairs are excited in a P-wave characterized by a slow rise of the cross section $\sigma \sim \beta^3$ with slepton velocity β. On the other hand, in $e^+_L e^-_L$ / $e^+_R e^-_R \to \tilde{e}^+_R \tilde{e}^-_L$ / $\tilde{e}^+_L \tilde{e}^-_R$ and $e^-_L e^-_L$ / $e^-_R e^-_R \to \tilde{e}^-_L \tilde{e}^-_L$ / $\tilde{e}^-_R \tilde{e}^-_R$ sleptons are excited in the S-wave giving steep rise of the cross sections $\sigma \sim \beta$. Therefore the shape of the cross section near threshold is sensitive to the masses and quantum numbers.

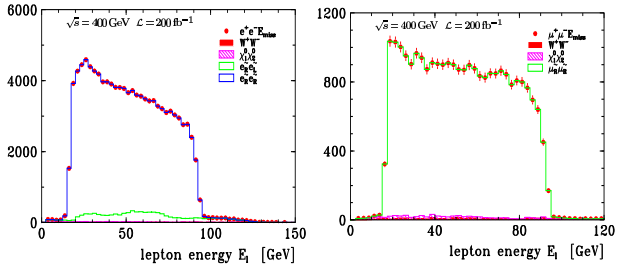

Figure 2: Lepton energy spectra in the processes $e^-_R e^+_L \to \tilde{e}^-_R \tilde{e}^+_R \to e^- \tilde{\chi}^0_1 e^+ \tilde{\chi}^0_1$ (left) and $e^-_R e^+_L \to \tilde{\mu}^-_R \tilde{\mu}^+_R \to \mu^- \tilde{\chi}^0_1 \mu^+ \tilde{\chi}^0_1 \to \mu^- \tilde{\chi}^0_1 \mu^+ \tilde{\chi}^0_1$ (right) at $\sqrt{s} = 400\,\mathrm{GeV}$, $\mathcal{L} = 200\,\mathrm{fb}^{-1}$; scenario SPS#1a [23].

The expected experimental precision requires higher order corrections, and finite sfermion width effects to be included. Examples of simulations for the SPS#1a point are shown in fig. 1. Using polarized e^+e^- beams and $\mathcal{L} = 50\ \mathrm{fb}^{-1}$ a (highly correlated) 2-parameter fit gives $\delta m_{\tilde{e}_R} = 0.20\,\mathrm{GeV}$ and $\delta\Gamma_{\tilde{e}_R} = 0.25\,\mathrm{GeV}$; the resolution deteriorates by a factor of ~ 2 for $\tilde{\mu}_R\tilde{\mu}_R$ production. For $e^-_R e^-_R \to \tilde{e}_R \tilde{e}_R$ the gain in resolution is a factor ~ 4 with only a tenth of the luminosity, compared to e^+e^- beams.

Above the threshold, slepton masses can be obtained from the endpoint energies of leptons coming from slepton decays. In the case of two-body decays, $\tilde{\ell}^- \to \ell^- \tilde{\chi}^0_i$ and $\tilde{\nu}_\ell \to \ell^- \tilde{\chi}^+_i$ the lepton energy spectrum is flat with endpoints (the minimum E_- and maximum E_+ energies)

$$E_\pm \;=\; \tfrac{1}{4}\sqrt{s}\,(1 \pm \beta)(1 - m^2_{\tilde{\chi}}/m^2_{\tilde{\ell}}) \qquad (4)$$

providing an accurate determination of the masses of the primary slepton and the secondary neutralino/chargino.

Simulations of the e and μ energy spectra of $\tilde{e}_R\tilde{e}_R$ and $\tilde{\mu}_R\tilde{\mu}_R$ (respectively) production, including beamstrahlung, QED radiation, selection criteria and detector resolutions, are shown in fig. 2 assuming mSUGRA scenario SPS#1a [23]. With a moderate luminosity of $\mathcal{L} = 200\ \mathrm{fb}^{-1}$ at $\sqrt{s} = 400$ GeV one finds $m_{\tilde{e}_R} = 143 \pm 0.10$ GeV, $m_{\tilde{\mu}_R} = 143 \pm 0.10$ GeV and $m_{\tilde{\chi}^0_1} = 96 \pm 0.10$ GeV from selectron, or $m_{\tilde{\chi}^0_1} = 96 \pm 0.18$ GeV from smuon production processes. Assuming the neutralino mass is known, one can improve slepton mass determination by a factor 2 from reconstructed kinematically allowed minimum $m_{min}(\tilde{\ell})$. A slightly better experimental error for the neutralino mass $\delta m_{\tilde{\chi}^0_1} = 0.08$ GeV from the smuon production has recently been reported in [24]. The partner $\tilde{\mu}_L$ is more difficult to detect because of large background from WW pairs and SUSY cascades. However, with the high luminosity of TESLA one may select the rare decay modes $\tilde{\mu}_L \to \mu\tilde{\chi}^0_2$ and $\tilde{\chi}^0_2 \to \ell^+\ell^-\,\tilde{\chi}^0_1$, leading to a unique, background free signature $\mu^+\mu^-\,4\ell^\pm \not{E}$. The achievable mass resolutions for $m_{\tilde{\mu}_L}$ and $m_{\tilde{\chi}^0_2}$ is of the order of 0.4 GeV [25].

One should keep in mind that the measurement of selectron masses is subject to two experimental difficulties: an overlap of flat energy distributions of leptons from $\tilde{e}^-_R\tilde{e}^+_L$, $\tilde{e}^-_R\tilde{e}^+_R$, $\tilde{e}^-_L\tilde{e}^+_L$, $\tilde{e}^-_L\tilde{e}^+_L$, and large SM background. Nevertheless, it has been demonstrated [26] that thanks to larger cross sections, both problems can be solved by a double subtraction of e^- and e^+ energy spectra and opposite electron beam polarizations $\mathcal{P}_{e^-} = +0.8$ and $\mathcal{P}_{e^-} = -0.8$, symbolically $(E_{e^-} - E_{e^+})_{e^-_R} - (E_{e^-} - E_{e^+})_{e^-_L}$. Such a procedure eliminates all charge symmetric background and clearly exhibits endpoints from the $\tilde{e}_R$ and $\tilde{e}_L$ decays, as seen in fig. 3. Simulations at $\sqrt{s} = 500\,\mathrm{GeV}$ in the SPS#1a scenario [26] show that both selectron masses can be determined to an accuracy of $\delta m_{\tilde{e}_R,\,\tilde{e}_L} \sim 0.8\,\mathrm{GeV}$.

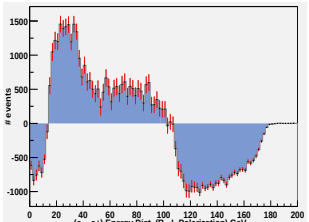

Figure 3: Energy spectrum $(E_{e^-} - E_{e^+})_{e^-_R} - (E_{e^-} - E_{e^+})_{e^-_L}$ for $e^-_{R,\,L}e^+ \to \tilde{e}_R\tilde{e}_L$ in the model SPS#1a at $\sqrt{s}$=500 GeV, $\mathcal{L}$=2·500 fb^{-1} [26].

Sneutrino production

At e^+e^- collisions sneutrinos are produced in pairs via the s-channel Z exchange; for the $\tilde{\nu}_e$ production there is additional t-channel chargino exchange. Their decay into the corresponding charged lepton and chargino, and the

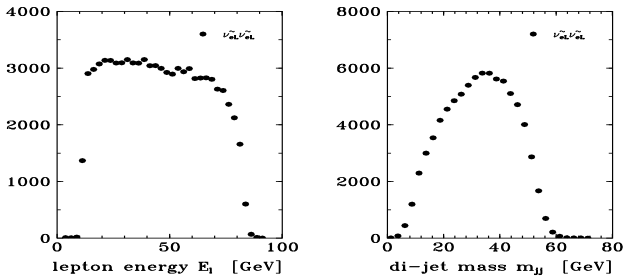

Figure 4: Lepton energy and di-jet mass spectra of $e^-_L e^+_R \to \tilde{\nu}_e \tilde{\nu}_e \to e^- \tilde{\chi}^+_1 e^+ \tilde{\chi}^-_1$ (left) with subsequent decay $\tilde{\chi}^\pm_1 \to q\bar{q}' \tilde{\chi}^0_1$ (right) [25]

subsequent chargino decay, make the final topology, e.g. $\tilde{\nu}_e\tilde{\nu}_e \to e^+e^-\ell^\pm 2j \not{E}$, very clean. The primary charged lepton energy, and di-jet energy and mass spectra, see fig. 4, can be used to determine $m_{\tilde{\nu}}$ and $m_{\tilde{\chi}^\pm_1}$ to 2 per mil (or better), and to measure the chargino couplings and the $\tilde{\chi}^\pm_1 - \tilde{\chi}^0_1$ mass difference; a resolution below 50 MeV, given essentially by detector systematics, appears feasible [25]. The detection and measurement of tau-sneutrinos $\tilde{\nu}_\tau$ is more problematic, due to neutrino losses in decay modes and decay energy spectra.

Study of staus

In contrast to the first two generations, the $L-R$ mixing for the third generation sleptons can be non-negligible due to the large τ Yukawa coupling. Therefore the $\tilde{\tau}$'s are very interesting to study since their production and decay is different from $\tilde{e}$ and $\tilde{\mu}$.

The $\tilde{\tau}$ masses can be determined with the usual techniques of decay spectra or threshold scans at the per cent level, while the mixing angle $|\cos\theta_{\tilde{\tau}}|$ can be extracted with high accuracy from cross section measurements with different beam polarisations. In a case study [27] for $m_{\tilde{\tau}_1} = 155$ GeV, $m_{\tilde{\tau}_2} = 305$ GeV, $\mu = 140$ GeV, $\tan\beta = 20$, $A_\tau = -254$ GeV it has been found that at $\sqrt{s} = 500$ GeV, $\mathcal{L} = 250\ \mathrm{fb}^{-1}$, $\mathcal{P}_{e^-} = +0.8$, $\mathcal{P}_{e^+} = -0.6$, the expected precision is as follows: $m_{\tilde{\tau}_1} = 155 \pm 0.8$ GeV, $\cos 2\theta_\tau = -0.987 \pm 0.08$, left panel of fig. 5.

The dominant decay mode $\tilde{\tau}_1 \to \tilde{\chi}^0_1 \tau$ can be exploited to determine $\tan\beta$ if $\tan\beta$ turns to be large [28]. In this case the non-negligible τ Yukawa coupling makes $\tilde{\tau}$ couplings sensitive to the neutralino composition in the decay process. Most importantly, if the higgsino component of the neutralino is sufficiently large, the polarization of τ's from the $\tilde{\tau}$ decay turns out to be a sensitive function of $\tilde{\tau}$ mixing, neutralino mixing *and* $\tan\beta$ [27]. This is crucial since for large $\tan\beta$ other SUSY sectors are not very sensitive to $\tan\beta$ and therefore cannot provide a precise determination of this parameter.

The τ polarization can be measured using the energy distributions of the decay hadrons, e.g. $\tau \to \pi\nu$ and $\tau \to \rho\nu \to \pi^\pm\pi^0\nu$. Simulations show that the τ polarization can be measured very accurately, $\delta\mathcal{P}_\tau = 0.82 \pm 0.03$, which in turn allows to determine $\tan\beta = 20 \pm 2$, as shown in the right panel of fig. 5.

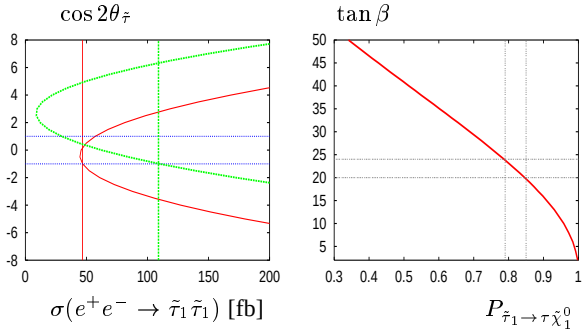

Figure 5: Left: $\cos 2\theta_{\tilde{\tau}}$ versus $\sigma(e^+e^- \to \tilde{\tau}_1\tilde{\tau}_1)$ at $\sqrt{s} = 500$ GeV for polarized (green, upper curve) and unpolarized (red, lower curve) beams; the expected cross sections shown by vertical lines. Unpolarised beams give a two-fold ambiguity in $\cos 2\theta_{\tilde{\tau}}$, while polarized beams give a unique physical solution. Right: $\tan\beta$ as a function of τ polarization. From simulations $P_\tau = 0.82 \pm 0.03$ leading to $\tan\beta = 22 \pm 2$ [27].

Squarks

For the third generation squarks, $\tilde{t}$ and $\tilde{b}$, the $L-R$ mixing is also expected to be important. As a result of the large top quark Yukawa coupling, it is possible that the lightest superpartner of the quarks is the stop $\tilde{t}_1 = \tilde{t}_L \cos\theta_{\tilde{t}} + \tilde{t}_R \sin\theta_{\tilde{t}}$. If the mass $m_{\tilde{t}_1}$ is below 250 GeV, it may escape detection at the LHC, while it can easily be discovered at the Linear Collider.

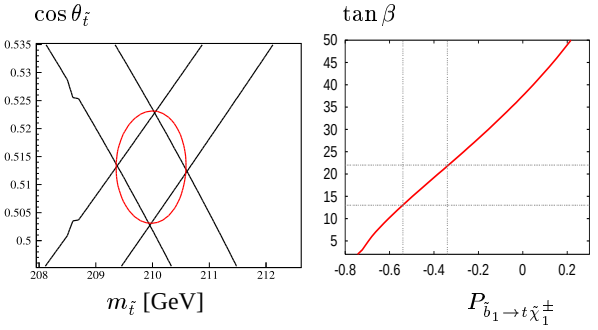

Figure 6: Left: Contours of $\sigma_R(\tilde{t}_1\tilde{t}_1)$ and $\sigma_L(\tilde{t}_1\tilde{t}_1)$ as a function of $m_{\tilde{t}_1}$ and $\cos\theta_{\tilde{t}}$ for $\sqrt{s} = 500$ GeV, $\mathcal{L} = 2 \cdot 500\ \mathrm{fb}^{-1}$ [29]. Right: $\tan\beta$ as a function of top polarization. From simulations $P_t = -0.44 \pm 0.10$ leading to $\tan\beta = 17.5 \pm 4.5$ [27].

The $\tilde{t}$ and $\tilde{b}$ phenomenology is analogous to that of the $\tilde{\tau}$ system. The masses and mixing angles can be extracted from production cross sections measured with polarized beams. The production cross sections for $e^+e^- \to \tilde{t}_1\bar{\tilde{t}}_1$ with different beam polarizations, $\sigma_R = \sigma_{e^-_R e^+_L}$ and $\sigma_L =$

$\sigma_{e_L^- e_R^+}$, have been studied for $\tilde{t}_1 \to b\,\tilde{\chi}_1^\pm$ and $\tilde{t}_1 \to c\,\tilde{\chi}_1^0$ decay modes including full-statistics SM background. New analyses have been performed for the SPS#5-type point: a dedicated "light-stop" scenario with $m_{\tilde{t}_1} = 210$ GeV, $m_{\tilde{\chi}_1^0} = 121.2$ GeV [29]. For this point the decay $\tilde{t}_1 \to b\,\tilde{\chi}_1^\pm$ is not open, and the SUSY background is small. The charm tagging, based on a CCD detector, helps to enhance the signal from the decay process $\tilde{t}_1 \to c\,\tilde{\chi}_1^0$. Generated events were passed through the SIMDET detector simulation. The results, shown in the left panel of fig. 6, provide high accuracies on the mass $\Delta m_{\tilde{t}_1} \sim 0.7$ GeV and mixing angle $\Delta \cos\theta_{\tilde{t}} \sim 0.01$.

If the heavier stop $\tilde{t}_2$ is too heavy to be produced at the LC, the precise measurement of the Higgs boson mass m_h together with measurements from the LHC can be used to obtain indirect limits on $m_{\tilde{t}_2}$ [30]. Assuming $m_{\tilde{t}_1} = 180 \pm 1.25$ GeV, $\cos\theta_{\tilde{t}} = 0.57 \pm 0.01$, $M_A = 257 \pm 10$ GeV, $\mu = 263 \pm 1$ GeV, $m_{\tilde{g}} = 496 \pm 10$ GeV, $A_{\tilde{b}} = A_{\tilde{t}} \pm 30\%$ and $m_{\tilde{b}_1} > 200$ GeV, fig. 7 shows the allowed region in the $m_{\tilde{t}_2}$–m_h plane. Only a lower bound $\tan\beta > 10$ has been assumed, which could for instance be inferred from the gaugino/higgsino sector. Intersection of the assumed

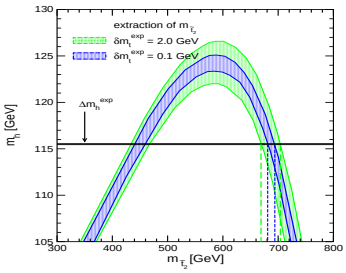

Figure 7: Indirect determination of $m_{\tilde{t}_2}$ from the m_h measurement for δm_t=2 GeV (LHC) and 0.1 GeV (LC) [30].

measured value $m_h = 115.5 \pm 0.05$ GeV with the allowed $m_{\tilde{t}_2}$–m_h region gives an indirect determination of $m_{\tilde{t}_2}$, yielding 670 GeV $\lesssim m_{\tilde{t}_2} \lesssim$ 705 GeV for the LHC precision $\delta m_t = 2$ GeV ($\tilde{t}_2$ must be above the LC reach). The LC precision of $\delta m_t = 0.1$ GeV reduces the range to 680 GeV $\lesssim m_{\tilde{t}_2} \lesssim$ 695 GeV, i.e. by a factor of more than 2.

Similarly to the $\tilde{\tau}$, the measurement of top quark polarization in the squark decay can provide information on $\tan\beta$. For this purpose the decay $\tilde{b}_1 \to t\tilde{\chi}_1^\pm$ is far more useful than $\tilde{t}_1 \to t\tilde{\chi}_k^0$ since in the latter the t polarization depends on $1/\sin\beta$ and therefore is only weakly sensitive to large $\tan\beta$.

A feasibility study of the reaction

$$e_L^+ e_R^- \;\to\; \tilde{b}_1\bar{\tilde{b}}_1 \;\to\; t\tilde{\chi}_1^- + \bar{t}\tilde{\chi}_1^+ \qquad (5)$$

has been performed in [27]. A fit to the angular distribution $\cos\theta_s^*$, where θ_s^* is the angle between the $\bar{s}$ quark and the primary $\tilde{b}_1$ in the top rest frame in the decay chain $e^+e^- \to \bar{\tilde{b}}_1 + t\,\tilde{\chi}_1^- \to \bar{\tilde{b}}_1 + bc\bar{s}\,\tilde{\chi}_1^-$, yields $P_t = -0.44 \pm 0.10$, consistent with the input value of $P_t^{th} = -0.38$. From such a measurement one can derive $\tan\beta = 17.5 \pm 4.5$, as illustrated in the right panel of fig. 6. After $\tan\beta$ is fixed, measurements of stop masses and mixing allow us to determine the trilinear coupling $A_{\tilde{t}}$ at the ten-percent level [27].

Quantum numbers

An important quantity is the spin of the sfermion which can directly be determined from the angular distribution of sfermion pair production in e^+e^- collisions [1, 25].

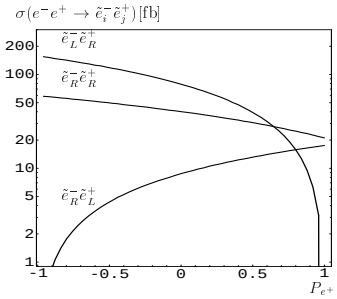

Figure 8: Production cross sections as a function of P_{e^+} for $\sqrt{s}$ =350 GeV, P_{e^-}=-0.8. ISR and beamstrahlung are included [31].

Due to small $L-R$ mixing of the first two generation sfermions, the mass eigenstates are chiral. As a result, of particular interest is the associated production of

$$e_R^- e_R^+ \to \tilde{e}_R^-\tilde{e}_L^+ \quad \text{and} \quad e_L^- e_L^+ \to \tilde{e}_L^-\tilde{e}_R^+ \qquad (6)$$

via t-channel $\tilde{\chi}^0$ exchange for the sfermion quantum number determination. For polarized beams the charge of the observed lepton is directly associated to the L, R quantum numbers of the selectrons and the energy spectrum uniquely determines whether it comes from the $\tilde{e}_R$ or the $\tilde{e}_L$ decay. However, in order to separate the t-channel neutralino exchange from the s-channel photon and Z-boson exchange, both the electron and positron beams must be polarized. By comparing the selectron cross-section for different beam polarizations the chiral quantum numbers of the selectrons can be disentangled, as can be seen in fig. 8, where other parameters are $m_{\tilde{e}_R} = 137.7$ GeV, $m_{\tilde{e}_L} = 179.3$ GeV, $M_2 = 156$ GeV, $\mu = 316$ GeV and $\tan\beta = 3$ [31].

Sfermion Yukawa couplings

Supersymmetry enforces gauge couplings and their supersymmetric Yukawa counterparts to be exactly equal at tree level. For example, the Yukawa coupling $\hat{g}_{\tilde{V}f\tilde{f}}$ between the gaugino partner $\tilde{V}$ of the vector boson V, the fermion f and the sfermion $\tilde{f}$ must be equal to the corresponding gauge coupling g_{Vff}.

The Yukawa couplings of selectrons can best be probed in the production of selectrons via the t-channel neutralino exchange contributions. For this purpose one can exploit the e^-e^- collider mode due to reduced background, larger production cross-sections, higher beam polarizability and no interfering s-channel contributions. Simulations have shown that these couplings can be determined with high accuracy [20, 32]. For example, errors for the extraction of the supersymmetric Yukawa couplings $\hat{g}_1$ and $\hat{g}_2$ (corresponding to the U(1) and SU(2) gauge couplings g_1

and g_2) are expected in the range $\delta\hat{g}_1/\hat{g}_1 \approx 0.2\%$ and $\delta\hat{g}_2/\hat{g}_2 \approx 0.8\%$. The values are for the SPS#1a scenario and integrated luminosity of 50 fb^{-1} of the e^-e^- collider running at $\sqrt{s} = 500\text{GeV}$, with no detector simulation included. Similar precision in the e^+e^- mode requires integrated luminosity of 500 fb^{-1}, see fig. 9.

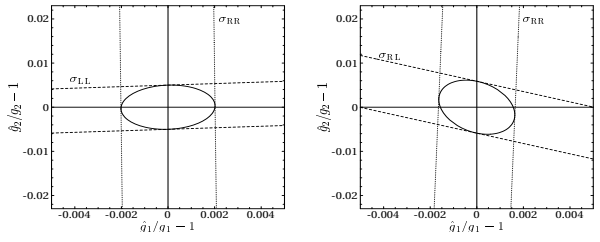

Figure 9: The 1σ bounds on the supersymmetric Yukawa couplings $\hat{g}_1$ and $\hat{g}_2$ in the SPS#1a scenario from e^-e^- with $\mathcal{L} = 50$ fb^{-1} (left) and e^+e^- with $\mathcal{L} = 500$ fb^{-1} (right), both running at $\sqrt{s} = 500$ GeV [32].

Such a high experimental precision requires radiative corrections to be included in the theoretical predictions for the slepton cross-sections. Far above threshold the effects of the non-zero slepton width are small, of the order $\Gamma_{\tilde{f}}/m_{\tilde{f}}$, and the production and decay of the sleptons can be treated separately. As mentioned, for both subprocesses the complete electroweak one-loop corrections in the MSSM have been computed [20, 21]. The electroweak corrections were found to be sizable, of the order of 5–10%. They include important effects from supersymmetric particles in the virtual corrections, in particular non-decoupling logarithmic contributions, e.g. terms $\propto \log m_{\tilde{f}}/m_{\rm weak}$ from fermion-sfermion-loops.

The equality of gauge and Yukawa couplings in the SU(3)$_{\rm C}$ gauge sector can be tested at a linear collider by investigating the associated production of quarks q and squarks $\tilde{q}$ with a gluon g or gluino $\tilde{g}$. While the processes $e^+e^- \to q\bar{q}g$ and $e^+e^- \to \tilde{q}\bar{\tilde{q}}g$ are sensitive to the strong gauge coupling of quarks and squarks, respectively, the corresponding Yukawa coupling can be probed in $e^+e^- \to q\bar{\tilde{q}}\tilde{g}$. In order to obtain reliable theoretical predictions for these cross-sections it is necessary to include next-to-leading order (NLO) supersymmetric QCD corrections. These corrections are generally expected to be rather large and they are necessary to reduce the large scale dependence of the leading-order result. The NLO QCD corrections to the process $e^+e^- \to q\bar{q}g$ within the Standard Model have been known for a long time. Recently, the complete $\mathcal{O}(\alpha_{\rm s})$ corrections to all three processes in the MSSM have been calculated [33]. The NLO contributions enhance the cross-section in the peak region by roughly 20% with respect to the LO result. Furthermore, the scale dependence is reduced by a factor of about six when the NLO corrections are included.

Mass universality

Most analyses are performed with a simplifying assumption of universal mass parameters at some high energy scale G: $\delta m^2(G) = m^2_{\tilde{l}_R}(G) - m^2_{\tilde{l}_L}(G)$=0. This assumption can be tested at the LC. For example, in [34] a quantity

$$\Delta^2 = m^2_{\tilde{e}_R} - m^2_{\tilde{e}_L} + \frac{m^2_{\tilde{\chi}^\pm_1}}{2\alpha_2^2}\left[\frac{3}{11}(\alpha_1^2 - \alpha_1^2(G)) - 3(\alpha_2^2 - \alpha_2^2(G))\right], \quad (7)$$

defined at the electroweak scale, is proposed as a probe of non-universality of slepton masses if only both selectrons and the light chargino are accessible at a linear collider (α_1 and α_2 are the U(1) and SU(2) couplings). It turns out that Δ^2 is strongly correlated with the slepton mass splitting, $\Delta^2 \sim 0.76\ \delta m^2(G)$. Assuming SUSY masses in the 150 GeV range to be measured with an experimental error of 1%, it has been found [34] that the non-universality can be detected for $|\delta m^2(G)| \geq 2500\,\text{GeV}^2$; knowing the gaugino mass M_2 to 1% increases the sensitivity down to $\delta m^2(G) = 1400\,\text{GeV}^2$.

Sfermions with complex CP phases

The soft SUSY breaking parameters: the gaugino masses and trilinear scalar couplings, and the Higgsino mass parameter μ, can in general be complex and the presence of non-trivial phases violates CP. This generalization is quite natural and is motivated by the analogy between fermions and sfermions: in the SM the CKM phase is quite large and the smallness of CP-violating observables results from the structure of the theory. Furthermore, large leptonic CP-violating phases together with leptogenesis may explain the baryonic asymmetry of the Universe.

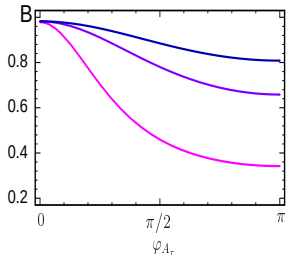

Figure 10: Branching ratios of $\tilde{\tau}_1 \to \tilde{\chi}^0_1\tau$ for $m_{\tilde{\nu}} = 233, 238, 243$ GeV (from bottom to top) [37].

In mSUGRA-type models the phase φ_μ of μ is restricted by the experimental data on electron, neutron and mercury electric dipole moments (EDMs) to a range $|\varphi_\mu| \lesssim 0.1$ – 0.2 if a universal scalar mass parameter $M_0 \lesssim 400$ GeV is assumed. However, the restriction due to the electron EDM can be circumvented if complex lepton flavour violating terms are present in the slepton sector [35]. The phases of the parameters $A_{\tilde{t},\tilde{b}}$ enter the EDM calculations only at two-loop level, resulting in much weaker constraints [36].

In the pure sfermionic sector the phases of $A_{\tilde{f}}$ and μ, eq. (3), enter the masses $m^2_{\tilde{f}_{1,2}}$ and mixing angle $\theta_{\tilde{f}}$ only through a term $m^2_{\tilde{f}}|A_{\tilde{f}}\mu|(\tan\beta)^{-2I^3_{\tilde{f}}}\cos(\varphi_{A_{\tilde{f}}} + \varphi_\mu)$.

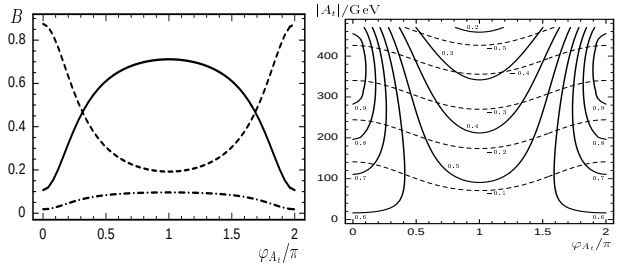

Figure 11: Left: Branching ratios of $\tilde{t}_1 \to \tilde{\chi}_1^+ b$ (solid), $\tilde{t}_1 \to \tilde{\chi}_1^0 t$ (dashed), $\tilde{t}_1 \to \tilde{\chi}_2^+ b$ (dashdotted). Right: Contours of $B(\tilde{t}_1 \to \tilde{\chi}_1^0 t)$ in the SPS#1a inspired scenario. The dashed lines denote the contours of $\cos\theta_{\tilde{t}}$ [38].

Therefore the $\tilde{t}_{1,2}$ masses are more sensitive to phases than masses of $\tilde{\tau}_{1,2}$ and $\tilde{b}_{1,2}$ because of the mass hierarchy of the corresponding fermions. The phase dependence of $\theta_{\tilde{f}}$ is strongest if $|A_{\tilde{f}}| \simeq |\mu|(\tan\beta)^{-2I_f^3}$ and $|m^2_{\tilde{f}_L} - m^2_{\tilde{f}_R}| \lesssim |a_{\tilde{f}} m_f|$ [37]. Since the $Z\tilde{f}_i\tilde{f}_i$ couplings are real, and for $\tilde{f}_1\bar{\tilde{f}}_2$ production only Z exchange contributes, the $\tilde{f}_i\bar{\tilde{f}}_j$ production cross sections do not explicitly depend on the phases – dependence enters only through the shift of sfermion masses and mixing angle. However, the various $\tilde{f}$ decay branching ratios depend in a characteristic way on the complex phases. This is illustrated in fig. 10, where branching ratios for $\tilde{\tau}_1$ are shown for $m_{\tilde{\tau}_1} = 240$ GeV, $\mu = 300$ GeV, $|A_{\tilde{\tau}}| = 1000$ GeV, $\tan\beta = 3$, and $M_2 = 200$ GeV [37]. The branching ratios for the light $\tilde{t}_1$ in the SPS#1a inspired scenario are shown in fig. 11, including the contour plot for the mixing angle $\cos\theta_{\tilde{t}}$ [38]. A simultaneous measurement of $B(\tilde{t}_1 \to \tilde{\chi}_1^0 t)$ and $\cos\theta_{\tilde{t}}$ might be helpful to disentangle the phase of $A_{\tilde{t}}$ from its absolute value. As an example a measurement of $B(\tilde{t}_1 \to \tilde{\chi}_1^0 t) = 0.6 \pm 0.1$ and $|\cos\theta_{\tilde{t}}| = 0.3 \pm 0.02$ would allow to determine $|A_{\tilde{t}}| \approx 320$ GeV with an error $\Delta(|A_{\tilde{t}}|) \approx 20$ GeV and $\varphi_{A_{\tilde{t}}}$ with a twofold ambiguity $\varphi_{A_{\tilde{t}}} \approx 0.35\pi$ or $\varphi_{A_{\tilde{t}}} \approx 1.65\pi$ with an error $\Delta(\varphi_{A_{\tilde{t}}}) \approx 0.1\pi$, see fig. 11 (right).

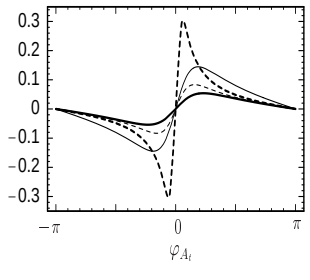

Figure 12: The CP sensitive asymmetry as a function of $\varphi_{A_{\tilde{t}}}$; $\tan\beta$=3 (thick), $\tan\beta$=10 (thin), μ=400 GeV (solid), μ=700 GeV (dashed) [39].

In principle, the imaginary parts of the complex parameters involved could most directly and unambiguously be determined by measuring suitable CP violating observables. For example, the polarization of the τ^+ normal to the $\tilde{t}_1$ decay plane in the decay $\tilde{t}_1 \to b\tilde{\nu}\tau^+$ is sensitive to CP violation. The asymmetry of the τ polarization perpendicular to the decay plane can go up to 30% for some SUSY parameter points where the decay $\tilde{t}_1 \to b\tilde{\nu}\tau^+$ has a sufficient branching ratio allowing for the measurement of this asymmetry, see fig. 12 where other parameters are taken as $m_{\tilde{t}_1} = 240$ GeV, $m_{\tilde{t}_2} = 800$ GeV, $m_{\tilde{\nu}} = 200$ GeV, $M_2 = 350$ GeV, $|A_{\tilde{t}}| = 1000$ GeV [39].

CP violation in the stau sector can generate electric and weak dipole moments of the taus. The CP-violating tau dipole form factors can be detected up to the level of $(3-5)\cdot 10^{-19} e\mathrm{cm}$ [40] at a linear collider with high luminosity and polarization of both e^+ and e^- beams. Although such a precision would improve the current experimental bounds by three orders of magnitude, it still remains by an order of magnitude above the expectations from supersymmetric models with CP-violation.

Lepton flavour violation

There are stringent constraints on lepton flavour violation (LFV) in the charged lepton sector, the strongest being $BR(\mu^- \to e^-\gamma) < 1.2 \times 10^{-11}$ [41]. However, neutrino oscillation experiments have established the existence of LFV in the neutrino sector with $\tan^2\theta_{Atm} \simeq 1$, $\tan^2\theta_\odot = 0.24 - 0.89$ and $\sin^2(2\theta_{13}) \lesssim 0.1$ [42].

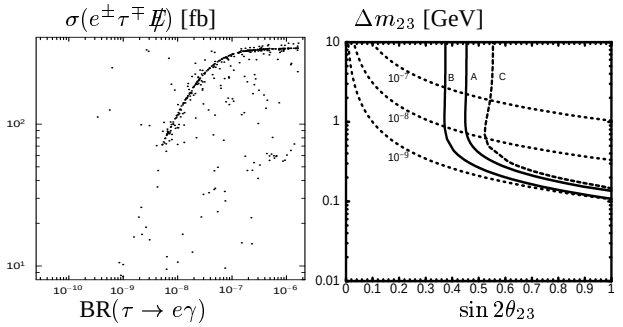

Figure 13: Left: Cross section for the signal $e^\pm\tau^\mp\not{E}$ as a function of BR($\tau \to e\gamma$) for $\sqrt{s} = 500$ GeV [45]. Right: 3σ significance contours for $\sqrt{s}$ =500 GeV and $\int \mathcal{L}$= 500 fb^{-1} (A), =1000 fb^{-1} (B). Line C: $\tilde{\nu}\tilde{\nu}^*$ contribution with luminosity 500 fb^{-1}. Dotted lines: BR($\tau \to \mu\gamma$)=10^{-7}, 10^{-8}, 10^{-9} [46].

In the MSSM the R–parity symmetry forces total lepton number conservation but still allows the violation of individual lepton number, e.g. due to loop effects in $\mu^- \to e^-\gamma$ [43]. Moreover, a large ν_μ-ν_τ mixing can lead to a large $\tilde{\nu}_\mu$-$\tilde{\nu}_\tau$ mixing via renormalization group equations. Therefore one can expect clear LFV signals in slepton and sneutrino production and in the decays of neutralinos and charginos into sleptons and sneutrinos at future colliders [44].

For the reference point SPS#1a a scan over the flavour non-diagonal ($i \neq j$) entries of slepton mass matrix eq. (2) shows [45] that values for $|M^2_{R,ij}|$ up to $8 \cdot 10^3$ GeV^2, $|M^2_{L,ij}|$ up to $6 \cdot 10^3$ GeV^2 and $|A_{ij} v_d|$ up to 650 GeV^2 are compatible with the current experimental constraints. In most cases, one of the mass squared parameters is at

least an order of magnitude larger than the others. However, there is a sizable part in parameter space where at least two of the off-diagonal entries have the same order of magnitude.

Possible LFV signals at an e^+e^- collider include $e\mu \not{E}$, $e\tau \not{E}$, $\mu\tau \not{E}$ in the final state plus a possibility of additional jets. In fig. 13 the cross section of $e^+e^- \to e^\pm\tau^\mp \not{E}$ at $\sqrt{s} = 500$ GeV versus BR($\tau \to e\gamma$) is shown for points consistent with the experimental LFV data which are randomly generated in the range $10^{-8} \leq |A_{ij}| \leq 50$ GeV, $10^{-8} \leq M_{ij}^2 \leq 10^4$ GeV^2. The accumulation of points along a band is due to a large $\tilde{e}_R$-$\tilde{\tau}_R$ mixing which is less constrained by $\tau^- \to e^-\gamma$ than the corresponding left-left or left-right mixing.

Note that the collider LFV signals can be very competitive to those from rare charged lepton decay, like $\tau \to \mu\gamma$. This is illustrated in fig. 13, where for simplicity the LFV has been restricted to the 2-3 generation subspace of sneutrinos with the mixing angle θ_{23} and $\Delta m_{23} = |m_{\tilde{\nu}_2} - m_{\tilde{\nu}_3}|$ as free parameters. [46].

Sgoldstinos

In the GMSB SUSY, not only the mass splittings Δm^2, but also the supersymmetry-breaking scale $\sqrt{F}$ is close to the weak scale: $G_F^{-1/2} \sim \Delta m^2 \lesssim \sqrt{F}$. Then the gravitino $\tilde{G}$ becomes very light, with $m_{\tilde{G}} = F/\sqrt{3}M_P' = F/(10\text{ TeV})^2 \times 0.03$ eV. The appropriate effective low-energy theory must then contain, besides the goldstino, also its supersymmetric partners, called sgoldstinos [47]. The spin-0 complex component of the chiral goldstino superfield has two degrees of freedom, giving rise to two sgoldstino states: a CP-even state S and a CP-odd state P. In the simplest case it is assumed that there is no sgoldstino-Higgs mixing, and that squarks, sleptons, gluinos, charginos, neutralinos and Higgs bosons are sufficiently heavy not to play a rôle in sgoldstino production and decay. Thus the S and P are mass eigenstates and, being R–even, they can be produced singly together with the SM particles.

During the Workshop new results on massive sgoldstino production at e^+e^- and $\gamma\gamma$ colliders have been presented [48]. The most interesting channels for the production of such scalars (ϕ will be used to indicate a generic state) are the process $e^+e^- \to \phi\gamma$, and the fusion $\gamma\gamma \to \phi$, followed by the ϕ decay to photons or gluons.

The $e^+e^- \to \phi\gamma \to gg\gamma$ process gives rise to events with one monochromatic photon and two jets. However, the brems- and beamstrahlung induces a photon energy smearing comparable to or larger than the experimental resolution. On the other hand, the signal can be searched for directly in the jet-jet invariant mass distribution. Results of the simulation are presented in fig. 14 where the exclusion region at the 95% CL is shown in the m_ϕ–$\sqrt{F}$ plane for two parameter sets: 1) M_1 = 200 GeV, M_2 = 300 GeV, M_3 = 400 GeV, 2) $M_1 = M_2 = M_3$ = 350 GeV.

For the $\gamma\gamma$ collider, despite the smaller decay branching ratio, only the two-photon final state has been considered

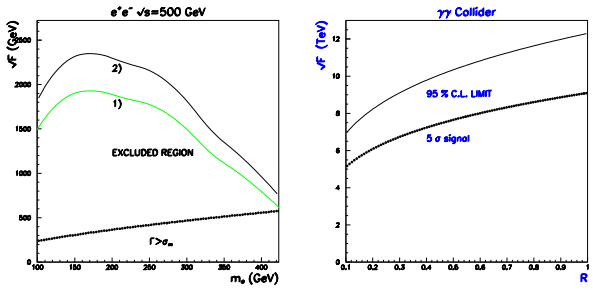

Figure 14: Left: Exclusion region at 95% CL at a 500 GeV e^+e^- collider. Right: Exclusion region at 95% CL and 5σ discovery at a $\gamma\gamma$ collider [48].

since it has a very little SM background. Taking as a reference point the value $(\sigma B)_0$ obtained for $M_{\gamma\gamma} = 350$ GeV and a 10% branching ratio to two photons, the 95 % CL exclusion limit on and the 5 σ discovery line for $\sqrt{F}$ is shown in fig. 14 in terms of the ratio $R = \sigma \times BR(\phi \to \gamma\gamma)/(\sigma B)_0$. Thus the sensitivity at a photon collider obtained from the same electron-positron beam energy is expected to be much higher for $m_\phi \sim 300 - 400$ GeV.

GAUGINOS AND HIGGSINOS

Supersymmetric partners of electroweak gauge and Higgs bosons mix due to the gauge symmetry breaking. The mass-eigenstates (with positive mass eigenvalues) are charginos ($\tilde{\chi}_i^\pm$, i=1,2, mixtures of the wino and charged higgsino) and neutralinos ($\tilde{\chi}_i^0$, i=1,2,3,4, mixtures of $\tilde{B}$, $\tilde{W}^3$, $\tilde{H}_1^0$ and $\tilde{H}_2^0$). At tree level the chargino sector depends on M_2, μ and $\tan\beta$; the neutralino sector depends in addition on M_1. The gaugino and higgsino mass parameters can be complex; without loss of generality M_2 can be assumed real and positive, and the non-trivial CP-violating phases may be attributed to $\mu = |\mu|e^{i\varphi_\mu}$ and $M_1 = |M_1|e^{i\varphi_1}$. The chargino mass matrix is diagonalized by two unitary matrices acting on left- and right-chiral weak eigenstates (parameterized by two mixing angles $\phi_{L,R}$ and three CP phases $\beta_{L,R}$ and γ) [49, 50]. The neutralino mass matrix is diagonalized by a 4×4 unitary rotation N parameterized in terms of 6 angles and 9 phases (three Majorana α_i and six Dirac β_{ij} phases) [51, 52]

$$N = \text{diag}\{1,\, \mathrm{e}^{i\alpha_1}, \mathrm{e}^{i\alpha_2}, \mathrm{e}^{i\alpha_3}\}\mathrm{R}_{34}\,\mathrm{R}_{24}\,\mathrm{R}_{14}\,\mathrm{R}_{23}\,\mathrm{R}_{13}\,\mathrm{R}_{12} \tag{8}$$

where R_{jk} are rotations in the $[jk]$ plane characterized by a mixing angle θ_{jk} and a (Dirac) phase β_{jk}.

Charginos and neutralinos are produced in pairs

$$e^+e^- \quad \to \quad \tilde{\chi}_i^+\tilde{\chi}_j^-, \quad \tilde{\chi}_i^0\tilde{\chi}_j^0 \tag{9}$$

via s-channel γ/Z and t-channel $\tilde{\nu}_e$ exchange for $\tilde{\chi}^\pm$, and via s-channel Z and t- and u-channel $\tilde{e}$ exchange for $\tilde{\chi}^0$ production. Beam polarizations are very important to study the $\tilde{\chi}$ properties and couplings. The polarized differential

cross section for the $\tilde{\chi}_i\tilde{\chi}_j$ production can be written as [52]

$$\frac{\mathrm{d}\sigma^{\{ij\}}}{\mathrm{d}\cos\theta\,\mathrm{d}\phi} = \frac{\alpha^2\lambda^{1/2}}{16\,s}[(1-P_l\bar{P}_l)\Sigma_u + (P_l-\bar{P}_l)\Sigma_l + P_t\bar{P}_t\cos(2\phi-\eta)\Sigma_t + P_t\bar{P}_t\sin(2\phi-\eta)\Sigma_n] \quad (10)$$

where $\lambda = [1-(\mu_i+\mu_j)^2][1-(\mu_i-\mu_j)^2]$ is the two–body phase space function with $\mu_i = m_{\tilde{\chi}_i^0}/\sqrt{s}$, P=$(P_t, 0, P_l)$ [$\bar{P}$=$(\bar{P}_t\cos\eta, \bar{P}_t\sin\eta, -\bar{P}_l)$] is the electron [positron] polarization vector; the electron–momentum direction defines the z–axis and the electron transverse polarization–vector the x–axis. The coefficients Σ_u, Σ_l, Σ_t and Σ_n depend only on the polar angle θ and their explicit form is given in [50] for charginos, and in [52] for neutralinos. The Σ_n, present only for non-diagonal neutralino production, is particularly interesting because it is non-vanishing only in the CP-violating case.

Given the high experimental precision in mass and cross section measurements expected at the LC, the radiative corrections will have to be applied to the above expressions. Recently full one-loop corrections to chargino and neutralino sector have been calculated [21, 53, 54, 55]. The numerical analysis based on a complete one loop calculation has shown that the corrections to the chargino and neutralino masses can go up to 10% and the change in the gaugino and higgsino components can be in the range of 30%, and therefore will have to be taken into account.

Charginos

Experimentally the chargino masses can be measured very precisely at threshold since the production cross section for spin 1/2 Dirac fermions rises as β leading to steep excitation curves. Results of a simulation for the reaction $e^+_Re^-_L \to \tilde{\chi}_1^+\tilde{\chi}_1^- \to \ell^\pm\nu_\ell\tilde{\chi}_1^0\,q\bar{q}'\tilde{\chi}_1^0$, fig. 15, show that the mass resolution is excellent of $\mathcal{O}(50\ \mathrm{MeV})$, degrading to the per mil level for the higher $\tilde{\chi}_2^\pm$ state. Above threshold, from the di-jet energy distribution one expects a mass resolution of $\delta m_{\tilde{\chi}_1^\pm} = 0.2$ GeV, while the di-jet mass distributions constrains the $\tilde{\chi}_1^\pm - \tilde{\chi}_1^0$ mass splitting within about 100 MeV. Since the chargino production cross sections are

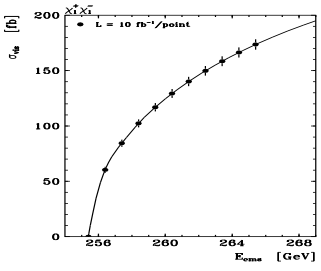

Figure 15: Cross section for $e^+_Re^-_L \to \tilde{\chi}_1^+\tilde{\chi}_1^- \to \ell^\pm\nu_\ell\tilde{\chi}_1^0\,q\bar{q}'\tilde{\chi}_1^0$ at threshold (in the RR 1 scenario [1, 25], errors for $10\ \mathrm{fb}^{-1}$ per point).

simple binomials of $\cos 2\phi_{L,R}$, see fig. 16, the mixing angles can be determined in a model independent way using polarized electron beams [56].

Once masses and mixing angles are measured, the fundamental SUSY parameters of the chargino sector can be

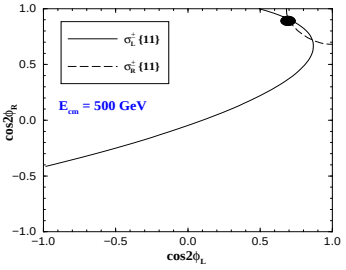

Figure 16: Contours of $\sigma(\tilde{\chi}_1^+\tilde{\chi}_1^-)$ with polarized beams in the plane $[\cos 2\phi_L, \cos 2\phi_R]$ [56].

extracted to lowest order in analytic form [56, 57]

$$M_2 = M_W[\Sigma - \Delta[\cos 2\phi_R + \cos 2\phi_L]]^{1/2} \quad (11)$$

$$|\mu| = M_W[\Sigma + \Delta[\cos 2\phi_R + \cos 2\phi_L]]^{1/2} \quad (12)$$

$$\cos\Phi_\mu = [\Delta^2 - (M_2^2-\mu^2)^2 - 4m_W^2(M_2^2+\mu^2) - 4m_W^4\cos^2 2\beta]/8m_W^2M_2|\mu|\sin 2\beta \quad (13)$$

$$\tan\beta = \left[\frac{1+\Delta(\cos 2\phi_R - \cos 2\phi_L)}{1-\Delta(\cos 2\phi_R - \cos 2\phi_L)}\right]^{1/2} \quad (14)$$

where $\Delta = (m^2_{\tilde{\chi}_2^\pm} - m^2_{\tilde{\chi}_1^\pm})/4M_W^2$ and $\Sigma = (m^2_{\tilde{\chi}_2^\pm} + m^2_{\tilde{\chi}_1^\pm})/2M_W^2 - 1$. However, if $\tilde{\chi}_2^\pm$ happens to be beyond the kinematic reach at an early stage of the LC, it depends on the CP properties of the higgsino sector whether they can uniquely be determined in the light chargino system alone:

(i) If μ is real, $\cos\Phi_\mu = \pm 1$ determines $m_{\tilde{\chi}_2^\pm}$ up to at most a two–fold ambiguity [50]; this ambiguity can be resolved if other observables can be measured, e.g. the mixed–pair $\tilde{\chi}_1^0\tilde{\chi}_2^0$ production cross sections.

(ii) In a CP non–invariant theory with complex μ, the parameters in eqs.(11–14) depend on the unknown heavy chargino mass $m_{\tilde{\chi}_2^\pm}$. Two solutions in the $\{M_2, \mu, \tan\beta\}$ space are parameterized by $m_{\tilde{\chi}_2^\pm}$ and classified by the two possible signs of $\sin\Phi_\mu$. The unique solution can be found with additional information from the two light neutralino states $\tilde{\chi}_1^0$ and $\tilde{\chi}_2^0$, as we will see in the next section.

The above methods fail for the light chargino if it happens to be nearly mass-degenerate with the lightest neutralino, as predicted in a typical AMSB scenario. In this case $\tilde{\chi}_1^\pm \to \tilde{\chi}_1^0 +$ *soft pion*, and very little activity is seen in the final state. However, one can exploit the ISR photons in $e^+e^- \to \tilde{\chi}_1^+\tilde{\chi}_1^-\gamma$ to measure both $m_{\tilde{\chi}_1^\pm}$ and the mass splitting $\tilde{\chi}_1^\pm - \tilde{\chi}_1^0$ [58]. The ISR photon recoil mass spectrum starts to rise at $2m_{\tilde{\chi}_1^\pm}$ allowing to determine the chargino mass at a percent level, fig. 17. Moreover, the pion energy spectrum for events with charginos produced nearly at rest peaks around $\tilde{\chi}_1^\pm - \tilde{\chi}_1^0$ and again precision of order 2 percent is expected.

Besides the e^+e^- option, chargino pair production

$$\gamma\gamma \to \tilde{\chi}_i^+\tilde{\chi}_i^-(i=1,2) \quad (15)$$

in the $\gamma\gamma$ mode of a Linear Collider has been studied [59]. In this case the production is a pure QED process (at tree level) and therefore it allows the chargino decay mechanism to be studied separately in contrast to the e^+e^- mode

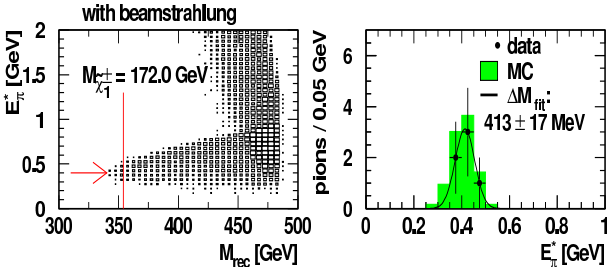

Figure 17: The ISR photon recoil mass and the pion energy scatter plot (left), and the pion energy spectrum across the red line (right) for $e^+_R e^-_L \to \tilde\chi^+_1 \tilde\chi^-_1 \gamma \to \pi^+\pi^-\gamma \not{E}$ [58].

where both production and decay are sensitive to the SUSY parameters.

Provided the chargino mass has been measured and the energy spectrum and polarization of the high energy photons are well under control, the production cross section and the polarization of the charginos in reaction eq. (15) are uniquely predicted. By manipulating the polarization of the laser photons and the converted electron beam various characteristics of the chargino decay can be measured and exploited to study the gaugino system. As an example, in [59] the forward-backward asymmetry (measured with respect to the e^+e^- beam direction)

$$A_{\rm FB} = \frac{\sigma_e(\cos\theta_{e^+} > 0) - \sigma_e(\cos\theta_{e^+} < 0)}{\sigma_e(\cos\theta_{e^+} > 0) + \sigma_e(\cos\theta_{e^+} < 0)} \qquad (16)$$

of the positron from the decay $\tilde\chi^+_1 \to \tilde\chi^0_1 e^+ \nu_e$, shown in fig. 18, has been studied to determine M_1 and $m_{\tilde\nu_e}$.

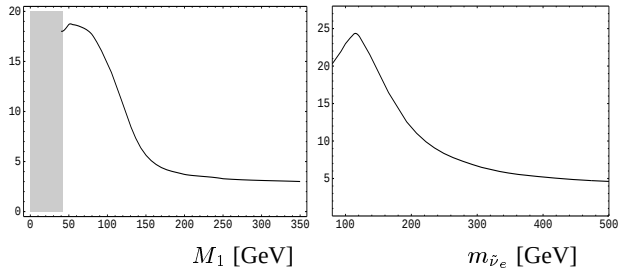

Figure 18: The e^+ forward-backward asymmetry (in %) in the ee-CMS of the decay positron from $\gamma\gamma \to \tilde\chi^+_1\tilde\chi^-_1$, $\tilde\chi^+_1 \to \tilde\chi^0_1 e^+\nu_e$ as a function of the parameter M_1 (left) and the sneutrino mass $m_{\tilde\nu_e}$ (right) at $\sqrt{s_{ee}} = 500$ GeV for $M_2 = 152$ GeV, $\mu = 316$ GeV, $\tan\beta = 3$. The shadowed region corresponds to the bound $m_{\tilde\chi^0_1} > 38$ GeV [59].

Neutralinos

Similarly to the chargino case, the di-lepton energy and mass distributions in the reaction $e^+e^- \to \tilde\chi^0_2\tilde\chi^0_2 \to 4\ell^\pm \not{E}$ can be used to determine $\tilde\chi^0_1$ and $\tilde\chi^0_2$ masses. Previous analyses of the di-lepton mass and di-lepton energy spectra performed in the $\tan\beta = 3$ case showed that uncertainties in the primary and secondary $\tilde\chi^0_2$ and $\tilde\chi^0_1$ masses of about 2 per mil can be expected [1, 25]. Higher resolution of order 100 MeV for $m_{\tilde\chi^0_2}$ can be obtained from a threshold scan of $e^+e^- \to \tilde\chi^0_2\tilde\chi^0_2$; heavier states $\tilde\chi^0_3$ and $\tilde\chi^0_4$, if accessible, can still be resolved with a resolution of a few hundred MeV. For the higher values of $\tan\beta \gtrsim 10$ the dominant decay mode of $\tilde\chi^0_2$ is to $\tau^+\tau^-\tilde\chi^0_1$. With τ's decaying in the final state the experimental selection of the signal from the SM and SUSY background becomes more difficult. Preliminary analyses nevertheless show [60] that an accuracy of 1-2 GeV for the mass determination seems possible from the process $e^+e^- \to \tilde\chi^0_1\tilde\chi^0_2$.

To resolve the light chargino case in the CP-violating scenario (ii) discussed in the previous section, we note that each neutralino mass $m_{\tilde\chi^0_i}$ satisfies the characteristic equation

$$(\Re{\rm e}M_1)^2 + (\Im{\rm m}M_1)^2 + u_i\,\Re{\rm e}M_1 + v_i\,\Im{\rm m}M_1 = w_i \qquad (17)$$

where u_i, v_i, w_i are functions of $m_{\tilde\chi^0_i}$, M_2, μ, $\tan\beta$; since physical masses are CP-even, v_i is necessarily proportional to $\sin\varphi_\mu$. Therefore each neutralino mass defines a circle in the $\{\Re{\rm e}M_1, \Im{\rm m}M_1\}$ plane, assuming other parameters fixed. With two light neutralino masses two crossing points in the ($\Re{\rm e}M_1$, $\Im{\rm m}M_1$) plane are found, fig. 19 (left). Since from the chargino sector $\{M_2, \mu\ \tan\beta\}$ are parameterized by the unknown $m_{\tilde\chi^\pm_2}$, the crossing points will migrate with $m_{\tilde\chi^\pm_2}$, fig. 19 (right). Using the measured cross section for $\tilde\chi^0_1\tilde\chi^0_2$, a unique solution for M_1 is obtained and the heavy chargino mass predicted. If the LC would run concurrently with the LHC, the LHC experiments might be able to verify the predicted value of $m_{\tilde\chi^\pm_2}$.

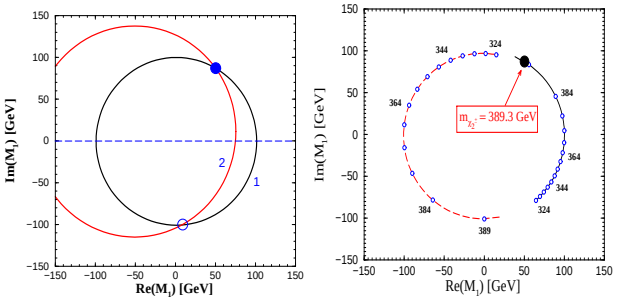

Figure 19: Two crossing points determined by two light neutralinos (left) and their migration with $m_{\tilde\chi^\pm_2}$ (right) [56].

Neutralinos with CP-violating phases

Particularly interesting is the threshold behavior since due to the Majorana nature of neutralinos [52], a clear indication of non–zero CP violating phases can be provided by studying the excitation curve for non–diagonal neutralino pair production near thresholds.

Like in the quark sector, it is useful [52, 61] to represent the unitarity constraints

$$M_{ij} = N_{i1}N^*_{j1} + N_{i2}N^*_{j2} + N_{i3}N^*_{j3} + N_{i4}N^*_{j4} \qquad (18)$$
$$D_{ij} = N_{1i}N^*_{1j} + N_{2i}N^*_{2j} + N_{3i}N^*_{3j} + N_{4i}N^*_{4j} \qquad (19)$$

on the neutralino mixing matrix N, eq. (8), in terms of unitarity quadrangles. For $i \neq j$ we get M_{ij}=D_{ij}=0 and the above equations define two types of quadrangles in the complex plane. The M-type quadrangles are formed by the sides $N_{ik}N^*_{jk}$ connecting two rows i and j, eq. (18), and the D-type by $N_{ki}N^*_{kj}$ connecting two columns i and j, eq. (19), of the mixing matrix. By a proper ordering of sides the quadrangles are assumed to be convex with areas

$$\text{area}[M_{ij}] = \tfrac{1}{4}(|J^{12}_{ij}| + |J^{23}_{ij}| + |J^{34}_{ij}| + |J^{41}_{ij}|) \quad (20)$$

$$\text{area}[D_{ij}] = \tfrac{1}{4}(|J^{ij}_{12}| + |J^{ij}_{23}| + |J^{ij}_{34}| + |J^{ij}_{41}|) \quad (21)$$

where J^{kl}_{ij} are the Jarlskog–type CP–odd "plaquettes" [62]

$$J^{kl}_{ij} = \Im\text{m} N_{ik} N_{jl} N^*_{jk} N^*_{il} \quad (22)$$

Note that plaquettes, and therefore the areas of unitarity quadrangles, are not sensitive to the Majorana phases α_i. Unlike in the quark or lepton sector, the orientation of all quadrangles is physically meaningful, and determined by the CP-phases of the neutralino mass matrix.

For a CP-conserving case with real M_1, M_2 and μ, the neutralino mixing matrix N has all Dirac phases $\beta_{ij} = 0$ mod π and Majorana phases $\alpha_i = 0$ mod $\pi/2$. Majorana phases $\alpha_i = \pm\pi/2$ describe only different CP parities of the neutralino states. In terms of quadrangles, CP is conserved if and only if all quadrangles have null area (collapse to lines or points) *and* are oriented along either the real or the imaginary axis.

The non–zero values of CP-odd quantities, like Σ_n or the polarization of the produced neutralino normal to the production plane, would unambiguously indicate CP-violation in the neutralino sector. In [63] the CP-odd asymmetry defined as

$$\mathcal{A} = \frac{\sigma(T > 0) - \sigma(T < 0)}{\sigma(T > 0) + \sigma(T < 0)} \quad (23)$$

where $T = \vec{p}(e^-) \times \vec{p}(l_1) \cdot \vec{p}(l_2)$ for the process $e^+e^- \to \tilde{\chi}^0_1\tilde{\chi}^0_2 \to \tilde{\chi}^0_1\tilde{\chi}^0_1 l_1 l_2$ with two visible leptons in the final state has been considered. In fig. 20 the expected cross section (left) and the asymmetry (right) are shown as functions of M_2 and μ assuming $\varphi_1 = \pi/2$.

One can also try to identify the presence of CP-phases by studying their impact on CP-even quantities, like neutralino masses, branching ratios etc. Since these quantities are non–zero in the CP-conserving case, the detection of CP-odd phases will require a careful quantitative analysis of a number of physical observables [64], in particular for numerically small CP-odd phases. For example, fig. 21 displays the unitarity quadrangles for the SPS#1a point assuming a small non-vanishing phase $\varphi_1 = \pi/5$ (consistent with all experimental constraints) [65]. The quadrangles are almost degenerate to lines parallel to either the real or the imaginary axis, and revealing a small phase of M_1 will be quite difficult. However, studying the threshold behavior of the production cross sections can be of great help [52, 65].

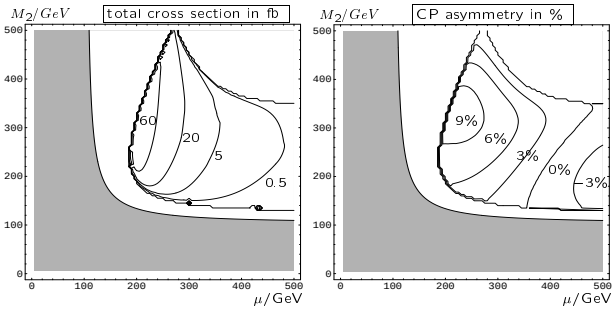

Figure 20: Cross section (left) and CP-odd asymmetry for $e^+e^- \to \tilde{\chi}^0_1\tilde{\chi}^0_2 \to \tilde{\chi}^0_1\tilde{\chi}^0_1 l_1 l_2$ at $\sqrt{s}$=500 GeV with m_0=100 GeV, $\tan\beta$=10 and gaugino mass universality. In shaded area $m_{\tilde{\chi}^\pm_1}$ <104 GeV [63].

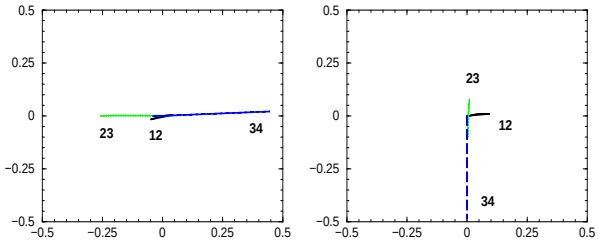

Figure 21: The D–type (left panel) and M–type (right panel) quadrangles in the complex plane, illustrated for $\tan\beta = 10$, $|M_1| = 100.5$ GeV, $\varphi_1 = \pi/5$, $M_2 = 190.8$ GeV, $|\mu| = 365.1$ GeV and $\varphi_\mu = 0$; ij as indicated in the figure [65].

If CP is conserved, the CP parity of a pair of Majorana fermions $\tilde{\chi}^0_i\tilde{\chi}^0_j$ produced in the static limit in e^+e^- collisions by a spin-1 current with positive intrinsic CP must satisfy the relation

$$\eta^i \eta^j (-1)^L = 1 \quad (24)$$

where $\eta^i = \pm i$ is the intrinsic CP parity of $\tilde{\chi}^0_i$ and L is the angular momentum [66]. Therefore neutralinos with the same CP parities (for example $i = j$) can only be excited in P-wave. The S-wave excitation, with the characteristic steep rise $\sim \beta$ of the cross section near threshold, can occur only for $i \neq j$ with opposite CP–parities of the produced neutralinos [67]. This immediately implies that if the $\{ij\}$ and $\{ik\}$ pairs are excited in the S–wave, the pair $\{jk\}$ must be excited in the P–wave characterized by the slow rise β^3 of the cross section, fig. 22, left panel.

If CP is violated, however, the angular momentum of the produced neutralino pair is no longer restricted by the eq. (24) and all non–diagonal pairs can be excited in the S–wave. This is illustrated in fig. 22, where the threshold behavior of the neutralino pairs $\{12\}$, $\{13\}$ and $\{23\}$ for the CP-conserving (left panel) case is contrasted to the CP-violating case (right panel). Even for a small CP–phase $\varphi_1 = \pi/5$, virtually invisible in the shape and orientation of unitarity quadrangles in fig. 21, the change in the energy

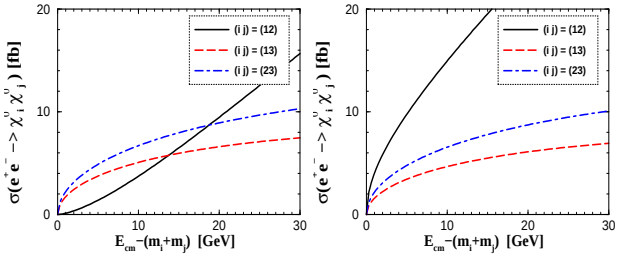

Figure 22: The threshold behavior of the neutralino production cross–sections $\sigma^{\{ij\}}$ for the CP–conserving (left panel) and the CP–violating (right panel) cases. Other parameters as in fig. 21 [65].

dependence near threshold can be quite dramatic. Thus, observing the $\{ij\}$, $\{ik\}$ and $\{jk\}$ pairs to be excited *all* in S–wave states would therefore signal CP–violation.

Gluinos

Strongly interacting gluinos will copiously be produced at the LHC. Only for rather light gluinos, $m_{\tilde{g}} \sim 200 - 300$ GeV, can a 1 TeV LC improve on the LHC gluino mass measurement.

In e^+e^- annihilation the exclusive production of gluino pairs proceeds only at the loop level: s-channel photons and Z^0 bosons couple to the gluinos via triangular quark and squark loops. Moreover, near threshold the pairs of identical Majorana gluinos are excited in a P-wave with a slow rise of the cross section. As a result, the production cross sections are rather small even for relatively light gluinos, see left panel of fig. 23. For $m_{\tilde{g}} \gtrsim 500$ GeV, no events at LC with luminosities of 1 ab^{-1} per year are expected irrespectively of their collision energy.

In the $\gamma\gamma$ option, the chances to observe gluinos are better. First, the gluino pairs can be excited in an S-wave with a faster rise of the cross section. Second, for $m_{\tilde{q}} \gg m_{\tilde{g}}$ the production can be enhanced by resolved photons. As seen in the right panel of fig. 23, the production cross sections in the polarized e^-e^- option can reach several fb in a wider range of gluino masses.

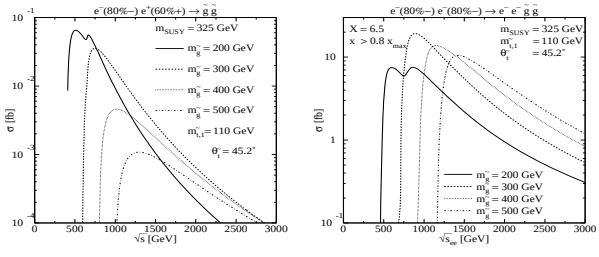

Figure 23: Gluino production cross section in e^+e^- annihilation (left), and in polarized direct photon collisions generated in e^-e^- (right). [68].

R–PARITY VIOLATING SUSY

In the MSSM the multiplicative quantum number R–parity is conserved. Under this symmetry all standard model particles have $R_p = +1$ and their superpartners $R_p = -1$. As a result, the lightest SUSY particle (LSP) is stable, SUSY particles are only produced in pairs with the distinct signature of missing energy in an experiment. However, R–parity conservation has no strong theoretical justification since the superpotential admits explicit R–parity violating ($\not{R}_p$) terms

$$W_{\not{R}_p} = \epsilon_i L_i H_u + \tfrac{1}{2}\lambda_{ijk} L_i L_j \bar{D}_k + \lambda'_{ijk} L_i Q_j \bar{D}_k + \tfrac{1}{2}\lambda''_{ijk} \bar{U}_i \bar{D}_j \bar{D}_k \quad (25)$$

where H_u, L, Q are the Higgs and left–handed lepton and squark superfields, and $\bar{E}, \bar{D}, \bar{U}$ are the corresponding right–handed fields. R–parity violation changes the SUSY phenomenology drastically. The LSP decays, so the characteristic signature of missing energy in the R_p conserving MSSM is replaced by multi–lepton and/or multi–jet final states.

The couplings ϵ, λ and λ' violate lepton number, while λ'' violate baryon number. If both types of couplings were present, they would induce fast proton decay. This can be avoided by assuming at most one type of couplings to be non-vanishing.

Bilinear R–parity violation

Models with explicit bilinear breaking of R–parity (BRpV) assume only $\epsilon_i \neq 0$ in eq. (25) and the corresponding terms in the soft SUSY breaking part of the Lagrangian $\mathcal{L}_{soft} \ni B_i \epsilon_i \tilde{L}_i H_u$ [69]. As a result, the sneutrinos develop non-zero vacuum expectation $v_i = \langle \tilde{\nu}_i \rangle$ in addition to the VEVs v_u and v_d of the MSSM Higgs fields H_u^0 and H_d^0. The bilinear parameters ϵ_i and v_i induce mixing between particles that differ only by R–parity: charged leptons mix with charginos, neutrinos with neutralinos, and Higgs bosons with sleptons. Mixing between the neutrinos and the neutralinos generates at tree level a non-zero mass $m_{\nu_3} \sim M_2 |\vec{\Lambda}|^2 / \mathrm{Det}(M_{\tilde{\chi}^0})$ (where $\Lambda_i = \epsilon_i v_d + \mu v_i$) for one of the three neutrinos and the mixing angle $\tan^2 \theta_{atm} \sim (\Lambda_2/\Lambda_3)^2$; the remaining two masses and mixing angles are generated at 1-loop. For example, the solar mixing angle scales as $\tan^2 \theta_{sol} \sim (\epsilon_1/\epsilon_2)^2$. Thus the model can provide a simple and calculable framework for neutrino masses and mixing angles in agreement with the experimental data, and at the same time leads to clear predictions for the collider physics [70].

For small $\not{R}_p$ couplings, production and decays of SUSY particles is as in the MSSM except that the LSP decays. Since the astrophysical constraints on the LSP no longer apply, a priori *any* SUSY particle could be the LSP. In a recent study [71] a sample of the SUSY parameter space with $\not{R}_p$ couplings consistent with neutrino masses shows that irrespectively of the LSP nature, there is always at least one correlation between ratios of LSP decay branching ratios

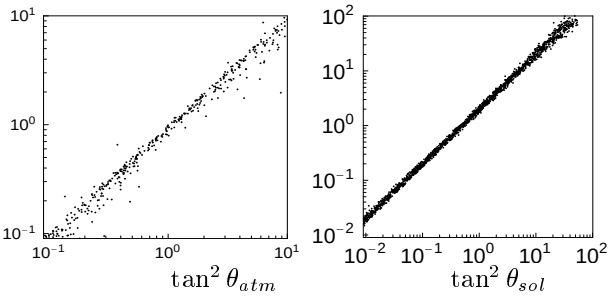

Figure 24: Left: BR($\tilde{\chi}_1^+ \to \mu^+ q\bar{q}$)/BR($\tilde{\chi}_1^+ \to \tau^+ q\bar{q}$) as a function of $\tan^2\theta_{atm}$. Right: BR($\tilde{b}_1 \to e^+ t$)/BR($\tilde{b}_1 \to \mu^+ t$) as a function of $\tan^2\theta_{sol}$ [71].

and one of the neutrino mixing angles. Two examples of chargino and squark being the LSP are shown in fig. 24.

Bilinear versus Trilinear $\not{R}_p$

In the case of charged slepton LSP, the collider physics might distinguish whether bilinear or trilinear couplings are dominant sources of $\not{R}_p$ and the neutrino mass matrix [72]. Possible final states of the LSP are either $l_j\nu_k$ or $q\bar{q}'$. If the LSP is dominantly right-chiral, the former by far dominate over the hadronic decay mode. In the case of TRpV, the two-body decay width for $\tilde{l}_i \to l_j + \Sigma_k \nu_k$ scales as $\Gamma \sim \Sigma_k \sin^2\theta_{l_i} \lambda^2_{kji}$ provided $\lambda' \lesssim \lambda$, while for the BRpV one has $\Gamma \sim Y_i \sin^2\theta_{l_i} \epsilon_j^2$ for $i \neq j$ (Y_i is the corresponding Yukawa coupling), and BR($\tilde{e}_1 \to e\Sigma_k\nu_k$) ~ 1. Immediately one finds then

$$\mathrm{BR}(\tilde{e}_1 \to e\Sigma_k\nu_k) = \begin{cases} \sim 1 & \text{for BRpV} \\ \lesssim 0.5 & \text{for TRpV} \end{cases} \qquad (26)$$

Therefore, the LC measurements of the $\tilde{l}_i$ decay modes can distinguish between bilinear or trilinear terms as dominant contributions to the neutrino masses [72].

For trilinear couplings of the order of current experimental upper bounds, in particular for the third generation (s)fermions, additional production as well as decay channels may produce strikingly new signatures. For example, sneutrinos could be produced as an s-channel resonance in e^+e^- annihilation. During this workshop single sneutrino production in association with fermion pairs at polarised photon colliders has been analysed [73]. The associate mode may also appear with fermions of different flavour [74], so that the signal is basically SM background free. Moreover, the advantage of exploiting $\gamma\gamma$ collisions in place of e^+e^- ones in producing single sneutrinos with a fermion pair of differnt flavour resides in the fact that the cross sections for the former are generally larger than those for the latter. As an example, fig. 25 shows the unpolarised production rates for both the $\gamma\gamma$ and e^+e^- induced $\tilde{\nu}\tau^\pm\mu^\mp$ modes at $\sqrt{s_{e^+e^-}} = 500$ GeV and 1 TeV. For illustration, the couplings are set $\lambda = \lambda' = 1$.

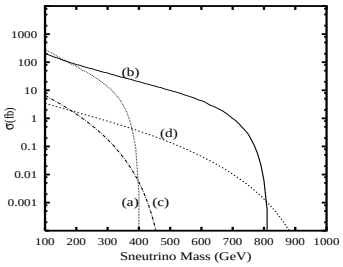

Figure 25: $\sigma(\tilde{\nu}\tau^\pm\mu^\mp)$ at $\gamma\gamma$ (a,b) and e^+e^- (c,d) collider with $\sqrt{s}$=100 GeV (a,c) and 1 TeV (b,d) [73].

EXTENDED SUSY

The NMSSM, the minimal extension of the MSSM, introduces a singlet superfield field S in the superpotential

$$W \supset \lambda H_u H_d S - \frac{1}{3}\kappa S^3 . \qquad (27)$$

In this model, an effective $\mu = \lambda x$ term is generated when the scalar component of the singlet S acquires a vacuum expectation value $x = \langle S \rangle$. The fermion component of the singlet superfield (singlino) will mix with neutral gauginos and higgsinos after electroweak gauge symmetry breaking, changing the neutralino mass matrix to the 5×5 form which depends on M_1, M_2, $\tan\beta$, x and the trilinear couplings λ and κ.

In some regions of the parameter space the singlino may be the lightest supersymmetric particle, weakly mixing with other states. In the extended SPS#1a scenario with large $x \gg |M_2|$, analysed in [75], the lightest neutralino $\tilde{\chi}_S^0$ with mass $\approx 2\kappa x$ becomes singlino-dominated while the other four neutralinos $\tilde{\chi}^0_{1,\ldots,4}$ have the MSSM characteristics. The exotic $\tilde{\chi}_S^0$ state can be searched for in the associated production of $\tilde{\chi}_S^0$ together with the lightest MSSM-like neutralino $\tilde{\chi}_1^0$ in e^+e^- annihilation. The unpolarized cross section, shown in fig. 26 for $m_{\tilde{\chi}_S^0} = 70$ GeV, is larger than 1 fb up to $x < 7.4$ TeV which corresponds to a singlino content of 99.7 %. Polarized beams can enhance the cross section by a factor 2–3, and provide discriminating power between different scenarios [76]. If the couplings of a singlino-dominated LSP to the NLSP are strongly suppressed at large values of x, displaced vertices in the NMSSM may be generated, fig. 26, which would clearly signal the extension of the minimal model. For a similar analysis in the E_6 inspired model we refer to [75].

However, if the spectrum of the four lighter neutralinos in the extended model is similar to the spectrum in the MSSM, but the mixing is substantial, discriminating the models by analysing the mass spectrum becomes very difficult. Studying in this case the summed-up cross sections of the four light neutralinos may then be a crucial method to reveal the structure of the neutralino system [52]. More specifically, in extended SUSY models with n SU(2) doublet and m SU(2) singlet chiral superfields, the sum rule reads

$$\lim_{s\to\infty} s \sum_{i\le j} \sigma\{ij\} = \frac{\pi\alpha^2}{48\, c_W^4 s_W^4} \times \left[n\,(8s_W^4 - 4s_W^2 + 1) + 48 s_W^4 + 3 \right] \qquad (28)$$

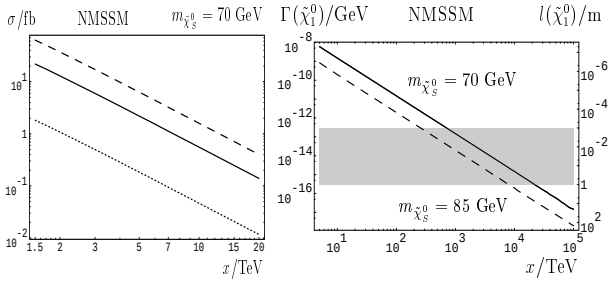

Figure 26: Left: Unpolarized $\sigma(\tilde{\chi}^0_S\,\tilde{\chi}^0_1)$ at $\sqrt{s}$=500 GeV (solid) and for polarized beams $\mathcal{P}_-$=0.8, $\mathcal{P}_+$=-0.6 (dashed), $\mathcal{P}_-$=-0.8, $\mathcal{P}_+$=0.6 (dotted). Right: Total decay widths of the lightest MSSM-like $\tilde{\chi}^0_1$ decaying into a singlino-dominated $\tilde{\chi}^0_S$. The shaded area shows where displaced vertices exist [75].

The right–hand side of eq. (28) is independent of the number m of singlets and it reduces to the sum rule in the MSSM for $n = 2$. In fig. 27 the exact sum rules, normalized to the asymptotic value, are compared for an NMSSM scenario giving rise to one very heavy neutralino with $m_{\tilde{\chi}^0_5} \sim 1000$ GeV, and to four lighter neutralinos with masses equal within 2 – 5 GeV to the neutralino masses in the MSSM. Due to the incompleteness of these states below the thresholds for producing the heavy neutralino $\tilde{\chi}^0_5$, the NMSSM value differs significantly from the corresponding sum rule of the MSSM. Therefore, even if the extended neutralino states are very heavy, the study of sum rules can shed light on the underlying structure of the supersymmetric model.

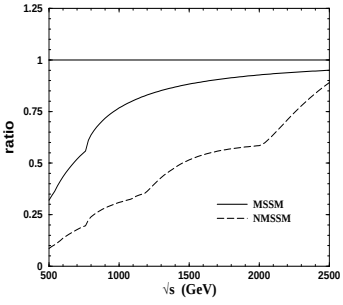

Figure 27: The sum of neutralino–pair production cross sections: all pairs in the MSSM (solid), and of the first four neutralino states in the NMSSM (dashed); both normalized to the asymptotic value [52].

RECONSTRUCTING FUNDAMENTAL SUSY PARAMETERS

Low energy SUSY particle physics is characterized by energy scales of order $\lesssim$ 1 TeV. However, the roots for all the phenomena we will observe experimentally in this range may go to energies near the Planck or the GUT scale. Fortunately, supersymmetry provides us with a stable bridge between these two vastly different energy regions [77]. To this purpose renormalization group equations (RGE) are exploited, by which parameters from low to high scales are evolved based on nothing but measured quantities in laboratory experiments. This procedure has very successfully been pursued for the three electroweak and strong gauge couplings, and has been expanded to a large ensemble of supersymmetry parameters [78] – the soft SUSY breaking parameters: gaugino and scalar masses, as well as trilinear couplings. This bottom-up approach makes use of the low-energy measurements to the maximum extent possible and it reveals the quality with which the fundamental theory at the high scale can be reconstructed in a transparent way.

Table 1: Representative gaugino/scalar mass parameters and couplings as determined at the electroweak scale and evolved to the GUT scale in the mSUGRA scenario based on LHC and LC simulations; masses are in GeV. The errors are 1σ [79].

	Exp. Input	GUT Value
M_1	102.31 ± 0.25	250.00 ± 0.33
M_2	192.24 ± 0.48	250.00 ± 0.52
M_3	586 ± 12	250.0 ± 5.3
μ	358.23 ± 0.28	355.6 ± 1.2
$M^2_{L_1}$	$(6.768 \pm 0.005) \cdot 10^4$	$(3.99 \pm 0.41) \cdot 10^4$
$M^2_{E_1}$	$(4.835 \pm 0.007) \cdot 10^4$	$(4.02 \pm 0.82) \cdot 10^4$
$M^2_{Q_1}$	$(3.27 \pm 0.08) \cdot 10^5$	$(3.9 \pm 1.5) \cdot 10^4$
$M^2_{U_1}$	$(3.05 \pm 0.11) \cdot 10^5$	$(3.9 \pm 1.9) \cdot 10^4$
$M^2_{D_1}$	$(3.05 \pm 0.11) \cdot 10^5$	$(4.0 \pm 1.9) \cdot 10^4$
$M^2_{H_1}$	$(6.21 \pm 0.08) \cdot 10^4$	$(4.01 \pm 0.54) \cdot 10^4$
$M^2_{H_2}$	$(-1.298 \pm 0.004) \cdot 10^5$	$(4.1 \pm 3.2) \cdot 10^4$
A_{tit}	-446 ± 14	-100 ± 54
$\tan\beta$	9.9 ± 0.9	—

A set of representative examples in this context has been studied [79]: minimal supergravity and a left–right symmetric extension; gauge mediated supersymmetry breaking; and superstring effective field theories. The anomaly mediated as well as the gaugino mediated SUSY breaking are technically equivalent to the mSUGRA case and therefore were not treated explicitly.

Gravity mediated SUSY breaking

The minimal supergravity scenario mSUGRA is characterized by the universal: gaugino mass $M_{1/2}$, scalar mass M_0, trilinear coupling A_0, sign of μ (the modulus $|\mu|$ determined by radiative symmetry breaking) and $\tan\beta$. The parameters $M_{1/2}$, M_0 and A_0 are defined at the GUT scale M_U where gauge couplings unify $\alpha_i = \alpha_U$. The RGE are then used to determine the low energy SUSY lagrangian parameters.

The point chosen for the analysis is close to the Snowmass Point SPS#1a [8], except for the scalar mass parameter M_0 which was taken slightly larger for merely illustrative purpose: $M_{1/2} = 250$ GeV, $M_0 = 200$ GeV, $A_0 = -100$ GeV, $\tan\beta = 10$ and $sign(\mu) = +$.

Based on simulations and estimates of expected preci-

sion, the low-energy 'experimental' values are taken as the input values for the evolution of the mass parameters in the bottom-up approach to the GUT scale. The results for the evolution of the mass parameters to the GUT scale M_U are shown in fig. 28. The left panel presents the evolution of the gaugino parameters M_i^{-1}, while the right panel shows the extrapolation of the slepton mass parameters squared of the first two generations. The accuracy deteriorates for the squark mass parameters and for the Higgs mass parameter $M_{H_2}^2$. The origin of the differences between the errors for slepton, squark and Higgs mass parameters can be traced back to the numerical size of the coefficients. The quality of the test is apparent from table 1, where it is shown how well the reconstructed mass parameters at the GUT scale reproduce the input values $M_{1/2} = 250$ GeV and $M_0 = 200$ GeV.

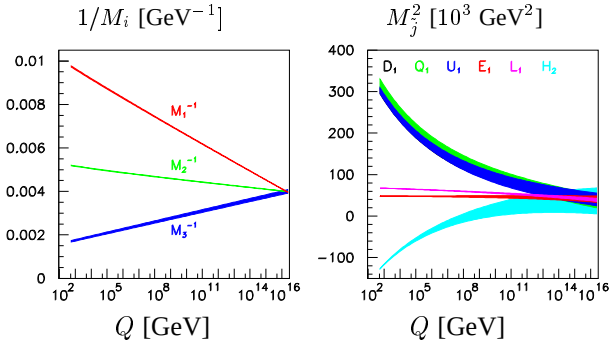

Figure 28: mSUGRA: Evolution, from low to high scales, of gaugino mass parameters (left), and first two generation sfermion mass parameters and the Higgs mass parameter $M_{H_2}^2$ (right). The widths of the bands indicate the 1σ CL [79].

The above analysis has also been extended [79] to a left–right supersymmetric $SO(10)$ model in which the $SO(10)$ symmetry is assumed to be realized at a scale between the standard $SU(5)$ scale $M_U \simeq 2 \cdot 10^{16}$, derived from the unification of the gauge couplings, and the Planck scale $M_P \simeq 10^{19}$ GeV. The right–handed neutrinos are assumed heavy, with masses at intermediate scales between $O(10^{10})$ GeV and $O(10^{15})$ GeV, so that the observed light neutrino masses are generated by the see-saw mechanism. The evolution of the gaugino and scalar mass parameters of the first two generations is not affected by the left–right extension. It is only different for the third generation and for $M_{H_2}^2$ owing to the enhanced Yukawa coupling in this case. The sensitivity to the intermediate ν_R scales is rather weak because neutrino Yukawa couplings affect the evolution of the sfermion mass parameters only mildly. Nevertheless, a rough estimate of the intermediate scale follows from the evolution of the mass parameters to the low experimental scale if universality holds at the Grand Unification scale.

Gauge mediated SUSY breaking

In GMSB the scalar and the F components of a Standard–Model singlet superfield S acquire vacuum expectation values $\langle S \rangle$ and $\langle F_S \rangle$ through interactions with fields in the secluded sector, thus breaking supersymmetry. Vector-like messenger fields M, carrying non–zero $SU(3) \times SU(2) \times U(1)$ charges and coupling to S, transport the supersymmetry breaking to the eigen–world. The system is characterized by the mass $M_M \sim \langle S \rangle$ of the messenger fields and the mass scale $\Lambda = \langle F_S \rangle / \langle S \rangle$ setting the size of the gaugino and scalar masses. M_M is expected to be in the range of 10 to 10^6 TeV and Λ has to be smaller than M_M.

The gaugino masses are generated by loops of scalar and fermionic messenger component fields, while masses of the scalar fields in the visible sector are generated by 2-loop effects of gauge/gaugino and messenger fields, and the A parameters are generated at 3-loop level and they are practically zero at M_M. Scalar particles with identical Standard–Model charges squared have equal masses at the messenger scale M_M, which is a characterictic feature of the GMSB model.

This scheme has been investigated for the point $\Lambda = 100$ TeV, $M_M = 200$ TeV, $N_5 = 1$, $N_{10} = 0$, $\tan\beta = 15$ and $\mu > 0$ corresponding to the Snowmass Point SPS#8. The evolution of the gaugino and sfermion mass parameters of the first two generations as well as the Higgs mass parameters, including 2-loop β–functions, is presented in fig. 29.

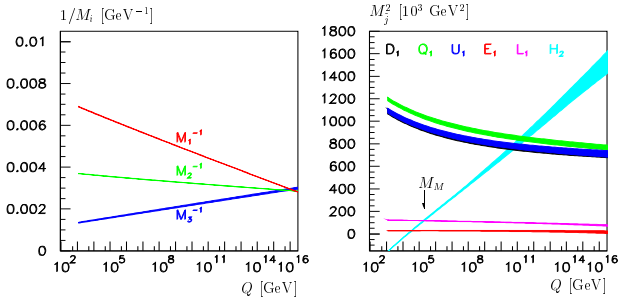

Figure 29: GMSB: Evolution, from low to high scales, of gaugino mass parameters (left), and first two generation sfermion mass parameters and the Higgs mass parameter $M_{H_2}^2$ (right). The widths of the bands indicate the 1σ CL [79].

The gaugino masses in GMSB evolve nearly in the same way as in mSUGRA. However, due to the influence of the A–parameters in the 2-loop RGEs for the gaugino mass parameters, they do not meet at the same point as the gauge couplings in this scheme. On the other hand the running of the scalar masses is quite different in both theories. The bands of the slepton L–doublet mass parameter $M_{\tilde{L}}^2$ and the Higgs parameter $M_{H_2}^2$, which carry the same moduli of standard–model charges, cross at the scale M_M. The crossing, indicated by an arrow in the fig. 29, is a neces-

sary condition (in the minimal form) for the GMSB scenario to be realized. Moreover, at the messenger scale the ratios of scalar masses squared in the simplest version of GMSB are determined solely by group factors and gauge couplings, being independent of the specific GMSB characteristics, i. e. messenger multiplicities and Λ mass scale.

The two scales Λ and M_M, and the messenger multiplicity $N_M = N_5 + 3N_{10}$ can be extracted from the spectrum of the gaugino and scalar particles. For the point analyzed in the example above, the following accuracy for the mass parameters and the messenger multiplicity has been found:

$$\Lambda = (1.01 \pm 0.03) \cdot 10^2 \text{ TeV} \quad (29)$$

$$M_M = (1.92 \pm 0.24) \cdot 10^2 \text{ TeV} \quad (30)$$

$$N_M = 0.978 \pm 0.056 \quad (31)$$

String induced SUSY breaking

Four–dimensional strings naturally give rise to a minimal set of fields for inducing supersymmetry breaking; they play the rôle of the fields in the hidden sectors: the dilaton S and the moduli T_m chiral superfields which are generically present in large classes of 4–dimensional heterotic string theories. In the analysis only one moduli field T has been considered. SUSY breaking, mediated by a goldstino field, originates in the vacuum expectation values of S and T generated by genuinely non–perturbative effects. The properties of the model depend on the composition of the goldstino which is a mixture of the dilaton field S and the moduli field T,

$$\tilde{G} = S \sin\theta + T \cos\theta \quad (32)$$

Universality is generally broken in such a scenario by a set of non-universal modular weights n_j that determine the coupling of T to the SUSY matter fields Φ_j. The gaugino and scalar mass parameters can be expressed to leading order by the gravitino mass $m_{3/2}$, the vacuum values $\langle S\rangle$ and $\langle T\rangle$, the mixing parameter $\sin\theta$, the modular weights n_j and the Green-Schwarz parameter $\delta_{\rm GS}$. The relations between the universal gauge coupling $\alpha(M_{\rm string})$ at the string scale $M_{\rm string}$ and the gauge couplings $\alpha_i(M_{\rm GUT})$ at the SU(5) unification scale $M_{\rm GUT}$:

$$\alpha_i^{-1}(\mathrm{M_{GUT}}) = \alpha^{-1}(\mathrm{M_{string}}) + \Delta\alpha_{\mathrm{i}}^{-1}[\mathrm{n_j}] \quad (33)$$

receive small deviations from universality at the GUT scale which are accounted for by string loop effects transporting the couplings from the universal string scale to the GUT scale. The gauge coupling at $M_{\rm string}$ is related to the dilaton field, $g_s^2 = 1/\langle S\rangle$.

A mixed dilaton/moduli superstring scenario with dominating dilaton field component and with different couplings of the moduli field to the (L,R) sleptons, the (L,R) squarks and to the Higgs fields, corresponding to O–I representation has been chosen for the analysis [79], for which $\sin^2\theta = 0.9$, $n_{L_i} = -3$, $n_{E_i} = -1$, $n_{H_1} = n_{H_2} = -1$, $n_{Q_i} = 0$, $n_{D_i} = 1$, $n_{U_i} = -2$, and the gravitino mass 180 GeV.

Table 2: Comparison of the experimentally reconstructed values with the ideal fundamental parameters in a specific example for a string effective field theory. [All mass parameters are in units of GeV.]

Parameter	Ideal	Reconstructed
$m_{3/2}$	180	179.9 ± 0.4
$\langle S\rangle$	2	1.998 ± 0.006
$\langle T\rangle$	14	14.6 ± 0.2
$\sin^2\theta$	0.9	0.899 ± 0.002
g_s^2	0.5	0.501 ± 0.002
δ_{GS}	0	0.1 ± 0.4
$\tan\beta$	10	10.00 ± 0.13

The evolution of the gaugino and scalar mass parameters is displayed in fig. 30. The pattern of the trajectories is remarkably different from other scenarios. The breaking of universality in the gaugino sector, induced by string threshold corrections, is shown in the insert.

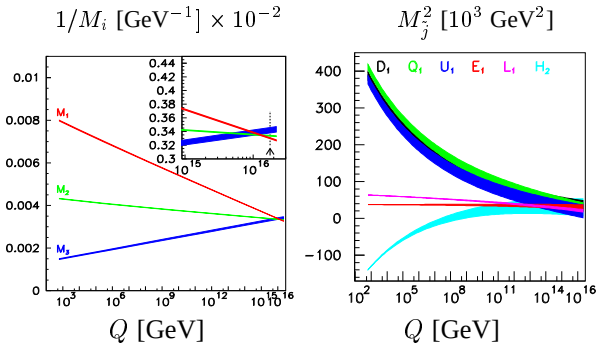

Figure 30: String scenario: Evolution, from low to high scales, of gaugino mass parameters (left), and first two generation sfermion mass parameters and the Higgs mass parameter $M_{H_2}^2$ (right). The widths of the bands indicate the 1σ CL [79].

The reconstructed values the fundamental parameters of the string effective field theory are compared with the ideal values in Table 2. Also the reproduction of moduli weights as 'integers' at the per-cent level provides a highly non-trivial check of the string model [79].

SUMMARY

Much progress has been achieved during the Extended ECFA/DESY Workshop. It has been demonstrated that a high luminosity LC with polarized beams, and with additional $e\gamma$, $\gamma\gamma$ and e^-e^- modes, can provide high quality data for the precise determination of low-energy SUSY Lagrangian parameters. In the bottom–up approach, through the evolution of the parameters from the electroweak scale, the regularities in different scenarios at the high scales can be unravelled if precision analyses of the supersymmetric particle sector at e^+e^- linear colliders are combined with

analyses at the LHC. In this way the basis of the SUSY breaking mechanism can be explored and the crucial elements of the fundamental supersymmetric theory can be reconstructed.

So far most analyses were based on lowest–order expressions. With higher order corrections now available, one of the goals of the SUSY WG in the new ECFA Study would be to refine the above program. Many new theoretical calculations and future experimental analyses will be necessary. However, the prospect of exploring elements of the ultimate unification of the interactions provides a strong stimulus in this direction.

REFERENCES

[1] J. A. Aguilar-Saavedra *et al.* [ECFA/DESY LC Physics Working Group Collaboration], "TESLA Technical Design Report Part III: Physics at an e+e- Linear Collider," arXiv:hep-ph/0106315.

[2] Understanding Matter, Energy, Space and Time: The Case for the e^+e^- Linear Collider, http://sbhepnt.physics.sunysb.edu/ grannis/ilcsc/lc_icfa_v6.3.pdf

[3] F. E. Paige, arXiv:hep-ph/0211017. J. G. Branson, D. Denegri, I. Hinchliffe, F. Gianotti, F. E. Paige and P. Sphicas (eds.) [ATLAS and CMS Collaborations], Eur. Phys. J. directC **4** (2002) N1.

[4] J. Kalinowski, arXiv:hep-ph/0212388.

[5] G. Weiglein, talk in Amsterdam. The web address of the LHC/LC Study Group: http://www.ippp.dur.ac.uk/ ˜georg/lhclc/.

[6] The web addresses of the Extended ECFA-DESY meetings:
Cracow http://fatcat.ifj.edu.pl/ecfadesy-krakow/
St. Malo http://www-dapnia.cea.fr/ecfadesy-stmalo/
Prague http://www-hep2.fzu.cz/ecfadesy/Talks/SUSY/
Amsterdam http://www.nikhef.nl/ecfa-desy/start.html

[7] G. Moortgat-Pick, talk in Amsterdam. The web address of the POWER Study Group: http://www.ippp.dur.ac.uk/ ˜gudrid/power/.

[8] B. C. Allanach *et al.*, in *Proc. of the APS/DPF/DPB Summer Study on the Future of Particle Physics (Snowmass 2001)* ed. N. Graf; Eur. Phys. J. C **25** (2002) 113 [eConf **C010630** (2001) P125] [arXiv:hep-ph/0202233] LC-TH-2003-022. The values of benchmarks are listed on http://www.ippp.dur.ac.uk/˜georg/sps

[9] H. Baer, F. E. Paige, S. D. Protopopescu and X. Tata, arXiv:hep-ph/0001086.

[10] N. Ghodbane and H. U. Martyn, in *Proc. of the APS/DPF/DPB Summer Study on the Future of Particle Physics (Snowmass 2001)* ed. N. Graf, arXiv:hep-ph/0201233, LC-PHSM-2003-055, LC-TH-2001-079. B. Allanach, S. Kraml and W. Porod, arXiv:hep-ph/0207314.

[11] B. C. Allanach, S. Kraml and W. Porod, JHEP **0303** (2003) 016 [arXiv:hep-ph/0302102] LC-TH-2003-017.

[12] B. C. Allanach, Comput. Phys. Commun. **143** (2002) 305 [arXiv:hep-ph/0104145].

[13] W. Porod, Comput. Phys. Commun. **153** (2003) 275 [arXiv:hep-ph/0301101] LC-TOOL-2003-042.

[14] A. Djouadi, J. L. Kneur and G. Moultaka, arXiv:hep-ph/0211331.

[15] S. Katsanevas and P. Morawitz, Comput. Phys. Commun. **112** (1998) 227 [arXiv:hep-ph/9711417].

[16] T. Sjostrand, L. Lonnblad and S. Mrenna, arXiv:hep-ph/0108264.

[17] M. Battaglia *et al.*, in *Proc. of the APS/DPF/DPB Summer Study on the Future of Particle Physics (Snowmass 2001)* ed. N. Graf, eConf **C010630** (2001) P347 [arXiv:hep-ph/0112013].

[18] A. Bartl *et al.* [ECFA/DESY SUSY Collaboration], arXiv:hep-ph/0301027, LC-TH-2003-039. A. Freitas *et al.*, [ECFA/DESY SUSY Collaboration], arXiv:hep-ph/0211108. LC-PHSM-2003-019.

[19] W. Majerotto, arXiv:hep-ph/0209137.

[20] A. Freitas, D. J. Miller and P. M. Zerwas, Eur. Phys. J. C 21 (2001) 361 [arXiv:hep-ph/0106198] LC-TH-2001-011. A. Freitas and D. J. Miller, in *Proc. of the APS/DPF/DPB Summer Study on the Future of Particle Physics (Snowmass 2001)* eds. R. Davidson and C. Quigg, [hep-ph/0111430]. A. Freitas and A. von Manteuffel, arXiv:hep-ph/0211105.

[21] J. Guasch, W. Hollik and J. Sola, JHEP **0210** (2002) 040 [arXiv:hep-ph/0207364]. J. Guasch, W. Hollik and J. Sola, arXiv:hep-ph/0307011, LC-TH-2003-033. W. Hollik and H. Rzehak, arXiv:hep-ph/0305328.

[22] M. Beccaria, F. M. Renard and C. Verzegnassi, arXiv:hep-ph/0203254, LC-TH-2002-005. M. Beccaria, M. Melles, F. M. Renard and C. Verzegnassi, arXiv:hep-ph/0210283.

[23] H.U. Martyn, LC-PHSM-2003-07, and talk in Prague.

[24] H. Nieto-Chaupis, LC-DET-2003-074, and talk in Amsterdam.

[25] H.U. Martyn, arXiv:hep-ph/0302024.

[26] M. Dima *et al.*, Phys. Rev. D 65 (2002) 071701.

[27] E. Boos, G. Moortgat-Pick, H. U. Martyn, M. Sachwitz and A. Vologdin, arXiv:hep-ph/0211040. E. Boos, H.U. Martyn, G. Moortgat-Pick, M. Sachwitz, A. Sherstnev and P.M. Zerwas, arXiv:hep-ph/0303110, LC-PHSM-2003-018.

[28] M.M. Nojiri, Phys. Rev. D **51** (1995) 6281 [arXiv:hep-ph/9412374]. M.M. Nojiri, K. Fujii and T. Tsukamoto, Phys. Rev. D **54** (1996) 6756 [arXiv:hep-ph/9606370].

[29] A. Finch, H. Nowak and A. Sopczak, arXiv:hep-ph/0211140, LC-PHSM-2003-075.

[30] S. Heinemeyer, S. Kraml, W. Porod and G. Weiglein, arXiv:hep-ph/0306181, LC-TH-2003-052.

[31] C. Blöchinger, H. Fraas, G. Moortgat-Pick and W. Porod, Eur. Phys. J. C 24 (2002) 297 [arXiv:hep-ph/0201282] LC-TH-2003-031.

[32] A. Freitas, DESY-THESIS-2002-023, A. Freitas, A. von Manteuffel, in [20], A. Freitas, A. von Manteuffel, P.M. Zerwas, in preparation.

[33] A. Brandenburg, M. Maniatis and M. M. Weber, arXiv:hep-ph/0207278. M. Maniatis, DESY-THESIS-2002-007

[34] H. Baer, C. Balazs, S. Hesselbach, J. K. Mizukoshi and X. Tata, Phys. Rev. D **63** (2001) 095008 [arXiv:hep-ph/0012205].

[35] A. Bartl, W. Majerotto, W. Porod and D. Wyler, arXiv:hep-ph/0306050.

[36] D. Chang, W. Y. Keung and A. Pilaftsis, Phys. Rev. Lett. **82** (1999) 900 [Erratum-ibid. **83** (1999) 3972] [arXiv:hep-ph/9811202]. A. Pilaftsis, Phys. Lett. B **471** (1999) 174 [arXiv:hep-ph/9909485].

[37] A. Bartl, K. Hidaka, T. Kernreiter and W. Porod, Phys. Rev. D **66** (2002) 115009 [arXiv:hep-ph/0207186] LC-TH-2003-027.

[38] A. Bartl, S. Hesselbach, K. Hidaka, T. Kernreiter and W. Porod, arXiv:hep-ph/0306281, LC-TH-2003-04.

[39] A. Bartl, T. Kernreiter and W. Porod, Phys. Lett. B **538** (2002) 59 [arXiv:hep-ph/0202198] LC-TH-2003-028.

[40] B. Ananthanarayan, S. D. Rindani and A. Stahl, Eur. Phys. J. C **27** (2003) 33 [arXiv:hep-ph/0204233] LC-PHSM-2002-006.

[41] K. Hagiwara *et al.* [Particle Data Group Collaboration], Phys. Rev. D **66** (2002) 010001.

[42] Y. Fukuda *et al.* [Super-Kamiokande Collaboration], Phys. Rev. Lett. **81**, 1562 (1998) Q. R. Ahmad *et al.* [SNO Collaboration], Phys. Rev. Lett. **89** (2002) 011301 [arXiv:nucl-ex/0204008]. Q. R. Ahmad *et al.* [SNO Collaboration], Phys. Rev. Lett. **89**, 011302 (2002) [arXiv:nucl-ex/0204009]. K. Eguchi *et al.* [KamLAND Collaboration], Phys. Rev. Lett. **90** (2003) 021802 [arXiv:hep-ex/0212021].

[43] F. Borzumati, A. Masiero, Phys. Rev. Lett. **57** (1986) 961.

[44] N. Arkani-Hamed, J. L. Feng, L. J. Hall and H. Cheng, Phys. Rev. Lett. **77** (1996) 1937 [hep-ph/9603431]. Hisano, M. M. Nojiri, Y. Shimizu and M. Tanaka, Phys. Rev. D **60** (1999) 055008 [hep-ph/9808410]. M. Guchait, J. Kalinowski and P. Roy, Eur. Phys. J. C **21** (2001) 163 [arXiv:hep-ph/0103161] LC-TH-2001-073. J. Kalinowski, Acta Phys. Polon. B **32** (2001) 3755.

[45] W. Porod, W. Majerotto, Phys. Rev. D **66** (2002) 015003 [arXiv:hep-ph/0201284] LC-TH-2003-030. W. Porod and W. Majerotto, arXiv:hep-ph/0210326.

[46] J. Kalinowski, Acta Phys. Polon. B **33** (2002) 2613 [arXiv:hep-ph/0207051] LC-TH-2003-040.

[47] E. Perazzi, G. Ridolfi and F. Zwirner, Nucl. Phys. B **574** (2000) 3 [arXiv:hep-ph/0001025].

[48] P. Checchia and E. Piotto, arXiv:hep-ph/0102208, LC-TH-2001-015.

[49] S. Y. Choi, A. Djouadi, H. S. Song and P. M. Zerwas, Eur. Phys. J. **C8** (1999) 669 [hep-ph/9812236].

[50] S. Y. Choi, M. Guchait, J. Kalinowski and P. M. Zerwas, Phys. Lett. B **479** (2000) 235 [hep-ph/0001175]; S. Y. Choi, A. Djouadi, M. Guchait, J. Kalinowski, H. S. Song and P. M. Zerwas, Eur. Phys. J. C **14** (2000) 535 [hep-ph/0002033].

[51] L. Chau and W. Keung, Phys. Rev. Lett. **53** (1984) 1802; H. Fritzsch and J. Plankl, Phys. Rev. D **35** (1987) 1732.

[52] S. Y. Choi, J. Kalinowski, G. Moortgat-Pick and P. M. Zerwas, Eur. Phys. J. C **22** (2001) 563 [arXiv:hep-ph/0108117] LC-TH-2003-024.

[53] T. Fritzsche and W. Hollik, Eur. Phys. J. C **24** (2002) 619 [arXiv:hep-ph/0203159]. T. Blank and W. Hollik, arXiv:hep-ph/0011092, LC-TH-2000-054.

[54] W. Öller, H. Eberl, W. Majerotto and C. Weber, arXiv:hep-ph/0304006. H. Eberl, M. Kincel, W. Majerotto and Y. Yamada, Phys. Rev. D **64** (2001) 115013 [arXiv:hep-ph/0104109].

[55] M. A. Diaz and D. A. Ross, arXiv:hep-ph/0205257. M. A. Diaz and D. A. Ross, JHEP **0106** (2001) 001 [arXiv:hep-ph/0103309].

[56] S. Y. Choi, J. Kalinowski, G. Moortgat-Pick and P. M. Zerwas, Eur. Phys. J. C **23** (2002) 769 [arXiv:hep-ph/0202039] LC-TH-2003-023.

[57] J. L. Kneur and G. Moultaka, Phys. Rev. D **59** (1999) 015005 [hep-ph/9807336]; V. Barger, T. Han, T. Li and T. Plehn, Phys. Lett. B **475** (2000) 342 [hep-ph/9907425]; J. L. Kneur and G. Moultaka, Phys. Rev. D **61** (2000) 095003 [hep-ph/9907360].

[58] C. Hensel, DESY-THESIS-2002-047, and talk in Cracow.

[59] T. Mayer, C. Blochinger, F. Franke and H. Fraas, Eur. Phys. J. C **27** (2003) 135 [arXiv:hep-ph/0209108].

[60] M. Ball, talk in Prague.
C. Tevlin, talk in Amsterdam.

[61] F. del Aguila and J. A. Aguilar-Saavedra, Phys. Lett. B **386** (1996) 241 [hep-ph/9605418]; J. A. Aguilar-Saavedra and G. C. Branco, Phys. Rev. D **62** (2000) 096009 [hep-ph/0007025].

[62] C. Jarlskog, Phys. Rev. Lett. **55** (1985) 1039.

[63] O. Kittel, talk in Prague. A. Bartl, H. Fraas, O. Kittel and W. Majerotto, arXiv:hep-ph/0308143, LC-TH-2003-065, and arXiv:hep-ph/0308141.

[64] B. Gaissmaier, arXiv:hep-ph/0211407, and talk in Amsterdam.

[65] J. Kalinowski, Acta Phys. Polon. B **34** (2003) 3441 [arXiv:hep-ph/0306272, LC-TH-2003-038].

[66] S. T. Petcov, Phys. Lett. B **178** (1986) 57. G. Moortgat-Pick and H. Fraas, Eur. Phys. J. C **25** (2002) 189 [arXiv:hep-ph/0204333].

[67] J. Ellis, J. M. Frère, J. S. Hagelin, G. L. Kane and S. T. Petcov, Phys. Lett. B **132** (1983) 436.

[68] S. Berge and M. Klasen, Phys. Rev. D **66** (2002) 115014 [arXiv:hep-ph/0208212]. S. Berge and M. Klasen, arXiv:hep-ph/0303032.

[69] M. Hirsch, W. Porod, J.C. Romão, J.W.F. Valle, Phys. Rev. D **66** (2002) 095006 [arXiv:hep-ph/0207334] LC-TH-2003-029.

[70] A. Bartl, M. Hirsch, T. Kernreiter, W. Porod and J. W. Valle, arXiv:hep-ph/0306071. W. Porod, M. Hirsch, J. Romão and J. W. Valle, Phys. Rev. D **63** (2001) 115004 [arXiv:hep-ph/0011248] LC-TH-2003-026.

[71] M. Hirsch and W. Porod, arXiv:hep-ph/0307364.

[72] A. Bartl, M. Hirsch, T. Kernreiter, W. Porod, J.W.F. Valle, Slepton LSP Decays: Trilinear versus Bilinear R-parity Breaking, LC-TH-2003-047, ZU-TH 10/03, UWThPh-2003-13.

[73] D. K. Ghosh and S. Moretti, Phys. Rev. D **66** (2002) 035004 [arXiv:hep-ph/0112288] LC-TH-2003-063.

[74] M. Chaichian, K. Huitu, S. Roy and Z. H. Yu, Phys. Lett. B **518** (2001) 261 [arXiv:hep-ph/0107111].

[75] F. Franke and S. Hesselbach, Phys. Lett. B **526** (2002) 370 [arXiv:hep-ph/0111285]. S. Hesselbach and F. Franke, arXiv:hep-ph/0210363, LC-TH-2003-006.

[76] S. Hesselbach, F. Franke and H. Fraas, arXiv:hep-ph/0003272.

[77] E. Witten, Nucl. Phys. B **188** (1981) 513.

[78] G. A. Blair, W. Porod and P. M. Zerwas, Phys. Rev. D 63 (2001) 017703; P. M. Zerwas *et al.*, hep-ph/0211076, LC-TH-2003-020. P. M. Zerwas *et al.*, [ECFA/DESY SUSY Collaboration], arXiv:hep-ph/0211076, LC-TH-2003-020.

[79] G. A. Blair, W. Porod and P. M. Zerwas, Eur. Phys. J. C **27** (2003) 263 [arXiv:hep-ph/0210058] LC-TH-2003-021.

...

...

HIGGS BOSON PRECISION STUDIES at a LINEAR COLLIDER *

Klaus Desch, University of Hamburg, Germany

Abstract

This report summarizes the progress in the study of Higgs physics at a future linear electron positron collider at center-of-mass energies up to about 1000 GeV and high luminosity. After the publication of the TESLA Technical Design Report [1], an extended ECFA/DESY study on linear collider physics and detectors was performed. The paper summarizes the status of the studies with main emphasis on recent results obtained in the course of the workshop.

OBJECTIVES OF THE STUDY

Elucidating the mechanism responsible for electro-weak symmetry breaking is one of the most important tasks of future collider based particle physics. Experimental and theoretical indications of a light Higgs boson make the precision study of the properties of Higgs bosons one of the major physics motivations of a linear collider (LC). Both the Higgs boson of the Standard Model (SM) and those of extended models will be copiously produced in e^+e^- collisions in various production mechanisms. A large variety of different decay modes can be observed with low backgrounds and high efficiency. These measurements allow us to extract the fundamental parameters of the Higgs sector with high precision. The series of ECFA/DESY workshops aims at a comprehensive study of the physics case, a determination of the achievable precisions on Higgs observables as well as on a fruitful cross-talk between theory, physics simulations and detector layout.

A future linear collider offers also the option of photon-photon collisions from back-scattered laser light. The physics potential and progress in Higgs physics at a photon collider is discussed elsewhere in these proceedings [2].

STANDARD MODEL HIGGS BOSON

Theoretical Predictions

In e^+e^- collisions, the SM Higgs boson is predominantly produced through the Higgs-strahlung process, $e^+e^- \to H^0Z$ [3] and through the vector boson fusion processes $e^+e^- \to \nu_e\bar{\nu}_e(e^+e^-)H^0$ [4]. The SM production cross-sections are precisely known including full electroweak corrections at the one-loop level. For a recent review of the theoretical calculations see e.g. [5]. Recently the full one-loop corrections to the WW-fusion process have been calculated [6, 7]. The radiatively corrected cross-sections for Higgs-strahlung and WW-fusion are shown in Fig. 1. For Higgs-strahlung the corrections are positive for small Higgs masses and negative for large Higgs masses and are of $\mathcal{O}(10\%)$. For WW-fusion the corrections are of similar size but always negative.

With the Higgs boson being responsible for mass generation its couplings to massive SM particles are proportional to their masses: $g_{ffH} = m_f/v$, $g_{VVH} = 2M_V^2/v$. Thus Higgs bosons decay preferentially into the heaviest kinematically possible final states. State-of-the-art branching ratio calculations including electro-weak and QCD corrections [8] are coded in the program HDECAY [9] for the SM and its minimal supersymmetric extension, the MSSM. Branching ratios of the neutral Higgs bosons in the MSSM can be also calculated with program FeynHiggsDecay [10]. The SM Higgs branching ratios in the mass range relevant to a LC are shown in Fig. 2.

Tools for Simulation

A variety of leading-order Monte Carlo generators exist which are commonly used for Higgs studies in e^+e^- collisions. They are PYTHIA [11], HERWIG [12], HZHA [13], CompHep [14], and WHiZard [15]. CompHep and WHiZard offer the possibility of generating the complete $2 \to 4$ and (in the case of WHiZard) also $2 \to 6$ processes including their interference with SM backgrounds.

* Most of the work reported in this talk was done by members of the Higgs working group of the Extended ECFA/DESY Study: V. Barger[a], M. Battaglia[b], M. Beccaria[c], E. Boos[d], J.C. Brient[e], S.Y. Choi[f], D. Choudhury[b], A. Datta[g], S. Dawson[h], S. DeCurtis[i], G. Degrassi[j,k], A. Denner[l], A. DeRoeck[b], N.G. Deshpande[m], S. Dittmaier[n], A. Djouadi[o], D. Dominici[i,p], M. Dubinin,[d] H. Eberl[q], J. Ellis[b], A. Ferrari[r], M. Frank[s], E. Gabrielli[g], A. Gay[t], I.F. Ginzburg[u], D.K. Ghosh[m], E. Gross[v], J. Guasch[l], J.F. Gunion[w], T. Hahn[n], T. Han[a],S. Heinemeyer[x], W. Hollik[n], K. Huitu[g], A. Imhof[y,z], J. Jiang[aa], A. Kiiskinen[g], T. Klimkovich[y,z], B.A. Kniehl[z], M. Krawczyk[bb], T. Kuhl[y] P. Langacker[cc], F. Madricardo [z], W. Majerotto[q], T. Maki[g], B. McElrath[a], B. Mele[j,k], N. Meyer[y,z], D.J. Miller[b], S. Moretti[b], M. Mühlleitner[l], K. Olive[dd], P. Osland[ee], S. Peñaranda[n], A. Pilaftsis[ff], A. Raspereza[y], F.M. Renard[o], M. Ronan[gg], M. Roth[n], H.J. Schreiber[y], M. Schumacher[hh], P. Slavich[n,s], A. Sopczak[ii], V.C. Spanos[dd], M. Steinhauser[y], S. Trimarchi[jj], C. Verzegnassi[jj], A. Vologdin[d], Z. Was[kk], M.M. Weber[l], G. Weiglein[ll], M. Worek[mm] M. Yao[gg], P.M. Zerwas[y], [a] University of Wisconsin, [b] CERN, [c] INFN, University di Lecce, [d] Moscow State University, [e] LPNHE Ecole Polytechnique , [f] Chonbuk National University, [g] Helsinki Instiute of Physics , [h] BNL Brookhaven National Laboratory, [i] INFN, Firenze, [j] INFN, Roma, [k] University La Sapienza, Roma, [l] PSI Villigen, [m] University of Oregon [n] MPI München, [o] Universite Montpellier, [p] University of Florence, [q] Inst.f.Hochenergiephysik Oesterr.Akademie d.Wissenschaften, Wien, [r] Uppsala University, [s] University Karlsruhe, [t] IRES Strasbourg, [u] NSC Novosibirsk, [v] Weizmann Institute, [w] University of California, Davis, [x] LMU München, [y] DESY Hamburg, [z] University of Hamburg, [aa] ANL Argonne, [bb] Warsaw University, [cc] University of Pennsylvania, [dd] University of Minnesota, [ee] University of Bergen, [ff] Manchester University, [gg] LBNL Berkeley, [hh] University of Bonn, [ii] Lancaster University, [jj] INFN, University Trieste, [kk] INP Cracow, [ll] University of Durham, [mm] University of Silesia, Katowice.

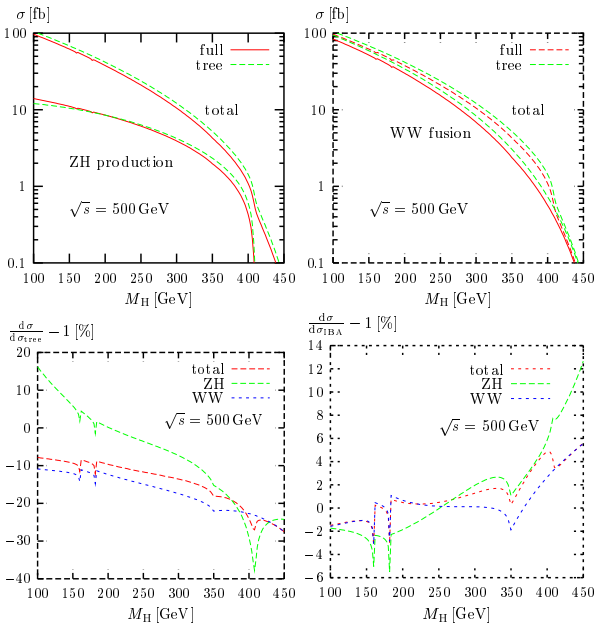

Figure 1: Upper plots: cross-section for the processes $e^+e^- \to ZH^0$ and $e^+e^- \to \nu_e\bar{\nu}_e H^0$ including complete one-loop electro-weak corrections for $\sqrt{s} = 500$ GeV. Lower plots: Relative amount of one-loop corrections relative to Born level result (left) and relative to an improved Born approximation (IBA) (from [7]).

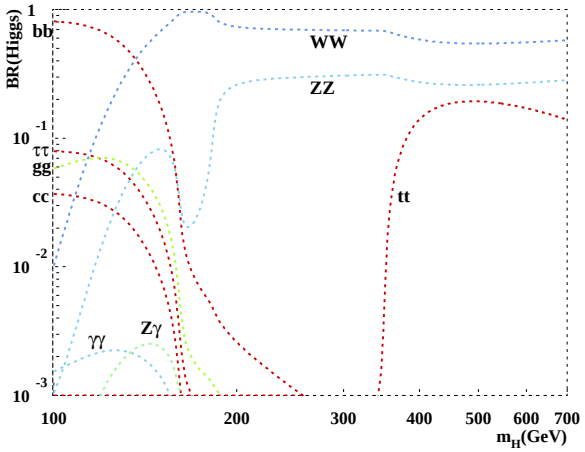

Figure 2: Branching ratios of the SM Higgs boson calculated with HDECAY [9].

Beamstrahlung was simulated in most analyses presented below using the parameterization CIRCE [16].

The vast majority of experimental analyses in this summary includes the simulation of complete SM backgrounds. The effects of limited detector acceptance and resolution have been incorporated using the parametric detector simulation program SIMDET [17] which is based on the detector performance specified for the TESLA detector in the TDR. A comparative study of different event generators and of different fast detector simulation programs was carried out in [18].

Most analyses which involve tagging of heavy quarks use a realistic event-wise neural-net algorithm based on ZVTOP [19] which was first used at the SLD detector.

A detailed simulation (BRAHMS [20]) of the TESLA TDR detector based on GEANT3 along with a reconstruction program is available and can be used for comparative studies.

Coupling to Z Bosons

The anchor of a model-independent precision analysis of Higgs boson properties at a LC is the measurement of the total cross-section for the Higgs-strahlung process, $e^+e^- \to H^0Z$. Z bosons can be selected in $Z \to e^+e^-$ and $Z \to \mu^+\mu^-$ decays. From energy-momentum conservation the invariant mass recoiling against the Z candidate can be calculated. Through a cut on the recoil mass, Higgs bosons can be selected independent of their decay mode, allowing for a model-independent measurement of the effective HZ coupling, g_{HZZ}. Once g_{HZZ} is known, all other Higgs couplings can be determined absolutely. The total Higgs-strahlung cross-section can be measured with an accuracy of 2.5% for $m_H = 120$ GeV and $\sqrt{s} = 350$ GeV for 500 fb^{-1} [21]. Assuming that the uncertainty scales with the square root of the cross-section and that the selection purity and efficiency is independent of the center-of-mass energy, one can obtain an accuracy between 1.2 % and 10% for $100 < m_H < 360$ GeV, for an integrated luminosity of $\sqrt{s}\times$ fb^{-1}/ GeV at a center-of-mass energy corresponding to the maximum of the cross-section for a given Higgs mass. The relative error is shown in Fig. 3 together with the optimal center-of-mass energy as a function of the Higgs mass.

The importance of a precise and model-independent determination of g_{HZZ} has e.g. recently been discussed in the context of supersymmetric models [22] and in the context of models with higher Higgs field representations, as well as in the context of extra-dimensional models [23].

Quantum Numbers

The measurements of differential production cross-sections and decay angular distributions provide access to the discrete quantum numbers of the Higgs boson: J^{PC}. In the TDR, the measurement of the β-dependence of the Higgs-strahlung cross-section close to the production threshold was exploited to determine the spin of the Higgs boson. The spin can also be determined from the invariant mass of the off-shell Z boson in the decay $H^0 \to ZZ^*$ for $m_H < 2m_Z$. This method is independent of the Higgs production process and thus potentially applicable also in $\gamma\gamma$ and gg collisions. The invariant mass distribution for $m_H = 150$ GeV is shown in Fig. 4. For m_H above $2m_Z$, azimuthal correlations of the two Z boson decay planes can

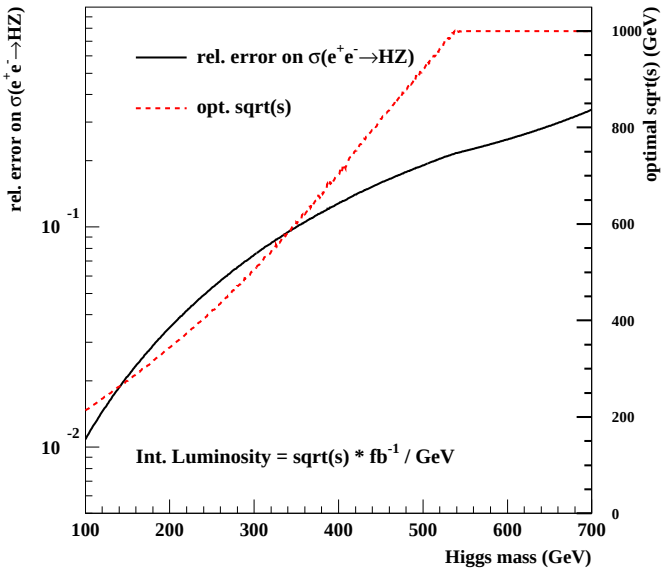

Figure 3: Achievable precision on the cross-section for $e^+e^- \to H^0Z$ as a function of the Higgs mass. An integrated luminosity proportional to the center-of-mass energy in fb^{-1}/GeV at a center-of-mass energy corresponding to the maximum of the cross-section is assumed. The center-of-mass energy which yields the largest cross-section is also shown (dashed line, right scale).

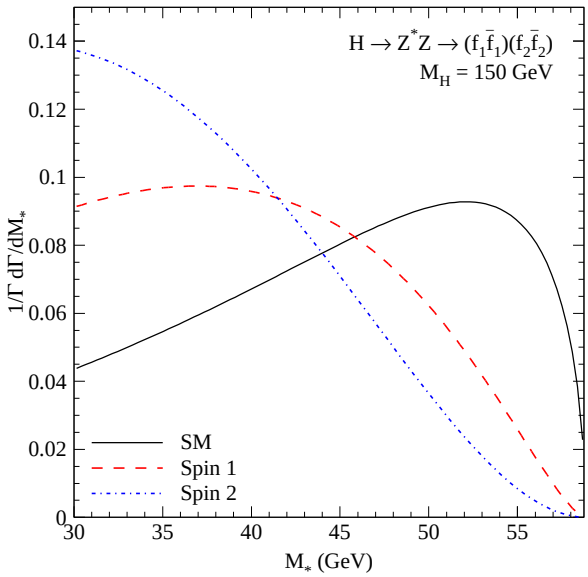

Figure 4: Distribution of the of the invariant mass of the decay products of the off-shell Z^* boson in $H^0 \to ZZ^*$ decays for the SM Higgs and for examples of spin-1 and spin-2 bosons for $m_H = 150$ GeV (from [25]).

be exploited to gain sensitivity to Higgs boson spin and CP [24, 25].

The CP quantum number, like the spin, can be determined from both Higgs boson production and decay [26]. In the TDR, the sensitivity of the angular distribution of the Z recoiling against the H^0 in Higgs-strahlung was exploited. Recently a method has been proposed which makes use of the transverse spin correlation in $H^0 \to \tau^+\tau^-$ decays. The spin correlations between the two τ leptons is probed through angular correlations of their decay products. In particular, events from $\tau^\pm \to \rho^\pm\nu_\tau \to \pi^\pm\pi^0\nu_\tau$ and from $\tau^\pm \to a_1^\pm\nu_\tau \to \rho^0\pi^\pm\nu_\tau \to \pi^\pm\pi^\mp\pi^\pm\nu_\tau$ can be used. The angle between the decay planes of the two ρ mesons from either τ decay provides a suitable observable [27, 28]. While this angle can be determined in the laboratory frame, ideally it is evaluated in the Higgs boson rest frame, which can be approximately reconstructed using τ lifetime information [29]. Preliminary results including detector simulation have shown that from a sample of 1 ab^{-1} of Higgs-strahlung events at $\sqrt{s} = 350$ GeV, a statistical separation between a CP-even and a CP-odd Higgs boson of eight standard deviations may be achieved assuming production cross section and branching ratio as for H^0_{SM} (see Fig. 5, note that background is not yet taken into account) [30].

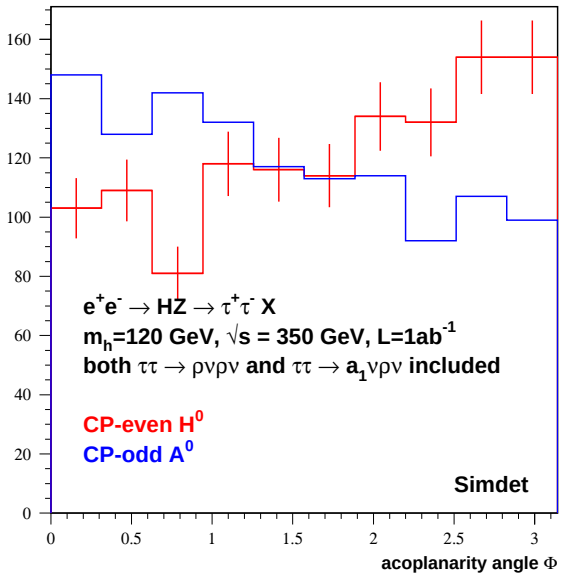

Figure 5: Acoplanarity angle between the two ρ decay planes from $H^0/A^0 \to \tau^+\tau^-$ decays (from [30]).

Decay Branching Ratios

The precise measurement of Higgs boson decay branching ratios is one of the key tasks in LC Higgs physics. In the TESLA TDR as well as in all other regional LC studies [31, 32] analyses have been performed to investigate the expected precisions on the branching ratio determination. For a light Higgs boson with $m_H < 160$ GeV, a large variety of Higgs decay modes can be measured. The hadronic decays into $b\bar{b}, c\bar{c}$, and gg are disentangled via the excellent capabilities of a LC vertex detector. Progress has been achieved recently in the level of detail at which the algorithms to tag b- and c-quarks are implemented into the simulation. Although these studies are not finished, it

looks conceivable that the results of the TDR study will essentially be confirmed [33].

There are two different methods to extract branching ratios from the observed events:

1. Measure the topological cross-section for a given final state, e.g. $\sigma(\mathrm{H^0Z} \to X\mathrm{Z})$ and divide by the total measured Higgs–strahlung cross-section (as obtained from the recoil mass measurement) [34].

2. Select a sample of unbiased $\mathrm{H^0Z}$ events (events in the recoil mass peak) and determine the fraction of events corresponding to a given $\mathrm{H^0} \to X$ decay within this sample.

The latter method was first applied to Higgs branching ratio studies in [35]. Since in this approach binomial (or in principle multi-nomial) statistics can be applied, smaller errors of the branching ratios can be inferred for the same number of events than from a rate measurement. Although only relying on events with $\mathrm{Z} \to \ell^+\ell^-$, the latter method yields errors very similar to those of the TDR method [34]. The achievable precision for the both methods for a SM Higgs boson of 120 GeV from a sample of 500 fb^{-1} is shown in Table 1. A possible combination of both methods is currently being investigated. While for the hadronic Higgs decays, there is a sizable overlap, for the $\mathrm{H^0} \to W^+W^-$ decay a significant improvement may be expected from combination.

Besides the decays into $\mathrm{b\bar{b}}, \mathrm{c\bar{c}}, \mathrm{gg}, \tau^+\tau^-, W^+W^-$, Z^0Z^0, and $\gamma\gamma$ further decay modes have been studied. The very rare decay $\mathrm{H^0} \to \mu^+\mu^-$ might be detectable in WW-fusion events at $\sqrt{s} = 800$ GeV for $\mathrm{m_H} = 120$ GeV. A measurement of the muon Yukawa coupling with approximately 15% relative accuracy may be obtained from a sample of 1 ab^{-1}. Here, the logarithmic rise of the signal cross-section with $\sqrt{s}$ is of advantage. A precision measurement of the $\mathrm{H^0} \to \mu^+\mu^-$ branching ratio however can only be performed at even higher luminosity or at higher energy [36]. The expected signal is shown in Fig. 6.

Another rare Higgs boson decay is the loop-induced $\mathrm{H^0} \to \mathrm{Z}\gamma$ decay. This decay has been studied in the $WW \to \mathrm{H^0} \to \mathrm{q\bar{q}}\gamma$ final state for a sample of $1\mathrm{ab}^{-1}$ at 500 GeV for 120 GeV $< \mathrm{m_H} <$ 160 GeV. Around the expected maximum of the branching ratio for a SM Higgs boson (140 GeV), a relative error of 27% can be expected while for lower (120 GeV) and higher (160 GeV) Higgs masses only upper limits at 70-80% of the SM branching ratio can be expected to be set [37]. The expected signal is shown in Fig. 7 together with the background.

Invisible Higgs Decays

In the TDR it was pointed out that the decay independent recoil mass technique allows us to extract a possible invisible decay width of the Higgs boson by comparing the rate of events in the recoil mass peak with the rate for all visible decays. This indirect technique is now complemented by a study which explicitly asks for missing energy and momentum compatible with an invisible Higgs decay. At $\sqrt{s} = 350$ GeV, the achievable precision on the invisible branching ratio is shown to be significantly higher than in the indirect approach, yielding e.g. a relative precision of $\sim$ 10% for a branching ratio of 5% and a 5σ observation down to a branching ratio of 1.5-2.0% with 500 fb^{-1} at $\sqrt{s} = 350$ GeV and Higgs masses between 120 and 160 GeV [38] (see Fig. 8).

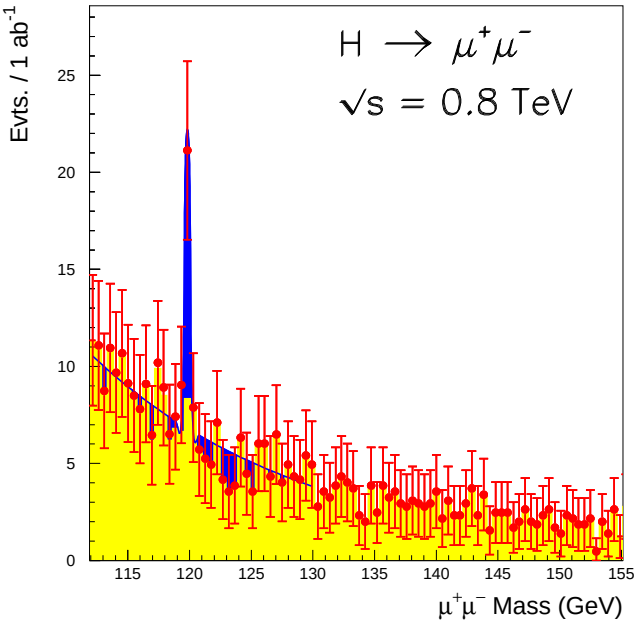

Figure 6: Expected mass spectrum for the decay $\mathrm{H^0} \to \mu^+\mu^-$ from a sample of $1\mathrm{ab}^{-1}$ at $\sqrt{s} = 800$ GeV for $\mathrm{m_H} = 120$ GeV (from [36]).

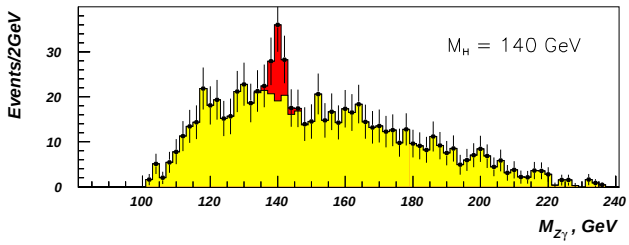

Figure 7: Expected mass spectrum for the decay $\mathrm{H^0} \to \mathrm{Z}\gamma$ from a sample of 1 ab^{-1} at $\sqrt{s} = 500$ GeV for $\mathrm{m_H} = 120$ GeV (from [37]).

Heavier SM Higgs Boson

Above a Higgs mass of approximately 2 $\mathrm{m_W}$, the phenomenology of the SM Higgs changes quite drastically. First, the bosonic decays into $\mathrm{W^+W^-}$ and ZZ rapidly become dominant, leaving only very little room for Yukawa couplings to be probed directly. Second, the total decay width increases rapidly with mass, exceeding 1 GeV for $\mathrm{m_H} > 190$ GeV.

In order to assess the question up to which Higgs mass a

Table 1: Summary of expected precisions on Higgs boson branching ratios from existing studies within the ECFA/DESY workshops. (a) for 500 fb^{-1} at 350 GeV; (b) for 500 fb^{-1} at 500 GeV; (c) for 1 ab^{-1} at 500 GeV; (d) for 1 ab^{-1} at 800 GeV; (e) as for (a), but method described in [35] (see text).

Mass(GeV)	120	140	160	180	200	220	240	280	320
Decay	Relative Precision (%)								
$b\bar{b}$	2.4 (a) / 1.9 (e)	2.6 (a)	6.5 (a)	12.0 (d)	17.0 (d)	28.0 (d)			
$c\bar{c}$	8.3 (a) / 8.1 (e)	19.0 (a)							
$\tau\tau$	5.0 (a) / 7.1 (e)	8.0 (a)							
$\mu\mu$	30. (d)								
gg	5.5 (a) /4.8 (e)	14.0 (a)							
WW	5.1 (a) / 3.6 (e)	2.5 (a)	2.1 (a)		3.5 (b)		5.0 (b)	7.7 (b)	8.6 (b)
ZZ			16.9 (a)		9.9 (b)		10.8 (b)	16.2 (b)	17.3 (b)
$\gamma\gamma$	23.0 (b) / 35.0 (e)								
$Z\gamma$		27.0 (c)							

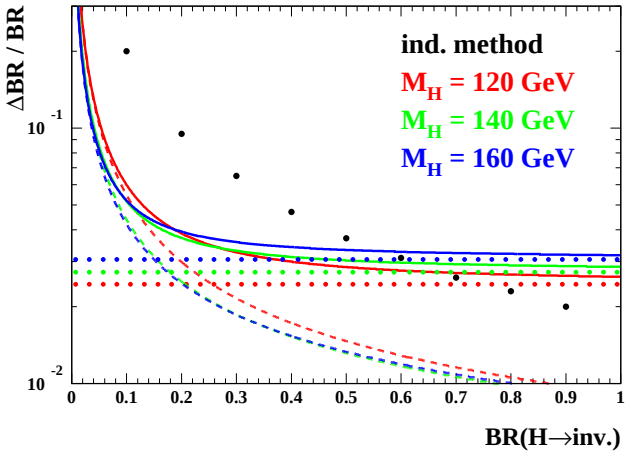

Figure 8: Accuracy on the branching ratio $H^0 \to invisible$, as a function of $BR(H^0 \to invisible)$ for three Higgs masses using 500 fb^{-1} at 350 GeV (full line). The dashed and dotted lines indicate the contributions from the measurement of the invisible rate and from the total Higgs-strahlung cross section measurement, respectively. The large dots are the result of the indirect method, presented in the TDR (from [38]).

direct Yukawa coupling measurement would still be possible, a study was performed which aims at selecting $H^0 \to b\bar{b}$ as a rare Higgs decay [39]. Like in the case of $H^0 \to \mu^+\mu^-$, the large number of Higgs bosons produced in the WW-fusion channel at high energy is favorable in comparison to using the Higgs-strahlung process at lower energies. For $1 ab^{-1}$ of data at $\sqrt{s} = 800$ GeV, a 5σ sensitivity to the bottom Yukawa coupling is achievable for $m_H < 210$ GeV. A measurement of the branching ratio $BR(H^0 \to b\bar{b})$ is possible with (12,17,28) % accuracy for m_H = (180,200,220) GeV.

The second question about heavier Higgs bosons is, whether the Higgs line-shape parameters (mass, decay width, Higgs-strahlung production cross section) can be measured. A complete study of the mass range 200 GeV $< m_H <$320 GeV has been performed [40]. The final state $q\bar{q}q\bar{q}\ell^+\ell^-$ resulting from $H^0Z \to ZZZ$ and from $H^0Z \to W^+W^-Z$ is selected. A kinematic fit is used to assign the possible di-jet combinations to bosons (W^+W^- or ZZ). The resulting di-boson mass spectrum can be fitted by a Breit-Wigner distribution convoluted with a detector resolution function. A relative uncertainty on the Higgs mass of 0.11 – 0.36 % is achievable from 500 fb^{-1} at 500 GeV for masses between 200 and 320 GeV. The resolution on the total width varies between 22 and 34% for the same mass range. Finally, the total Higgs-strahlung cross-section can be measured with 3.5 – 6.3% precision. Under the assumption that only $H^0 \to W^+W^-$ and $H^0 \to ZZ$ decays are relevant, their branching ratios can be extracted with 3.5–8.6% and 9.9–17.3%, respectively (see Table 2). The expected mass spectra for $m_H = 200$ GeV and $m_H = 320$ GeV are shown in Fig. 9.

Table 2: Expected precision on Higgs boson line-shape parameters for $200 < m_H < 320$ GeV at a LC with $\sqrt{s} = 500$ GeV.

m_H (GeV)	$\Delta\sigma$ (%)	Δm_H (%)	$\Delta\Gamma_H$ (%)
200	3.6	0.11	34
240	3.8	0.17	27
280	4.4	0.24	23
320	6.3	0.36	26

Top Yukawa Coupling

For $m_H < 2m_t$, the top quark Yukawa coupling is not directly accessible from Higgs decays. The only relevant tree level process to access the top quark Yukawa coupling is the process $e^+e^- \to H^0t\bar{t}$ [41]. Due to the large

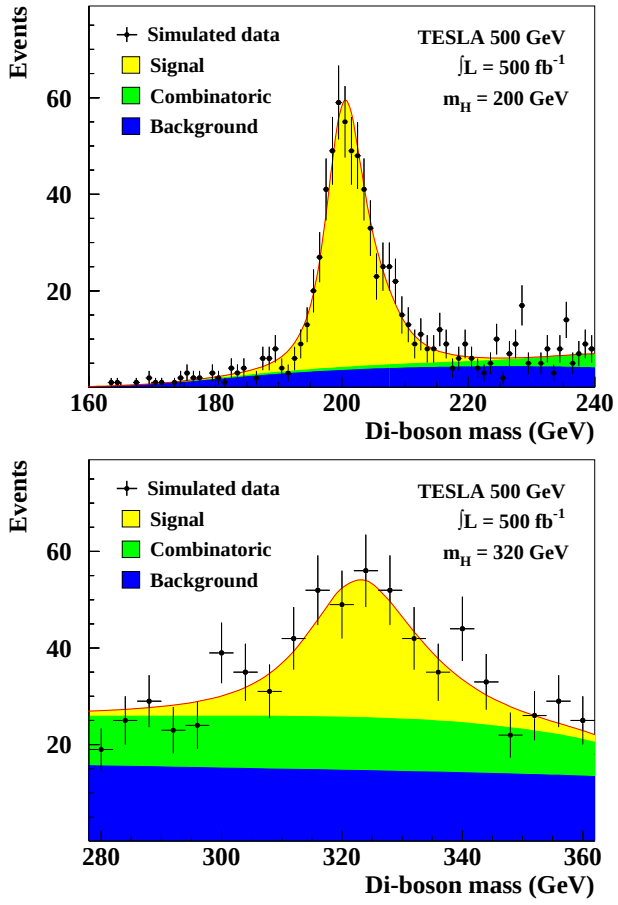

Figure 9: Expected reconstructed Higgs boson mass spectra for $m_H = 200$ GeV and $m_H = 320$ GeV from 500 fb^{-1} at 500 GeV (from [40]).

masses of the final state particles, the process only has a significant cross-section at center-of-mass energies significantly beyond 500 GeV. Higher order QCD corrections to the process have been calculated and are significant [42]. Recently, also the full $\mathcal{O}(\alpha)$ electro-weak corrections became available [43]. Experimental studies have been performed for $m_H < 130$ GeV in the TDR [44] and in the NLC study [45]. Recently a completely new study has been performed with refined b-tagging simulation as well as for an extended mass range of up to $m_H = 200$ GeV, exploiting also the $H^0 \to W^+W^-$ decay [46]. For the $H^0 \to b\bar{b}$ case, both the $t\bar{t} \to b\bar{b}q\bar{q}\ell^-\bar{\nu}$ and the $t\bar{t} \to b\bar{b}q\bar{q}q\bar{q}$ channels have been analyzed. For the $H^0 \to W^+W^-$ case, the 2-like-sign lepton plus 6-jet and the single lepton plus 8-jet final states were studied. The events were selected by neural networks. The generic 6-fermion background is fully taken into account. The expected uncertainties on the top Yukawa coupling for $1 ab^{-1}$ at 800 GeV range from 6–14% for $120 < m_H < 200$ GeV and are shown in Fig. 10.

Higgs Potential

The observation of a non-zero self-coupling of the Higgs boson is the ultimate proof of spontaneous symmetry breaking being responsible for mass generation of the SM bosons and fermions since it probes the shape of the Higgs potential and thus the presence of a vacuum expectation value. Higgs boson self-coupling in general leads to triple and quartic Higgs boson couplings out of which only the former is accessible. For 500 GeV center-of-mass energy, the double Higgs-strahlung process, $e^+e^- \to H^0H^0Z$ is most promising for observation, the small cross-section of 0.1 - 0.2 fb however demands the highest possible luminosity and calls for ultimate jet energy resolution since only if the most frequent six jet final state $b\bar{b}b\bar{b}q\bar{q}$ can be reconstructed, the signal rate becomes significant. The cross-section has been calculated in [47] and radiative corrections became known recently [48]. In the TDR, an experimental analysis for $m_H = 120$ GeV was presented [49] which concluded that with $1 ab^{-1}$ of data at 500 GeV, a precision of 17 - 23 % for $120 < m_H < 140$ GeV on the $e^+e^- \to H^0H^0Z$ cross-section can be achieved. Recently, the potential of the WW-fusion channel for higher Higgs boson masses at higher energies was discussed and compared to the possibilities at the LHC in [50]. Furthermore, it was discussed how the existing analyses might be improved by exploiting kinematic differences between the signal diagram and diagrams which lead to the same final state without involving the triple Higgs coupling (dilution diagrams), namely the sequential radiation of two Higgs bosons from one Z boson and the diagram which involves the quartic ZZHH coupling [51]. In particular, the invariant mass of the hadronic system which is formed by the two Higgs boson decay products is sensitive to the different contributions to the HHZ final state. Its distribution is shown in Fig. 11. A reduction of the uncertainty on the trilinear coupling from 0.23 to 0.20 can be obtained.

MINIMAL SUPERSYMMETRIC HIGGS SECTOR

Theoretical Predictions

The Higgs sector of the Minimal Supersymmetric Standard Model (MSSM) comprises two complex scalar field doublets which acquire vacuum expectation values v_1 and v_2. After electro-weak symmetry breaking, two charged Higgs bosons ($H^\pm$) and three neutral Higgs bosons emerge, two of which are CP-even (h^0, H^0) and one is CP-odd (A^0), if CP is conserved. In contrast to the SM, the Higgs masses are predicted in terms of the fundamental parameters of the MSSM. At tree level, the mass spectrum is determined by $\tan\beta = v_2/v_1$ and m_A and the mass of the h^0 has to fulfill $m_h < m_Z$. Higher order corrections, predominantly from loops involving third generation fermions and their supersymmetric partners, have large influence. In particular, m_h can be as large as 135 GeV [52]. A compilation of more recent higher order corrections can be found in [53].

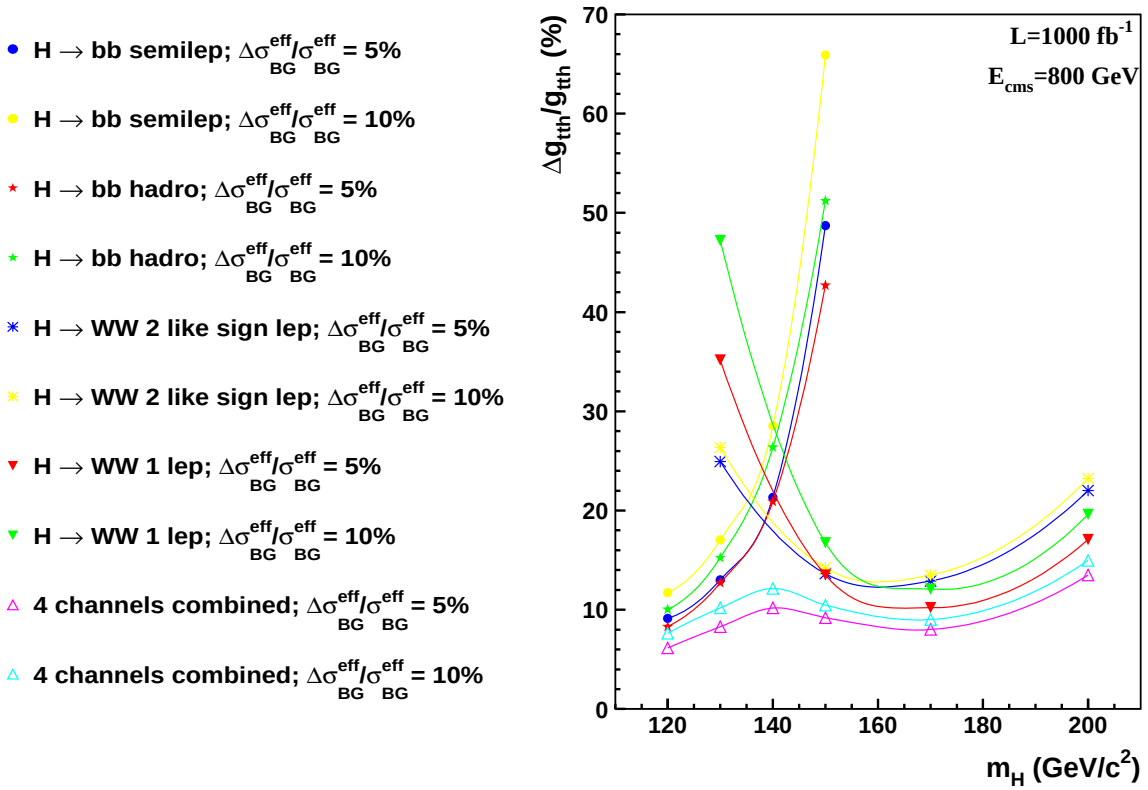

Figure 10: Expected relative precision on the top Yukawa coupling for $120 < m_H < 200$ GeV from 1 ab^{-1} at 800 GeV for various final states and for two different assumptions of the systematic uncertainty on the background (BG) normalization (from [46]).

The value of m_h as a function of $\tan\beta$ is shown for two different cases of scalar-top mixing (no-mixing and m_h^{max} scenarios of [56]) in Fig. 12. The complete 1-loop and dominant 2-loop SUSY corrections to the production cross-sections for $e^+e^- \to h^0Z$ [54, 55] and the 1-loop corrections from stop-sbottom loops for $e^+e^- \to \nu_e\bar{\nu}_e h^0$ [57, 58] are calculated.

The MSSM Higgs sector exhibits a so-called decoupling limit as m_A becomes large, in which the h^0 approaches the properties of the SM Higgs boson [59] This limit is approached relatively fast for $m_A > 200$ GeV in a large portion of the MSSM parameter space. However, also scenarios far away from decoupling (e.g. *the intense coupling scenario* [60]) is experimentally not excluded and theoretically possible. In such a scenario, all Higgs bosons are accessible already at 500 GeV and a rich phenomenology is waiting to be disentangled. The closer the MSSM scenario moves towards the decoupling limit the more difficult it becomes to distinguish the Higgs sector from the SM. Therefore most analyses focus on a close-to-decoupling scenario. In this case, the analyses for a light SM Higgs apply also for h^0. It is the task of the LC to employ the precise measurements of the properties of this lightest Higgs boson to distinguish it from a SM Higgs and draw conclusions on the supersymmetric parameters.

Study of Heavy Neutral SUSY Higgs Bosons

If $\cos^2(\beta-\alpha)$ is small[1], the heavy neutral MSSM Higgs bosons are predominantly produced through the process, $e^+e^- \to H^0A^0$. With the mass splitting between H^0 and A^0 being small for a large part of the parameter space, the mass reach of the LC for H^0 and A^0 is approximately $\sqrt{s}/2$. In this case, the coupling of the H^0 to gauge bosons is small, therefore the dominant decays of both H^0 and A^0 are $b\bar{b}$ and $\tau^+\tau^-$. During the workshop, a new experimental study was started to fully determine the sensitivity of the LC to the heavy MSSM Higgs bosons through the pair production process [62]. For the first time, both the $b\bar{b}b\bar{b}$ and $b\bar{b}\tau^+\tau^-$ final states are analyzed including detector simulation and complete standard model backgrounds. Preliminary results at 500 GeV and 800 GeV center-of-mass energy were obtained. The following assumptions are made: 500 fb^{-1} at 500 GeV and at 800 GeV, $\cos^2(\beta-\alpha) = 0$, BR($H^0 \to b\bar{b}$) = 90%, BR($H^0 \to \tau^+\tau^-$) = 10%. Mass reconstruction is performed using a kinematic fit which imposes energy-momentum conservation. Therefore a good mass reconstruction is achieved both in the $b\bar{b}b\bar{b}$ and $b\bar{b}\tau^+\tau^-$ final states, see Fig. 13 and 14. The achievable precisions on masses and topological cross-sections are listed in Table 3 for various choices of m_H and m_A.

[1] α is the mixing angle in the CP-even neutral Higgs sector

Table 3: Expected precision on the properties of heavy MSSM Higgs bosons from 500 fb^{-1} at 500 GeV (a) and 800 GeV (b), respectively (from [62]).

	m_A	m_H	precision on			
			$(m_A + m_H)$	$(\lvert m_A - m_H \rvert)$	$\sigma(\mathrm{bbbb})$	$\sigma(\mathrm{bb}\tau^+\tau^-)/\sigma(\tau^+\tau^-\mathrm{bb})$
	(GeV)	(GeV)	(GeV)	(GeV)	(%)	(%)
(a)	140	150	0.2	0.2	1.5	7.2/6.3
(a)	150	200	0.3	0.4	2.3	9.7/8.7
(a)	200	200	0.4	0.4	2.7	8.1
(a)	200	250	0.4	1.2	6.5	-
(b)	250	300	0.5	0.7	3.0	13.8/11.9
(b)	300	300	0.6	0.7	3.5	10.0
(b)	300	400	1.9	2.8	7.0	-

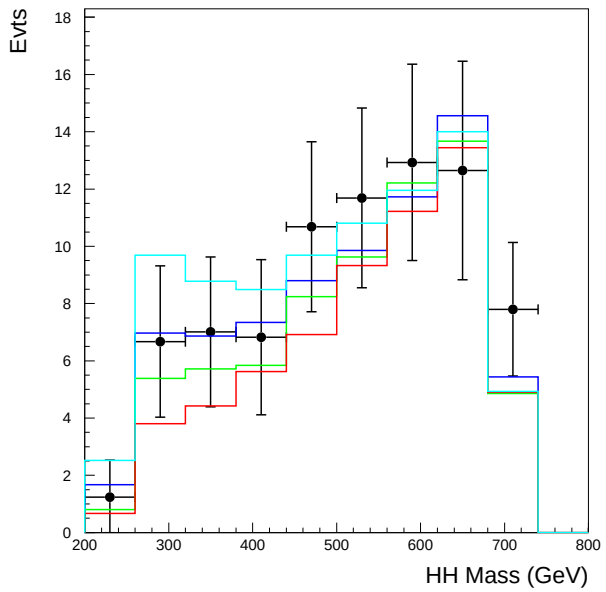

Figure 11: Distribution of the $\mathrm{H}^0\mathrm{H}^0$ invariant mass in $\mathrm{e}^+\mathrm{e}^- \to \mathrm{H}^0\mathrm{H}^0\mathrm{Z}$ events for $m_H = 120$ GeV (1 ab^{-1} at 800 GeV). The histograms are for predictions of the trilinear Higgs coupling ranging from 1.25 to 0.5 (top to bottom) times the SM coupling. (from [51]).

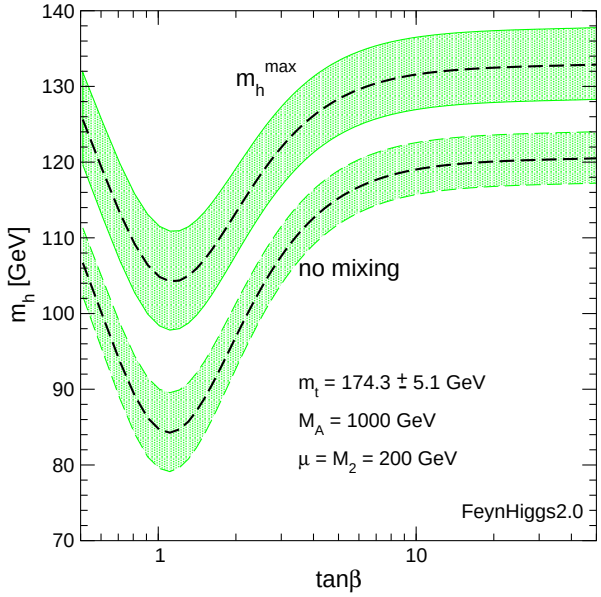

Figure 12: Largest mass of the light CP even Higgs boson of the MSSM as a function of $\tan\beta$ for two scenarios of scalar-top mixing (no-mixing and m_h^{max} scenarios of [56]). The bands indicate the effect of varying the top quark mass by 1 standard deviation of its current error.

Since at the tree level and in the decoupling limit the heavy neutral MSSM Higgs bosons decouple from the Z, the mass reach for their discovery at a LC is limited to approximately $\sqrt{s}/2$ from the pair production process. It has been investigated during the workshop, how single production mechanisms could extend the mass reach of an $\mathrm{e}^+\mathrm{e}^-$ LC. In particular, the WW-fusion process $\mathrm{e}^+\mathrm{e}^- \to \nu_e\bar{\nu}_e\mathrm{H}^0$ has been investigated [57]. Its tree level cross-section is proportional to $\cos(\beta - \alpha)$. Depending on the SUSY parameters, radiative corrections might increase the cross-section for $\mathrm{e}^+\mathrm{e}^- \to \nu_e\bar{\nu}_e\mathrm{H}^0$, possibly allowing discovery beyond the pair production kinematic limit for certain choices of the MSSM parameters. Using left-polarized electron beams and right-polarized positron beams the cross-section can further be enhanced. A particular scenario where this is the case has been chosen in [57] ($M_{\mathrm{SUSY}} = 350$ GeV, $\mu = 1000$ GeV, $M_2 = 200$ GeV and large stop mixing). Cross-section contours for this scenario are shown in Fig. 15.

Charged Higgs Bosons

Charged Higgs bosons can be pair-produced at the LC via $\mathrm{e}^+\mathrm{e}^- \to \mathrm{H}^+\mathrm{H}^-$ if $m_{\mathrm{H}^\pm} < \sqrt{s}/2$. A complete simulation of this process for the decay $\mathrm{H}^+ \to t\bar{b}$ has been performed for $\sqrt{s} = 800$ GeV, 1 ab^{-1}, and $m_{\mathrm{H}^\pm} = 300$ GeV [63]. The expected signal and background are shown in Fig. 16. The mass resolution is approximately 1.5%. A 5σ discovery will be possible for $m_{\mathrm{H}^\pm} < 350$ GeV.

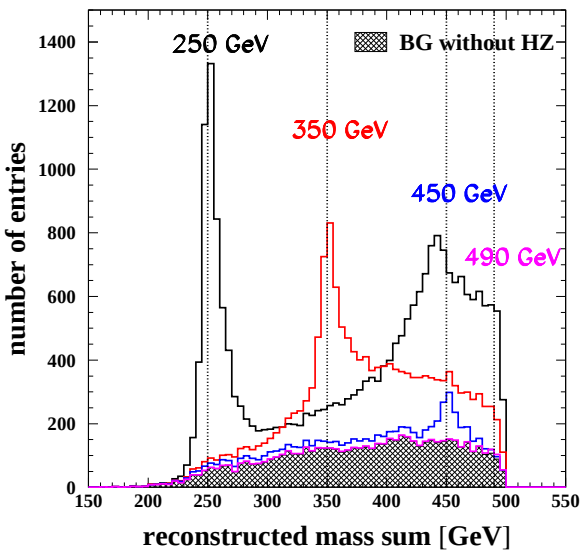

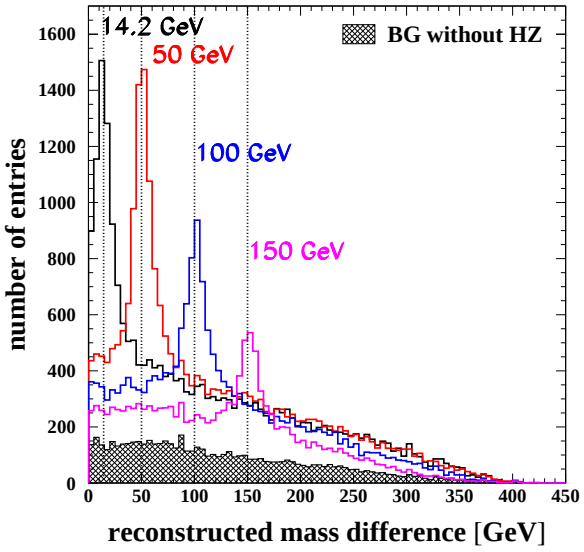

Figure 13: Simulated signals and background of the process $e^+e^- \to H^0A^0 \to b\bar{b}b\bar{b}$. Top: reconstructed sum of the two Higgs candidate masses. Bottom: reconstructed difference of the two Higgs boson candidate masses. The study was performed at 500 GeV center-of-mass energy and for 500fb^{-1}. BR($H^0 \to b\bar{b}$) = BR($A^0 \to b\bar{b}$) = 0.9 was assumed (from [62]).

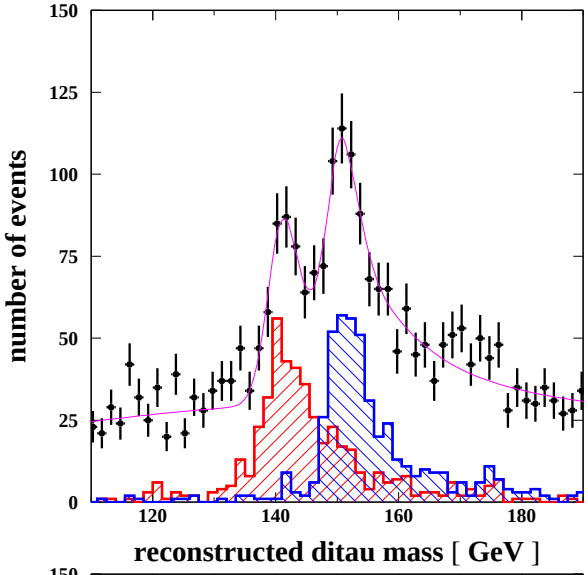

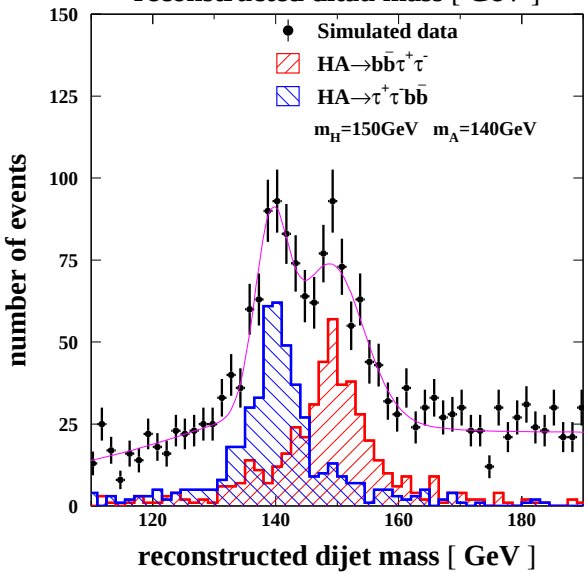

Figure 14: Simulated signal and background of the process $e^+e^- \to H^0A^0 \to b\bar{b}\tau^+\tau^-(\tau^+\tau^-b\bar{b})$ for $m_A = 140$ GeV and $m_H = 150$ GeV at 500 GeV center-of-mass energy (500fb^{-1}). Top: reconstructed $\tau\tau$ invariant mass from a kinematic fit. Bottom: reconstructed $b\bar{b}$ invariant mass from a kinematic fit. BR($H^0 \to \tau^+\tau^-$) = BR($A^0 \to \tau^+\tau^-$) = 0.1 was assumed (from [62]).

Since in pair production the mass reach for charged Higgs bosons is limited to $\sqrt{s}/2$, also the rare processes of single charged Higgs production may be considered. The dominant processes for single charged Higgs production are $e^+e^- \to b\bar{t}H^+, e^+e^- \to \tau^-\bar{\nu}_\tau H^+$, and $e^+e^- \to W^-H^+$. Their cross-sections have been calculated at leading order in [64]. QCD corrections to $e^+e^- \to b\bar{t}H^+$ have recently become available [65] and are sizable. In general, parameter regions for which the production cross-section exceeds 0.1 fb are rather small for charged Higgs masses beyond the pair production threshold. Cross-section contours for $\sqrt{s} = 500$ GeV and 800 GeV are shown in Fig. 17.

Constraints on SUSY Parameters

At tree level, the MSSM Higgs sector only depends on $\tan\beta$ and m_A. Thus, if m_A would be measured, $\tan\beta$ could in principle be uniquely determined from the observed Higgs properties. In particular, the coupling of A^0 to down-type fermions is directly proportional to $\tan\beta$. Therefore this coupling which appears in the rate of the $e^+e^- \to b\bar{b}A^0$ and $e^+e^- \to A^0H^0 \to b\bar{b}b\bar{b}$ processes, as well as in the total decay width Γ_A can be used to extract

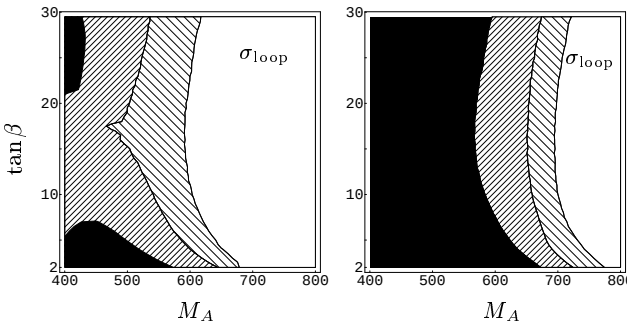

Figure 15: Cross-section contours for $e^+e^- \to H^0\nu\bar{\nu}$ for a particular MSSM scenario (see text) in the $m_A - \tan\beta$-plane for $\sqrt{s} = 1$ TeV. The different shadings correspond to: white: $\sigma \leq 0.01$fb, light shaded: $0.01\text{fb} \leq \sigma \leq 0.02$fb, dark shaded: $0.02\text{fb} \leq \sigma \leq 0.05$fb, black: $\sigma \geq 0.05$fb (from [57]). The left figure is for unpolarized beams, the right figure for an electron (positron) polarization of 0.8 (0.6).

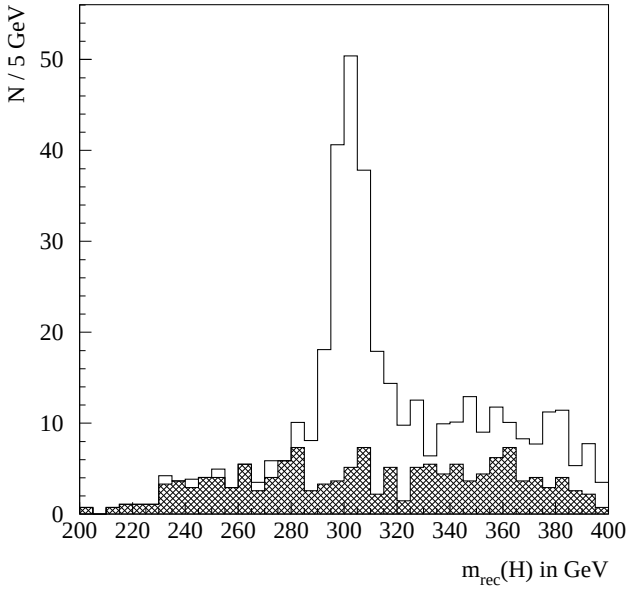

Figure 16: Simulated signal and background of the process $e^+e^- \to H^+H^- \to t\bar{b}\bar{t}b$ for $m_{H^\pm} = 300$ GeV at 800 GeV center-of-mass energy (1ab^{-1}) (from [63]).

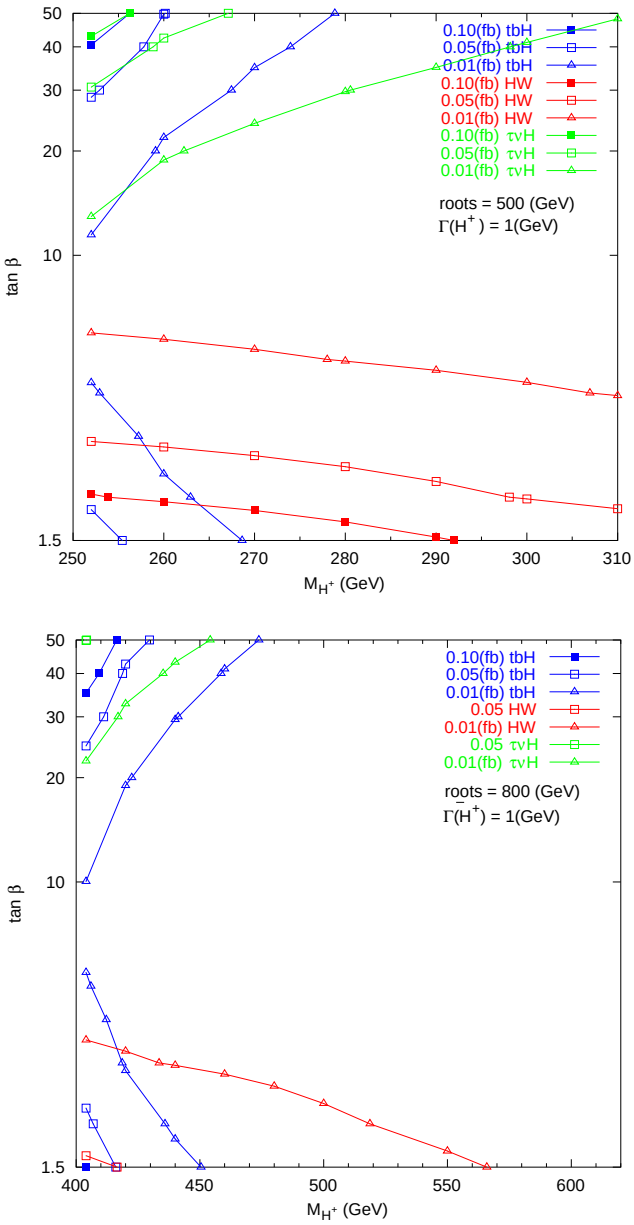

Figure 17: Cross-section contours for the processes $e^+e^- \to b\bar{t}H^+(blue/dark), e^+e^- \to \tau^-\bar{\nu}_\tau H^+$ (green/light grey), and $e^+e^- \to W^-H^+$ (red/medium grey) at $\sqrt{s} = 500$ GeV (upper) and at 800 GeV (lower). (from [66]).

$\tan\beta$ in principle. This has been studied in [67]. Due to the large radiative corrections the predictions for the observables also depend on other SUSY parameters (in particular the sfermion masses and mixings) which are fixed in this analysis. Therefore the resulting errors (see 18) are only valid if all other SUSY parameters, were precisely known.

A different approach to $\tan\beta$ determination has been proposed in [68]. In a scenario where all SUSY particles are light compared to the center-of-mass energy, the dependence of the cross-section for charged Higgs production on $\sqrt{s}$ in the 1 TeV domain can be compared to the logarithmic Sudakov expansion of the cross-section. In particular, it has been shown, that the first coefficient of the expansion depends only on $\tan\beta$.

A complete study of SUSY parameter determination in the full MSSM is only possible when studies of the Higgs sector are combined with information on sparticle production. Within more constrained SUSY models which assume specific SUSY breaking schemes Higgs observables alone can lead to significant constraints [69]. As an example, the NUHM (non-universal Higgs mass) model has been considered in [70]. The NUHM model assumes unification of sfermion masses and mixing terms as well as unification of gaugino mass terms at a high scale. However, in con-

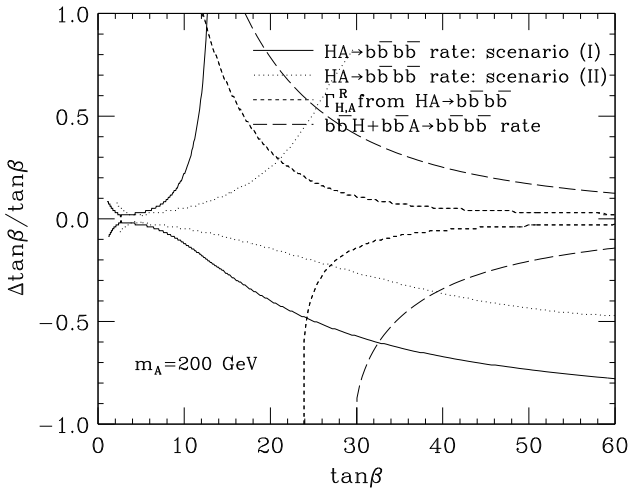

Figure 18: Sensitivity of the $e^+e^- \to H^0A^0 \to b\bar{b}b\bar{b}$ and $e^+e^- \to b\bar{b}A^0/H^0$ cross-sections and the total decay widths $\Gamma_{H/A}$ on $\tan\beta$. Assumed measurement errors are for 2 ab^{-1} at 500 GeV without detector simulation (except for $e^+e^- \to b\bar{b}A^0/H^0$). $m_A = m_H = m_{H^\pm} =$ 200 GeV and all SUSY parameters except $\tan\beta$ are fixed (from [67]).

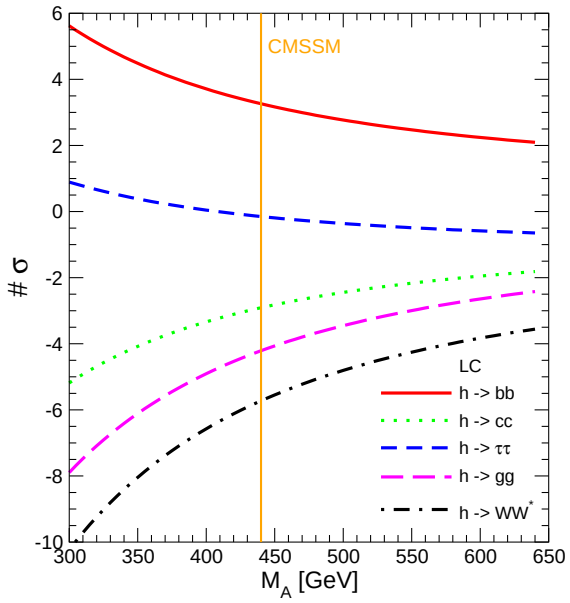

Figure 19: Deviation of decay branching ratios of the lightest CP even Higgs in the constrained MSSM with non-universal Higgs mass (NUHM) (for $\tan\beta = 10, A_0 = 0, m_{1/2} = 300$ GeV and $m_0 = 0$) from their SM values in terms of standard deviations of the prospective measurement error at the LC as a function of $\tan\beta$. The dependence on μ is weak (from [70]). The errors are taken from [1].

trast to the mSUGRA (minimal supergravity) model, both μ and m_A are free parameters. In Fig. 19, the deviation of branching ratios of the lightest Higgs boson from the SM is shown for the NUHM scenario as a function of m_A. The deviation is plotted in terms of standard deviations of the prospective measurement error at the LC as described in the TDR. It can be seen that in particular $h^0 \to b\bar{b}$ and $h^0 \to W^+W^-$ provide good sensitivity to m_A while the dependence on μ is only weak. As a caveat, the values of $\tan\beta$ as well as the other model parameters are fixed in this study and thus have to be allowed to vary freely in the study or assumed to be known from elsewhere in order to translate the plotted deviations into expected errors on the parameter measurements.

Another study utilizes the ratio $\mathcal{R} = BR(h^0 \to b\bar{b})/BR(h^0 \to \tau^+\tau^-)$ [71]. At tree level, in the MSSM, this ratio is constant since both b quarks and τ leptons are down-type fermions, coupling proportionally to $\sin\alpha/\cos\beta$ to the h^0. A precise measurement of this ratio is therefore sensitive to the difference of the radiative corrections to these two decays. In particular at large $\tan\beta$ these corrections become relevant, allowing to gain sensitivity to the value of $\tan\beta$ itself if all other SUSY parameters are fixed. The ratio of $\mathcal{R}^{MSSM}/\mathcal{R}^{SM}$ as a function of $\tan\beta$ is shown in Fig. 20.

CP violation in the SUSY Higgs Sector

In the MSSM the Higgs potential is invariant under the CP transformation at tree level. However, it is possible to break CP symmetry in the Higgs sector by radiative corrections, especially by contributions from third generation scalar-quarks [72, 73, 74]. Such a scenario is theoretically attractive since it provides a possible solution to the cosmic baryon asymmetry [75]. In a CP violating scenario the three neutral Higgs bosons, H_1, H_2, H_3, are mixtures of the CP even and CP odd Higgs fields. Consequently, they all couple to the Z boson and to each other. These couplings may be very different from those of the CP conserving case. In the CP violating scenario the Higgs-strahlung processes $e^+e^- \to H_iZ$ ($i = 1, 2, 3$) and pair production processes $e^+e^- \to H_iH_j$ ($i \neq j$) may all occur, with widely varying cross-sections.

In a case study, for $m_{H^\pm} = 200$ GeV and $\tan\beta = 3$, the sensitivity of the observable Higgs masses m_{H_1}, m_{H_2} and of the observed cross-section for $e^+e^- \to H_1H_2 \to b\bar{b}b\bar{b}$ to the real and imaginary part of the trilinear coupling A_t has been analyzed. Under the assumption that the other SUSY parameters are known, the complex phase of A_t may be extracted from these observables [62]. Clearly, further studies are needed in order to extract CP-violating SUSY parameters from the Higgs sector.

EXTENDED MODELS

Genuine Dimension-Six Higgs Operators

If a light Higgs boson is discovered at the LHC but no additional particles are seen at the LHC or the LC, it is important to search for small deviations of the Higgs boson

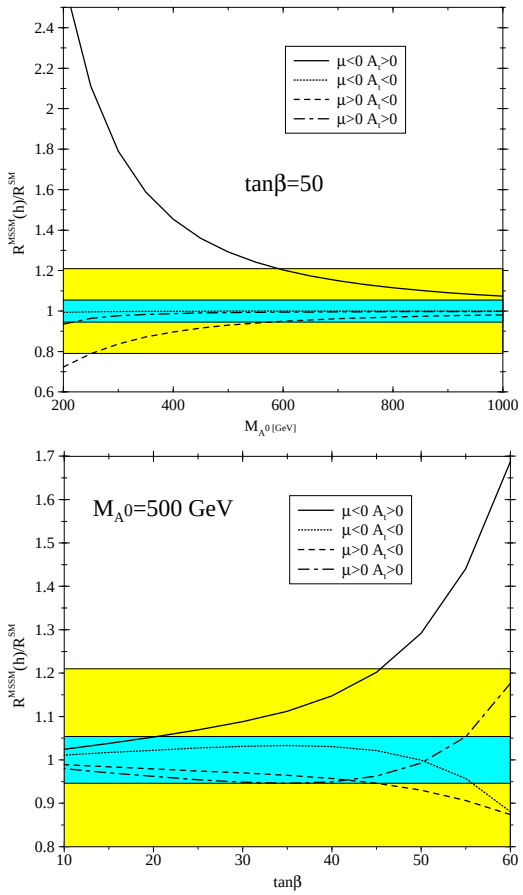

Figure 20: Deviation of the ratio $\mathcal{R} = BR(\mathrm{h}^0 \to \mathrm{b\bar{b}})/BR(\mathrm{h}^0 \to \tau^+\tau^-)$ as a function of $\mathrm{m_A}$ (top) and $\tan\beta$ (bottom). (from [71]. The inner band represents the expected measurement error taken from [1].

potential from the SM predictions to probe new physics scales. If the reason for such small deviations is beyond-SM physics at large scales Λ, the effective operator approach can be chosen to parameterize the low-energy behavior of such models. Recently, operators of dimension six have been studied, which involve only the Higgs field and which are not severely constrained by precision electro-weak data [76]. These operators are

$$\mathcal{O}_1 = \frac{1}{2}\partial_\mu(\Phi^\dagger\Phi)\partial^\mu(\Phi^\dagger\Phi) \quad \text{and} \quad \mathcal{O}_2 = -\frac{1}{3}(\Phi^\dagger\Phi)^3, \quad (1)$$

which lead to a Lagrangian

$$\mathcal{L}' = \sum_i^2 \frac{a_i}{v^2}\mathcal{O}_i. \quad (2)$$

In [76], it has been shown that the parameter a_1 can be measured to an accuracy of $0.005(0.003)$ corresponding to a scale $\Lambda \approx 4$ TeV, from 1 ab^{-1} of data at 500 (800) GeV through the measurement of the production cross-sections from Higgs-strahlung and WW/ZZ-fusion for $\mathrm{m_H} = 120$ GeV. The parameter a_2 modifies the form of the Higgs potential and thus the Higgs pair production cross-section.

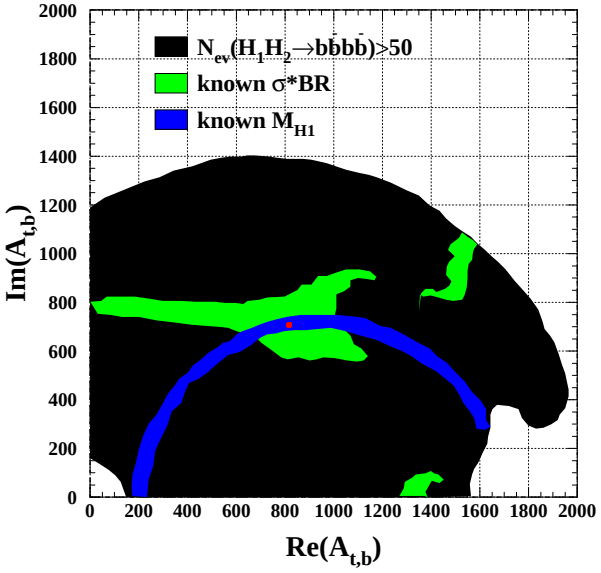

Figure 21: Plane of the real and imaginary part of the trilinear coupling A_t in a CP violating MSSM scenario. In the black region, the Higgs pair production process $\mathrm{e^+e^-} \to H_1H_2$ is observable at $\sqrt{s} = 500$ GeV with 500 fb^{-1}. The chosen model point is (750,800) GeV for the (real,imaginary) part of A_t. The dark grey band is the region which is consistent with the measured lightest Higgs mass, the medium grey region is consistent with the measured $\mathrm{e^+e^-} \to H_1H_2 \to \mathrm{b\bar{b}b\bar{b}}$ rate. The real and imaginary part of A_t can thus be constrained to the overlapping region. Parameters are $\mathrm{m_{H^\pm}} = 200$ GeV and $\tan\beta = 3$ (from [62]).

With the same integrated luminosity, for $\mathrm{m_H} = 120$ GeV, a_2 can be measured to $0.13(0.07)$ at 500 (800) GeV corresponding to a scale $\Lambda \approx 1$ TeV.

Two Higgs Doublet Models

The prospects for the exploration of general Two Higgs Doublet Models (2HDM) at a LC have been discussed e.g. in [1]. During the workshop, a 2HDM scenario has been discussed in which the lightest CP-even Higgs boson has absolute values of the tree level couplings to fermions and massive gauge bosons exactly as in the SM and the other Higgs bosons are heavy ($\mathcal{O}(\mathrm{TeV})$) [77]. Within the 2HDM such a scenario can be realized differently from the SM in two ways: (A) the tree level couplings have the same sign as in the SM or (B) either up-type or down-type fermions have opposite sign couplings as in the SM. The only possibility to distinguish such a scenario from the SM is through loop-induced processes, in particular through the loop-induced $\gamma\gamma\mathrm{h}^0$ and ggh^0 couplings. Depending on $\mathrm{m_h}$ the effect can be large enough to be distinguishable from the SM at the LC (and LHC) from Higgs branching ratio measurements or at a photon collider through the $\gamma\gamma \to \mathrm{h}^0$ process (see Fig. 22).

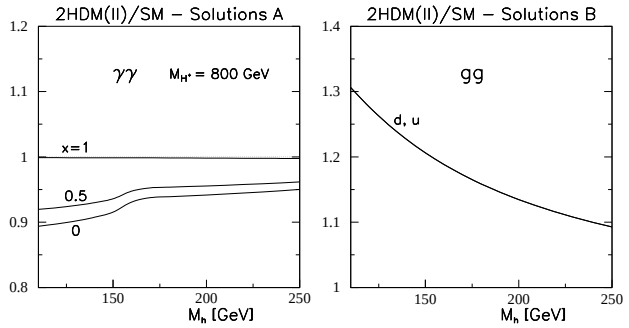

Figure 22: Higgs boson decay widths in the SM-like 2HDM (II) relative to the SM decay widths as functions of M_h. Left: $h \to \gamma\gamma$ decay widths for a 2HDM scenario with all tree-level couplings as in the SM up to an overall sign for $M_{H^\pm} = 800$ GeV and $\mu/\sqrt{2} = xM_{H^\pm}$. Right: $h \to gg$, for a 2HDM scenario with absolute values of tree level couplings as in the SM but opposite relative sign between up-type and down-type fermions (from [77]).

NMSSM

The addition of a Higgs singlet field defines the Next-to-minimal MSSM (NMSSM). This addition is theoretically motivated mainly since it allows a naturally small μ parameter. If the associated Peccei-Quinn symmetry were unbroken, it would lead to a massless CP odd Higgs boson which is ruled out. The LC phenomenology of the model depends on how strong this symmetry is broken. The Higgs spectrum of the NMSSM consists of three CP-even and two CP-odd neutral Higgs bosons and two charged Higgs bosons. The complete LC phenomenology has recently been reviewed in [78]. As an example, the masses of the neutral and charged Higgs bosons and the coupling of the CP-even Higgs bosons to the Z are shown in Fig. 23 as a function of $\mathrm{m_A}$ (defined as the top left parameter of the CP-odd Higgs mixing matrix, see [78]). It can be seen that in a large portion of the parameter space, all three CP-even Higgs bosons would have significant couplings to the Z, thus significant Higgs-strahlung cross-sections at the LC.

Higgs Bosons and Extra Dimensions

Models which postulate the existence of additional space dimensions in order to explain the hierarchy between the electro-weak and the Planck scale have been discussed extensively in recent years. Their common feature is that the apparent weakness of gravity in our 4-dimensional world is a result of its dilution in the extra dimensions. Two scenarios, that of large extra dimensions (ADD) [79] and that of warped extra dimensions (RS) [80] have been discussed in particular. The 'classic' signatures involve deviations of SM processes like $\mathrm{e^+e^- \to f\bar{f}}$ and $\mathrm{e^+e^- \to W^+W^-}$ from the virtual exchange of towers of (ADD) [81] or single [82] Kaluza-Klein (KK) excitations of gravitons, or their real emission together with SM fermions or gauge bosons [83]. These modes have been studied experimentally e.g. in the

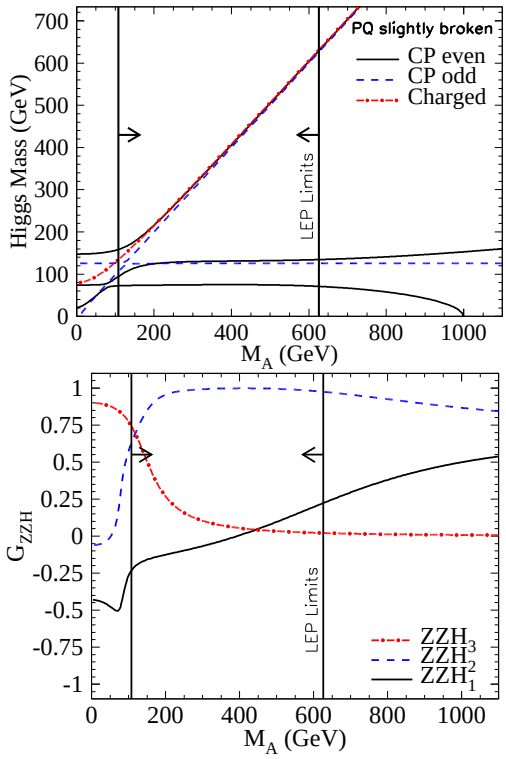

Figure 23: NMSSM Higgs boson properties: masses (upper plot) and couplings of the CP even Higgs bosons to the Z(lower plot) (from [78]) for a scenario with slightly broken Peccei-Quinn symmetry (for $\lambda = 0.05$, $\kappa = 0.02$, $v_s = 15\,v$, $\tan\beta = 3$ and $A_\kappa = -100$ GeV). The arrows denote the region allowed by LEP searches with 95% confidence.

TESLA TDR.

More recently, also the impact of extra dimensions on the Higgs boson phenomenology has been studied. In the ADD scenario, two effects have been analyzed:

1. A modification of the quasi-resonant $\mathrm{W^+W^- \to H^0}$ production process through interference of the SM amplitude with the imaginary part of the graviton/graviscalar KK exchange amplitude [84]. In order to yield a significant modification, a large total Higgs width is needed (i.e. large $\mathrm{m_H}$), which implies on the other hand a large center-of-mass energy. While the graviscalar contribution only modifies the normalization of the cross-section (by few percent for $\sqrt{s} = 1$ TeV, $\mathrm{m_H} = 500$ GeV and 2 extra dimensions at a fundamental Planck scale of 1 TeV), a significant change of the angular distribution is expected from the spin-2 graviton exchange.

2. A modification of the process $\mathrm{e^+e^- \to H^0H^0Z}$ and the existence of the process $\mathrm{e^+e^- \to H^0H^0\gamma}$ which is absent at tree level in the SM [85]. For a 1 TeV LC and $\mathrm{m_H} = 120$ GeV, a sizable correction to $\mathrm{e^+e^- \to H^0H^0Z}$ both in normalization and angular distribution is expected for fundamental Planck scale up to a few TeV. Furthermore, the cross-section for $\mathrm{e^+e^- \to H^0H^0\gamma}$ exceeds 0.1 fb for a fundamental Planck scale below approximately 2 TeV. In [85],

expected 5 σ discovery limits on the fundamental Planck scale of 880–1560 (1640–2850) GeV have been derived at $\sqrt{s} = 500$ (1000) GeV for 6–3 extra dimensions.

In the RS scenario, the influence on the Higgs sector might be much more drastic. Besides the spin-2 KK graviton excitations, graviscalar excitations, called Radions, are predicted [86]. They are predicted to couple to SM particles through the trace of the energy-momentum tensor, i.e. up to the trace anomaly of QCD, very similar to the Higgs boson. The lightest Radion might in fact be lighter than the lightest graviton excitation and thus the discovery channel for the model. Higgs boson and Radion may exhibit kinetic mixing, which leads to a modification of both Higgs boson and Radion properties, in particular their couplings to gauge bosons and fermions. For a review of the Radion phenomenology, see e.g. [87]. The Radion sector is governed by 3 parameters: the strength of the Radion-matter interactions described by an energy scale Λ_ϕ, the mass of physical Radion, m_ϕ, and the Radion-Higgs mixing parameter ξ. In Fig. 24, the effective couplings squared of the Higgs boson and the Radion (relative to those of a SM Higgs boson) are shown for the choice $\Lambda_\phi = 5$ TeV, and three values of the Radion mass (20, 55, 200 GeV) as a function of ξ. Large deviations of the Higgs couplings from their SM values are expected if there is large Radion Higgs mixing present. The Radion itself has couplings which are reduced by a factor v/Λ_ϕ with respect to those of a SM Higgs in the case of no mixing, which requires high luminosity for direct discovery. The sensitivity of the trilinear Higgs coupling to Radion admixtures has been studied as well in [87].

The LC capability of precisely measuring the Higgs branching ratios $H^0 \to b\bar{b}$ and $H^0 \to W^+W^-$ has been exploited in [88]. In Fig. 25, the regions where the LC would observe larger than 2.5σ deviations of the Higgs branching ratios due to Radion Higgs mixing is shown together with the regions where the LHC can observe the Higgs bosons. In particular the regions in which the LHC might be blind to the Higgs boson are well covered by the LC. A study of the sensitivity of the WW-fusion channel to Radion effects has also been presented at the workshop [89].

RELATION TO THE LHC

A Higgs boson with SM-like properties will most likely be discovered at the Large Hadron Collider LHC. In recent years, the potential of the LHC to make measurements of Higgs boson properties has been investigated. For a recent summary of the ATLAS studies, see [90]. In most cases the capabilities of a LC are superior to those of the LHC as far as Higgs physics is concerned. In particular, *no model-independent measurements* of Higgs boson couplings are possible at the LHC. However, there are cases where the synergy of both colliders is vital and rewarding. Examples are in the determination of the top Yukawa coupling, in the mass reach for heavy SUSY Higgs bosons, and

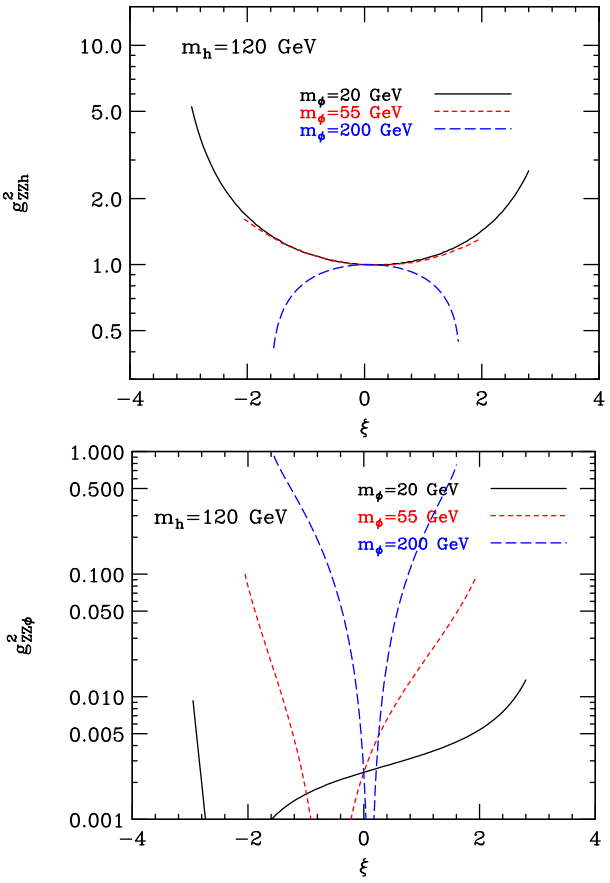

Figure 24: Effective coupling of the Higgs boson (upper) and the Radion (lower) to Z boson (from [87]).

in LHC measurements on third generation squark properties in order to constrain the interpretation of a supersymmetric Higgs sector. These examples are currently been worked out in more detail in a world-wide LHC/LC study group [91].

SUMMARY AND OUTLOOK

The precision study of Higgs bosons is at the core of the physics program of a future linear collider. In the course of the extended ECFA/DESY study 2001-2003 this physics case has been developed further: the precision of theoretical calculations has been improved, the implication of new theoretical models has been investigated and the experimental studies of the LC sensitivity have been extended and improved.

The studies are vital for the preparation of the worldwide LC project and will be continued both in the three regions America, Asia, and Europe and in worldwide workshops. In Europe, the study will continue in the framework of a new ECFA study. Major goals of this new study are to continue to incorporate new theoretical ideas and to improve the precision of theoretical predictions. On the experimental side, a more detailed study of systematic limitations, impact of machine conditions and in particular dependence of

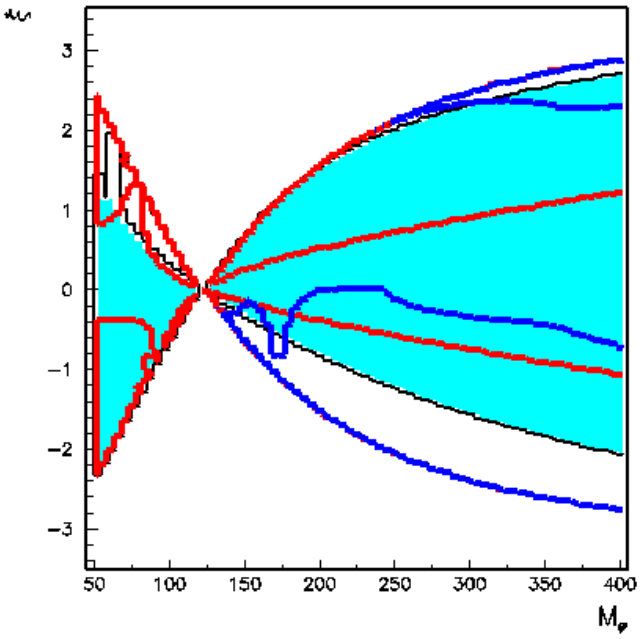

Figure 25: Sensitivity to Radions at LHC and LC: parameter plane of the Radion Higgs mixing angle ξ and the Radion mass M_ϕ for $m_H = 120$ GeV. In the shaded regions, the LHC can observe the Higgs boson in the $gg \to H^0 \to \gamma\gamma$ channel with 30 fb^{-1} in one experiment. The dark (blue) lines indicate the regions where LHC can observe the Radion in the $gg \to \Phi \to 4\ell$ channel. The grey (red) lines indicate the regions where at the LC a $> 2.5\sigma$ deviation of the Higgs branching ratio BR($H^0 \to b\bar{b}$) is observable. For more details see [88].

the precision on specific detector properties are of utmost importance.

ACKNOWLEDGMENTS

I would like to warmly thank all contributors to the Higgs working group for their huge efforts to make the workshop a success. In particular the work of my co-convenors M. Battaglia, A. Djouadi, E. Gross, and B. Kniehl is greatly acknowledged.

REFERENCES

[1] ECFA/DESY LC Physics Working Groups, J. A. Aguilar-Saavedra *et al.*, *TESLA Technical Design Report Part III: Physics at an e+e- Linear Collider,* hep-ph/0106315, DESY-2001-011.

[2] A. de Roeck, these proceedings.

[3] J. R. Ellis, M. K. Gaillard and D. V. Nanopoulos, Nucl. Phys. B **106** (1976) 292; B. L. Ioffe and V. A. Khoze, Sov. J. Part. Nucl. **9** (1978) 50; B. W. Lee, C. Quigg and H. B. Thacker, Phys. Rev. Lett. **38** (1977) 883.

[4] D. R. Jones and S. T. Petcov, Phys. Lett. B **84** (1979) 440; R. N. Cahn and S. Dawson, Phys. Lett. B **136** (1984) 196; G. L. Kane, W. W. Repko and W. B. Rolnick, Phys. Lett. B **148** (1984) 367; G. Altarelli, B. Mele and F. Pitolli, Nucl. Phys. B **287** (1987) 205; W. Kilian, M. Kramer and P. M. Zerwas, Phys. Lett. B **373** (1996) 135, hep-ph/9512355.

[5] B. A. Kniehl, hep-ph/0210176.

[6] A. Denner, S. Dittmaier, M. Roth, M.M. Weber, *Electroweak radiative corrections to e+ e- → nu nubar H,* Nucl. Phys. B **660** (2003) 289, hep-ph/0302198, LC-TH-2003-007 (2003).

[7] G. Belanger, F. Boudjema, J. Fujimoto, T. Ishikawa, T. Kaneko, K. Kato and Y. Shimizu, Phys. Lett. B **559** (2003) 252, hep-ph/0212261; Nucl. Phys. Proc. Suppl. **116** (2003) 353, hep-ph/0211268;
F. Jegerlehner and O. Tarasov, Nucl. Phys. Proc. Suppl. **116** (2003) 83, hep-ph/0212004;
A. Denner, S. Dittmaier, M. Roth, M.M. Weber, *Electroweak radiative corrections to single Higgs-boson production in e+ e- annihilation,* Phys. Lett. B **560** (2003) 196, hep-ph/0301189, LC-TH-2003-008 (2003).

[8] A. Djouadi, M. Spira and P. M. Zerwas, Z. Phys. C **70** (1996) 427, hep-ph/9511344.

[9] A. Djouadi, J. Kalinowski and M. Spira, Comput. Phys. Commun. **108** (1998) 56.

[10] S. Heinemeyer, W. Hollik and G. Weiglein, *Decay widths of the neutral CP-even MSSM Higgs bosons in the Feynman-diagrammatic approach,* Eur. Phys. J. C **16** (2000) 139, hep-ph/0003022, LC-TH-2001-064.

[11] T. Sjöstrand, Comp. Phys. Comm. **82** (1994) 74;
T. Sjöstrand, LU TP 95-20.

[12] G. Corcella *et al.*, JHEP 01 (2001) 010, hep-ph/0011363; hep-ph/0107071, hep-ph/0201201, hep-ph/0210213.
S. Moretti, *HERWIG: an event generator for e^+e^- Linear Colliders,* hep-ph/0209209, LC-TOOL-2002-009.

[13] P. Janot, *Physics at LEP2*, CERN 96-01, Vol.2, 309.

[14] A. Pukhov *et al.*, hep-ph/9908288.

[15] W. Kilian, LC-TOOL-2001-039.

[16] T. Ohl, Comput. Phys. Commun. **101** (1997) 269

[17] M. Pohl, H.J. Schreiber, *SIMDET - Version 4: A parametric Monte Carlo for a TESLA detector,* LC-DET-2002-005.

[18] M. Ronan, *Multi-Jet Higgsstrahlung Analysis,* LC-PHSM-2003-048 (2003).

[19] D. J. Jackson, Nucl. Instrum. Meth. A **388** (1997) 247.

[20] T. Behnke *et al.*, *BRAHMS: A Monte Carlo for a Detector at a 500/800 GeV Linear Collider,* LC-TOOL-2001-005.

[21] P. Garcia-Abia and W. Lohmann, Eur. Phys. J. directC **2** (2000) 2.

[22] S. Dawson, S. Heinemeyer, *The Higgs Boson Production Cross-Section as a Precision Observable?,* Phys. Rev. D **66** (2002) 055002, hep-ph/0203067, LC-TH-2003-005 (2003).

[23] D. Choudhury, A. Datta and K. Huitu, hep-ph/0302141.

[24] V. D. Barger, K. m. Cheung, A. Djouadi, B. A. Kniehl and P. M. Zerwas, Phys. Rev. D **49** (1994) 79, hep-ph/9306270.

[25] S. Y. Choi, D. J. Miller, M. M. Mühlleitner and P. M. Zerwas, *Identifying the Higgs Spin and Parity in Decays to Z Pairs,* Phys. Lett. B **553** (2003) 61, hep-ph/0210077, LC-TH-2003-036 (2003).

[26] M. Kramer, J. H. Kühn, M. L. Stong, and P. M. Zerwas, Z. Phys. **C64** (1994) 21, hep-ph/9404280;
B. Grządkowski and J. F. Gunion, Phys. Lett. **B350** (1995) 218, hep-ph/9501339.

[27] G.R. Bower, T. Pierzchala, Z. Was, M. Worek, Phys. Lett. B **543** (2002) 227, hep-ph/0204292;
M. Worek, *Higgs CP from H/A → tau tau decay,* Acta Phys. Polon. B34 (2003) 4549, hep-ph/0305082, LC-PHSM-2003-050 (2003).

[28] Z. Was and M. Worek, *"Transverse spin effects in H/A → tau+ tau-, tau+- → nu X+-, Monte Carlo approach,*Acta Phys. Polon. B **33** (2002) 1875, hep-ph/0202007], LC-PHSM-2003-049 (2003).

[29] K. Desch, Z. Was and M. Worek, *Measuring the Higgs boson parity at a linear collider using the tau impact parameter and tau → rho nu decay,*Eur. Phys. J. C **29** (2003) 491, hep-ph/0302046, LC-PHSM-2003-003 (2003).

[30] A. Imhof, *Measurement of the Higgs boson parity at TESLA,* talk given at the ECFA/DESY workshop on physics and detectors for a future linear collider, Amsterdam, Spring 2003, LC note in preparation.

[31] T. Abe *et al.* [American Linear Collider Working Group Collaboration], *Linear collider physics resource book for Snowmass 2001,* hep-ex/0106055 (part 1), hep-ex/0106056 (part 2), hep-ex/0106057 (part 3), and hep-ex/0106058 (2001).

[32] K. Abe *et al.* [ACFA Linear Collider Working Group Collaboration], *Particle physics experiments at JLC,* hep-ph/0109166.

[33] T. Kuhl, *Higgs branching ratios with SIMDET4+ZVTOP: first results,* talk given at the ECFA/DESY workshop on physics and detectors for a future linear collider, Amsterdam, Spring 2003, LC note in preparation.

[34] M. Battaglia, hep-ph/9910271.

[35] J-C. Brient, *The direct method to measure the Higgs branching ratios at the future e+ e- linear collider,* LC-PHSM-2002-003 (2002).

[36] M. Battaglia and A. De Roeck, in *Proc. of the APS/DPF/DPB Summer Study on the Future of Particle Physics (Snowmass 2001)* ed. N. Graf, eConf **C010630** (2001) E3066, hep-ph/0111307.

[37] M. Dubinin, H.J. Schreiber, A. Vologdin, *Measurement of the HZgamma coupling at the future linear e+e- collider,* LC-PHSM-2003-004 (2003).

[38] M. Schumacher, *Investigations of invisible decays of the Higgs boson at a futire e+e- linear collider,*LC-PHSM-2003-096.

[39] M. Battaglia, *Rare Higgs Dacays: bb and mumu,* talk given at the ECFA/DESY workshop on physics and detectors for a future linear collider, St. Malo, Spring 2002;
M. Battaglia,hep-ph/0211461.

[40] N. Meyer, *Measuring Resonance Parameters of Heavy Higgs Bosons at TESLA,* LC-PHSM-2003-066, hep-ph/0308142 (2003).

[41] A. Djouadi, J. Kalinowski and P. M. Zerwas, Mod. Phys. Lett. A **7** (1992) 1765.

[42] S. Dittmaier, M. Kramer, Y. Liao, M. Spira and P. M. Zerwas, Phys. Lett. B **441** (1998) 383;
S. Dawson and L. Reina, Phys. Rev. D **59** (1999) 054012.

[43] Y. You, W. G. Ma, H. Chen, R. Y. Zhang, S. Yan-Bin and H. S. Hou, Phys. Lett. B **571** (2003) 85, hep-ph/0306036;
G. Belanger *et al.*, Phys. Lett. B **571** (2003) 163, hep-ph/0307029;
A. Denner, S. Dittmaier, M. Roth and M. M. Weber, hep-ph/0307193;

[44] A. Juste and G. Merino, hep-ph/9910301.

[45] H. Baer, S. Dawson and L. Reina, Phys. Rev. D **61** (2000) 013002.

[46] A.Gay, *Top Yukawa coupling* , talk given at the ECFA/DESY workshop on physics and detectors for a future linear collider, Amsterdam, Spring 2003, LC note in preparation.

[47] A. Djouadi, W. Kilian, M. Mühlleitner and P. M. Zerwas, Eur. Phys. J. C **10** (1999) 27, hep-ph/9903229.

[48] Z. Ren-You, M. Wen-Gan, C. Hui, S. Yan-Bin and H. Hong-Sheng, hep-ph/0308203;
G. Belanger *et al.*, Phys. Lett. B **576** (2003) 152, hep-ph/0309010.

[49] C. Castanier, P. Gay, P. Lutz and J. Orloff, *Higgs self coupling measurement in e+ e- collisions at center-of-mass energy of 500 GeV* , LC-PHSM-2000-061 (2000).

[50] U. Baur, T. Plehn and D. Rainwater, *Examining the Higgs boson potential at lepton and hadron colliders: A comparative analysis,* hep-ph/0304015.

[51] M. Battaglia, E. Boos and W. M. Yao, in *Proc. of the APS/DPF/DPB Summer Study on the Future of Particle Physics (Snowmass 2001)* ed. N. Graf, eConf **C010630** (2001) E3016, hep-ph/0111276.

[52] G. Degrassi, S. Heinemeyer, W. Hollik, P. Slavich and G. Weiglein, *Towards high-precision predictions for the MSSM Higgs sector,* Eur. Phys. J. C **28** (2003) 133, hep-ph/0212020, LC-TH-2002-015.

[53] S. Heinemeyer, W. Hollik and G. Weiglein, Phys. Rev. **D58**, 091701 (1998) [hep-ph/9803277]; Phys. Lett. **B440**, 296 (1998) [hep-ph/9807423]; Eur. Phys. J. **C9**, 343 (1999) [hep-ph/9812472]; M. Carena, H.E. Haber, S. Heinemeyer, W. Hollik, C.E.M. Wagner and G. Weiglein, Nucl. Phys. **B580**, 29 (2000) [hep-ph/0001002]; R.-J. Zhang, Phys. Lett. **B447**, 89 (1999) [hep-ph/9808299]; J.R. Espinosa and R.-J. Zhang, JHEP **0003**, 026 (2000) [hep-ph/9912236]; Nucl. Phys. **B586**, 3 (2000) [hep-ph/0003246]; J.R. Espinosa and I. Navarro, Nucl. Phys. **B615**, 82 (2001) [hep-ph/0104047]; G. Degrassi, P. Slavich and F. Zwirner, Nucl. Phys. **B611**, 403 (2001) [hep-ph/0105096]; A. Brignole, G. Degrassi, P. Slavich and F. Zwirner, Nucl. Phys. **B631**, 195 (2002) [hep-ph/0112177]; Nucl. Phys. **B643**, 79 (2002) [hep-ph/0206101]; A. Dedes, G. Degrassi and P. Slavich, Nucl. Phys. B **672** (2003) 144, hep-ph/0305127; Computer programs developed for computing the radiatively-corrected Higgs masses, FeynHiggs and FeynHiggsFast, are described respectively in S. Heinemeyer, W. Hollik and G. Weiglein, Comput. Phys. Commun. **124**, 76 (2000) [hep-ph/9812320]; and CERN-TH-2000-055 [hep-ph/0002213].

[54] P.H. Chankowski, S. Pokorski and J. Rosiek, *Nucl. Phys.* **B 423** (1994) 437, hep-ph/9303309; *Nucl. Phys.* **B 423** (1994)

497;
V. Driesen and W. Hollik, *Z. Phys.* **C 68** (1995), 485, hep-ph/9504335;
V. Driesen, W. Hollik and J. Rosiek, *Z. Phys.* **C 71** (1996) 259, hep-ph/9512441.

[55] S. Heinemeyer, W. Hollik, J. Rosiek and G. Weiglein, *Eur. Phys. J.* **C 19** (2001) 535, hep-ph/0102081;
S. Heinemeyer and G. Weiglein, *Nucl. Phys. Proc. Suppl.* **89** (2000) 210.

[56] M. Carena, S. Heinemeyer, C. E. Wagner and G. Weiglein, Eur. Phys. J. C **26** (2003) 601, hep-ph/0202167.

[57] T. Hahn, S. Heinemeyer and G. Weiglein, *MSSM Higgs-boson production at the linear collider: Dominant corrections to the W W fusion channel*, Nucl. Phys. B **652** (2003) 229, hep-ph/0211204, LC-TH-2002-018.
T. Hahn, S. Heinemeyer, G. Weiglein, *Very Heavy MSSM Higgs-Boson Production at the LC*, Nucl. Phys. Proc. Suppl. **116** (2003) 336, LC-TH-2002-019 (2002).

[58] H. Eberl, W. Majerotto and V. C. Spanos, Nucl. Phys. B **657** (2003) 378, hep-ph/0210038].

[59] J. F. Gunion and H. E. Haber, Phys. Rev. D **67** (2003) 075019, hep-ph/0207010.

[60] E. Boos, A. Djouadi, M. Mühlleitner and A. Vologdin, Phys. Rev. D **66** (2002) 055004, hep-ph/0205160.

[61] J. F. Gunion *et al.*, Phys. Rev. D **38** (1988) 3444; A. Djouadi, J. Kalinowski, P. Ohmann and P. M. Zerwas, Z. Phys. C **74** (1997) 93, hep-ph/9605339.

[62] T. Klimkovich, *Experimental study of heavy SuSy Higgs bosons at the LC*, talk given at the ECFA/DESY workshop on physics and detectors for a future linear collider, Amsterdam, Spring 2003, LC note in preparation. A. Raspereza, *CP properties of Higgs bosons and $H_i H_j \to b\bar{b}\tau^+\tau^-$ selection*,talk given at the ECFA/DESY workshop on physics and detectors for a future linear collider, Prague, Autumn 2002,
A. Raspereza, T. Klimkovich, T. Kuhl, K. Desch, LC note in preparation.

[63] M. Battaglia, A. Ferrari, A. Kiiskinen and T. Maki, in *Proc. of the APS/DPF/DPB Summer Study on the Future of Particle Physics (Snowmass 2001)* ed. N. Graf, eConf **C010630** (2001) E3017, hep-ex/0112015].

[64] S. Kanemura, S. Moretti and K. Odagiri, JHEP **0102** (2001) 011, hep-ph/0012030.
H. E. Logan and S. f. Su, Phys. Rev. D **67** (2003) 017703, hep-ph/0206135.
S. Moretti, *Detection of heavy charged Higgs bosons at future Linear Colliders via $\tau^-\bar{\nu}_\tau H^+$ production*, hep-ph/0209210, LC-TH-2002-010 (2002).
O. Brein, hep-ph/0209124.

[65] B. A. Kniehl, F. Madricardo and M. Steinhauser, Phys. Rev. D **66** (2002) 054016.

[66] S. Kiyoura, private communication.

[67] J. Gunion, T. Han, J. Jiang, A. Sopczak, *Determining tan(beta) with Neutral and Charged Higgs Bosons*, Phys. Lett. B **565** (2003) 42, LC-PHSM-2003-064 (2003).

[68] M. Beccaria, F. M. Renard, S. Trimarchi and C. Verzegnassi, hep-ph/0212167.

[69] A. Dedes, S. Heinemeyer, S. Su and G. Weiglein, hep-ph/0302174, to appear in Nucl. Phys. B.

[70] J. Ellis, S. Heinemeyer, K. Olive, G. Weiglein, *Precision Analysis of the Lightest MSSM Higgs Boson at Future Colliders*, JHEP **0301** (2003) 006, hep-ph/0211206, LC-TH-2002-013 (2002).

[71] J. Guasch, W. Hollik and S. Peñaranda, Phys. Lett. B **515** (2001) 367;
J. Guasch, W. Hollik, S. Peñaranda, *Some results on distinction of Higgs boson models*, LC-TH-2003-043 (2003).

[72] A. Pilaftsis and C. E. Wagner, Nucl. Phys. B **553** (1999) 3, hep-ph/9902371.

[73] M. Carena, J. R. Ellis, A. Pilaftsis and C. E. Wagner, Nucl. Phys. B **586** (2000) 92, hep-ph/0003180.

[74] S. Heinemeyer, Eur. Phys. J. C **22** (2001) 521, hep-ph/0108059.
M. Frank, S. Heinemeyer, W. Hollik, G. Weiglein, *The Higgs-Boson Masses of the Complex MSSM: A Complete One-Loop Calculation* , hep-ph/0212037, LC-TH-2002-016 (2002).

[75] M. Carena *et al.*, Nucl. Phys. B **599** (2001) 158, hep-ph/0011055.

[76] V. Barger, T. Han, P. Langacker, B. McElrath and P. M. Zerwas, *Effects of Genuine Dimension Six Higgs Operators*, Phys. Rev. D **67** (2003) 115001, LC-TH-2003-035 (2003).

[77] I. F. Ginzburg, M. Krawczyk, P. Osland, *Two-Higgs-Doublet Models with CP violation*, LC-TH-2003-037 (2003), hep-ph/0211371.

[78] D. J. Miller, R. Nevzorov and P. M. Zerwas, *The Higgs Sector of the Next-to-Minimal Supersymmetric Standard Model*, hep-ph/0304049, LC-TH-2003-034 (2003).

[79] N. Arkani-Hamed, S. Dimopoulos, and G. R. Dvali, Phys. Lett. **B429** (1998), 263.

[80] L. Randall and R. Sundrum, *Phys. Rev. Lett.* **83** (1999) 3370, *Phys. Rev. Lett.* **83** (1999) 4690.

[81] J. L. Hewett, Phys. Rev. Lett. **82** (1999) 4765.

[82] H. Davoudiasl, J. L. Hewett and T. G. Rizzo, Phys. Rev. Lett. **84** (2000) 2080.

[83] G. F. Giudice, R. Rattazzi and J. D. Wells, Nucl. Phys. B **544** (1999) 3, hep-ph/9811291.

[84] A. Datta, E. Gabrielli, B. Mele, *Large extra dimension effects in Higgs boson production at linear colliders and Higgs factories*, LC-TH-2003-011 (2003), hep-ph/0303259.

[85] N. G. Deshpande and D. K. Ghosh, Phys. Rev. D **67** (2003) 113006, hep-ph/0301272.

[86] G. F. Giudice, R. Rattazzi, and J. D. Wells, *Nucl. Phys.* **B595** (2001) 250.
C. Csaki, M. L. Graesser, and G. D. Kribs, *Phys. Rev.* **D63** (2001) 065002.

[87] D. Dominici, B. Grzadkowski, J. F. Gunion and M. Toharia, hep-ph/0206192.

[88] M. Battaglia, S. De Curtis, A. De Roeck, D. Dominici and J. F. Gunion, *On the complementarity of Higgs and radion searches at LHC*, hep-ph/0304245, Phys. Lett. B **568** (2003) 92.

[89] A. Datta and K. Huitu, hep-ph/0306241.

[90] M. Dührssen, *'Prospects for measurement of Higgs boson coupling parameters in the mass range from 110 - 190 GeV'*, ATLAS physics note ATL-PHYS-2003-030 (2003).

[91] LHC/LC Study Group, http://www.ippp.dur.ac.uk/˜ georg/lhclc/ .

PHYSICS at a $\gamma\gamma$, $e\gamma$ and e^-e^- OPTION for a LINEAR COLLIDER

A. De Roeck*, CERN, 1211 Geneva 23, Switzerland

Abstract

This report presents a review of the studies made in the working group on "$\gamma\gamma$ and $e\gamma$ physics" of the ECFA/DESY workshop on linear collider physics. It reports on several new physics studies, in particular s-channel Higgs production. A summary of R&D activities for the interaction region is presented. The merits of e^-e^- collisions are briefly recalled.

INTRODUCTION

A future e^+e^- linear collider (LC) offers excellent new opportunities for the study of high energy particle collisions. The idea to convert the electron beams of a LC into photon beams, by laser backscattering, and thus create a photon collider (PC), was first discussed about 20 years ago in [1]. Projects for a future LC collider are studied in Europe (TESLA,CLIC), the US (NLC) and Asia (JLC), and all consider a PC as a possible additional option. Recently, in the context of the ECFA-DESY LC study, a detailed discussion of the physics and design of a PC was presented in the TESLA-TDR [2] and in [3]. This paper reviews the work done during the last two years in the study group "$\gamma\gamma$ and $e\gamma$ physics" of the extended ECFA/DESY workshop on physics and detectors at a linear collider.

A plethora of new and exciting measurements become accessible with a PC, in particular Higgs boson studies, but also searches for new physics and electroweak, top and QCD measurements can be made often in a complementary way compared to e^+e^- collisions. The precision reached at a PC is competitive if sufficiently high luminosities can be reached.

Examples of advantages of a PC include:

- Higher cross sections for charged particles than in e^+e^-.
- Different J^{PC} states than for e^+e^-.
- Higgs can be s-channel produced as a resonance.
- CP analysis opportunities for Higgs bosons
- Precise test of the coupling to photons
- Possible higher mass discovery range for e.g. H, A, and sleptons

Note that a PC needs no positron drive beam but electron beams, which can be produced with relatively high polarisation, are sufficient.

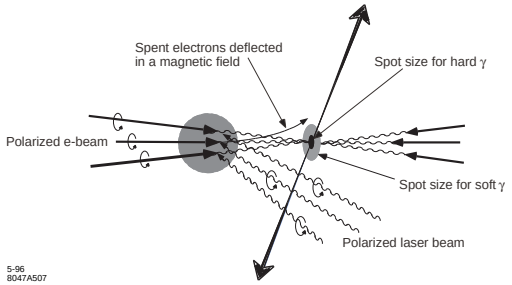

Figure 1: A sketch of the creation of a photon beam by Compton backscattering of laser photons off beam electrons.

The proposed technique for a PC consists of using laser backscattering as shown in Fig. 1. A low energy (typically 1 eV) laser beam of photons collides with the high energy (typically 250-500 GeV) electron beam and is backscattered receiving a major fraction of the incoming electron energy. The maximum energy of the generated photons is given by $E_\gamma^{max} = xE_e/(1+x)$, with E_e the electron beam energy and $x = 4E_eE_L\cos^2(\theta/2)/m_e^2c^4$ with E_L and θ the laser photon energy and angle between the electron and laser beam. The distance of the conversion to the interaction point is in the range of several mm. A typical value for x is 4.8, which leads to photon spectra which peak around $0.8E_e$. The energy distribution depends on the polarisation of the photon (P_c) and electron beam (λ_e), the most peaked spectrum is obtained when $P_c\lambda_e = -1$. In reality, due to the maximum polarizability of the electron beam a value close to $P_c\lambda_e = -0.8$ can be reached. Sometimes it is advantageous to have a broader spectrum, e.g. to discover particles with unknown masses, in which case the configuration $P_c\lambda_e = +0.8$ will be more useful.

The polarization of both beams can be further used to produce interactions with the same ($J_z = 0$) or opposite ($J_z = 2$) photon helicities, useful e.g. for Higgs studies. Higher geometrical luminosities can be achieved

* The work reported in this talk was done by the members of the "$\gamma\gamma$ and $e\gamma$ physics" working group of the Extended ECFA/DESY Study; D. Anipko (Nowosibirsk), E. Asakawa (Tokyo U.), D. Asner (Cornel), I. Bozovic (VINCA Belgrade), W. Da Silva (Paris VI), A. De Roeck (CERN), A. Finch (Lancaster), I. Ginzburg (Nowosibirsk), R. Godbole (Bangalore), J. Gronberg (LLNL Livermore), C. Heusch (Santa Cruz), G. Klemz (DESY-Zeuthen), M. Krämer (Edinburgh), F. Kraus (Dresden), M. Krawczyk (Warsaw), J. Kwiecinski (Krakow), V. Makarenko (NC PHEP Minsk), I. Marfin (NC PHEP Minsk), S. Maxfield (Liverpool), D. Miller (CERN), K. Moenig (DESY-Zeuthen), M. Mühlleitner (PSI), F. Nagel (Uni Heidelberg), P. Niezurawski (Warsaw), A.V. Pak (Novisibirsk), D.V. Pavluchenko (Novisibirsk), S.S. Petrosyan (Novisibirsk), A. Rosca DESY-Zeuthen), S. Schumann (Dresden), J. Sekaric (DESY Zeuthen), V.G. Serbo (Novisibirsk), T. Shishkina (NC PHEP Minsk), S. Soeldner-Rembold (Manchester), A. Stahl (DESY Zeuthen), V. Telnov (Novisibirsk), M. Velasco (Northwestern), M. Wing (Bristol Univ. & DESY), A.F.Żarnecki (Warsaw),

for photon colliders than for genuine e^+e^- colliders, due to the absence or strong reduction of beamstrahlung in the interaction region. The 'luminosity' is usually defined to be the luminosity corresponding to the region $\sqrt{s_{\gamma\gamma}} > 0.8\sqrt{s_{\gamma\gamma,max}}$ and is typically 10% of the geometrical e^+e^- luminosity. For the TESLA parameters, but including a smaller horizontal β function at the interaction point namely 1.5 mm in x, compared to 15 mm for the e^+e^- beam design, and reducing the horizontal emittance from 553 nm to 140 nm, leads to $L_{\gamma\gamma}(\sqrt{s_{\gamma\gamma}} > 0.8\sqrt{s_{\gamma\gamma,max}}) \sim \frac{1}{3}L_{e+e-}$. This gives event samples corresponding to $O(100)$ fb^{-1} per year for the PC. A PC

- needs a second interaction point
- needs a cross angle
- has a rather peaked but somewhat smeared centre of mass system (CMS) energy spectrum

Both high energy $e\gamma$ and $\gamma\gamma$ interactions can be provided, depending on whether only one or both lepton beams are converted.

TOOLS

During this workshop major progress was made on the development and completion of the tools to study physics at a $\gamma\gamma$ collider. These tools have now reached a high level of maturity.

Luminosity spectra at photon colliders can not be described completely by effective photon spectra due to the energy-angle correlation in Compton scattering and beam collision effects. Fully detailed luminosity distributions were obtained by a complete simulation of beam collisions, resulting in 'collision events' that contain the types of colliding particles (photon, electron, positron), their energies and polarizations. The PHOCOL program [4] was used to generate these collision events for several e^-e^- CMS energies and laser configurations. PHOCOL includes nonlinear corrections and contributions of higher order processes. An example of a $\gamma\gamma$ CMS energy distribution is shown in Fig. 2. The event files can be used by the CIRCE program [5]. These luminosity spectra are also used to tune a simple model based on analytical formulae for the Compton scattering (CompAZ [6]). The results of such a tune are shown in Fig. 2 as well. While being an approximation, these spectra are nevertheless extremely convenient for studies e.g. at different energies other than the (few) ones for which event files were produced.

A version of the fast detector simulation package SIMDET, including modifications for the PC interaction point (IP) has been used. Overlap events from the QCD background can be added to the signal events. For TESLA luminosities, we expect typically on average about one overlaying event at low energy ($\sqrt{s_{ee}} \sim 200$ GeV, also called the Higgs mode since it would be best suited for the study of a light Higgs with mass ~ 120 GeV) and two events at nominal energy ($\sqrt{s_{ee}} \sim 500$ GeV).

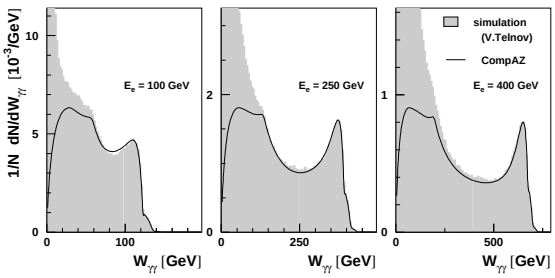

Figure 2: Comparison of the center of mass energy distribution obtained from full simulation of the luminosity spectrum [4] with results from CompAZ, for three electron beam energies [6]

Background studies [7] have been made for incoherent and coherent e^+e^- pair production. A new two-mask design in the IP reduces the background by a factor 2-3 with respect to the previous layout; the details are still being optimized. Tracks in the TPC and hits in the vertex detector from incoherent and coherent pairs were found to be tolerable and similar to the expected background at an e^+e^- collider interaction region. Hence there is now evidence that a similar vertex detector as for an e^+e^- collider detector can be used for a PC detector, and therefore a similar quality in b-tagging can be achieved. The neutron background is still under study but the first results show that it is tolerable as well [8].

During this workshop we also had direct contact with MC developers which resulted in getting requirements implemented in e.g. the new SHERPA generator [9], and getting good MC parameter tunes for PYTHIA and HERWIG (using mostly HERA γp data) from the JETWEB team [10].

On the web page of the working group a link directing to the page with the tools can be found: http://www-h1.desy.de/˜maxfield/ggcol/lcgg.html.

LUMINOSITY

One of the topics studied in detail is the precision with which the luminosity can be measured. The following processes are proposed for the $\gamma\gamma$ mode [11, 12]:

- $ee \to ee\,(\mu\mu)$
- $ee \to ee\gamma\,(\mu\mu\gamma)$
- $ee \to 4$ leptons

The cross sections for these channels are shown in Fig. 3. The first channel can give the highest precision $\sim 0.1\%$ (stat) but cannot be used for $J_z = 0$, i.e. for the Higgs study, because it is suppressed as m_l^2/s, with m_l the lepton mass. In that case, however, the second channel can be used. For two years of running the statistical precision for

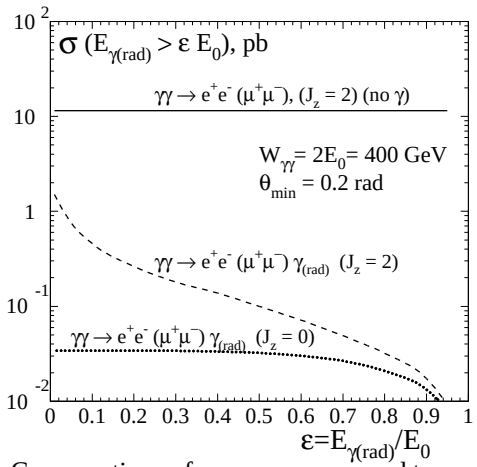

Figure 3: Cross sections of processes proposed to measure luminosity at a $\gamma\gamma$ collider [12].

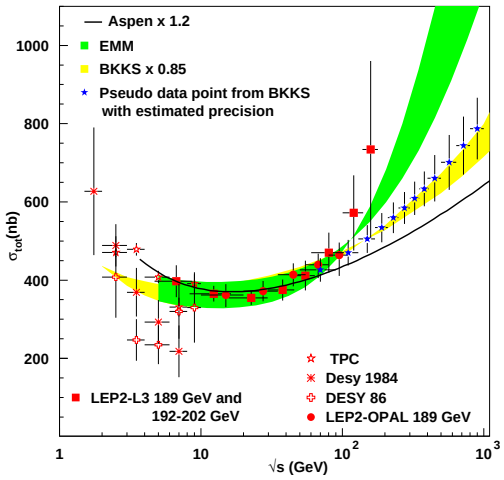

Figure 4: The total $\gamma\gamma$ cross-section as function of the $\gamma\gamma$ collision energy, compared with model calculations [17]: BKKS band (upper and lower limits correspond to different photon densities) and EMM band (Eikonal Minijet Model for total and inelastic cross-section, with different photon densities and different minimum jet transverse momentum).

the channel $ee \to ee\gamma$, using realistic detector cuts, is

$$\frac{\Delta L}{L}(\sqrt{s} > 0.8\sqrt{s_{\gamma\gamma,max}}) = 0.4\% \qquad (1)$$

$$\frac{\Delta L}{L}(m_H \pm 2\mathrm{GeV}) = 1.0\% \qquad (2)$$

For $e\gamma$ collisions the following processes are suggested:

- $e\gamma \to e\gamma, eZ$
- $e\gamma \to eee$.

The statistical precision that can be achieved is better than 1% for one year of running.

PHYSICS TOPICS

Two-photon physics is not new. Most e^+e^- colliders have or had a program of two-photon physics, by using the photons emitted from the lepton beams, which follow the well known WWA [13] energy dependence. The known disadvantage is the rapidly decreasing photon flux with photon energy: for collisions with a fractional energy $\sqrt{s_{\gamma\gamma}}/2E_e^{beam}$ larger than 0.1 (0.5) the $\gamma\gamma$ luminosity is reduced by a factor 100 (10000) with respect to the e^+e^- luminosity. Hence the PC opens a new opportunity for truly *high* energy two-photon physics, which is not limited to QCD but competes in searches for new physics and measurements of Higgs properties.

The cross sections for charged particle pair productions are considerably larger in $\gamma\gamma$ collisions than for e^+e^- collisions and decrease more slowly with energy. Hence one can study new particles far from threshold with higher rate. E.g. WW pair production in $\gamma\gamma$ at 500 GeV is a factor 20 larger than in e^+e^-. Cross sections for charged scalars, lepton and top pairs are a factor $5-10$ higher at a PC, compensating for the reduced luminosity compared to e^+e^-.

QCD

First we consider the QCD aspects of two-photon collisions in the reaction $\gamma\gamma \to$ hadrons. The nature of the photon is complex. A high energy photon can fluctuate into a fermion pair or into a bound state, i.e. a vector meson with the same quantum numbers as the photon $J^{PC} = 1^{--}$. These quantum fluctuations lead to the so-called hadronic structure of the photon.

Many QCD studies of photon-photon collisions were made for the TDR [2] and will not be repeated here. During this workshop we got new paramterizations of the energy dependence of the total cross section [14, 15], and new LO parametrizations of the photon structure functions [16].

As an example the total $\gamma\gamma$ cross-section is briefly discussed, a quantity that is not yet understood from first principles. Fig. 4 shows the present photon-photon cross-section data in comparison with recent phenomenological models [14]. All models predict a rise of the cross-section with the collision energy, $\sqrt{s}_{\gamma\gamma}$, but the amount of the rise differs and predictions for high photon-photon energies show noticable differences. *Proton-like-models* follow closely the rise of the proton-proton cross-section, while in *QCD based* models, a stronger rise is predicted using the eikonalized pQCD jet cross-section.

The figure demonstrates that large differences between the models become apparent in the energy range of a future 0.5-1 TeV e^+e^-collider. An overview of new model predictions is reported in [14]. The absolute precision with which these cross-sections can be measured ranges from

5% to 10%, where the largest contributions to the errors are due to the control of the diffractive component of the cross-section, Monte Carlo models used to correct for the event selections, the absolute luminosity and knowledge on the shape of the luminosity spectrum [17]. These prospects for measurement have been updated to the TeV range and are shown in Fig. 4.

Higgs Studies

The quest for the Higgs particle(s) and the measurement of its properties will be one of the most important topics for high energy collider physics in the coming years. The PC is an ideal place to study the Higgs boson since it can be produced as an s-channel resonance. The mass reach of the PC is up to 80% of the CMS energy of the e^-e^- collider. A detailed study of the $\gamma\gamma H$ vertex is only possible at a PC. Accurate measurements of mass and width are extremely important and can be used to compare the SM predictions with those of alternative models e.g. based on SUSY. Since the two-photon decay width of the Higgs is sensitive to all heavy charged particles which acquire mass via the Higgs mechanism, the partial width could be modified by 5-10% in these models.

For a light Higgs, the most promising channel is $\gamma\gamma \rightarrow H \rightarrow b\overline{b}$. A first study based on detector simulation, showed that a 2% statistical precision for the partial width could be reached [18], for a Higgs with mass of 120 GeV. During this workshop we have

- Revisited the $H \rightarrow b\overline{b}$ channel in detail
- Studied the $H \rightarrow WW, ZZ$ channels
- Studied analysis methods for the spin and CP properties of the Higgs
- Studied the model separation power
- Studied the MSSM higgs

Members of the US PC study group have been reporting to us on their Higgs analyses as well, in particular H, A production and discovery, the $H \rightarrow \gamma\gamma$ decay mode, and charged Higgs studies.

First we discuss the $H \rightarrow b\overline{b}$ studies. Selecting $J_z = 0$ strongly suppresses the (Leading Order) contributions of $b\overline{b}$ and $c\overline{c}$ production, but a good tagging of bottom quarks with simultaneous rejection of charm quarks is needed. During this workshop two new complete analyses were finalized [19, 20]. The two studies use a different approach for the background process, but come to the same conclusions. The simulated mass spectrum for a Higgs particle with mass of 120 GeV, is shown in Fig. 5 for signal and background. The PC will determine the quantity $\Gamma(H \rightarrow \gamma\gamma) \cdot BR(H \rightarrow b\overline{b})$. A feasibility study for a light Higgs, using a parametrized simulation of the detector, has confirmed that the quantity above can be determined with a typical statistical accuracy of about 2-3%, as shown in Fig. 6. These studies use as before the NLO QCD backgrounds [21]. New in these studies are the use of a more realistic photon spectrum, inclusion of overlap background QCD events (on average one event per bunch crossing), b-tagging using a neural net, and using a correction method for the reconstructed Higgs mass, accounting for escaping neutrinos from the heavy flavour decays.

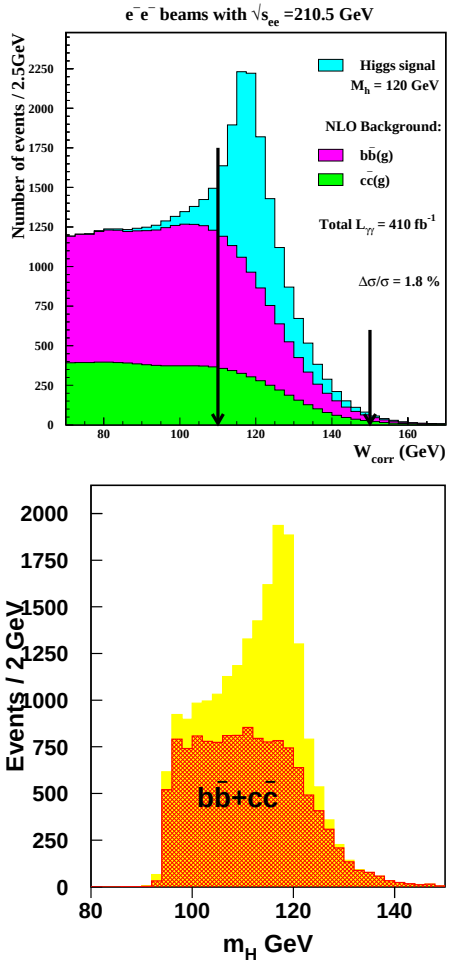

Figure 5: Reconstructed invariant mass distribution, W_{rec} (top [19]) and M_H (below[20]), for selected $b\overline{b}$ events. Contributions for background and signal are shown separately. In the top plot the arrows show the optimized mass window for the partial width measurement.

Since the $b\overline{b}$ branching ratio can be measured at an e^+e^- collider with a precision of 1-2%, $\Gamma(H \rightarrow \gamma\gamma)$ can be determined with a statistical accuracy of approx. 2% for an integrated luminosity of 85 fb^{-1}, i.e one year running.

In [22] the processes $\gamma\gamma \rightarrow H \rightarrow WW$ and $\gamma\gamma \rightarrow H \rightarrow ZZ$ have been studied for the region 180 GeV $< m_H <$ 350 GeV via $q\overline{q}q\overline{q}$ decays for the WW channel and $llq\overline{q}$ decays for the ZZ channel. Typical mass plots are shown in Fig. 7. Due to the interference with the standard model background the processes $\gamma\gamma \rightarrow$ Higgs $\rightarrow WW/ZZ$ turn out to be also sensitivity to the phase

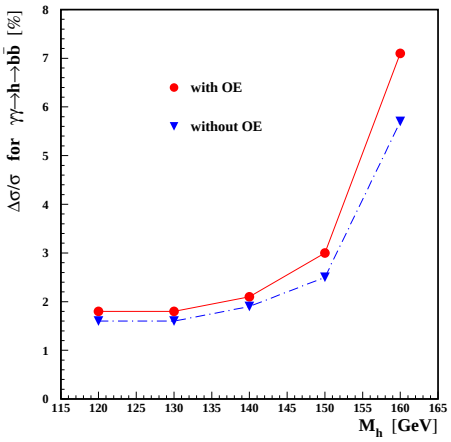

Figure 6: Statistical precision of $\Gamma(h \to \gamma\gamma)Br(h \to b\bar{b})$ measurements for the SM Higgs boson with mass 120-160 GeV, with and without overlaying events (OE). The lines are drawn to guide the eye [19].

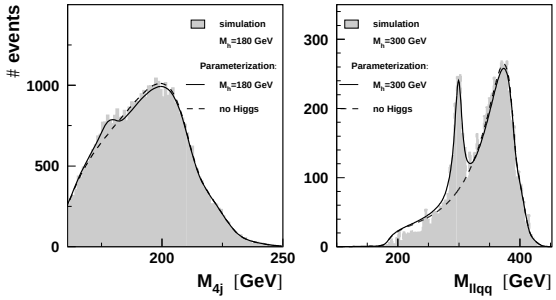

Figure 7: Distribution of the reconstructed invariant mass $\gamma\gamma \to WW, ZZ$ for Higgs mass/electron beam of 180/152.5 GeV and 300/250 GeV respectively [22].

of the $\gamma\gamma \to$ Higgs coupling, $\phi_{\gamma\gamma}$. The measurement of both the phase and partial width gives powerful tools to discriminate a SM Higgs from that of an extended model. A plot showing the sensitivity that can be reached on the partial two-photon width and the phase versus the mass of the Higgs is given in Fig. 8, using the same simulation tools as for the light Higgs discussed above. Over a large region a sensitivity of 3-5% can be achieved. The deviation from the SM prediction expected by a Higgs in a 2HDM is also indicated [22]

Furthermore the CP structure of the Higgs boson can be verified by studying the decay into ZZ, WW and measuring the azimuthal angle $\Delta\phi$ between the decay planes of the two Z, W bosons. An example of the sensitivity of the angle $\Delta\phi$ is shown in Fig. 9 for the decay channels $H \to ZZ, WW$, using a realistic simulation and for one year of data taking. In [22] one can find a very extensive discussion on sensitivities to CP properties using this and other variables, showing that a PC is an excellent tool for

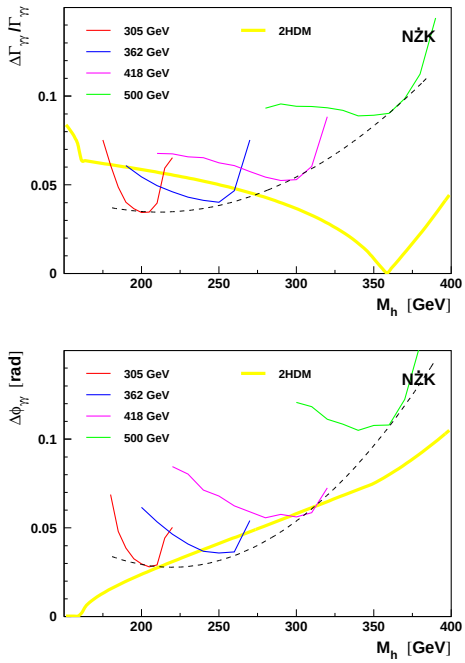

Figure 8: Statistical determination of the Higgs boson width (upper plot) and phase (lower plot) from the combined fit to the observed WW and ZZ mass spectra as a function of M_H [22]. The yellow (thick) line shows the size of the deviation expected in the SM-like 2HDM II [23], with an additional charged Higgs of 800 GeV. The dashed line is to guide the eye.

such analyses.

Further interesting CP studies include the study of the channel $\gamma\gamma \to t\bar{t}$, measuring asymmetries composed of the initial lepton beam polarization and the decay lepton charge [24]. A sensitivity plot is shown in Fig. 10.

Our US colleagues have reported to us on studies of $\gamma\gamma \to H \to \gamma\gamma$ and charged Higgs production. The first channel is quadratically sensitive to the two photon Higgs partial width. The event rate is however small and an excellent calorimeter is need for the signal to be observable. In the analysis a calorimeter energy resolution $\sigma_e/E = ((0.015/\sqrt{E})^2 + (0.0045)^2)^{1/2}$ was assumed which is better than the CMS experiment EM calorimeter resolution. This would be also a different calorimeter than what is currently envisaged for the TESLA detector. The signal for one year of running is shown in Fig. 11. The mass resolution on the peak is 0.4 GeV, allowing for a measurement of $\Delta m_H \sim 100$ MeV and $\Delta\sigma/\sigma$ of 24%. A crucial issue will be the understanding of the background.

An analysis of the production of charged Higgses, which appear in extended Higgs doublet models, is reported in [25]. The cross section is about a factor 20 larger than for e^+e^- collisions. Taken into account the branching ratios, for a charged Higgs below 200 GeV generally the channel $\gamma\gamma \to H^+H^- \to \tau\nu\tau\nu$ is the most promising. With suitable cuts (albeit with a very low efficiency of a few %) a

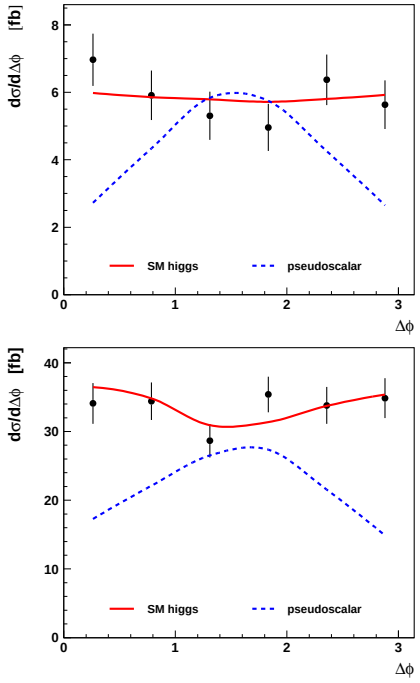

Figure 9: Statistical error on the determination of the azimuthal angle $\Delta\phi$, as explained in the text, for $H \to WW$ and $H \to ZZ$.

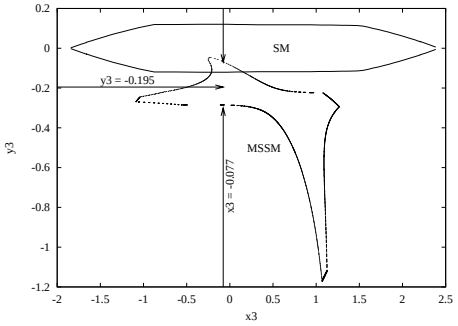

Figure 10: The boundaries of blind regions in the parameter space at 95% C.L. in the $x_3 - y_3$ plane for a luminosity of 100 fb^{-1} for E_B = 310 GeV, given for both the SM and an example of a MSSM point. Details on this analysis and definitions of the x_3, y_3 variables can be found in [24].

S/B of about 3 can be achieved. This decay mode does not allow to reconstruct the mass. To get mass information the channel $H^+H^- \to \tau\nu q\overline{q}$ is under study. More PC studies of the US group are reported in [25, 26].

An important "golden" channel for the PC is the production $\gamma\gamma \to H, A$. Indeed, a PC may help to discover H, A bosons in the MSSM SUSY extension of the SM when these are inaccessible by other machines. For example the LHC cannot extract the H, A signals out of the background

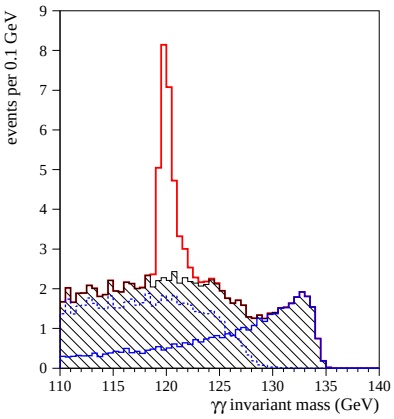

Figure 11: The $\gamma\gamma$ invariant mass distribution including backgrounds from $\gamma\gamma \to \gamma\gamma$ (dashed lines) and $e\gamma \to e\gamma$ (heavy solid line) as well as the Higgs signal peak [25]. The hatched histogram shows the sum of the background contributions.

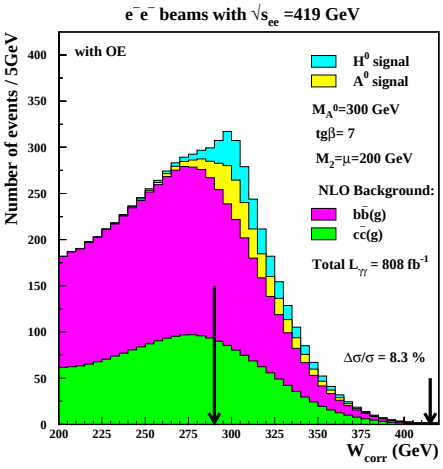

Figure 12: Reconstructed invariant mass, W_{rec}, distribution for selected $b\overline{b}$ events for H, A. Contributions for background and signal are shown separately. The arrows show the optimized mass window for the partial width measurement [28].

(except perhaps for SUSY decay modes of the H, A) if the mass is larger than about 200-300 GeV at medium $\tan\beta$. Fig. 12 shows the mass distribution of the H, A in the $b\overline{b}$ decay channel. This mass distribution [28] was estimated using exactly the same tools as for the light Higgs $H \to b\overline{b}$ analysis [19]. Fig. 13 shows the region that could be covered by a PC for several years of running (assuming a 630 GeV collider) [27] in the $b\overline{b}$ decay mode. The e^+e^- mode of that collider can reach $M_{H,A}$ masses up to about 300 GeV only. The PC essentially closes the wedge left by the LHC, up to masses of 500 GeV. Fig. 14 shows the precision with which the cross section can measured for M_A in the range of 200-350 GeV and $\tan\beta = 7$, with and without

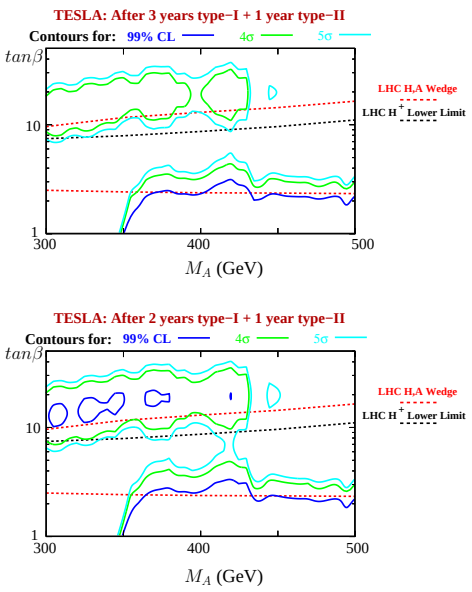

Figure 13: Regions in M_A, $\tan\beta$ where the LHC has problems discovering the heavy Higgs, A and H, with the statistical sensitivity at a PC based on a 630 GeV e^+e^- collider, after several years of running [27].

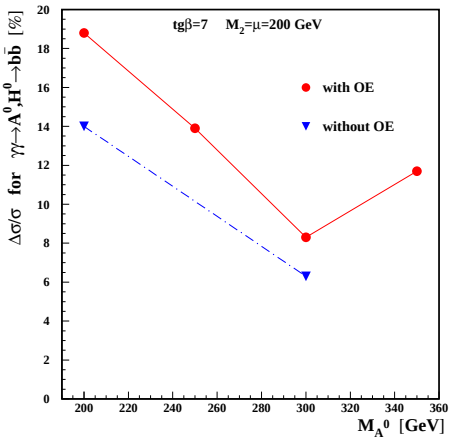

Figure 14: Statistical error on the determination of the $\sigma(\gamma\gamma \to A, H \to b\bar{b})$ measurements shown for $M_A = 200 - 350$ GeV and $\tan\beta = 7, M_2 = \mu = 200$ GeV, with and without overlaying events (OE) [28]. The lines are to guide the eye.

overlaying events.

Standard Model

Due to the large cross sections, several precise measurements of SM parameters or particle properties can be made at a PC.

Triple gauge couplings were studied in detail, using realistic luminosity spectra and detector simulation [29]. The WHIZARD [30] Monte Carlo was used for the signal. The

(GeV)	$\sqrt{s_{e\gamma}}$= 450	$\sqrt{s_{\gamma\gamma}}$= 400	$\sqrt{s_{ee}}$= 500
$\int L\Delta t$	$110 fb^{-1}$	$110 fb^{-1}$	$500 fb^{-1}$
ΔL	0.1%	0.1 %	
ΔK_γ	$9.9 \cdot 10^{-4}$	$6.7 \cdot 10^{-4}$	$3.1 \cdot 10^{-4}$
$\Delta\Lambda_\gamma$	$2.6 \cdot 10^{-4}$	$(6.0) \cdot 10^{-4}$	$4.3 \cdot 10^{-4}$

Table 1: Precision achievable on triple gauge couplings for a $\gamma\gamma$, $e\gamma$ and ee collider.

study shows that these couplings can be measured at a PC with a precision similar to the one achieved at an e^+e^- collider, see Table 1. The sensitivity is proportional to the momentum of the particles involved in the triple gauge boson vertex. The analysis [29] includes detector simulation and 3D fits including the azimuthal decay angle (not yet done for the $\gamma\gamma$ study).

Top quark production was studied in [3]. The $e\gamma$ scattering gives a good sensitivity to the anomalous top couplings, as detailed in that report. The reaction $\gamma\gamma \to t\bar{t}$ allows for an extraction of the electric dipole moment: for 20 fb^{-1} and an electron beam energy of 250 GeV a sensitivity on the dipole moment of $1.3 \cdot 10^{-16}$ ecm can be achieved, when assuming a realistic luminosity spectrum [31].

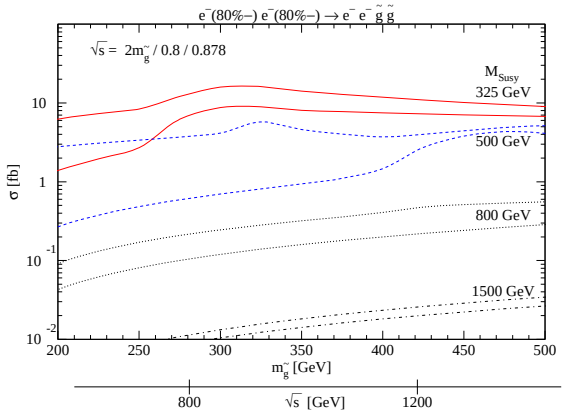

Figure 15: Cross section for gluino production in $\gamma\gamma$ collisions versus the gluino mass and for different squark masses [33] (maximal stop mixing (thin lines) and no mixing (thick lines)).

Beyond the Standard Model

Supersymmetry is presently the most popular theory for physics beyond the standard model. A few examples are given where a PC can make significant contributions.

If the LSP is light, the process $e\gamma \to \tilde{e}\chi_1^0 \to e\chi_1^0\chi_1^0$ can extend the range of discovery for heavy sleptons. Indeed LHC has difficulties discovering sleptons for masses above 300-350 GeV, and the e^+e^- collider has to pair produce sleptons, hence its range is limited to $\sqrt{s}_{ee}/2$. In case of a $e\gamma$ collider the reach is $0.9 \cdot \sqrt{s}_{ee} - m_{\chi_1^0}$, e.g. 350 GeV for 250 GeV electron beams and a LSP of 100 GeV [32].

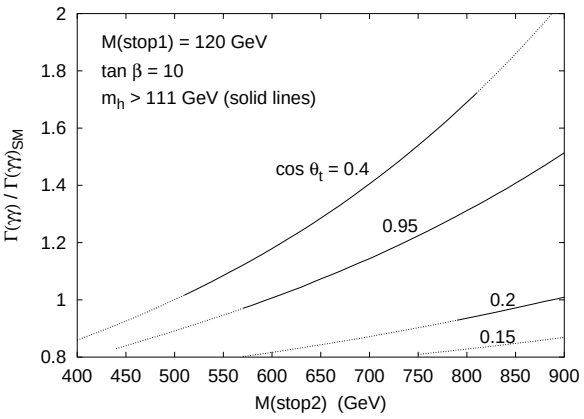

Figure 16: Dependence of the partial two photon width of the Higgs on $M_{\tilde{t}_2}$ for various values of $M_{\tilde{t}_1}$. Here M_A is 1 TeV, $\tan\beta = 10$ and $M_2 = -\mu = 200$ GeV, other SUSY mass parameters are set to 1 TeV [25].

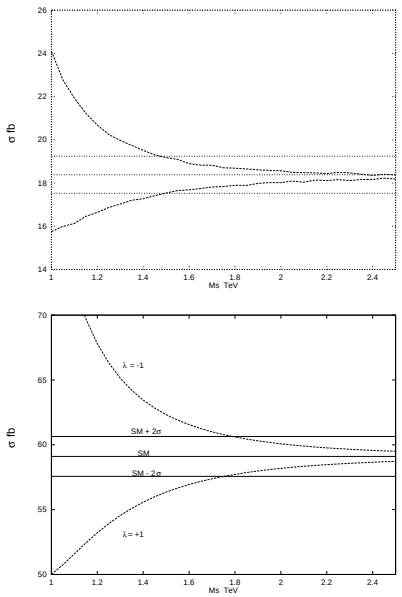

Figure 17: The sensitivity to ADD extra dimensions in the channel $\gamma\gamma \to t\bar{t}$, for an ideal Compton spectrum (top) and for a realistic one using CompAZ (bottom).

Another channel of interest at a PC is $\gamma\gamma \to$ gluinos. This reaction is only accessible at an e^+e^- collider if the squarks are heavier than the gluinos and the decays $\tilde{q} \to \tilde{g}q$ are open. Photons couple to squarks and quarks and can produce gluinos via box diagrams. The yield is shown in Fig. 15. Typically 2000 gluinos pairs can be produced/year for light quarks (325 GeV) [33]. It remains to be seen what one can learn more at a PC than what is known from the LHC at that point.

Measuring the two photon width at a PC can also help to pin down masses of sparticles which cannot be directly produced at the e^+e^- collider. An example is shown in Fig. 16, where we assume a scenario of large mass splitting between the $\tilde{t_1}$ and $\tilde{t_2}$. If the $\tilde{t_1}$ mass and $\tilde{t}$ mixing angle are known from e^+e^- studies then using a precise measurement of the two-photon partial width of the Higgs one can constrain the mass of $\tilde{t_2}$ as shown in the Figure [26].

Other new theories propose the existence of extra dimensions. It appears that the reaction $\gamma\gamma \to WW$ is very sensitive to ADD type of effects [34]. The sensitivity scales with a CMS energy as 11 $\sqrt{s}$. For $e^+e^- \to f\overline{f}$ the sensitivity is 6.5 $\sqrt{s}$, and for the LHC using the process $pp \to jj$ it is 9 TeV for 100 fb^{-1}. A new study shows the sensitivity to ADD extra dimensions in the channel $\gamma\gamma \to t\overline{t}$ in Fig. 17 [35]: the top figure takes the ideal Compton spectrum while the lower figure includes the luminosity via CompAZ. The sensitivity is reduced from $M_s = 1.7$ TeV to 1.4 TeV for one year of running.

TECHNOLOGY FOR A PC

A photon collider IP introduces new challenges: The laser part, the optics, stability and control in the IP (to 1 nm), length control in case of a cavity, beam extraction line, etc. Both the European and the US groups have an R&D effort on the hardware part.

Europe is developing a scheme for an optical cavity, shown in Fig. 18 [36], and plans are considered to make a 1:9 scale model. The use of a cavity allows multi-passing of the laser signal and thus reduces the required laser power. The US group of LLNL follows a full power laser design, as the short bunch distance at the NLC is less favourable to benefit from such a cavity option.

The US group has commissioned a laser with 20 J pulses at 10 Hz. The full power (100 Hz at 10 Hz) is expected to be reached next year. In total 10 of these lasers would be required. They have also studied interferometry for alignment, built a half-size focusing optics setup in the lab, studied a beam-beam deflection feedback system, and are preparing a proposal for a PC testbed at SLAC, using the SLC and perhaps even parts of the SLD [37]. A picture of the set-up of the optics is shown in Fig. 19.

In all there is progress but funding is presently certainly and issue to continue the R&D. The developments during the coming years will be of vital importance.

E-E- COLLISIONS

The PC will be based on e^-e^- collisions. These collisions can be of great interest by itself. No new studies have been presented in the context of this workshop, but an excellent overview paper can be found in the proceedings of the LCWS2002 [38]. Here we recall on a few of the outstanding advantages of e^-e^-

- Large polarization for both beams, hence (almost) pure e_L, e_R initial states.
- Excellent discovery potential for states with exotic quantum numbers (e.g such as H^{--})

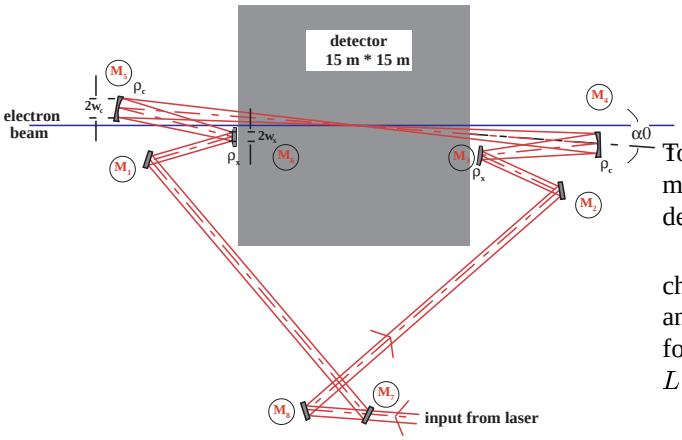

Figure 18: The optical cavity for the TESLA PC IP design.

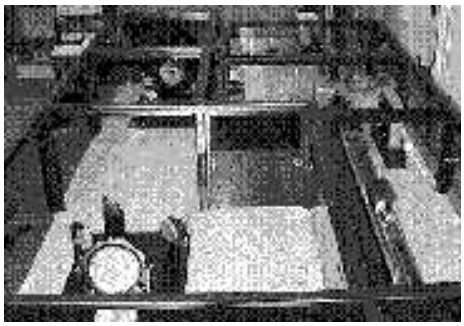

Figure 19: The optics setup at LLNL.

- Larger sensitvity (for identical luminosity) than e^+e^- e.g. for contact interactions, non-commutative scales (via Moller scattering)
- Special processes can be very clean, e.g. $e^-e^- \to e^-e^-H$
- Sharper onset of e.g. the slepton production threshold

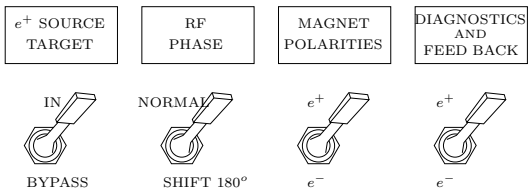

Figure 20: Since the e^-e^- collider requires only minor changes to the hardware of the e^+e^- machine and detector, its programme could be pursued during the first face of the facility..." International Linear Collider Technical Review Committee Report- 1995 [38].

than in e^+e^-

- Possibility to identify TeV level Majorana neutrinos through the lepton number violation reaction $e^-e^- \to W^-W^-$

To be fully convincing these studies need to reach the same maturity as for the e^+e^- collider or PC studies: i.e. include detector simulation, backgrounds, beamstrahlung, ...

On the downside there are of course no classical s-channel processes in e^-e^-, and since the beams show an anti-pinch effect, the luminosity in general is lower than for e^+e^-. One finds typically numbers in the ball-park of $L_{e^-e^-} = 0.15 - 0.3 \cdot L_{e^+e^-}$ [39].

Unlike for the PC there are however no major changes required in the interaction region or accelerator. The e^-e^- option is the extra option which for TESLA would be most easily to realize. Fig. 20 shows how easy it could be for the machine shift leader to switch from e^+e^- to e^-e^- collisions: just four switches to turn... Clearly we must keep it on the roadmap and the future new physics will decide how valuable this option will be for us.

CONCLUSION

An $\gamma\gamma$ and $e\gamma$ collider will provide exciting physics opportunities, many of which have been developed in detail during the last two years. The development of specific PC study tools has allowed that several of the studies have now reached the necessary maturity.

At the LCWS2002 in Jeju a panel discussion was organized on the PC option [40]. The conclusion was a clear plea to continue the R&D and physics studies such that we can be in a good position to incorporate a PC in the overall planning of a LC, when that day comes. A PC will be largely complementary to its drive LC and will therefore strengthen the case for such an e^+e^- collider. A PC option should be considered from the onset within the planning of the project. A vigorous R&D plan for a PC will need to be put in place, preferably on a world-wide level.

Finally an (updated) short list of processes which are considered to be most important for the physics program of the photon collider option of the LC, is presented in Table 2, taken from ref. [3]. Additionally to this list are the processes $e\gamma \to e^*$, leptoquark production, strong WW scattering and $e\gamma \to eH$. It summarizes the rich physics program that becomes accessible at a Photon Collider!

ACKNOWLEDGMENTS

I would like to thank my co-conveners M. Krämer, M. Krawczyk, and S. Maxfield of the ECFA/DESY Future LC study group on "$\gamma\gamma$ and $e\gamma$ Collider Physics", for the two years pleasant collaboration and critically reading the manuscript.

Reaction	Remarks
$\gamma\gamma \to H, h \to b\bar{b}$	SM/MSSM Higgs, $M_{H,h} < 160$ GeV
$\gamma\gamma \to H \to WW(^*)$	SM Higgs, 140$< M_H <$ 190 GeV
$\gamma\gamma \to H \to ZZ(^*)$	SM Higgs, 180$< M_H <$ 350 GeV
$\gamma\gamma \to H \to \gamma\gamma$	SM Higgs, 120$< M_H <$ 160 GeV
$\gamma\gamma \to H \to t\bar{t}$	SM Higgs, $M_H > 350$ GeV
$\gamma\gamma \to H, A \to b\bar{b}$	MSSM heavy Higgs, interm. $\tan\beta$
$\gamma\gamma \to \tilde{f}\bar{\tilde{f}},\ \tilde{\chi}_i^+\tilde{\chi}_i^-$	large cross sections
$\gamma\gamma \to \tilde{g}\tilde{g}$	measurable cross sections
$\gamma\gamma \to H^+H^-$	large cross sections
$\gamma\gamma \to S[\tilde{t}\bar{\tilde{t}}]$	$\tilde{t}\bar{\tilde{t}}$ stoponium
$e\gamma \to \tilde{e}^-\tilde{\chi}_1^0$	$M_{\tilde{e}^-} < 0.9 \times 2E_0 - M_{\tilde{\chi}_1^0}$
$\gamma\gamma \to \gamma\gamma$	non-commutative theories
$e\gamma \to eG$	extra dimensions
$\gamma\gamma \to \phi$	Radions
$e\gamma \to \tilde{e}\tilde{G}$	superlight gravitions
$\gamma\gamma \to W^+W^-$	anom. W inter., extra dimensions
$e\gamma \to W^-\nu_e$	anom.W couplings
$\gamma\gamma \to 4W/(Z)$	WW scatt., quartic anom. W,Z
$\gamma\gamma \to t\bar{t}$	anomalous top quark interactions
$e\gamma \to \bar{t}b\nu_e$	anomalous Wtb coupling
$\gamma\gamma \to$ hadrons	total $\gamma\gamma$ cross section
$e\gamma \to e^-X, \nu_e X$	NC and CC structure functions
$\gamma g \to q\bar{q},\ c\bar{c}$	gluon in the photon
$\gamma\gamma \to J/\psi\, J/\psi$	QCD Pomeron

Table 2: Update of the Gold–plated processes at photon colliders.

REFERENCES

[1] I. F. Ginzburg, G. L. Kotkin, V. G. Serbo, and V. I. Telnov, *Nucl. Instr. and Meth.* **205**, (1983) 47;
I. F. Ginzburg et al., *Nucl. Instr. and Meth.* **219**, (1984) 5;
V. Telnov, *Nucl. Instr. and Meth.* **A294**, (1990) 72;
V. Telnov, *Nucl. Instr. and Meth.* **A355**, (1995) 3.

[2] B. Badelek et al., hep-ex/0108012.

[3] E. Boos et al, *Nucl. Instrum. Meth.* **A472** (2001) 100, hep-ph/0103090.

[4] V. Telnov, PHOCOL program, private comm.

[5] T. Ohl, *Comput. Phys. Commun.* **101** (1997) 269, hep-ph/9607454.

[6] A.F. Żarnecki, *Acta Phys. Polon.* **B34** (2003) 2741, hep-ex/0207021 (2002).

[7] K. Mönig, J. Sekaric, talks during this workshop.

[8] V. Telnov, Talk at the ECFA/DESY meeting in Amsterdam April 2003.

[9] F. Kraus, talks during this workshop.

[10] J. Butterworth, M. Wing, talks at ECFA/DESY workshops, Prague Nov. 2002 and Amsterdam, April 2003;
J. M. Butterworth, S. Butterworth, hep-ph/0210404, *Comp. Phys. Comm.* **153** (2003) 164.

[11] V. Makarenko, K. Mönig, T. Shishkina, LC-PHSM-2003-016.

[12] A.V. Pak et al., LC-PHSM-2003-057.

[13] V. Budnev et al., *Phys. Rep.* **C15** 181 (1975).

[14] R. M. Godbole, G. Pancheri *Eur. Phys. J.* **C19** (2001) 129, hep-ph/0010104

[15] N. Timmeanu, J. Kwiecinski and L. Motyka, *Eur. Phys. J.* **C23** (2002) 513, hep-ph/0110409.

[16] F. Cornet, P. Jankowski, M. Krawczyk and A. Lorca, *Phys. Rev.* **D68** (2003) 014010, hep-ph/0212160.

[17] R.M. Godbole, A. De Roeck, A. Grau, G. Pancheri *JHEP* **0306**, (2003) 61, hep-ph/0305071.

[18] S. Soldner-Rembold and G. Jikia, *Nucl. Instrum. Meth.* **A472** (2001) 133, hep-ex/0101056.

[19] P. Niezurawski, A.F.Żarnecki, M. Krawczyk, hep-ph/0307183 and LC-PHSM-2003-086;
P.Niezurawski, A.F.Żarnecki, M.Krawczyk, *Acta Phys. Polon.* **B34** (2003) 177, hep-ph/0208234.

[20] A. Rosca and K. Mönig, LC-PHSM-2003-084.

[21] G. Jikia and A. Tkabladze, *Nucl. Inst. Meth* **A355**, (1995) 91; *Phys. Rev.* **D54** (1996) 2030, hep-ph/9406428.

[22] P. Niezurawski, A.F.Żarnecki, M. Krawczyk, hep-ph/0307175 and LC-PHSM-2003-088;
P.Niezurawski, A.F.Żarnecki, M.Krawczyk, *JHEP* 0211 (2002) 034, hep-ph/0207294.

[23] See e.g.. I. Ginzburg, M Krawczyk and P. Osland LC-PHSM-2003-037 and references therein.

[24] R. M. Godbole, S. D. Rindani, R. K. Singh, *Phys. Rev.* **D67** (2003) 095009, hep-ph/0211136.

[25] D. Asner et al, 2002, hep-ph/0208219.

[26] D. Asner et al 2003, hep-ph/0308103.

[27] D. Asner, J. Gronberg, J. Gunion, *Phys. Rev.* **D67** (2003) 035009, hep-ph/0110320.

[28] P. Niezurawski, A.F.Żarnecki, M. Krawczyk, hep-ph/0307180 and LC-PHSM-2003-088.

[29] K. Mönig, J. Sekaric, LC-PHSM-2003-072, I. Marfin, V. Mossolov, T. Shishkina, LC-PHSM-2003-085.

[30] W. Kilian, Procs of the Int. Conf. on High Energy Physics (ICHEP 2002), Amsterdam, p831.

[31] R.M. Godbole, P. Poulose and S.D. Rindani, LC Note to appear.

[32] I. Watanabe et al., KEK-REPORT-97-17 (1998).

[33] Stefan Berge, Michael Klasen, hep-ph/0303032.

[34] T. Rizzo, *Nucl. Instrum. Meth.* XS**A472** (2001) 37, hep-ph/0008037.

[35] R.M. Godbole, P. Mathews and S.D. Rindani, LC Note to appear.

[36] G. Klemz et al., talks during this workshop.

[37] J. Gronberg, talks at meetings during this workshop;
A.J. Bayramian, R.J. Beach, W. Behrendt, C. Bibeau, et al., Tech. digest OSA TOPS on Advanced Solid-State Lasers, Vol. 83, pp. 268-275.

[38] C. Heusch, Proc. of LCWS02, p763, (2002).

[39] S. Schreiber, *Int. J. Mod. Phys.* **A18** (2003) 2827.

[40] E. Gross, Proc. of LCWS02, p83, (2002);
M. Krawczyk, hep-ph/0307314.

The TESLA DETECTOR CONCEPT*

M.A. Thomson,
Cavendish Laboratory, University of Cambridge, Cambridge, UK

Abstract

The high precision physics goals of a future e^+e^- linear collider place strict requirements on the design of the detector. This paper gives an overview of the TESLA detector concept concentrating on the physics motivation for the design choice and the detector performance.

INTRODUCTION

Within the particle physics community there is increasing consensus that the world's next large accelerator project will be an e^+e^- linear collider (LC) operating in the energy range 500 GeV$-$1 TeV. The TESLA (TeV Energy Superconducting Linear Accelerator) project [1] offers one technological route to realising such a LC. The luminosities provided by TESLA would be approximately three orders of magnitude greater than those achieved at LEP. This, coupled with the clean environment of e^+e^- collisions, would make TESLA the ideal place for precision studies of physics beyond the Standard Model (SM). The physics potential of a LC, such as understanding the nature of any Higgs-like particle, places stringent requirements on all aspects of the detector design.

*This article summarises both detector R&D work and the studies of the impact of the detector performance on the physics potential of the TESLA linear collider. Much of the work was performed in the extended ECFA/DESY study by: K. Ackermann, L. Andricek, H.M. Araujo, S. Ask, J.E. Augustin, M. Battaglia, H. Bauke, M. Baulillier, T. Behnke, A.C. Benvenuti, M. Berggren, J.-D. Berst, F. Bieser, G. Blair, W. de Boer, A. Bondar, I. Bozovic, J.C. Brient, I. Britvich, K. Buesser, A. Buzulutskov, T. Camporesi, B. Canton, R.C. Carnegie, C. Carimalo, P. Checchia, R. Cizeron, G. Claus, P. Cloarec, P. Colas, C. Colledani, C. Damerell, A. Delbart, G. Deptuch, F. Le Diberder, M.S. Dixit, V. Djordjadze, M. Doucet, J. Dubeau, W. Dulinski, W. Da Silva, V. Eckardt, W. Edwards, M. Elsing, C. Fanin, A. Feniouk, P. Fischer, B. Gastineau, P. Gay, G. Genolini, N. Ghodbane, Y. Giomataris, Y. Gornushkin, H. van der Graaf, N. de Groot, M. Gruwe, P. Hassler, M. Hamann, K. Harder, J. Hauschildt, R. Hawkings, V. Hedberg, R.D. Heuer, Y. Hu, D. Imbault, A. Imhof, D.J. Jackson, J. Jeanjean, J. Kaminski, A. Kaoukher, S. Kappler, F. Kapusta, A. Karar, D. Karlen, M. Killenberg, F. Kircher, V. Klioukhine, M. Kock, V. Korbel, T. Kuhl, J. Kuhlmann, H. Lebbolo, B. Ledermann, V. Lepeltier, V. Lishin, S. Lotze, G. Lutz, T. Lux, S. Magill, M. Margoni, C. Martens, J.-P. Martin, M. Mazzucato, H. Mes, N. Meyners, D.J. Miller, J. Mnich, K. Moenig, S. Monteil, P. Mora de Freitas, V. Morgunov, T. Müller, D. Nygren, V. Obraztsov, D. Orlando, Y. Pabot, M. Paganoni, J. Peyré, M. Pohl, V. Poliakov, V. Popov, J. Pouthas, P. Rebourgeard, D. Reid, R. Richter M. Ronan, F. Rossel, S. Roth, K. Sachs, V. Saveliev, A. Savoy-Navarro, H.J. Schreiber, H. Schröder, R. Schulte, M. Schumacher R. Settles, L. Shekhtman, M. Siemens, F. Simonetto K. Sinram, B. Sobloher, A. Stahl, K. Stefanov, W. Struczinski, S. Shuvalov, Ch. de la Taille, V.I. Telnov, F. Terranova, J. Timmermans, M. Tonutti, M. Trimpl, R. Turchetta, J. Ulrici, A. Vasilev, H. Videau, D. Vincent, E. Vlasov, N. Wermes, D. Wicke, M. Wing, M. Winter H. Wieman, S.M. Xella-Hansen, R. Zimmermann

THE PHYSICS ENVIRONMENT

It is foreseen that the TESLA LC would operate at centre-of-mass energies of $90-800\,\mathrm{GeV}$. In the TESLA design, the colliding beams arrive in five bunch trains per second with each train consisting of 2820 bunches separated by 337 ns. The nominal luminosity (at 500 GeV) is $3.4\times10^{34}\,\mathrm{cm^{-2}\,s^{-1}}$ which is more than 1000 times that achieved at LEP 2. The corresponding event rates are indicated in Table 1. In addition to the listed processes there is a significant background from the multi-peripheral "two photon" process, $e^+e^- \to e^+e^- + \mathrm{hadrons}$, which corresponds to approximately 0.02 events with visible tracks per bunch crossing (BX) at 500 GeV. The relatively long time between successive BXs (337 ns) should allow association of tracks with BX. In addition to the two photon background, there are also significant beam related backgrounds corresponding to approximately 600 hits per BX in the Vertex detector. These background levels, although high compared to those experienced at LEP, are much lower than those anticipated at the LHC. Consequently the detector design is dictated by the physics goals and not by issues of radiation hardness.

Table 1: Event rates at a 500 GeV e^+e^- collider assuming the TESLA design luminosity of $3.4\times10^{34}\,\mathrm{cm^{-2}\,s^{-1}}$. The event rate from $e^+e^- \to q\overline{q}$ refers to the rate summed over all quarks other than the top quark.

Process	**Event Rate**
$e^+e^- \to e^+e^-$ ($\theta > 20$ mrad)	$350\ \mathrm{s^{-1}}$
$e^+e^- \to q\overline{q}(\gamma)$	$1600\ \mathrm{h^{-1}}$
$e^+e^- \to W^+W^-$	$930\ \mathrm{h^{-1}}$
$e^+e^- \to t\overline{t}$	$70\ \mathrm{h^{-1}}$
$e^+e^- \to ZH$ (M_H=120 GeV)	$7\ \mathrm{h^{-1}}$

PHYSICS AT A LINEAR COLLIDER

The physics case for a future LC is well documented in the TESLA Technical Design Report [1] (TDR). The main goals of the physics programme are summarised below:

- *Higgs Physics:* If the Higgs boson exists, it is likely that it will be discovered at the LHC or Tevatron. At a LC the emphasis will be on establishing the nature of the Higgs through precise measurements of its properties, such as mass, fermionic branching fractions and the Higgs boson trilinear coupling.
- *Supersymmetry:* Supersymmetry (SUSY) is a widely touted candidate for physics beyond the SM. How-

ever, SUSY encompasses a wide range of theoretical scenarios, both in terms of the mechanism by which SUSY is broken and the large number of free parameters within SUSY models. The wealth of precise measurements possible at the LC would provide a powerful probe of the underlying structure of the SUSY theory.

- *Strong Electroweak Symmetry Breaking:* If the Higgs boson is not discovered at the LHC or Tevatron, an alternative mechanism for electroweak symmetry breaking is required. The golden physics process in the absence of the Higgs boson is that of longitudinal W-boson scattering, $\mathrm{W_L^+W_L^-} \rightarrow \mathrm{W_L^+W_L^-}$ which, without contributions from the s-channel Higgs exchange, grows and violates quantum mechanical unitarity. To avoid unitarity violation it is required that the interactions between the vector-bosons become strong at energies of order 1 TeV. This would be manifested in anomalous triple or quartic gauge boson couplings. Observation of the $\mathrm{W^+W^-}$ and ZZ scattering processes will be possible using the final states $\nu_e\overline{\nu}_e\mathrm{W^+W^-}$ and $\nu_e\overline{\nu}_e\mathrm{ZZ}$. Anomalous gauge boson couplings can be studied using similar techniques to those used at LEP, such as the reconstruction of angular distributions and correlations.

- *Top-quark Physics:* An $\mathrm{e^+e^-}$ LC provides a clean environment in which to study the properties of the top quark. In particular, the mass of the top quark is a key input in fits to high precision electroweak data. At the LC the top quark mass can be determined with a precision of ~ 200 MeV compared to $1-2$ GeV at LHC.

DETECTOR REQUIREMENTS

Before considering explicitly the requirements for a detector at a future LC it is worth considering the impact of the performance of the LEP detectors on the physics sensitivity. The main goal at LEP was to perform precision measurements of the properties of the W and Z gauge bosons. Physics sensitivity did not usually depend strongly on the detector performance. A good example is the measurement of the W-boson mass where the four LEP collaborations obtain similar statistical uncertainties [2] with significantly different jet energy resolutions. This is a direct consequence of the kinematic fit where the total energy of the final state fermions is constrained to be equal to the energy of the $\mathrm{e^+e^-}$ collisions; as a result the mass resolution is significantly better than achieved using the raw measured jet energies, as indicated in Fig. 1 [3]. At a LC, kinematic fitting will be far less useful due to Beamstrahlung and increased initial state radiation (ISR). In addition, many of the potentially interesting final states at a future LC involve two or more unobserved particles, for example, $\mathrm{e^+e^-} \rightarrow \nu_e\overline{\nu}_e\mathrm{W^+W^-}$ and many SUSY processes, and kinematic constraints will be of limited use. As a result, the physics performance at a LC depends critically on being able to reconstruct the gauge bosons directly from jets and leptons. This places strict performance requirements on the detector.

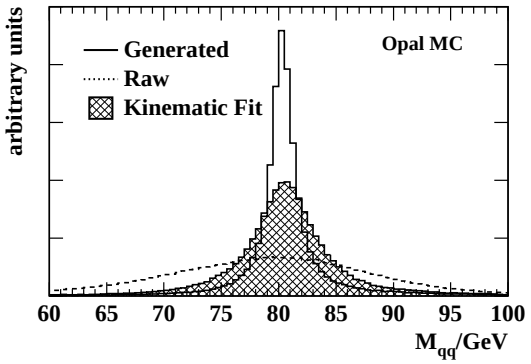

Figure 1: A comparison of the reconstructed invariant mass distribution from the $\mathrm{q\overline{q}}$ system in $\mathrm{W^+W^-} \rightarrow \mathrm{q\overline{q}}\ell\overline{\nu}_\ell$ events at LEP using the measured quantities (Raw) and the result of the kinematic fit [3]. Also shown is the underlying generated distribution.

Detector Requirements at TESLA

The main requirements for a TESLA detector are summarised below:

- *Momentum resolution:* $\sigma_{1/p} \sim 5 \times 10^{-5}\,\mathrm{GeV}^{-1}$ (a factor of ten better than that achieved at LEP). Good momentum resolution is important for the reconstruction of the leptonic decays of Z bosons. This is particularly relevant for $\mathrm{e^+e^-} \rightarrow \mathrm{ZH}$ events where the Higgs boson properties, including its mass, are best studied by considering the system recoiling against the Z, with the golden channel being $\mathrm{Z} \rightarrow \mu^+\mu^-$.

- *Impact parameter resolution:* Efficient b and c quark tagging which implies good impact parameter (d_0) resolution:

$$\sigma_{d_0}^2 < (5.0\,\mu\mathrm{m})^2 + \left(\frac{5.0\,\mu\mathrm{m}}{p(\mathrm{GeV})\sin^{\frac{3}{2}}\theta}\right)^2 .$$

  This is a factor of three better resolution than obtained at SLD.

- *Jet energy resolution:* $\sigma_E/E \sim 0.3/\sqrt{E(\mathrm{GeV})}$ in order to be able to directly reconstruct and identify gauge bosons from their hadronic decays to jets, *i.e.* $\mathrm{W} \rightarrow \mathrm{q\overline{q}}$ and $\mathrm{Z} \rightarrow \mathrm{q\overline{q}}$. This is a factor of two better than the best achieved at LEP.

- *Hermiticity:* Hermetic down to 5 mrad for searches for missing energy signals from new physics.

- *High Granularity:* Events at the LC will have high track densities due to the boosted final states and the

fact that many of the interesting physics processes result in final states with six or more jets. A LC detector is required to have high granularity and good two track resolution.

THE TESLA DETECTOR CONCEPT

The baseline TESLA detector concept is discussed in detail in the TESLA TDR [1]. The general detector layout consists of a cylindrical barrel region and two endcaps and is shown in Fig. 2. Tracking of charged particles is performed using a high precision Silicon-based microvertex detector (VTX) surrounded by a large gaseous time projection chamber (TPC) which provides a large number of space points along a track and enables momentum determination. The tracking is supplemented by additional Silicon forward tracking detectors (FTD) perpendicular to the beam axis. The high granularity electromagnetic calorimeter (ECAL) consists of alternate layers of Silicon and Tungsten. A high granularity hadronic calorimeter (HCAL) is located outside the ECAL, but still inside the magnet coil. The superconducting magnet, which is based on the CMS magnet [4], provides a highly homogeneous 4 T solenoidal field. Muon chambers are located within the magnet return yoke. There is no hardware trigger, with deadtime-free continuous readout over a complete 1 ms bunch train. Zero suppression, hit recognition and digitisation is performed in the front-end electronics.

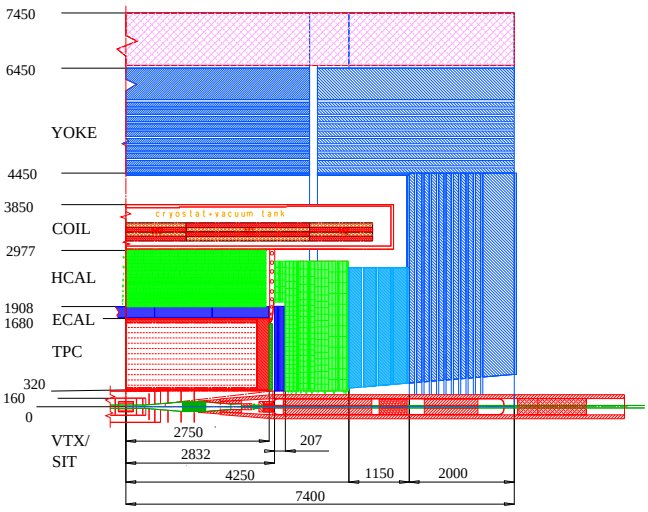

Figure 2: A quadrant of the TDR concept of a detector for TESLA [1] (dimensions in mm).

The main features of the detector components are described below, concentrating on the tracking detectors, in particular the vertex detector and central tracker, and the calorimetry.

OVERVIEW OF THE TRACKING SYSTEM

The primary requirements of the tracking system for a detector at TESLA are: excellent momentum resolution, $\sigma_{1/p} \sim 5 \times 10^{-5}\,\mathrm{GeV}^{-1}$; excellent heavy flavour tagging capability and efficient track reconstruction down to small angles. A subsidiary, but nevertheless important, requirement is to minimise the amount of material in the central tracker in order to minimise multiple scattering, to reduce the occupancy from converting background photons, and to avoid compromising the performance of the calorimeters. The components of the tracking system are:

- a multilayer micro-vertex detector (VTX) from radii of $1.5 - 6.0\,\mathrm{cm}$ consisting of five concentric barrels of Silicon pixel detectors;
- a large volume Time Projection Chamber (TPC) between radii $32 - 170\,\mathrm{cm}$ to provide precise momentum measurements;
- additional Silicon tracking between the vertex detector and the TPC consisting of 2 cylinders of Silicon in the barrel region (SIT) and discs in the forward region (FTD);
- a precise forward straw chamber or Silicon tracker behind the TPC endplate (FCH/Si-FCH).

The layout of the tracking system is shown in Fig. 3. One advantage of the proposed system is that tracks can be reconstructed independently in the TPC and in the combined seven layers of the VTX and SIT detectors, thus aiding both alignment and calibration. The physics motivation and the design of the main components of the tracking system are described below.

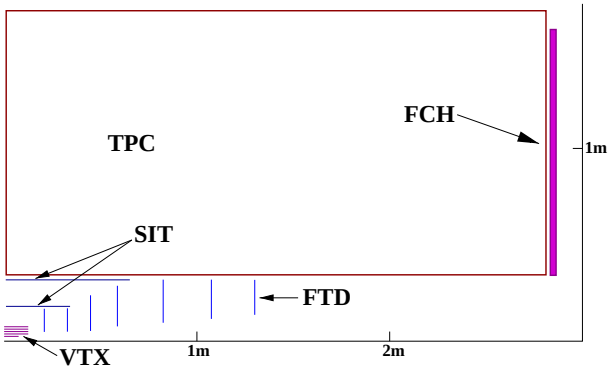

Figure 3: The components of the tracking system [1].

VERTEX DETECTOR

Precise measurements of the properties of as yet undiscovered new particles form the cornerstone of the LC physics programme. It is assumed that if the Higgs boson and/or SUSY exist, they are likely to have been discovered at the LHC or Tevatron before the linear collider is operational. At a LC the emphasis will be on establishing the nature of these new particles by making precise measurements of their properties. Heavy-flavour tagging will be of prime importance in many of these studies as

many signatures of new physics result in final states containing b-quarks, for example, $e^+e^- \to ZHH$ and $e^+e^- \to H^0A^0 \to b\bar{b}b\bar{b}$. One particularly important question is whether the Higgs boson, if it is observed, has production and decay properties consistent with being the SM Higgs. In the SM the Higgs boson coupling to fermions, g_{Hff}, is proportional to the fermion mass. If the Higgs boson is light ($M_H < 150\,GeV$), which is consistent with the current electroweak data [2], one important test of the Higgs sector will be the measurement of its fermionic branching fractions, shown in Fig. 4. Here the ability to be able to tag efficiently charm quarks is important for separating $H \to c\bar{c}$ and $H \to b\bar{b}$. Efficient heavy flavour tagging will also play a major rôle in the event identification of many final states involving quarks.

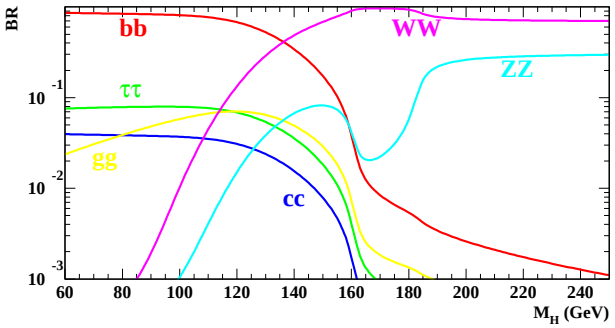

Figure 4: The decay branching fractions of the SM Higgs boson as a function of Higgs boson mass, M_H.

Design Issues

Heavy flavour tagging requires a precise measurement of the impact parameter d_0, the transverse ($r\phi$), distance of a charged particle track from the primary vertex. In general, the impact parameter resolution can be expressed as the quadrature sum of two terms:

$$\sigma_{d_0}^2 = a^2 + \left(\frac{b}{p(\mathrm{GeV}) \sin^{\frac{3}{2}} \theta} \right)^2 .$$

The first term, a, depends on the single point resolution and the second term is the degradation in resolution arising from multiple scattering in the vertex detector which depends on both polar angle θ and momentum p. The TESLA detector goal is for both a and b to be smaller than $\sim 5\,\mu m$. This would represent a significant improvement over previous vertex detectors, *e.g.* this is approximately a factor three better than that achieved at SLD.

In light of the success of the SLD vertex detector it is generally accepted that a vertex detector at the next linear collider will consist of approximately one billion Silicon pixels arranged in concentric cylindrical layers, as shown schematically in Fig. 5.

Given the rapid evolution of semi-conductor devices, it is too early to decide on a specific detector technology, however there are a number of widely accepted design principles:

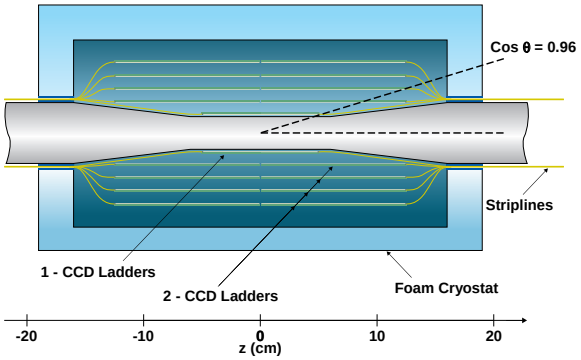

Figure 5: General layout of a CCD-based vertex detector [1].

- the inner layer should be as close to the interaction region as possible. This is particularly important for charm tagging. In the TESLA TDR design [1] the inner radius is 15 mm. Ultimately the minimum inner radius is determined by the size of the beam pipe, which depends on the accelerator design.

- at TESLA beam related backgrounds, even at a radius of 12.5 mm, are not a significant problem as most e^+e^- pairs from beam-beam interactions are confined to the beam pipe by the 4 T magnetic field.

- the detector should consist of five layers to allow full track reconstruction independent of the central tracking chamber.

- space points should be measured with a precision of $< 5\,\mu m$ which is obtainable with CCD pixel sizes of $\sim 20 \times 20\,\mu m^2$ by charge centroid fitting. In addition, to giving to good space point resolution, a small pixel size is important to separate hits from multiple tracks in dense event environments, *e.g.* the cores of high multiplicity jets.

- the thickness of the layers should be reduced from $0.004\,X_0$ (SLD) to less than $0.001\,X_0$. This not only improves the d_0 resolution by reducing multiple scattering, but also suppresses γ conversions allowing clean electron identification in heavy flavour decays.

Although the general concept and performance goals are well defined the technological route is uncertain and forms an active area of research and development. The main options currently being considered are: CCD pixel devices [5]; CMOS monolithic active pixel sensors (MAPS) [6]; hybrid active pixel sensors (HAPS) [7] and depleted Field Effect Transistors (DEPFET) [8].

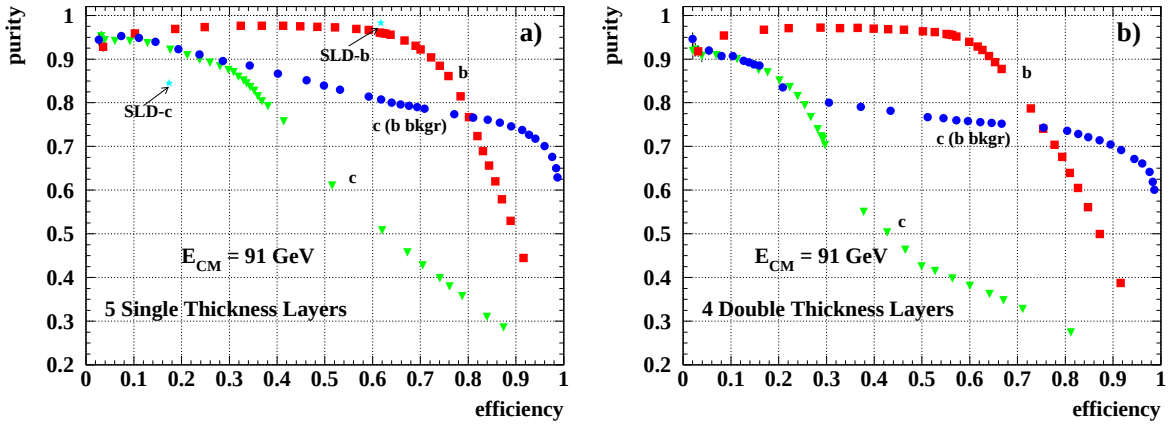

Figure 6: Efficiency and purity for tagging a heavy flavour jet in Z decays [10]. Figure a) shows the performance of a slightly modified version of the TDR VTX detector. Figure b) shows the degradation in performance if the inner layer is removed and the layer thickness doubled. The c(b bkgr) points represent the charm tagging efficiency when only bottom jets constitute the background. For comparison the best results from SLD are also indicated.

Performance

The baseline VTX detector of the TESLA TDR consists of 5 concentric cylinders of $20 \times 20\,\mu\mathrm{m}^2$ CCD pixels located at radii of 15 mm, 26 mm, 38 mm, 48 mm and 60 mm. Each layer corresponds to a thickness of 0.06 % of a radiation length. The expected performance of such a device has been evaluating using the sophisticated tracking and heavy flavour tagging algorithms [9, 10] developed at LEP and SLD. For the TDR baseline design the impact parameter resolution is

$$\sigma_{d_0}^2 = (4.2\,\mu\mathrm{m})^2 + \left(\frac{4.0\,\mu\mathrm{m}}{p(\mathrm{GeV})\sin^{\frac{3}{2}}\theta}\right)^2 .$$

For comparison the values obtained for the SLD detector were $a = 9\,\mu\mathrm{m}$ and $b = 38\,\mu\mathrm{m}$. The flavour tagging used in the TESLA studies is based primarily on the ZVTOP [11] topological vertexing method pioneered at SLD. This algorithm parametrises tracks as Gaussian probability tubes in three dimensional space and identifies vertices as regions of high tube overlap. In addition to ZVTOP, a 1-prong charm tag and an impact parameter joint probability tag [12] are combined in a neural net approach similar to that used by OPAL [13]. Recent studies [10] using the GEANT3 [14] based BRAHMS [15] simulation and these sophisticated (*i.e.* realistic) tagging algorithms compared the performance of different VTX detector configurations. Fig. 6a) shows the simulated heavy flavour tagging performance for a slightly modified version of the TDR VTX detector for a single jet in $\mathrm{Z} \to \mathrm{q\bar{q}}$ events. Although the b-tagging performance is similar to that obtained at SLD, there is a significant improvement of the charm tag; in the high purity region the charm tagging efficiency is approximately a factor two better than that obtained at SLD. Good charm tagging is particularly important for the Higgs to fermion pair branching ratio measurement. Fig. 6b shows the charm tagging efficiency versus purity curves obtained for a four layer VTX detector with the inner layer at 2.7 mm. In this case the layers have double the nominal thickness, *i.e.* 0.11 % X_0. The charm tagging performance is significantly degraded. Other detector configurations have been studied [10] and the most important factor influencing the VTX detector performance is having the inner layer as close to the interaction region as possible.

THE CENTRAL TRACKER

The main purpose of the large volume central tracker is to provide precise momentum measurements. The performance requirements are set by the ability to reconstruct precisely Z bosons from their leptonic decays. This is particularly important for measurements of the properties of the Higgs boson. Current SM fits to electroweak data from LEP, the Tevatron and SLD suggest a relatively light Higgs boson mass, $M_{\mathrm{H}} < 219\,\mathrm{GeV}$ (95 % confidence level) [2]. In this mass range the cross-section for the SM Higgs-strahlung process, $\mathrm{e^+e^-} \to \mathrm{Z^*} \to \mathrm{ZH}$, shown in Fig. 7, is relatively large (a few tens of fb at $\sqrt{s} = 500\,\mathrm{GeV}$).

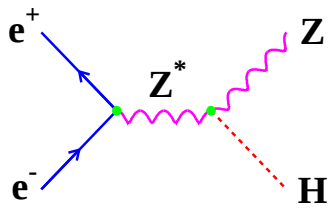

Figure 7: The SM Higgs-strahlung process. Note at a future linear collider the SM Higgs boson is also produced in the WW fusion process and to a lesser extent in the ZZ fusion process.

The Higgs boson typically decays into final states in-

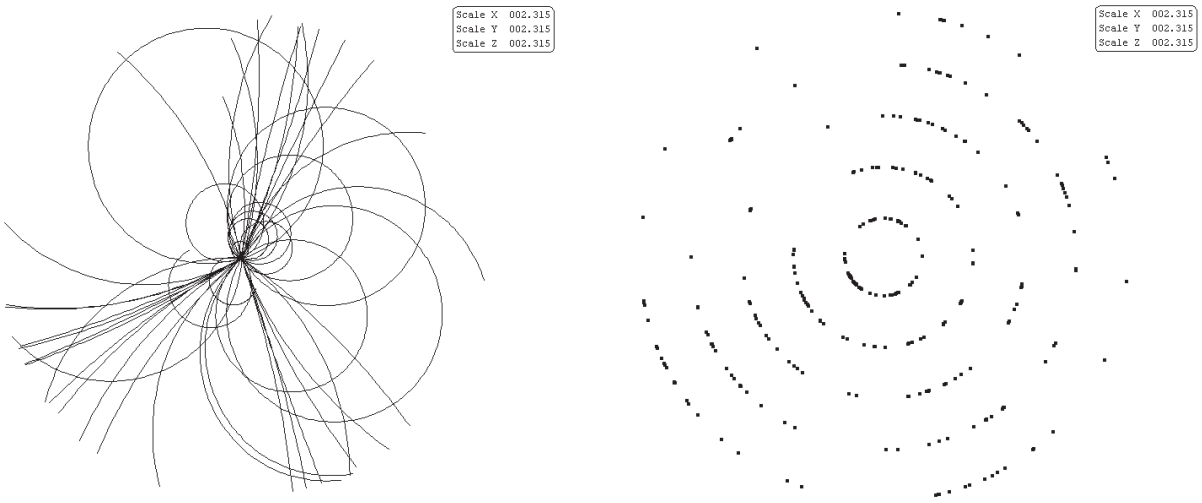

Figure 8: a) A typical linear collider event as seen in a TPC with sampling in more than 100 radial layers. b) The same event as seen in a 5 layer Silicon tracker.

volving jets (*e.g.* $\mathrm{H} \rightarrow \mathrm{b\overline{b}}$ or for higher Higgs masses $\mathrm{H} \rightarrow \mathrm{W^+W^-}$). As jet energies are relatively poorly measured the most precise measurements of the Higgs boson properties can be obtained from well measured Z decays. Consequently, the "golden" channel is the Higgs-strahlung process with $\mathrm{Z} \rightarrow \mu^+\mu^-$. Such events can be precisely reconstructed, independent of the Higgs decay mode, from the $\mu^+\mu^-$ system. For example, the mass of the Higgs boson can be determined from the mass recoiling against the $\mu^+\mu^-$ system. Two factors determine the precision of this measurement: the Z width, Γ_{Z}, and the event-by-event measurement error on the recoil mass which is of order the momentum resolution, σ_{p}. For the momentum resolution term to be significantly smaller than that from Γ_{Z} imposes the requirement on the momentum resolution of the entire tracking system (including the precisely measured hits in the VTX and SIT detectors) of $\sigma_{1/\mathrm{p}} \sim 5 \times 10^{-5}\,\mathrm{GeV}^{-1}$. This is an order of magnitude better than achieved at LEP. To achieve this goal, the momentum resolution from the central tracking chamber alone must be $\sigma_{1/\mathrm{p}} \sim 2 \times 10^{-4}\,\mathrm{GeV}^{-1}$.

Choice of Central Tracker Technology

A number of options for the large volume central tracker have been considered. These fall into two main categories: i) gaseous detectors which provide a large number of relatively coarse spatial measurements along a charged particle track and ii) Silicon detectors which provide a few very precise measurements. The TESLA baseline choice is a Time Projection Chamber (TPC) such as those successfully operated by the ALEPH [16] and DELPHI [17] collaborations at LEP. A TPC has a number of significant advantages:

- it provides a large number of three-dimensional space points which enables good pattern recognition in a dense track environment. This point is illustrated by Fig. 8, where the TPC hit pattern is compared with that which would be observed using a 5 layer Silicon central tracker.
- it provides adequate two hit resolution enabling separation of nearby charged particle tracks, an important point for the reconstruction of jet energies.
- as gas forms the active medium, the amount of material in front of the ECAL is minimised. This reduces multiple scattering and also reduces the occupancy in the tracking chamber arising from conversions of background photons.
- it provides dE/dx information allowing particle identification.
- it allows easy identification of 'non-pointing' tracks, *i.e.* tracks which do not originate from the interaction region, thereby allowing the reconstruction of decaying neutrals, *e.g.* $\mathrm{K_S} \rightarrow \pi^+\pi^-$. This is also important in searches for signals for physics beyond the Standard Model. For example, one possible signal for Gauge Mediated SUSY Breaking (GMSB) would be the observation of kinked tracks in the process $\mathrm{e^+e^-} \rightarrow \tilde{\mu}^+\tilde{\mu}^- \rightarrow \mu^+\mu^-\tilde{\mathrm{G}}\tilde{\mathrm{G}}$.

TPC Conceptual Design

The baseline design of the TPC is shown in Fig. 9. The active volume consists of two drift regions (forward/backward) each of 2.5 m in length. The inner radius, determined by the size of the forward mask system which extends inside the TPC bore, is 0.32 m and the outer radius is 1.7 m. The outer radius of the TPC plays an important rôle in determining the cost and performance of the detector. On the one hand the TPC has to be sufficiently large to achieve the desired momentum resolution for the baseline

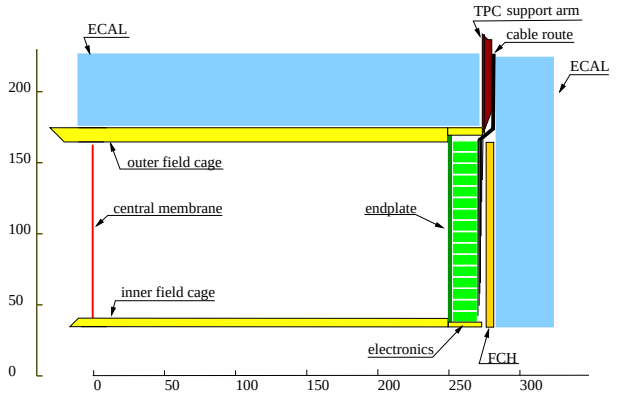

Figure 9: General layout of the TDR baseline TPC design [1] (dimensions in cm).

4 T magnetic field, on the other, the TPC dimensions determine the size of the ECAL, HCAL and solenoid, and thus significantly impacts the cost of the whole detector.

The TPC would be read out on the two end planes, each consisting of approximately 200 rings of readout pads. In the baseline design the readout pads have transverse and radial dimensions of $2 \times 6\,\mathrm{mm}^2$. The performance of the TPC depends on the choice of gas, which not only affects the resolution through the transverse and longitudinal diffusion of the drifting charge cloud but also influences the design of the field cage (as the total voltage at the cathode depends on the desired drift velocity). In addition, gas mixtures with high hydrocarbon content present a large cross-section to neutron background, leading to higher TPC occupancy. The baseline choice for the TESLA TPC is a three-gas mixture of Ar-CO_2-CH_4 (93-2-5), although there are many other options [18]. With this choice of gas a single hit resolution of 140 μm can be achieved [19]. The ultimate aim is $\sigma \sim 100\,\mu$m which can be reached using 90-10 Ar-CH_4 which has a smaller transverse diffusion constant, although it is more sensitive to neutron background. The longitudinal granularity of a TPC is limited by the longitudinal diffusion of the charge cloud. In Ar-CO_2-CH_4 the longitudinal (transverse) diffusion constants in a 4 T solenoidal field are 300(70) $\mu\mathrm{m\,cm}^{-1/2}$. Hence, for typical drift distances of 1 m, the longitudinal spread of the electron cloud is about 3 mm. For a drift velocity of $5\,\mathrm{cm}\,\mu\mathrm{s}^{-1}$, this corresponds to a time resolution of 60 ns requiring a readout rate of at least 20 MHz.

There are two main drawbacks inherent to a TPC. Firstly, there is a significant amount of material in the endcap regions due to the endplanes and the readout electronics. Ideally the amount of material in front of the ECAL should be minimised and the goal is for the contribution from the TPC to be less than $0.3\,X_0$. Secondly, due to the finite drift time, the TPC integrates over multiple bunch crossings within a bunch train. This enhances the detector occupancy from beam background and gamma-gamma interactions [20] which could lead to a degradation in the pattern recognition capability. For a drift velocity of $5\,\mathrm{cm}\,\mu\mathrm{s}^{-1}$, the maximum drift time is approximately $50\,\mu$s. This corresponds to 160 bunch-crossings for which the estimated background is 80000 hits in the TPC at $\sqrt{s} \sim 500\,\mathrm{GeV}$ (and twice as much at $\sqrt{s} \sim 800\,\mathrm{GeV}$). However, the sensitive TPC volume corresponds to approximately 10^9 three-dimensional electronic readout pixels ($\sim 1.5 \times 10^6$ pads $\times\ 10^3$ longitudinal time samples). Consequently, the resulting occupancy from beam and gamma-gamma backgrounds is less than 1 % [20]. This would not present a significant problem for pattern recognition/track reconstruction even if the machine background calculations are wrong by a large factor.

TPC Readout

In a conventional TPC the number of drift electrons is amplified by avalanche multiplication in the high electric fields generated near the thin wires of multi-wire proportional chambers and the signal is read out via the induced charge on pads placed behind the wires. There are a number of problems with this traditional approach if applied to a TPC operating at TESLA:

- The resolution is limited by $\vec{E} \times \vec{B}$ effects in the strong magnetic field of the TESLA detector. This occurs because close to the proportional chamber wires the electric and magnetic fields are no longer parallel and electrons drifting in this region are subject to significant transverse forces which broaden the electron cloud and therefore degrade the resolution. This is significant for traditional multi-wire readout because the region over which $\vec{E} \times \vec{B}$ effects are important is determined by the relatively large separation of the wires (which sets the scale for the distance over which electrons drift with a non-zero velocity component perpendicular to the magnetic field).

- Positive ions produced in the gas amplification process migrate back into the drift region and can distort the electric field, termed ion feedback. In previous TPCs ion feedback was reduced by installing a gating plane just in front of the amplification region which effectively blocked positive ions drifting back into the TPC drift region except for after a trigger. Due to the bunch structure at TESLA and triggerless readout, this is only an option between bunch-trains.

- The large number of wires in the endplane and the structure required to keep the wires under tension constitutes a significant amount of material.

Because of the above disadvantages of conventional multi-wire readout alternative technologies form the basis of the baseline TESLA detector TPC design. Two options are currently being considered: Gas Electron Multipliers [21] (GEMs) or MicroMEGAS [22]. Here only GEMs will be discussed as MicroMEGAS share many of the advantages and difficulties of GEMs.

A GEM, shown schematically in Fig. 10, consists of two metal foils separated by a thin polymer film with a typical thickness of $50\,\mu$m. The device has a high density of small holes typically separated by $100-200\,\mu$m. By applying a potential difference across the two sides of the GEM, high electric fields are generated in the region of the small holes ($40-80\,\mathrm{kV\,cm^{-1}}$). Nearly all the electrons drifting from the TPC volume are funnelled into these holes where gas amplification occurs. The amplified charge is directly collected on readout pads located a few millimetres behind the GEM.

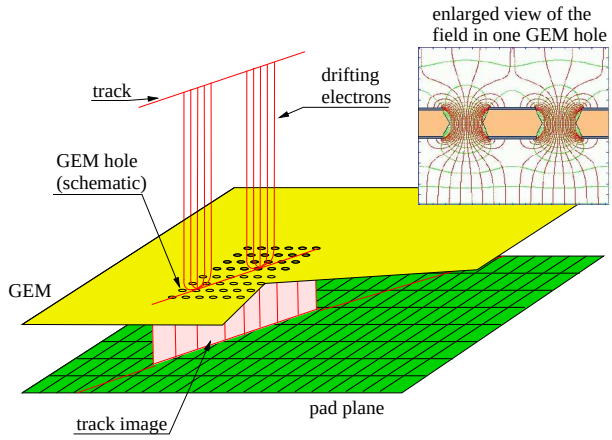

Figure 10: Schematic view of a single layer Gas Electron Multiplier (GEM).

GEMs offer a number of advantages over multi-wire readout:

- because of the small hole separation the region over which the electrons move transverse to the magnetic field is small and $\vec{E}\times\vec{B}$ effects are greatly reduced. Consequently the intrinsic resolution of the TPC is improved.
- ion feedback is naturally suppressed as the majority of the positive ions are swept onto the metal foils of the GEM and do not reach the TPC drift region (as can been seen from the electric field lines shown in Fig. 10). Ion suppression to the level 10^{-2} has already been achieved. However for stable operation of the chamber the goal is 10^{-4}. If this cannot be reached one solution would be to add a gating plane which is open for the entire TESLA bunch train.
- as there are no wires to keep under tension it should be possible to produce thinner endplanes.

GEMs have a number of advantages over wire chamber readout, however they also bring a number of new challenges. The avalanche region is relatively small and only limited amplification is achieved (typically less than a factor 100). Consequently, it is likely that a cascade of at least two GEMs will be required to achieve the necessary gas amplification, for example see [23]. In multi-wire chamber readout, the electron avalanche induces charge on the readout pads, resulting in a signal which is spread across several pads. By using a centre-of-gravity algorithm the resolution is not limited by the pad size. In GEMs and MicroMEGAS the amplified charge is directly transferred onto the readout pads. Here the electron clouds arriving at the readout planes have typical dimensions of $20-50\,\mu$m, determined by diffusion over the $1-5\,$mm drift distance from the GEM to the readout plane (for GEM towers there is further diffusion in the gaps between the GEMs). Unless the readout pad sizes are matched to the electron cloud size, which would result in a prohibitively large number of channels, the signal will be often localised to a single pad. In this case it is the pad size (nominally two millimetres) rather than the GEM hole separation ($\sim 100\,\mu$m) which determines the resolution of the device. However, in the absence of the induction signal it is still possible to achieve good resolution. A number of approaches have been considered. For example, by using "chevron" rather than rectangular shaped readout pads, as indicated in Fig. 11, it is possible to spread the charge cloud over more than one pad and obtain the necessary improvement in resolution [19]. Another promising idea is to spread the charge across a number of pads by inserting a resistive layer in front of the pads [24]. It seems likely that a solution to this particular aspect of using GEMs to readout the TPC will be found.

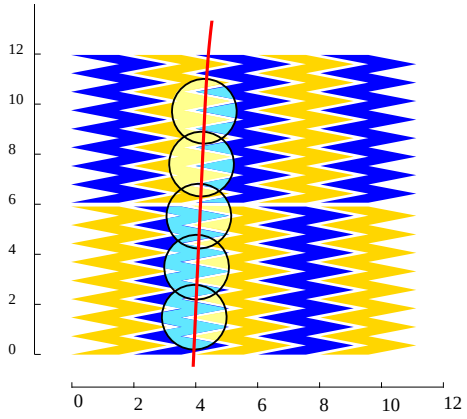

Figure 11: Possible layout of "Chevron" shaped pads, with a track superimposed to illustrate the sharing of charge between different pads (dimensions in mm) [19]. The circles indicate the typical size of the charge cloud arriving at the pads for a structure consisting of two GEMs.

TPC Summary

Since the production of the TESLA TDR there has been an active programme of R&D into the possible use of TPCs as the central tracking chamber for a detector at the TESLA linear collider. Although, to date, no major pitfalls have been identified, more work is required before it can concluded that a TPC will provide the necessary performance and stability. Fortunately there are a significant number of

groups worldwide actively involved in R&D [25] work for a TPC option for a future LC detector.

Tracking Performance

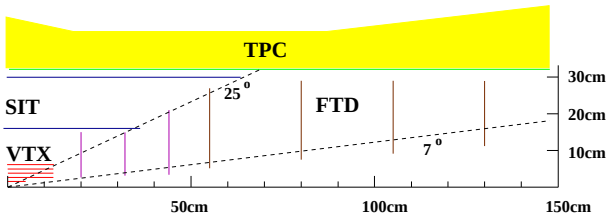

Figure 12: Layout of the TDR concept of the intermediate and forward tracking chambers [1].

In the TESLA detector design the tracking capabilities of the VTX and TPC are complemented by a series of Silicon detectors in the region between the vertex detector/beam pipe and the TPC, as shown in Fig. 12. The main purpose of these detectors is to improve the momentum resolution particularly in the forward region. The SIT consists of two cylinders of double-side Silicon strips with resolution $\sigma_{r\phi} = 10\,\mu$m. Such a detector poses few technological problems; similar detectors have already been successfully used in the DELPHI microvertex detector. The SIT is useful for the purpose of pattern recognition, providing a link between VTX and TPC tracks. However, its main purpose is to provide two well measured space points at a relatively large distance from the interaction point. Using a combination of the TPC and hits in the five layers of the VTX detector, supplemented by the SIT, the resolution goal of $\sigma_{1/p} = 5 \times 10^{-5}\,\mathrm{GeV}^{-1}$ is reached (see Table 2). It should be noted that the momentum resolution of the TESLA TDR tracking system was obtained from a full simulation of the detector [15] using sophisticated track fitting code adapted from that used at LEP [26].

Table 2: Momentum resolution for tracks in the barrel region.

Detector	$\sigma_{1/p}$
TPC	$1.5 \times 10^{-4}\,\mathrm{GeV}^{-1}$
+VTX	$0.7 \times 10^{-4}\,\mathrm{GeV}^{-1}$
+SIT	$0.5 \times 10^{-4}\,\mathrm{GeV}^{-1}$

Monte Carlo studies have been performed to determine the physics sensitivity for the above momentum resolution. These studies used a fast simulation program[27] which uses a parametrisation of the detector resolutions obtained from the full simulation. Fig 13a) shows the resulting invariant mass distribution of the $\mu^+\mu^-$ system in simulated $\mathrm{e^+e^-} \to \mathrm{HZ}$ events. The width is dominated by the natural width of the Z and not the experimental momentum resolution. Fig. 13b) shows the invariant mass of the Higgs boson as measured from the $\mu^+\mu^-$ recoil mass. Here the distribution, which has a peak at the assumed Higgs mass ($M_\mathrm{H} = 120\,\mathrm{GeV}$), displays a significant tail towards higher masses. The origins of this tail are Beamstrahlung (discussed below) and ISR.

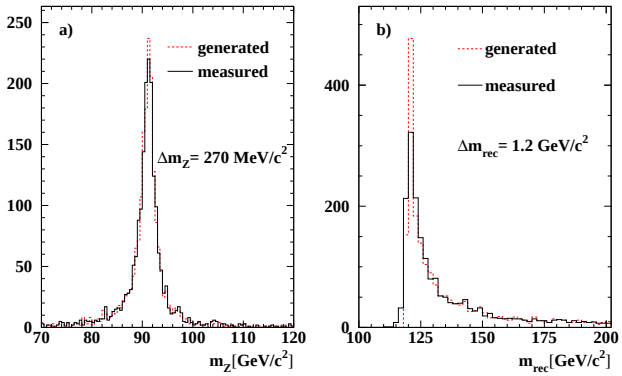

Figure 13: a) Generated and reconstructed Z mass and b) recoil mass for $\mathrm{e^+e^-} \to \ell^+\ell^-\mathrm{H}$ Higgs-strahlung events at $\sqrt{s} = 350\,\mathrm{GeV}$ (M_H=120 GeV) [1].

FORWARD TRACKING

Forward tracking is particularly important at TESLA for three main reasons:

- One undesirable aspect of a future LC is Beamstrahlung. Beamstrahlung is the induced photon radiation from an electron (positron) in one bunch in the coherent field of the positrons (electrons) in the colliding bunch. The amount of Beamstrahlung depends strongly on the machine design and corresponds to an average energy loss of around $1.5\,\%$ for TESLA [28]. The effect of Beamstrahlung on the effective centre-of-mass energy spectrum after photon radiation, $\sqrt{s'}$, is shown in Fig. 14. To make precise mass measurements, *e.g.* M_W from a threshold cross-section scan and to a lesser extent M_H from the recoil mass spectrum, the effects of Beamstrahlung must be quantified. Fortunately, the luminosity spectrum can be obtained from data by studying the acollinearity distribution of Bhabha scattering events for which the cross-section is highly forward peaked. Consequently, a LC detector requires excellent *polar angle* resolution for forward tracks [29].

- Many of the physics processes at a LC are forward-peaked, for example $\mathrm{e^+e^-} \to \mathrm{W^+W^-}$. Here, due to the highly boosted W bosons, the jets from a hadronic W-decay are not only forward-peaked but also tend to overlap.

- Missing energy is the main signature for many SUSY processes and good forward tracking is required to improve the missing-energy resolution.

For tracks with polar angles below 25° the polar angle resolution, and to lesser extent the momentum resolution, is

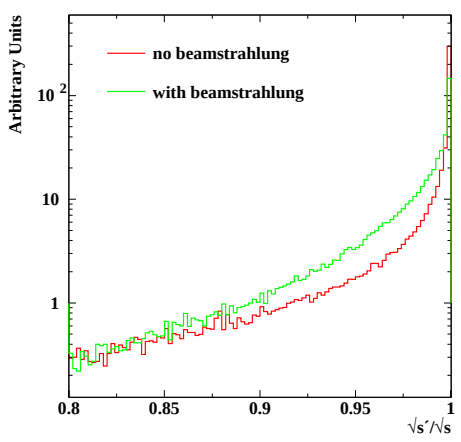

Figure 14: The $\sqrt{s'}/\sqrt{s}$ distribution for e^+e^- collisions at a nominal centre-of-mass energy of 500 GeV. The effects of ISR alone and ISR plus Beamstrahlung are shown [29].

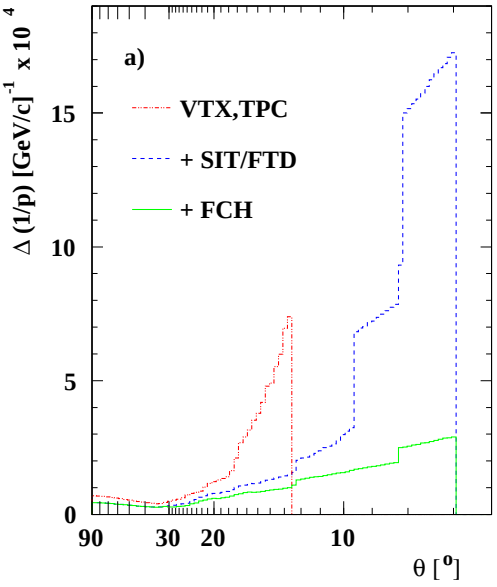

Figure 15: Momentum resolution for 250 GeV muons as a function of polar angle. In this case the FCH is the TDR straw chamber option.

improved using the forward tracking detector (FTD) which consists of a series of seven Silicon disks. The first three layers of the FTD consist of Silicon pixel detectors with a pixel size of $50 \times 300\,\mu\mathrm{m}^2$. The four layers furthest from the interaction point consist of Silicon strips with a resolution of $90\,\mu\mathrm{m}$. The excellent polar angle resolution obtained from the FTD not only allows the mean energy loss due to Beamstrahlung to be measured with a statistical precision of 5×10^{-5}, but also provides a measurement of the beam energy spread with statistical precision of 0.5×10^{-5} [29].

Forward Chambers

The FTDs primarily measure the polar angle of forward tracks. However, in the forward direction the momentum resolution of the TPC is degraded due to the decreased lever-arm and the reduced number of hits. To improve the momentum resolution in this region, forward chambers (FCH) with a point resolution of approximately $50\,\mu$m, are positioned directly behind the TPC end planes. In the TESLA TDR three planes of straw tubes were foreseen. Recently it has been suggested that Silicon strip detectors forming a "Silicon Envelope" around the entire TPC would be a better choice [30] (see below). Independent of the technological choice, the importance of additional tracking in the forward region can be seen from Fig. 15 which shows the momentum resolution for 250 GeV muons as a function of polar angle when information from different detectors is included.

Silicon Envelope

It has been suggested that the TDR tracking system could be complemented by an envelope of Silicon surrounding the TPC [30]. The original proposal [31] considered only the barrel region, the Silicon External Tracker (SET). The SET would consist of three cylindrical layers of Silicon detectors just beyond the TPC at radii 160.5 cm, 165 cm and 169.5 cm. Recently this idea was extended to replacing the straw-tube FCH with a six layer Silicon tracker (Si-FCH) [30]. Preliminary studies [30] which assumed a single-layer point-resolution of $25\,\mu$m and that each layer represented 0.5 % of a radiation length, indicate that the SET could improve the momentum resolution in the barrel region by upto 20 %. However, at this stage the merits of the SET should be taken with some caution as the improvement in momentum resolution depends strongly on the assumed performance of the TPC. Nevertheless, a Si-envelope may offer other advantages:

- The addition of a precisely measured space point, outside the material of the TPC support structure could aid the calorimeter reconstruction and improve the energy flow measurement.
- The addition of the Silicon-envelope would complement the tracking in the VTX, SIT and FTD Silicon detectors, forming a large lever arm tracker independent of the TPC. As such, the Silicon-envelope would help in monitoring/calibrating the TPC.

CALORIMETRY

The majority of the interesting physics processes at a future linear collider are characterised by multi-jet final states, often accompanied by charged leptons and/or missing transverse energy associated with neutrinos or the lightest super-symmetric particles (LSPs). The reconstruction of the invariant mass of two or more jets will provide a powerful tool both for event reconstruction and for event identification. For example:

- the identification of the rare, but nevertheless important, ZHH $\rightarrow 6j$ final state from background processes will rely on the ability to identify pairs of jets with the invariant masses of the Z and Higgs;

- the identification and separation of $\nu_e\overline{\nu}_e\mathrm{W^+W^-}$ and $\nu_e\overline{\nu}_e\mathrm{ZZ}$ events, of great interest in strong EWSB models, will rely almost entirely on di-jet mass reconstruction.

In general it will important to be able to identify jet pairs arising from the hadronic decays of W and Z bosons. Since the reconstruction of the invariant mass of two or more jets will play a major rôle in the analyses of numerous processes at the LC, a good measurement of jet energy is of great importance.

The LEP Experience

At LEP is was found that the jet energy resolution was limited by the ability to separate and correctly associate tracks and energy deposits in electromagnetic and hadronic calorimeters, rather than the intrinsic momentum and energy resolution of the tracking chambers and calorimeters respectively. Measurements of jet fragmentation at LEP have provided detailed information on the particle composition of jets (e.g. [32, 33]). On average, after the decay of short-lived particles, roughly 62% of the energy of jets is carried by charged particles (mainly hadrons), around 27% by photons, about 10% by long-lived neutral hadrons (*e.g.* n/$\mathrm{K^0_L}$), and around 1.5% by neutrinos. The momenta of charged particles are measured accurately in the tracking detectors and the energy obtained by assuming the $\pi^{\pm}$ mass. Photon energies are measured in the electromagnetic calorimeter (ECAL), and the energies of neutral hadrons in the hadron calorimeter (HCAL). To obtain the energy of the jet, the information from tracks, ECAL clusters and HCAL clusters has to be combined taking into account correlated energy deposits. For example, a charged hadron will typically deposit energy in both calorimeters, while a neutral hadron may start showering in the ECAL. The most successful algorithms for jet reconstruction at LEP used the so-called *energy flow* approach, in which geometrical associations between tracks and calorimeter clusters and between clusters in the ECAL and HCAL are used to minimise the double counting of energy. Using the energy flow technique the ALEPH experiment obtained a jet-energy resolution of $\sigma_E/E = 60\%(1 + |\cos\theta|)/\sqrt{E(\mathrm{GeV})}$ [34]. Although the OPAL lead-glass calorimeter had a better intrinsic energy resolution, OPAL achieved a jet-energy resolution of only $\sigma_E/E \sim 80\%/\sqrt{E(\mathrm{GeV})}$. The main reason for the relatively good performance of the ALEPH calorimeter was that it had significantly better spatial resolution, permitting better matching and separation of the various energy deposits within a jet. At LEP the beam-energy constraint used in the kinematic fits reduced the sensitivity to the jet energy resolution; despite having very different jet energy resolutions, the four LEP experiments achieved similar M_{W} sensitivity (a measurement where most of the information comes from the reconstructed jet-jet invariant mass distribution).

Jet-Energy Resolution

At a LC kinematic fitting will play a less significant rôle than at LEP as many final states involve missing energy and the beam energy constraint is less useful due to Beamstrahlung. Consequently, good jet-energy resolution is of paramount importance. A jet energy resolution of $\Delta E = \alpha\sqrt{E}$ leads to a di-jet mass resolution of roughly $\Delta M/M = \alpha/\sqrt{E_{jj}}$ where E_{jj} is the energy of the di-jet system. A reasonable goal is to match ΔM for the W or Z bosons to their natural widths, i.e. $\sim$ 2 GeV. Since E_{jj} $\sim$250 GeV at the LC, this suggests a goal of

$$\sigma_E/E = 30\,\%/\sqrt{E(\mathrm{GeV})},$$

which is a factor of two better than the best achieved at LEP. The importance of achieving this goal is well illustrated by considering the process $\mathrm{e^+e^-} \rightarrow \nu_e\overline{\nu}_e\mathrm{W^+W^-}$. If the Higgs mechanism is not responsible for Electroweak symmetry breaking then the quartic gauge coupling process, shown in Fig. 16, is of great interest; without the SM s-channel Higgs exchange contribution, the cross-section for longitudinal W-boson scattering, $\mathrm{W^+_L W^-_L} \rightarrow \mathrm{W^+_L W^-_L}$, grows with $\sqrt{s}$ and ultimately violates quantum mechanical unitarity. In strong EWSB scenarios it will be important fully to investigate quartic gauge couplings in both $\mathrm{e^+e^-} \rightarrow \nu_e\overline{\nu}_e\mathrm{W^+W^-}$ and $\mathrm{e^+e^-} \rightarrow \nu_e\overline{\nu}_e\mathrm{ZZ}$. For fully-hadronic decays, the $\nu_e\overline{\nu}_e\mathrm{W^+W^-}$ and $\nu_e\overline{\nu}_e\mathrm{ZZ}$ final states can only be distinguished on the basis of the invariant masses of the pairs of jets. Fig. 17 shows the improvement in separation obtained in going from a LEP-like resolution to the TESLA goal. In statistical terms the improved separation is equivalent to a $40\,\%$ increase in luminosity [35].

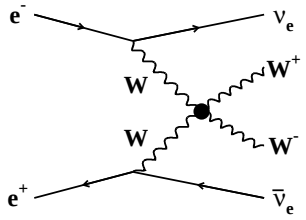

Figure 16: The process $\mathrm{e^+e^-} \rightarrow \nu_e\overline{\nu}_e\mathrm{W^+W^-}$.

Calorimetry at the Linear Collider

The requirements for calorimetry at a future LC can be summarised as:

- Excellent energy resolution for jets: $\sigma_E/E = 30\,\%/\sqrt{E(\mathrm{GeV})}$.

- Good energy and angular resolution for photons needed, for example, for the identification of H$\rightarrow \gamma\gamma$ events.

Table 3: Contributions from the different particle components to the jet-energy resolution (all energies in GeV). The table lists the approximate fractions of charged particles, photons and neutral hadrons in a jet and the assumed single particle energy resolution. The contribution to the overall jet energy resolution from all particles in each category is also shown. For photons and neutral hadrons this is given by the quadrature sum of the resolutions for individual particles which yields a term proportional to the total energy in that component. For charged particles only a maximum value can be given; this corresponds to there being a single charged particle in the jet. In general there will be many charged particles and this term will be negligible.

Component	**Detector**	**Energy Fraction**	**Energy Res.**	**Jet Energy Res.**
Charged Particles ($X^{\pm}$)	Tracker	$\sim 0.6\, E_{\rm jet}$	$10^{-4}\, E^2_{X^{\pm}}$	$< 3.6 \times 10^{-5}\, E^2_{\rm jet}$
Photons (γ)	ECAL	$\sim 0.3\, E_{\rm jet}$	$0.11\, \sqrt{E_{\gamma}}$	$0.06\, \sqrt{E_{\rm jet}}$
Neutral Hadrons (h^0)	HCAL	$\sim 0.1\, E_{\rm jet}$	$0.40\, \sqrt{E_{h^0}}$	$0.13\, \sqrt{E_{\rm jet}}$

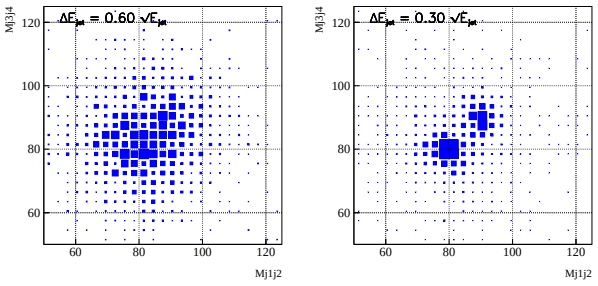

Figure 17: Impact of the jet energy resolution on the separation of $\nu_e\overline{\nu}_e\mathrm{W}^+\mathrm{W}^-$ and $\nu_e\overline{\nu}_e\mathrm{ZZ}$ final states where both gauge bosons decay hadronically [35]. The first plot shows the separation for the best LEP jet-energy resolution, $\sigma_E/E = 60\,\%/\sqrt{E(\mathrm{GeV})}$, and the second shows the separation for the TESLA goal of $\sigma_E/E = 30\,\%/\sqrt{E(\mathrm{GeV})}$.

- The ability to identify non-pointing photons which can arise, for example, in GMSB scenarios where a long-lived neutralino may decay in the detector volume to a photon and an unobserved stable gravitino, $\tilde{\chi}^0_1 \to \gamma\tilde{\mathrm{G}}$.
- Excellent hermeticity.
- Ideally both the ECAL and HCAL should be placed inside the magnet coil to avoid degradation in energy resolution. For this to be affordable the calorimeters have to be compact.

Of the above requirements it is that of jet-energy resolution which drives the calorimeter design. To understand the dominant source of uncertainty it is useful to decompose the jet-energy resolution into its components. In an ideal world one would measure the energy of charged particles using the tracking chambers, the energy of photons using the ECAL and the energy of neutral hadrons using the HCAL. Table 3 (adapted from [36]) shows the different contributions to the jet-energy resolution assuming no double-counting of energy deposits. It should be noted that although the neutral hadron component comprises only 10 % of the jet energy this is the largest single contribution to the uncertainty. From the sum of the contributions from the individual components, a jet-energy resolution of $\sigma_E/E = 14\,\%/\sqrt{E(\mathrm{GeV})}$ is obtained. This is far better than the best achieved for the TESLA TDR detector, $\sigma_E/E = 30\,\%/\sqrt{E(\mathrm{GeV})}$. From this it is clear that, in practice, the dominant contribution to the jet-energy uncertainty comes from double-counting energy deposits in more than one detector component or missing energy deposits due to overlapping tracks and showers. Consequently, one can conclude that the jet-energy resolution is driven mainly by the ability to resolve energy deposits from different particles. This is particularly difficult in the dense environment of (potentially highly boosted) hadronic jets at a LC, as can be seen from Fig. 18. Consequently, for the purposes of jet-energy resolution granularity is more important than energy resolution.

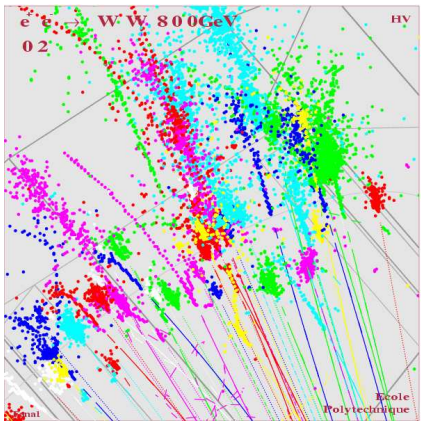

Figure 18: View of a di-jet in $\mathrm{e}^+\mathrm{e}^- \to \mathrm{W}^+\mathrm{W}^-$ at $\sqrt{s} = 800\,\mathrm{GeV}$ [35].

TESLA Calorimeter Concept

The calorimeters at TESLA should be able to:

- *separate of energy deposits from different nearby particles.* Therefore the ECAL should have a small Molière radius, ρ_{M}, to limit the transverse spread of electromagnetic showers and a high lateral segmentation (of the order ρ_M).

- *discriminate between electromagnetic and hadronic showers.* Therefore the ECAL (and HCAL) should have a large ratio of the interaction length, λ_I, to the radiation length, X_0, so that hadronic showers start relatively deep in the calorimeter. It also implies longitudinal as well as transverse segmentation of the calorimeters.
- *contain electromagnetic showers in the ECAL.* This suggests that the ECAL should be $\sim 20 - 25\, X_0$ in depth, sufficient to contain the highest energy showers. This is a further argument for choosing a material with small X_0 in order to arrive at a compact ECAL.

The preferred solution adopted for the TESLA TDR, shown in Fig. 19 envisages a Silicon-tungsten ECAL, followed by an HCAL, both located inside the magnet coil. The barrel regions have an octagonal geometry. Specialised calorimetry in the forward region would complete the angular coverage.

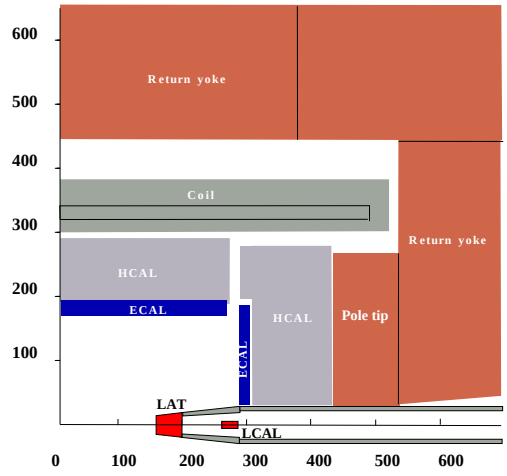

Figure 19: Side view of the TESLA TDR calorimeters [1] (dimensions in cm).

Electromagnetic Calorimeter

Tungsten is an attractive choice for the showering medium in the ECAL, having a very low radiation length, a small Molière radius of 9 mm and a large ratio of λ_I / X_0, see Table 4. By using Silicon as the detecting medium, the gaps between tungsten layers can be kept thin, so that the whole ECAL of 24 radiation lengths thickness can be fitted into a thickness of about 20 cm. Keeping the gaps between the tungsten layers to a minimum also avoids a significant increase in the effective Molière radius of the Si-W sandwich. The transverse granularity of the Silicon readout, *i.e.* the size of the Silicon pads is determined by the Molière radius, which defines the transverse size of electromagnetic showers. If the pad size is significantly greater than the Molière radius the shower can only be localised to within the area of one pad and the spatial resolution is degraded. Consequently a pad size of $\sim$1 cm^2 is envisaged. The present design of the ECAL has 40 longitudinal samples. The high granularity leads to an excellent angular resolution for photons:

$$\sigma_\theta = (0.063/\sqrt{E/\mathrm{GeV}} \oplus 0.024)\ \mathrm{mrad},$$

allowing the identification of 'non-pointing' photons arising from possible GMSB signals from purely neutral decays in the TPC volume. The jet-energy resolution of the TDR ECAL design yields an energy resolution for single photons of

$$\sigma_{E_\gamma}/E_\gamma = (0.11/\sqrt{E_\gamma/\mathrm{GeV}} \oplus 0.01).$$

Table 4: Comparison of interaction length, λ_I, radiation length, X_0, and Molière radius, ρ_M, for Iron, Copper, Tungsten and Lead. Also given is the ratio of λ_I / X_0.

material	λ_I**/cm**	X_0**/cm**	ρ_M**/cm**	λ_I / X_0
Fe	16.8	1.76	1.69	9.5
Cu	15.1	1.43	1.52	10.6
W	9.6	0.35	0.93	27.4
Pb	17.1	0.56	1.00	30.5

Hadronic Calorimeter

The total ECAL depth for normal incident particles corresponds to $24\, X_0$ (sufficient to mostly contain even the highest energy electromagnetic showers) but corresponds to only $0.9\, \lambda_I$, consequently hadronic showers tend to develop late in the ECAL. For the purposes of energy-flow the HCAL should be highly segmented, both in the transverse and longitudinal directions. However, the overall cost impact of the HCAL design is determined by its size, which determines the coil radius. Hence cost arguments suggest a compact detector and the ideal showering material would be Tungsten which has a particularly short hadronic interaction length (see Table 4). Unfortunately Tungsten is relatively expensive and price considerations tend to favour using stainless steel which has a somewhat larger λ_I. The total area of the active layers of the HCAL is approximately 5000 m^2, which would require 5×10^7 electronics channels for a 1 cm^2 lateral segmentation. To avoid the prohibitively high cost of the readout a compromise is likely to be made: either degrading the lateral segmentation, which reduces the number of channels, or by reducing the information read out from a single channel. In the latter case, the *digital HCAL* option, multiple active elements are read out on a single channel. For the digital readout one records whether or not there was an energy deposit in a particular detector cell but not amount of energy itself, *i.e.* a simple binary yes/no outcome. The baseline design consists of a 1 m thickness HCAL consisting of approximately 40 layers, providing $4.5\lambda_I$ ($6.2\lambda_I$) of material in the barrel (endcap) region. To reduce the number of readout channels the

layers are grouped into 9 (12) longitudinal readout layers in the barrel (endcap).

Among the preferred options for the HCAL are stainless steel plates instrumented with either $\sim 5 \times 5\,\mathrm{cm}^2$ scintillator tiles (providing analogue readout) or resistive plate chambers (RPCs) providing digital readout with a granularity of between $1 \times 1\,\mathrm{cm}^2$ and $2 \times 2\,\mathrm{cm}^2$. The digital option has the advantage that multiple detector elements can be readout on the same electronics channel, thus reducing the cost of the associated readout which would otherwise be prohibitively high for a highly segmented large volume HCAL. The choice between a moderately segmented HCAL with analogue readout or a highly segmented HCAL with digital readout is a matter of great debate and ongoing studies (*e.g.* see [37]). Naively one might expect the digital option to result in a degraded energy resolution as energy is not explicitly recorded. However, for hadronic showers this is not necessarily the case. Hadronic showers consist of a number of distinct components: the ionisation from the primary particle (if charged); a relatively compact electromagnetic component *e.g.* arising from π^0 decays; and a broad (typically transverse size of a few λ_I) hadronic component from secondary hadrons. The response of the HCAL to these different components influences the performance:

- The charged hadron (predominantly $\pi^{\pm}$) component of the shower is essentially track-like, consisting of a number of near minimum ionising particles. Here the total path length, summed over all tracks, provides a good energy estimate. This is exactly what is measured in the digital option, providing that the typical transverse separation of the particles is larger than the segmentation of the HCAL. The energy resolution for the charged hadron component in the analogue option has an additional contribution. In an analogue sampling calorimeter it is the ionisation in the active detector volume that is recorded rather than the total energy. For a charged particle crossing a single active detector element the ionisation follows the (asymmetric) Landau distribution which has a long tail towards high values. Consequently a single sample of the ionisation energy loss of a single charged hadron is subject to large fluctuations. As only a small fraction of the total energy loss is sampled, the inclusion of these large fluctuations may degrade the energy resolution for the track-like component of the shower.

- The electromagnetic component of a hadronic shower consists of many electrons, positrons and photons in a small transverse region, information which is lost in the digital option. Hence the electromagnetic component can only be directly measured in the analogue HCAL, although in the digital HCAL there is information in shower size.

- The TESLA HCAL designs are implicitly non-compensating, having different responses for the hadronic and electromagnetic components of the shower. In a highly segmented calorimeter it might be possible to identify tracks and electromagnetic showers, allowing the possibility of software compensation. This argues for a transverse granularity of order the Molière radius. In addition the higher granularity of the digital HCAL would provide better separation of energy deposits from nearby hadronic showers, potentially improving the performance of the energy flow algorithm.

Based on the above arguments it is difficult to foresee which option will give the best jet-energy performance in the context of an energy-flow algorithm. Since many of the effects are subtle, sophisticated Monte Carlo simulation and energy flow algorithms will be required to address this interesting question of digital versus analogue HCAL.

Calorimeter Performance

As an example of the TDR calorimeter performance, Fig. 20 shows the distribution of reconstructed minus true Z mass for jets from $\mathrm{e^+e^-} \to \mathrm{q\overline{q}}$ at $\sqrt{s} = M_{\mathrm{Z}}$ obtained using for the digital HCAL option [35]. A mass resolution of 2.89 GeV is achieved, which corresponds to a jet energy resolution of $0.3/\sqrt{\mathrm{E(GeV)}}$, the TESLA goal.

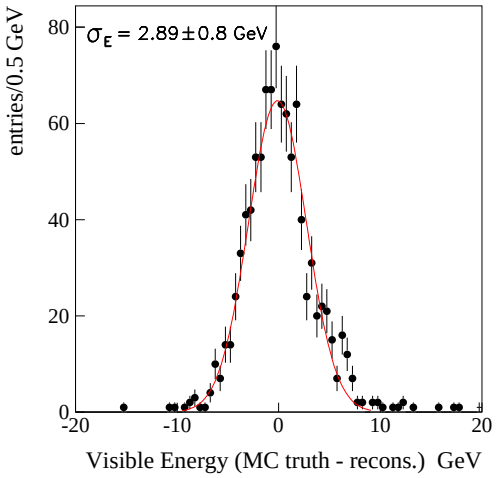

Figure 20: The jet-jet mass resolution for Z decays at rest [35].

Finally, given the relatively large cost of the TDR calorimeters, it is worth re-emphasising the physics impact. A good example of the importance of excellent jet-energy resolution is the SM process $\mathrm{e^+e^-} \to \mathrm{ZHH} \to \mathrm{q\overline{q}b\overline{b}b\overline{b}}$. This process involves the trilinear Higgs coupling, as shown in Fig. 21, providing a direct probe of the Higgs potential. Here the signal cross-section is small (~ 0.5 fb) and the background large. In addition, the six jet final state results in a large combinatorial background arising from the association of the six jets to the two Higgs bosons and the Z. However, providing one has sufficiently good jet-energy resolution, the invariant masses of the re-

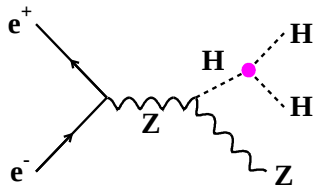

Figure 21: The process $e^+e^- \rightarrow ZHH$ which probes the Higgs trilinear self-coupling.

constructed di-jet pairs may be used to significantly reduce the backgrounds. A useful discriminating variable is

$$D = \sqrt{(m_{12} - m_H)^2 + (m_{34} - m_H)^2 + (m_{56} - m_Z)^2},$$

where the m_{ij} are the reconstructed invariant masses of the jet pairs hypothesised as being associated with Higgs/Z boson. Figure 22 shows the distributions of D for signal and background for two cases: $\sigma_E/E = 0.3/\sqrt{E(\mathrm{GeV})}$ (the TESLA goal) and $\sigma_E/E = 0.6(1 + |\cos\theta|)/\sqrt{E(\mathrm{GeV})}$ (LEP-like) [38]. The increased significance of the signal above the background expectation in going from a LEP-like jet-energy resolution to the TESLA goal is equivalent to a fourfold increase in luminosity. Given the smallness of the cross-section, a jet-energy resolution of a least $\sigma_E/E = 0.35/\sqrt{E(\mathrm{GeV})}$ is required to establish a signal for an integrated luminosity of 1 ab^{-1}. Here the excellent jet-energy resolution makes the difference between observing the process or not.

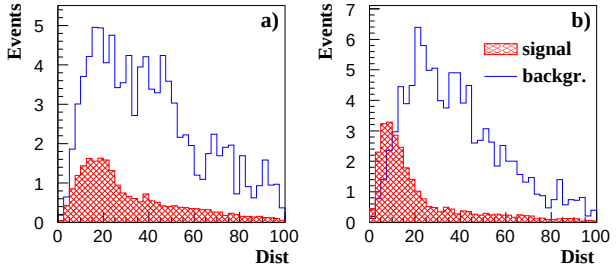

Figure 22: Distributions of the discriminating variable D for $ZHH \rightarrow 6$ jet signal and background, for two values of jet energy resolution: a) $\sigma_E/E = 0.6(1 + |\cos\theta|)/\sqrt{E(\mathrm{GeV})}$ (LEP-like); b) the TESLA goal of $\sigma_E/E = 0.3/\sqrt{E(\mathrm{GeV})}$.

OTHER DETECTORS

In addition to the detector components described above, the TESLA TDR detector includes muon chambers and forward calorimeters, described briefly below.

Muon Chambers

The basic task of the muon system is to identify muons which penetrate the HCAL. The muon system would be embedded in the 2 m thickness of iron of the magnetic return yoke, see Fig. 2. The muon system may also be useful as a "tail-catcher" for hadronic showers which are not fully contained in the HCAL. A number of options exist for the muon detectors, both Plastic Streamer Tubes and RPCs are considered in the TESLA TDR.

Forward Calorimeters

The ECAL coverage of the TESLA detector concept is completed by two devices in the very forward region: the Low Angle Tagger (LAT) and the Luminosity Calorimeter (LCAL), as indicated in Fig. 19. The LAT improves the detector hermeticity by providing calorimetric coverage down to polar angles of 30 mrad. In addition, the LAT allows a precise Measurment of the luminosity using low angle Bhabha scattering events. It is foreseen that the LAT would be a Silicon-Tungsten sampling calorimeter along the lines of the luminosity monitors employed by ALEPH[39] and OPAL[40]. The LCAL covers the region down to polar angles of 5 mrad; its main purpose is to provide fast monitoring of the luminosity and beam. The backgrounds in this low angle region are high and a Tungsten sampling calorimeter with either oxygenated Silicon or Diamond sensors[41] are being considered.

CONCLUSIONS AND OUTLOOK

Two years after the publication of the Tesla TDR[1], the basic detector concept remains the same, providing a viable route to achieving the basic performance goals necessary at a future LC. The emphasis now has shifted towards R&D to investigate the technical issues surrounding the main detector components: there are a number of active R&D programmes investigating the issues specific to the operation of a TPC at a future LC; the CALICE collaboration [42] will soon commence a major test-beam study of the proposed ECAL and HCAL designs; and there are a number groups investigating possible Silicon technologies for the VTX detector. In addition to the technical issues, there many open questions. For example, is a Silicon central tracker a realistic alternative to a TPC ? In this case one would have essentially the same (*i.e.* Silicon-based) technology for the entire detector which is an attractive idea. There is also the important question of the analogue versus digital versions of the HCAL. Furthermore, there are many issues related to the optimisation of the detector design, for example, what is the optimal length and outer radius of the TPC ? To address these issues will require full simulation studies of the whole detector as the design of one detector component may affect the performance of another. For example, the TPC outer radius impacts not only the tracking performance, but also the ECAL inner radius and the jet-energy resolution. Studies of this kind, considering the performance of the detector as whole, are just starting in earnest. It is important that we obtain answers to many of these questions as soon as possible as, in the not too distant future, hopefully we will have to start designing and constructing the real detector.

ACKNOWLEDGEMENTS

I would like to acknowledge the following people for many useful and illuminating discussions over the past year: Jean-Eudes Augustin, Jean-Claude Brient, Chris Damerell, David Miller, Vasily Morgunov, Markus Schumacher, Ron Settles, Jan Timmermans, Henri Videau, and David Ward.

REFERENCES

[1] TESLA Technical Design Report, DESY 2001-011, ECFA 2001-2009.

[2] The ALEPH, DELPHI, L3 and OPAL Collaborations, the LEP Electroweak Working Group, and the SLD Electroweak and Heavy Flavour Working Groups, "A Combination of Preliminary Electroweak Results and Constraints on the Standard Model", hep-ex/0312023.

[3] M. Thomson, "The Measurement of the Mass and Width of the W Boson at LEP", to appear in the proceedings of the EPS Conference on HEP, Aachen, July 2003.

[4] CMS Collaboration, "The Magnet Project", Technical Design Report, CERN/LHCC 97-10, May 1997.

[5] C. Damerell and K. Stefanov, "A CCD-based Vertex Detector for the Future Linear Collider", LC-DET-2003-060.

[6] M. Winter *et al.*, "Development of CMOS Sensors for a Linear Collider Vertex Detector", DESY Physics Research Committee progress report, May 2003. `http://www-zeus.desy.de/~gregork/MAPS/Papers/MAPS_PRC_REPORT_2003.pdf`.

[7] M. Battaglia, "Hybrid Pixel Detector Development for the Linear Collider Vertex Detector", Proc. IEEE Nuclear Science Symposium, Lyon, October 2000. `http://home.cern.ch/~caccia/IEEE.pdf`.

[8] P. Fischer *et al.*, "A DEPFET based pixel vertex detector for the detector at TESLA", LC-DET-2002-004.

[9] S.M. Xella-Hansen, D.J. Jackson, R. Hawkings, and C. Damerell, "Flavour Tagging Studies for the TESLA Linear Collider", LC-PHSM-2000-021.

[10] S.M. Xella-Hansen, M. Wing, D.J. Jackson, N. de Groot and C. Damerell, "Update on Flavour Tagging Studies for the Future Linear Collider using the BRAHMS simulation", LC-PHSM-2003-061.

[11] D. Jackson, Nucl. Instr. and Meth. **A388** (1997) 247.

[12] ALEPH Collaboration, D. Buskulic *et al.*, Phys. Lett. **B313** (1993) 535.

[13] OPAL Collaboration, G. Abbiendi *et al.*, Eur. Phys. J. **C8** (1999) 217.

[14] S. Giani *et al.*, "GEANT Detector Description and Simulation Tool", CERN Program Library Long Writeup W5013.

[15] T. Behnke *et al.*, "BRAHMS: A Monte Carlo for a Detector at a 500/800 GeV Linear Collider", LC-TOOL-2001-005.

[16] P.S. Marrocchesi *et al.*, Nucl. Instr. and Meth. **A283** (1989) 573.

[17] Delphi Collaboration, C. Brand *et al.*, Nucl. Instr. and Meth. **A283** (1989) 576.
Delphi Collaboration, P. Abreu *et al.*, Nucl. Instr. and Meth. **A378** (1996) 57.

[18] M. Gruwe, "Gas Studies for a TPC of a detector for the future linear collider TESLA", LC-DET-1999-003-TESLA.

[19] M. Shumacher, "Pad readout geometries for a TPC with GEM readout for the TESLA linear collider", LC-DET-2001-014.

[20] C. Hensel, "Beam Induced Background at a TESLA Detector", LC-DET-2000-001.

[21] F. Sauli, Nucl. Instr. and Meth. **A386** (1997) 531.

[22] Y. Giomataris *et al.*, Nucl. Instr. and Meth. **A376** (1996) 29.

[23] M. Killenberg, "Modelling and Measurement of Charge Transfer in Multiple GEM Structures", LC-DET-2002-022.

[24] M.S. Dixit, J. Dubeau, J.-P. Martin and K. Sachs, "Position Sensing from Charge Dispersion in Micro-Pattern Gas Detectors with a Resistive Anode", LC-DET-2003-080.

[25] The LC TPC Group, R. Settles *et al.*, "A TPC for a Future Linear Collider", LC-DET-2002-008.

[26] T. Behnke *et al.*, "Performance study of the proposed TESLA detector using a realistic track reconstruction package", LC-DET-2001-029.

[27] M. Pohl and H.J. Schreiber, "SIMDET-Version 3: A parametric Monte Carlo for a TESLA detector", DESY 99-030.

[28] See for example contributions by R. Brinkmann, T. Tauchi and K.A. Thompson *et al.*, in Vol.2 of the Proceedings of the Worldwide Study on Physics and Experiments with Future Linear e^+e^- Colliders, Stiges, April 1999.

[29] K. Moenig, "Measurement of the Differential Luminosity using Bhabha events in the Forward-Tracking region at TESLA", LC-PHSM-2000-060.

[30] J.E. Augustin *et al.*, "A Silicon Envelope for the TPC", LC-DET-2003-013.

[31] J.E. Augustin, M. Berggren and A. Savoy-Navarro, "Study of a Silicon External Tracker: SET", LC-DET-2001-075.

[32] I.G. Knowles and G.D. Lafferty, J. Phys. **G23** (1997) 731.

[33] M. G. Green, S. L. Lloyd, P. N. Ratoff and D. R. Ward, "Electron-Positron Physics at the Z", IoP Publishing (1998).

[34] ALEPH Collaboration, D. Buskulic et al., Nucl. Inst. Meth. **A360** (1995) 481.

[35] J.-C. Brient and H. Videau, "The calorimetry at the future e^+e^- linear collider", LLR 02-001, hep-ex/0202004 (revised June 2003).

[36] V. Morgunov, proceedings of the Calor2002 conference, Caltech, March 2002.

[37] S. Magill, "Comparison of simulated analog versus digital energy measurement in a finely-segmented hadron calorimeter", LC-DET-2003-009.

[38] F. Badaud et al., *Si-W calorimeter performances*, LC-DET/2001-058.

[39] D. Bederede *et al.*, ALEPH Collaboration, Nucl. Instr. and Meth. **A365** (1995) 117.

[40] G. Abbiendi *et al.*, OPAL Collaboration, Eur. Phys. J. **C14** (2000) 373.

[41] T. Behnke, M. Doucet, N. Ghodbane and A. Imhof, "Radiation hardness and linearity studies for a diamond luminosity calorimeter", LC-DET-2002-001.

[42] The CALICE Collaboration, see for example: `http://polywww.in2p3.fr/flc/calice.html`.

The SILICON DETECTOR (SiD) and LINEAR COLLIDER DETECTOR R&D in ASIA and NORTH AMERICA*

James E. Brau, University of Oregon, USA
Martin Breidenbach, SLAC, USA
Yoshiaki Fujii, KEK, Japan

Abstract

In Asia and North America research and development on a linear collider detector has followed complementary paths to that in Europe. Among the developments in the US has been the conception of a detector built around silicon tracking, which relies heavily on a pixel (CCD) vertex detector, and employs a silicon tungsten calorimeter. Since this detector is quite different from the TESLA detector, we describe it here, along with some of the sub-system specific R&D in these regions.

INTRODUCTION

The TESLA detector, which has been developed by the ECFA-DESY Studies over the past several years, optimizes the design of the detector around a specific set of assumptions. Alternative assumptions exist, and to a varying degree, have been applied to the design of other possible linear collider detectors, such as the JLC [1] Detector, the North American Large Detector, and the North American Silicon Detector (so-called SiD). Table 1 summarizes the properties of these differing choices. This table shows a number of similarities between the detectors:

- both TESLA and the Large Detector use TPC trackers.
- both TESLA and the Silicon Detector use silicon/tungsten for the EM calorimeter.
- The Large Detector and the JLC Detector choose scintillator tile with lead for EM and hadron calorimetry.

Other details vary, including the choice of magnetic field, which ranges from 3 up to 5 Tesla.

Each of these designs is guided by the physics goals, which lead to the following principal detector goals:

- Two-jet mass resolution, comparable to the natural widths of the W and Z for an unambiguous identificaion of the final states.
- Excellent flavor-tagging efficiency and purity.
- Momentum resolution capable of reconstructing the recoil-mass to di-muons in Higgs-strahlung with resolution better than the beam-energy spread.
- Hermeticity (both crack-less and coverage to very forward angles) to precisely determine the missing momentum.
- Timing resolution capable of separating bunch-crossing to suppress overlapping of events.

THE SILICON DETECTOR

The "Silicon Detector" (SiD, illustrated in Figure 1) was conceived as a high performance detector for the NLC, achieving all of the physics goals enumerated above, with reasonably uncompromised performance, but constrained to a rational cost. The strategy of the "Silicon Detector" is based on the assumption that energy flow calorimetry will be important. While this has not yet been demonstrated in simulation by the US groups, the TESLA Collaboration has accepted this and it seems probable that the US community will eventually agree.

Figure 1: The Silicon Detector.

The strategy of energy-flow calorimetry leads directly to a reasonably large value of BR^2 to provide charged-neutral separation in a jet, and to an electromagnetic calorimeter (EMCal) design with a small Moliere radius and small pixel size. Additionally, it is desirable to read out each layer of the EMCal to provide maximal information on shower development. This leads to the same nominal solution as TESLA: a series of layers of about 0.5 X_0 Tungsten sheets alternating with arrays of silicon diodes. Such

* The authors acknowledge the help of the following people in preparing this overview: Gene Fisk, Ray Frey, John Jaros, Tom Markiewicz, Bruce Schumm, Eric Torrence, and Jae Yu.

[1] The name JLC was changed to GLC in April, 2003.

	TESLA	SiD	LD	JLC
Tracker type	TPC	Silicon	TPC	Jet-cell drift
ECal				
$R_{\min}$ barrel (m)	1.68	1.27	2.00	1.60
Type	Si pad/W	Si pad/W	scint tile/Pb	scint tile/Pb
Sampling	$30 \times 0.4X_0$ $+10 \times 1.2X_0$	$30 \times 0.71X_0$	$40 \times 0.71X_0$	$38 \times 0.71X_0$
Gaps,active(mm)	2.5 (0.5 Si)	2.5 (0.3 Si)	1 (scint)	2 (1 scint)
Long. readouts	40	30	10	3
Trans. seg. (cm)	≈ 1	0.5	5.2	4
Channels ($\times 10^3$)	32000	50000	135	144
$z_{\min}$ endcap (m)	2.8	1.7	3.0	1.9
HCal				
$R_{\min}$ (m) barrel	1.91	1.43	2.50	2.0
Type	T: sc. tile/steel D: digital/steel	digital/RPC Cu or steel	scint tile/Pb	scint tile/Pb
Sampling	$38 \times 0.12\lambda$ (B), $53 \times 0.12\lambda$ (EC)	$34 \times 0.12\lambda$	$120 \times 0.047\lambda$	$130 \times 0.047\lambda$
Gaps,active(mm)	T: 6.5 (5 scint) D: 6.5 (TBD)	1 (TBD)	2 (scint)	3 (2 scint)
Longitudinal readouts	T: 9(B), 12(EC) D: 38(B), 53(EC)	34	3	4
Transverse segment. (cm)	T: 5–25 D: 1	1	19	14
$\theta_{\min}$ endcap	5°	6°	6°	8°
Coil				
$R_{\min}$ (m)	3.0	2.5	3.7	3.7
B (T)	4	5	3	3
Comment	Shashlik ECal option in TDR discontinued		option: Si pad sh. max det	sc. strip (1cm) shower max det (2 layers)

Table 1: Comparison of Detector Configurations

a calorimeter is expensive, and its cost is moderated by keeping the scale of the inner detectors down. This has two implications: the space point resolution of the tracker should be excellent to meet momentum resolution requirements in a modest radius detector; and the design should admit high performance endcaps so that the barrel length (or cosθ_{Barrel}) will be small.

It is expected that track finding will largely be done in the 5 layer pixellated vertex detector, and the so-called tracker will primarily make the momentum measurement("Momenter"?), and improve the impact parameter measurement, and consequently refine the vertex reconstruction, as well as participate in the reconstruction of neutral strange particles. Strange particle decays in the tracker will be reconstructed from stubs in the EM calorimeter matched to hits in the silicon strips.

The last real strategic question is whether the Hadronic Calorimeter (HCAL) will be inside or outside the coil. Locating the HCAL inside the coil permits reasonably hermetic calorimetry, but it costs a larger, more expensive coil and more iron to return the flux. It is assumed that the detector will have a "standard" ultra high performance vertex detector based on CCD's (or an equivalent thin, small pixel technology), and that a muon tracker will be interleaved in

the iron flux return utilizing reliable RPC's or equivalent.

These considerations lead to a first trial design with a tracking radius of 1.25 m and a field of 5 T. The field is set high to get a large BR^2, and also provides a safety margin of protection for the vertex detector against the massive number of electron-positron pairs at the interation point. This choice makes BR^2 = 8, compared to 10 for TESLA and 12 for the North American Large Detector. The baseline tracker is 5 layers of silicon microstrips (silicon drift detectors are under consideration as an option) with a cosθ_{Barrel} of 0.8. A set of 5 silicon strip disks is arranged as to complete the acceptance. It is made of thinned silicon squares daisy chained together and read out on the ends, and supported by a low mass carbon fiber space frame. The HCAL is chosen inside the coil, and the radiator is Stainless Steel. The quadrant view is shown in Figure 2, and the major dimensions are tabulated in Table 2.

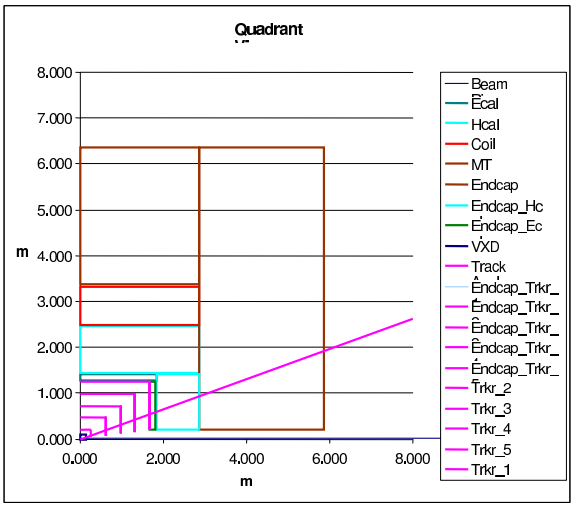

Figure 2: Quadrant View of the Silicon Detector.

Tracker

The tracker resolution versus cosθ is shown in Figure 3. The resolution at 90^0 as a function of the tracker radius is shown in Figure 4 for the high momentum of p = 250 GeV/c, illustrating the choice of the 1.25 m outer radius. The high momentum resolution of the tracker is analyzed as a system with the 5-layer vertex detector. The low momentum track finding performance has not yet been calculated. Note that the tracker should be considered with the 5 layer vertex detector as a tracking system. It is assumed that the barrel readout is only at the ends of each layer, and that its mass has been minimized by ASIC's. Note that the required duty factor of a few hundred nanoseconds (a few microseconds in probable reality) every 8 milliseconds, is tiny compared to ATLAS, and that thermal management should be straightforward assuming power pulsing. The reasons for considering a silicon strip tracker are that its point resolution is excellent, leading to excellent high momentum resolution; that its barrel end structure should be thin compared to a TPC leading to better performance from disk endcaps; and that the silicon should be extremely robust in the questionable backgrounds of a linear collider. On the other hand, it will be challenging to read out the long strips with good noise performance and to keep the overall thickness of the structure very small.[2]

Detector	Radius (m)		Axial(z)(m)	
	Min	Max	Min	Max
Vertex Detector	0.01	0.10	0.00	0.15
Central Tracking	0.20	1.25	0.00	1.67
Endcap Tracker	0.04	0.20	0.27	1.67
Barrel Ecal	1.27	1.42	0.00	1.84
Endcap Ecal	0.20	1.25	1.68	1.83
Barrel Hcal	1.44	2.46	0.00	2.86
Endcap Hcal	0.20	1.42	1.84	2.86
Coil	2.49	3.34	0.00	2.86
Barrel Iron	3.37	6.36	0.00	2.87
Endcap Iron	0.20	6.36	2.87	5.86

Table 2: SiD Major Dimensions

The vertex detector is assumed to be a CCD vertex detector, built of CCDs of optimal shape, with multiple readout nodes ($\sim$20) for speed, thinned ($< 100\mu$m), with improved radiation hardness, and low power. A readout ASIC is mounted at the CCD, with output through fiber optics. This is a modest extrapolation from SLD's VXD3, with about 3 times the number of pixels.

EM Calorimeter

The EMCal consists of layers of tungsten with gaps sufficient for arrays of silicon diode detectors mounted on G10 mother boards and for a thermal conductor to provide heat removal. The diode arrays are hexagonal pixels, approximately 5 mm across. The thickness of these gaps is a major issue, in that it drives the Moliere radius of the calorimeter. A thickness of 2.5 mm seems plausible now, accommodating a 0.3-0.5 mm silicon wafer, a 0.5 mm G10 carrier, a 1 mm Cu thermal conduction sheet, and 0.5 mm of clearance. Conversely, 1.5 mm seems barely plausible but is an interesting goal! A stacked assembly rather than insertion into a slot is assumed. For now, we assume a 2.5 mm gap.[3]

The readout electronics from preamplification through digitization and zero suppression will be developed on a single chip that will be bump or diffusion bonded to the

[2]Recent designs are considering individual readout of each detector to provide timing tags and lower occupancies.

[3]Recent work indicates that 1.5 mm or somewhat less should be possible.

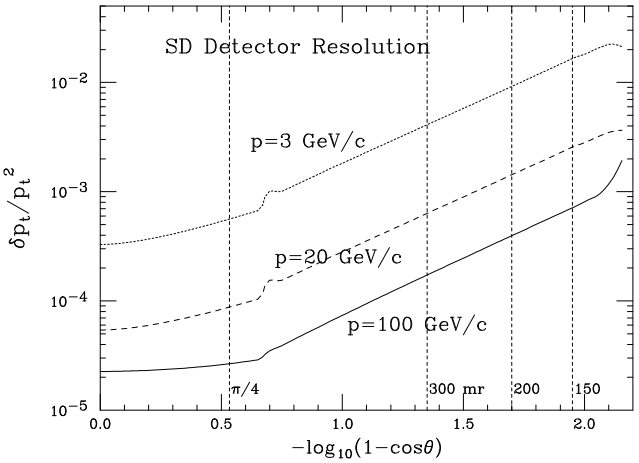

Figure 3: Momentum resolution $\Delta p_t/p_t^2$ as a function of cosθ, specifically $-log_{10}$(1-cosθ), for momenta of 3 GeV/c, 20 GeV/c, and 100 GeV/c. The values of the function for θ = π/4, 300 mr, 200 mr, and 150 mr are indicated by the vertical dashed lines.

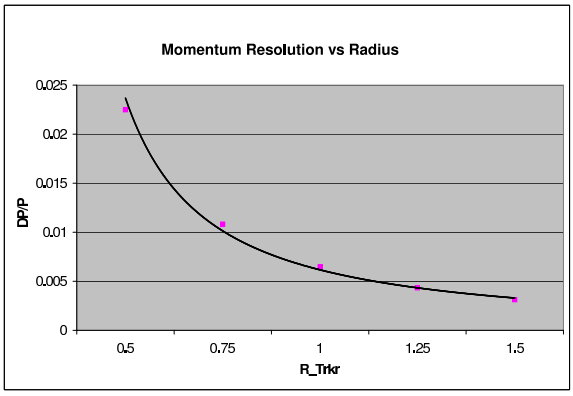

Figure 4: Momentum Resolution at p = 250 GeV/c vs. radius for the SiD tracker system.

wafer of detector diodes. Figure 5 illustrates the center of one 1000 pixel silicon wafer, with the bump bond array at the center, and the traces from the pixels to the bump bond array. Thus it is expected that the pixel size on the wafer will not affect the cost directly. Shaping times would be optimized for the (small) capacitance of the depleted diode. Recent work indicates that it may be possible to get timing information from each pixel, with localization to about a bunch within a train. Figure 6 is a cross-sectional view in the vicinity of the readout chip.

Thermal management is a fundamental problem for the EM Calorimeter as envisoned here with the deeply embedded electronics. With a power pulsing duty factor of 10^{-3} (which is possible for the X-Band collider), each wafer might generate 20 mW average power. Preliminary calculations indicate a water cooled heat sink at the outer edge of an octant, conducting heat through a 1 mm thick copper plane sandwiched with tungsten and G10, will develop a 14^0C temperature differential. This is acceptable. Whether

W Thickness	2.5 mm
Gap	2.5 mm
Layers	30
Total X_0	21.4

Table 3: SiD Electromagnetic Calorimeter Parameters

the electronics can maintain adequately low noise in the presence of this power pulsing remains to be demonstrated.

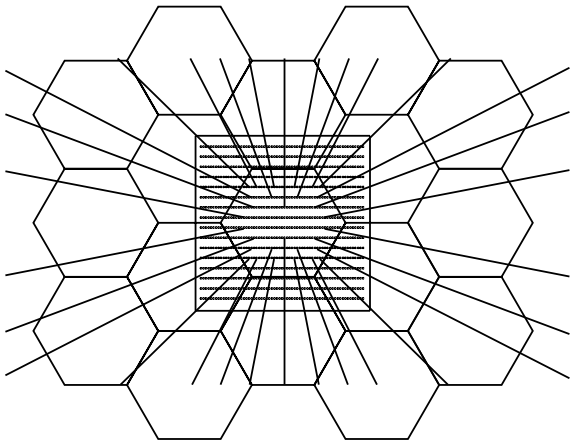

Figure 5: The center of one 1000 pixel silicon wafer showing the bump bond array at the center for the single readout chip. A few representative traces from pixels to bump bond array are shown.

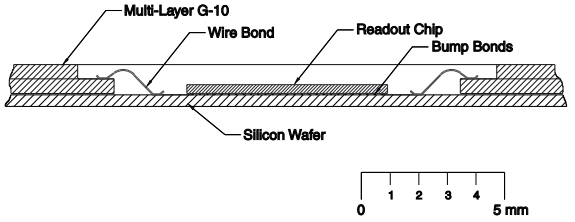

Figure 6: Cross-sectional view in the vicinity of the EM Calorimeter readout chip.

Hadron Calorimeter

The HCal is chosen to lie inside the coil. This choice permits much better hermeticity for the HCal, and extends the solenoid to the endcap flux return. This makes a more uniform field for the track finding, and simplifies the coil design. The HCal radiator is a non-magnetic metal, probably copper or stainless steel. Lead is possible, but is mechanically more difficult, particularly since the EMCal is supported by the inner layer of the HCal. The detectors could be “digital”, with high reliability RPC’s assumed. Studies

are underway to determine the performance of the "digital" approach.

The HCal is assumed to be 4 λ thick, with 46 layers of radiator 5 cm thick alternating with 1.5 cm gaps.

Coil and Muon Tracker

The coil concept is based on the CMS design, with two layers superconductor and stabilizer. The stored energy is 1.4 GJ, compared to about 2.4 GJ for the TESLA detector and 1.7 GJ for the "L" detector. The coil ΔR is 85 cm.

The flux return and muon tracker is designed to return the flux from the solenoid, although the saturation field for the iron is assumed to be 1.8 T, which may be optimistic. The iron is laminated in 5cm slabs with 1.5 cm gaps for detectors.

Forward Detector

Figure 7 shows the SiD forward system. This figure illustrates the forward masking and magnets, and the tracking, calorimetry, and luminosity-pair monitor. Figure 8 shows the beampipe openings in the luminosity-pair monitor located 3.5 meters from the IP.

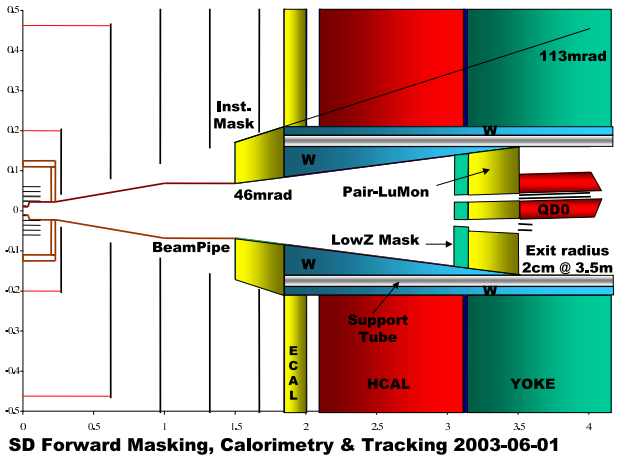

Figure 7: Schematic of the forward region of SiD, showing the forward masking and magnets, and the tracking, calorimetry, and luminosity-pair monitor.

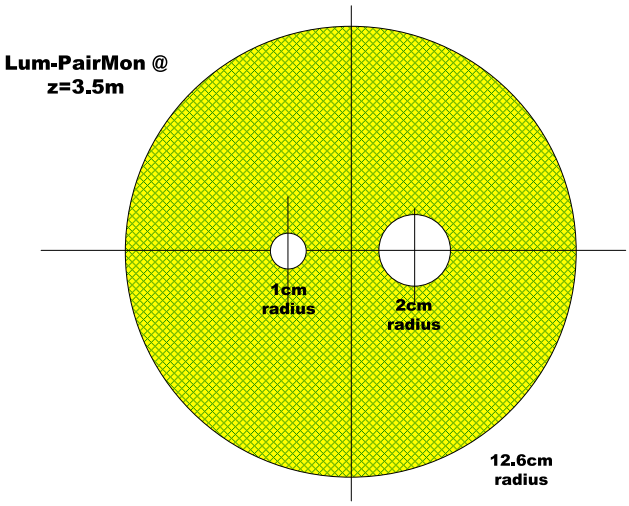

Figure 8: Cross section of the luminosity-pair monitor in the SiD forwrad system at z=3.5m.

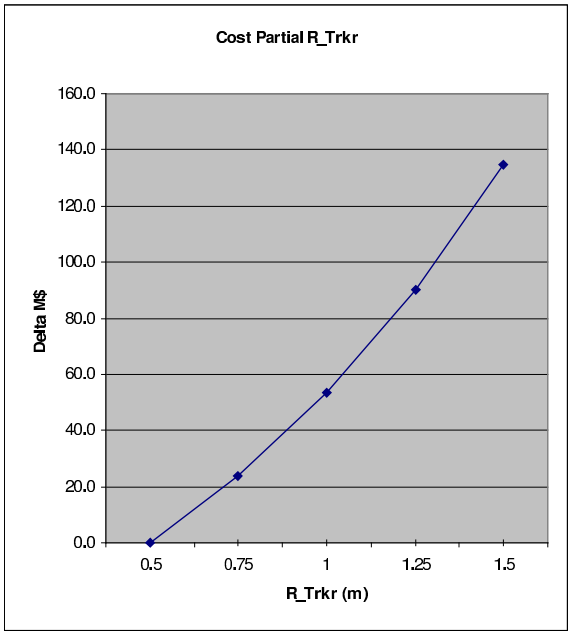

Figure 9: Cost differential versus tracker radius.

Costs

The "complete" cost estimate is in a separate document. A crude design code was written in Excel to keep the detector nominally consistent as parameters were varied which allows the estimation of some of the cost partial derivatives. The reader is cautioned that these are rather preliminary estimates.

The detector cost derivatives due to the major tracker parameters are shown in Figures 9 and 10.

The SiD tracker outer radius is nominally set to 1.25 m and cos θ_{Barrel}=0.8. A further interesting partial is the cost dependence on the thickness of the HCal. Although the HCal itself is not particularly expensive, it drives the coil and flux return size. The estimated values are shown in Figure 11.

The "more complete but extraordinarily preliminary" SiD total cost estimate is calculated mostly using numbers from the other North American detector costing exercises.[2] At this time the total materials and supplies (M&S) estimate is \$183M, the Labor estimate is \$55M, and contingency is \$84M, for a total of \$322M.

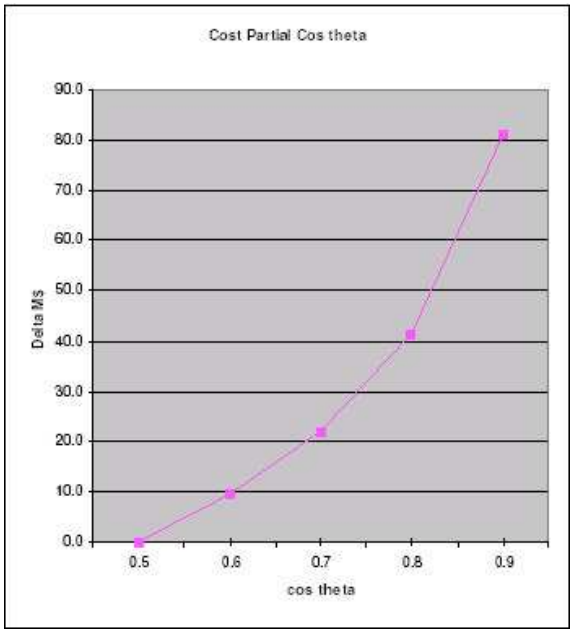

Figure 10: Cost differential versus tracker barrel angle.

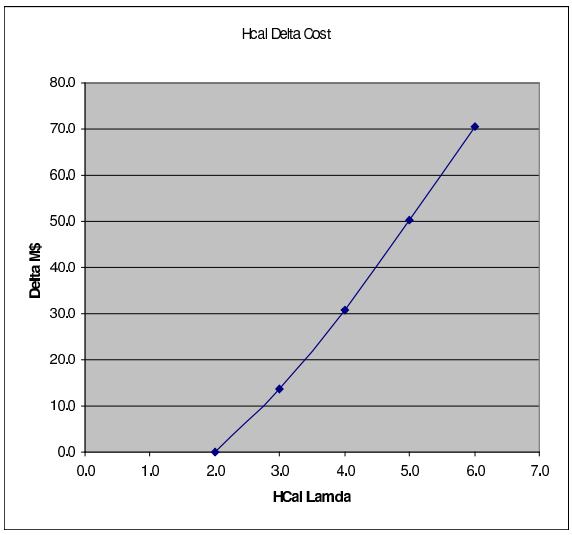

Figure 11: Cost differential versus hadron calorimeter thickness.

DETECTOR R&D IN NORTH AMERICA

The detector R&D in North American on linear collider detectors is diverse, and has not been aimed at any specific detector configuration. Following several years of support for simulation, the effort is now transitioning into an invigorated hardware effort. Funding for this new era is now established.

Below we list many of the tasks that are under investigation (this is not an inclusive list; there are other efforts).

Tracking

Tracking has focussed on three main R&D thrusts:

- Simulation
- Gaseous Tracking (TPC)
- Solid-state Tracking (μ-strips and silicon drift)

The simulation has been aimed at establishing tracking specifications, such as resolution and coverage, and in comparing and qualifying technologies.

Future goals for the simulation will include:

- Refine Tracker Requirements
  - SUSY (central at Michigan, forward at USCS)
- Explore Alternatives (not yet fully underway)
  - TPC vs. silicon drift
  - All-axial central μ-strip tracking
  - Forward tracking scenarios
  - With GEANT-based background included
- Tracking/Calorimeter Interface Issue
  - Track-cluster matching
  - Calorimeter-assisted VEE finding

Several Canadian and US groups are working on gaseous tracking. Their objectives are:

- Explore readout choice and design
- Gas selection (neutron backgrounds, diffusion)
- Compact electronics

Test chambers are being studied at Carleton, Victoria, and Cornell. GEM production is carried out at MIT (Microsystems Technology Laboratory) and proposed at Louisiana Tech.

Solid-state tracking R&D includes both microstrip detectors and silicon drift detectors:

- Long Shaping-time μ-strips
  - Ultra-thin (for momentum resolution and energy-flow)
  - ASIC development at UC Santa Cruz
  - Long (2m) ladders under development at UCSC
- Silicon Drift R&D (Wayne State, Brookhaven)
  - Intrinsically 3-dimensional
  - Proven (STAR VTX detector at RHIC)
  - Longer, thinner sensors; low-power readout
- Mechanical Issues
  - Space frame
  - Interferometeric position monitoring (Michigan)

Vertex Detection

Three groups are working now or plan to start work on vertex detection. The Oregon/Yale/SLAC group is investigating CCDs, as a next step from the success of the 307 Mpixel CCD vertex detector of SLD, VXD3. This studies include:

- Radiation hardness studies
  - removal of SLD VXD3 for analysis
  - spare ladder studies
- Developing new CCD detector prototype
- Studying mechanical issues
- Design readout for X-Band operation

The Oklahoma/Boston/Fermilab group plans to develop a design for a linear collider ASIC for CCD readout, and the Purdue group is planning studies of the mechanical behavior of thin silicon and the development of hybrid silicon pixels for the linear collider.

Calorimetry

Calorimetry R&D is summarized in Table 4.

The calorimeter group has the following test beam plan:

- ECal module (roughly 20 cm x 20 cm x 30 layers)
- HCal module (roughly 1m x 1m x 1m)
- Starting 2004-5; site(s) to be determined
- Goal: Full validation of simulations (GEANT4)

Some additional details of these efforts:

Si/W - SLAC/Oregon/BNL

- Integrated Electronics
  - Analog + digital preliminary design
    - 0.20x0.25 mm^2/pixel
    - Full charge and time
    - Heat looks ok (power pulsing)
- Silicon Detectors
  - Prototype design finalized
    - 5x5 mm^2 pixels
    - 6" wafers
  - Vendor order in progress

Colorado's scintillator tile concept uses an offset type configuration to improve performance. Simulations and detector work is in progress.

Kansas is developing a hybrid scintillator/silicon/tungsten module to provide optimize performance.

RPCs - Argonne/Chicago/BU/FNAL

- Emphasize reliability
- Glass
- Avalanche mode
  - Requires integrated amplification (ASIC)
- Plans for 1 m^3 test beam module underway

GEMs - UT Arlington

- Triple GEM
- GEM foils/prototypes fabricated in Texas
- Simulations underway

Scint. tiles - N. Illinois

- Extensive R&D and simulation progress

Muons

An active group including Fermilab, Northern Illinois, Notre Dame, UC Davis, Wayne State, Rice and UT Austin, is working on a scintillator based muon detector.[1] This effort spans the tasks from simulation of muon detection, to prototype planning. The hardware plan includes:

- Test 16 pixel MAPMT - specification and parameters.
- Test extruded MINOS-style scintillator and fiber.
- Develop prototype modules (2.5m W x 5.0m L) to:
  1. Understand mechanical design/construction issues such as basic scint. Layout, WLS fiber laying, WLS - clear fiber connections, fiber routing, bundling, optical multiplexing, mechanical engineering, etc.
  2. Understand FE electronics, calibration and readout specifications.
  3. Understand safety, testing, and QA procedures.
  4. Implement cosmic ray tests and eventually beam tests.
  5. Make detailed cost estimates for a scintillator-based muon system.

Beamline Instrumentation

A very active group is working on beam-line instrumentation in North America. The high priority items are:

- dL/dE analysis
  - complete analysis to extract both tail and core
  - understand external inputs (asymmetries, offsets)
  - possible to extract correlations (energy, polarization)?

Ecal	Silicon/W	SLAC/Oregon/BNL	Designs and prototyping
	Scint/Si/W hybrid	Kansas	Initial ideas
	Scint tile/W	Colorado	Ideas under study
Hcal	Digital - Scint. Tiles	N. Illinois	Designs and prototyping
	Digital - RPCs	Argonne/Chicago/BU/FNAL	Designs and prototyping
	Digital - GEMs	UT Arlington	Initial designs and prototyping

Table 4: Calorimeter Detector R&D in North America

- Extraction line studies
  - expected distributions with disrupted beam
  - expected backgrounds at detectors
- Forward Tracking/Calorimetry
  - Realistic conceptual design for NLC detector
  - Expected systematics eg: alignment
- Beam Energy Width
  - Understand precision of beam-based techniques
  - Possible with extraction line energy spectrometer based on SLD approach of Wire Imaging Synchrotron Radiation Detectors (WISRD)

The ongoing R&D work including the following

- Luminosity
  - dL/dE analysis (SLAC, Wayne St.)
  - Beamstrahlung Monitor (Wayne St.)
  - Pair monitor (Hawaii, in collab. with Tohoku)
  - Forward calorimeter (Iowa St.)
- Energy
  - WISRD spectrometer (UMass, Oregon)
  - BPM spectrometer (Notre Dame)
- Polarization
  - x-line simulations (SLAC, Tufts)
  - Quartz fiber calorimter (Iowa, Tennessee)

There are many important topics uncovered.

Testbeams

Test beams will be required to develop the detectors needed for the linear collider. We must begin now to plan for these beams. An assessment is underway across the regions. Some understanding of these needs is being to develop. Table 5 summarizes the known needs at the present time.

Accelerator R&D

Within the US there is a large interest within the university community in working on linear collider accelerator R&D. This is now funded by DOE at roughly the same level as the linear collider detector R&D and a similar level of support is being considered at NSF.

R&D ON THE JLC DETECTOR

The JLC strategy for choice of technologies in the baseline R&D has been taken with two principles: 1.) there will be no “proof-of-principle” R&D, and 2.) the detector must be constructible within an affordable budget.

The overall layout of the JLC Detector is shown in Figure 12 in the 3T field configuration.

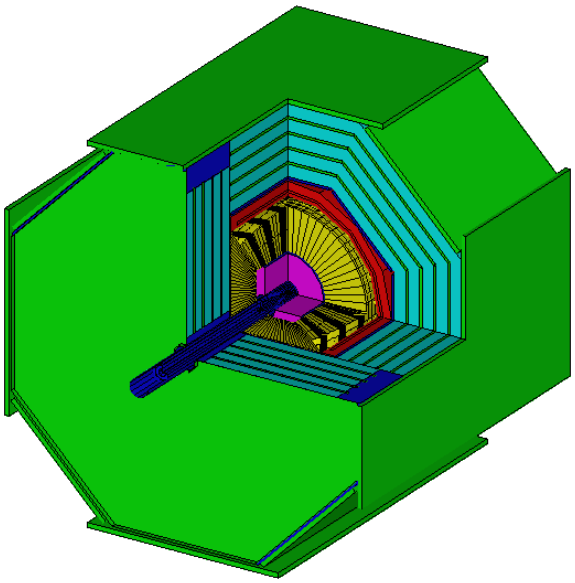

Figure 12: GEANT drawing of the baseline JLC Detector for 3 Tesla.

There is progress in several areas of the detector. In each, we list below the work that is completed, or nearly so, and the work that is in progress, or yet to do.

	Group	Apparatus	Beam Conditions	When/Where
1	TESLA/CALICE J.-C. Brient/P. Dauncy et al	E_Cal/H_Cal E-flow Tests	e,μ,π,p e 1-100 GeV	Mid 2004 - 2005 Fermilab/Protvino? Setup; DESY/CERN Fermilab/Protvino?
2	JLC-Cal - Y. Fujii et al	EM/H Cal Prototypes	e,μ,π,p 1-200 GeV	KEK/2004 US/Europe 2004-8
3	LC- Cal - R. Frey et al	E_Cal H_Cal Prototypes	e to 10 GeV e,μ,π,p $\rightarrow$ 120	E_cal at SLAC '04; E & H_Cal @ FNAL?
4	Digital H_Cal - Argonne, NIU, UTA, et al	H-Cal Prototypes	e,μ,π,p $\rightarrow$ 120	Fermilab - 2005-'06
5	IP Instrumentation Woods/Torrence et al	Gas C counter/cal Quartz fiber cal Sec. Emission det. W. angle, vis light beamstrahlung Synchrotron rad BPM E spectro	e/γ to 100 GeV; LINX for beamstrahlung; Polarized e's	Various
6	IP Instr and Calorimetry Onel/Winn et al	Compton polar. w/ quartz fiber cal; Sec. Emission det. C compensated cal	e,π, p $\rightarrow$ 120 $<$ 20, $<$ 300 GeV	Fermilab CERN PS & SPS
7	Tile/fiber Tests R. Ruchti	Detector prototypes, timing,	e,μ,π 10 - 100 GeV	Fermilab
8	Muon Prototype Detectors TESLA/ALC	RPCs and Scintillator based	e's 50-750 MeV e,μ,π $\rightarrow$ 120GeV	Frascati 2004 Fermilab 2005

Table 5: Test Beam Requirements (incomplete list).

Vertex Detector

- done or finishing soon:
  1. excellent spatial resolution (see Figure 13);
  2. room-temperature operation (good S/N by Multi-Pinned Phase operation);
  3. radiation hardness measurement : ^{90}Sr, ^{252}Cf, electron-beam irradiation; analysis is underway.
- in progress or to do:
  1. CTI improvement: two-phase clocking, thermal charge injection, notch structure (see Figure 14);
  2. fast readout : test-board fabrication in progress ;
  3. thinned CCD (20micrometer): flatness, stability, reproducibility;
  4. precise estimation of background by a full simulation with detailed beamline components.

Intermediate Tracker

- in progress or to do:
  1. Si-sensor fabrication and test-module construction;
  2. Simulation study of VTX-IT-CT combined tracking (see Figure 15).

Central Tracker

- done or finishing soon:
  1. spatial resolution;

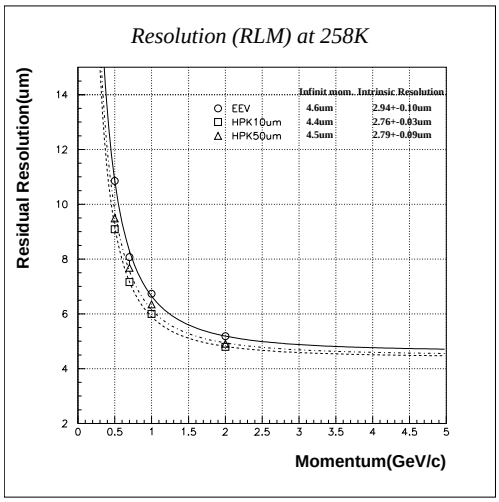

Figure 13: Position resolution of CCD test module obtained with minimum-ionizing pions at KEK $pi2$ testbeam measurement. Intrinsic resolutions, after subtraction of multiple-scattering effects, are written as insight of the figure.

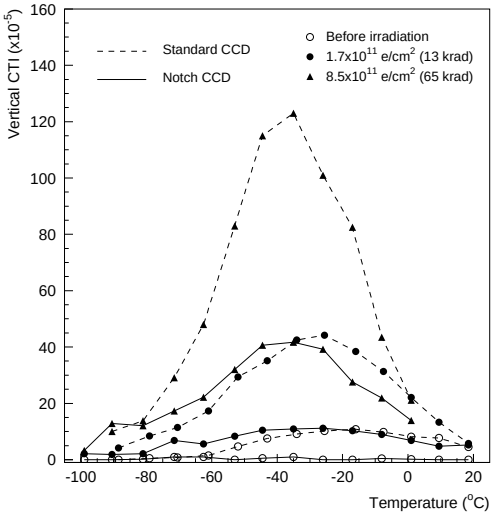

Figure 14: Charge-Transfer Inefficiency of CCDs. Dashed lines are for standard CCD, while solid lines are for 'notched-structure' CCD. Notched structure improves CTI significantly. Notched structure has small deeper well to concentrate charge in a well.

2. effect of gas contamination;
3. Lorentz angle measurement;
4. dE/dx measurement;
5. positive-ion space-charge effect (see Figure 16).

- in progress or to do:

1. two-track separation performance with a test chamber using parallel laser beam (see Figure 17);

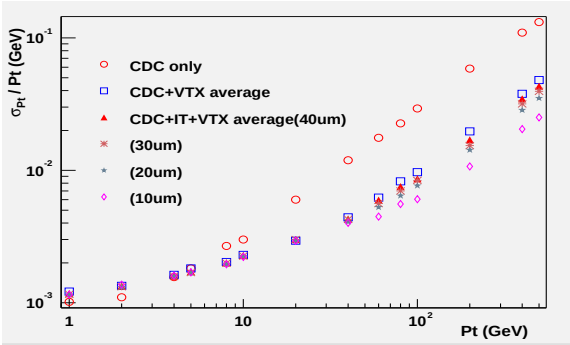

Figure 15: Single-track Pt-resolution (full-simulation) compared for three tracking cases.

2. z-measurement with charge division;
3. solve creeping of aluminum wire;
4. full-simulation study on Pt resolution;
5. bunch-tagging capability and its impact on physics sensitivity.

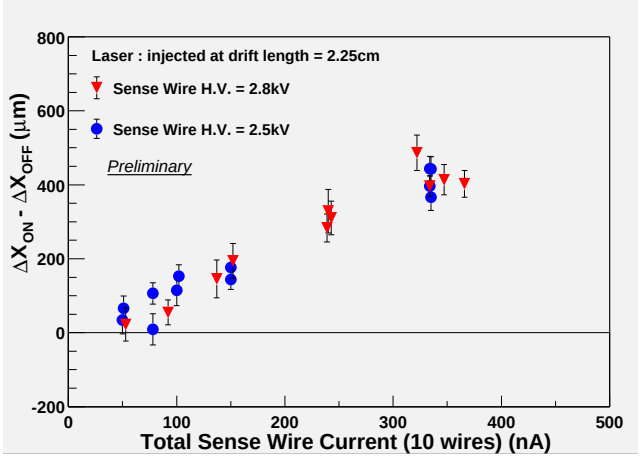

Figure 16: Effect of drift-field deformation caused by positive-ions on position measurement. For higher beam intensity (higher sense current) measured position shifts. However in the actual operation, inter-train time is long enough to sweep out all the positive ions.

Calorimeter

- done or finishing soon:

1. hardware compensation, energy response linearity, energy resolution (stochastic term);
2. machine-ability of tiny tiles, assemble-ability;
3. performance of WLS-readout shower-position detector.

- in progress or to do:

1. granularity optimization with a full simulation;

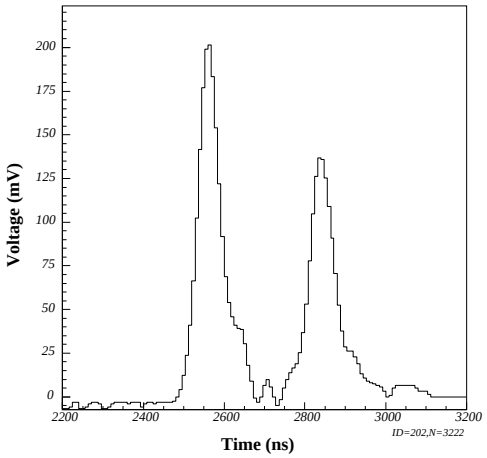

Figure 17: Sense-wire FADC spectrum when two parallel laser tracks are injected into a test chamber with distance of 2.2mm. 2mm-separation is assured.

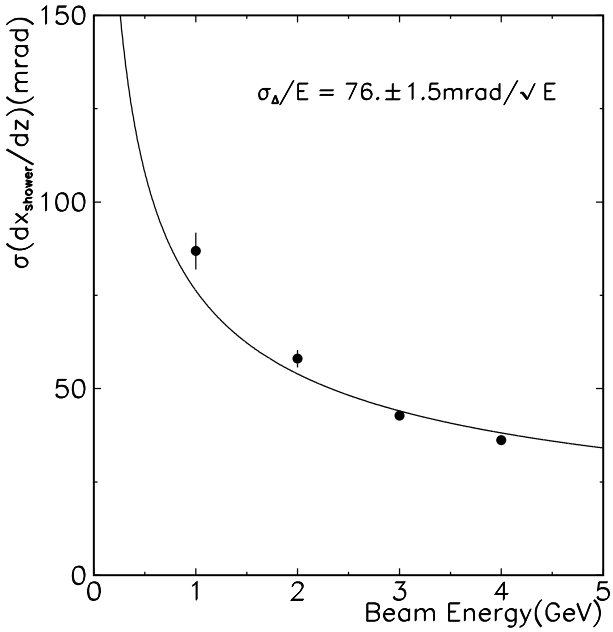

Figure 18: Shower axis angular resolution (preliminary) of a scintillator-strip-array EMcal obtained by a testbeam measurement at KEK. Strip width is 1cm, and the module has 6 superlayers (17 radiation length).

2. photon yield and non-uniformity improvement for conventional tile/fiber EMcal;
3. performance study of strip-array EMcal : beamtest, simulation, ghost-rejection (see Figure 18);
4. shower-position detector with directly-mounted APD-readout;
5. photon detectors (multi-channel HPD/HAPD, EBCCD etc.).

Muon System

There is no effort on the muon system for the JLC Detector.

CONCLUSION

The Detector R&D underway in the different regions of the world shows there is no unique solution, and differing optimizations can lead to quite different detector configurations. The advantages and disadvantages of each approach needs to be confronted with honest assessment and comparison.

REFERENCES

[1] http://www-d0.fnal.gov/∼maciel/LCD/awg_lcdmu.html.

[2] Linear Collider Physics Resource Book for Snowmass 2001, http://www.slac.stanford.edu/grp/th/LCBook/, 412-413.

...

...

A BRIEF REVIEW of the FINDINGS of the INTERNATIONAL LINEAR COLLIDER TECHNICAL REVIEW COMMITTEE (ILC-TRC)

N. J. Walker, DESY, Hamburg

Abstract

In the beginning of 2003, the ILC-TRC published its second report on the status of R&D towards the current proposed designs for an e^+e^- linear collider [1]. The nearly 500 page report was the end result of over one year of intense work by over 30 scientists from the various linear collider related laboratories around the world. Charged with making a critical review of the machine designs, while identifying outstanding R&D items, the end result in itself represents a unique resource of information for anyone interested in the subject (both expert and novice alike). In the following report, I will summarise the findings of the committee, with perhaps a slightly personal perspective. Those readers who are interested in the subject are encouraged to read at least the executive summary (on which this report is loosely based), if not the entire report.

INTRODUCTION

At the Snowmass workshop in July 2001, the then newly formed Steering Committee of the second ILC-TRC met for the first time. Chaired once again by Greg Loew (SLAC), the Steering Committee reflected the five current proposals for a 500 GeV and beyond centre of mass e^+e^- linear collider:

- R. Brinkmann (DESY) for TESLA [2];
- G. Guignard (CERN) for CLIC [3];
- T. Raubenheimer (SLAC) for NLC [4];
- K. Yokoya (KEK) for the JLC-C and JLC-X [5].

This meeting marked the beginning of a process that would take over one year to complete, and would keep some 30 accelerator physicists fully occupied for that time. The second study was formally commissioned by chair of ICFA (Prof. H. Sugawara) in February of 2001.

The charge broadly sketched by ICFA to the ILC-TRC and then later refined read as follows (taken verbatim from [1]):

- To assess the present technical status of the four LC designs at hand, and their potential for meeting the advertised parameters at 500 GeV c.m. Use common criteria, definitions, computer codes, *etc.*, for the assessments.
- To assess the potential of each design for reaching higher energies above 500 GeV c.m.
- To establish, for each design, the R&D work that remains to be done in the next few years.
- To suggest future areas of collaboration.

By 'present status' it was agreed to take the baseline designs as outlined in (for example) the TESLA TDR [2] and the 2001 NLC Snowmass Report (the so-called copper book [4]). The Steering Committee decided to address these charges by forming three working groups, each containing 14-15 international experts in accelerator physics:

- **Technology, RF Power, and Energy Performance Assessments** – chaired by Daniel Boussard, (CERN *retired*);
- **Luminosity Performance Assessments** – chaired by Gerry Dougan (Cornell University);
- **Reliability, Availability and Operability** – co-chaired by Nan Phinney (SLAC) and Ralph Pasquinelli (FNAL).

Once in place, these three working groups worked primarily by exchange of emails (Gbytes!), and numerous conference calls (sometimes several per week). In addition, four pivotal meetings were held at SLAC (February 2002), CERN (April 2002), Paris (June 2002) and finally DESY (September 2002).

THEN AND NOW

Before discussing the findings of the current (and second) ILC-TRC, it is interesting to look back at the first report, published at the end of 1995 [6]. At that time, there were no less than 8 proposed machines, of which 3 have since disappeared. Of the remaining five, the X-band machines proposed by SLAC (NLC) and KEK (JLC*) have become virtually identical in design; as a result, the ILC-TRC treated them as one design, resulting in four separate machines to be compared. Tables 1 and 2 show some key parameters for the 500 GeV c.m. machines from the first and second (current) ILC-TRC reports respectively.

Since 1994, the four remaining designs have matured significantly, reflecting both the advances in hardware R&D and in simulation. Comparing the example parameters listed in tables 1 and 2, we immediately see that the proposed peak luminosity for these machines has increased by almost a factor of 6! This factor alone has significantly strengthened the physics case for an e^+e^- linear collider, ultimately leading to the unprecedented situation today of a world-wide consensus on the need for such a machine. But the factor of 6 does not come for free, and the machine designers have pushed ever closer to the edge of the envelope to achieve it. I believe the increase has been primarily driven by the

* as of writing, KEK have renamed their X-band accelerator proposal from JLC to GLC for 'Global Linear Accelerator'.

		TESLA	SBLC	JLC-S	JLC-C	JLC-X	NLC	VLEPP	CLIC
f_{RF}	GHz	1.3	3.0	2.8	5.7	11.4	11.4	14.0	30.0
L	$\times 10^{33}$ cm^{-2}s^{-1}	6	4	4	9	5	7	9	1-5
P_{beam}	MW	16.5	7.3	1.3	4.3	3.2	4.2	2.4	~1-4
P_{AC}	MW	164	139	118	209	114	103	57	100
$\gamma\varepsilon_y$	$\times 10^{-8}$ m	100	50	4.8	4.8	4.8	5	7.5	15
σ_y*	nm	64	28	3	3	3	3.2	4	7.4

Table 1: Example parameters for the 500 GeV c.m. linear collider designs reviewed as part of the first ILC-TRC in 1994 [2].

		TESLA	JLC-C	JLC-X/NLC	CLIC
f_{RF}	GHz	1.3	5.7	11.4	30.0
L	$\times 10^{33}$ cm^{-2}s^{-1}	34	14	20	21
P_{beam}	MW	11.3	5.8	6.9	4.9
P_{AC}	MW	140	233	195	175
$\gamma\varepsilon_y$	$\times 10^{-8}$ m	3	4	4	1
σ_y*	nm	5	4	3	1.2

Table 2: Example parameters for the remaining 500 GeV c.m. linear colliders for the current (second) ILC-TRC [1].

competition between the warm and cold designs (good for the consumer?). If that is true we might ask if the push towards this very ambitious high luminosity is technically justified? That questions is one of the reasons why the second ILC-TRC was convened. As we will see, the outcome looks good, although it should be stressed that the experts within the ILC-TRC all agreed that this was as far as it goes: there is almost certainly no more factors to be had between now and building the machine.

ORGANISATION AND METHODOLOGY

Figure 1 shows that overall organisation of the ILC-TRC. The three working groups were made up of a total of 28 accelerator experts; of these many were taken directly from the centres of linear collider R&D, but several *neutrals* form accelerator fields outside the immediate LC community were also included. The *Reliability, Availability and Operability* working group was not originally foreseen at the beginning of the committee's work, the subject being considered separately for each of the original two working groups. It soon became clear, however, that the subject could not be dealt with separately within the contexts of the two groups, and a third amalgamated working group was formed.

The approach taken by the three groups was to divide the scope into smaller sub-groups:

- **Tech., RF Power and Energy Performance**
  - Injectors, Damping Rings and Beam Delivery
  - Klystrons, Power Supplies, Modulators and Low Level RF
  - Power Distribution (RF pulse compression, waveguides, two-beam acceleration)
  - Accelerator Structures
- **Luminosity Performance**
  - Electron and Positron Sources
  - Damping Rings
  - Low Emittance Transport (DR to IP)
  - Machine Detector Interface
- **Reliability, Availability and Operability**
  - Compilation of data from existing machines
  - Component reliability issues
  - Machine protection system (MPS)
  - Commissioning, tuning, and maintenance

For all three working groups, the overall philosophy (methodology) was the same:

- review current designs and status (achievements) of R&D, particularly the test facilities;
- identify the positive aspects of the designs;
- identify those areas of concern and
- identify R&D that needs to be done to address these issues;
- categorise (rank) the R&D items.

By the nature if its charge, the technology working group was a traditional review of the hardware designs of the machines, and the current R&D and test facilities. Although mandated with looking at all aspects of the machine, the focus was clearly on the main linac, specifically the power generation and distribution, and the structure and cavity status. By contrast, the luminosity group set about repeating many beam dynamics simulations related to the machine performance.

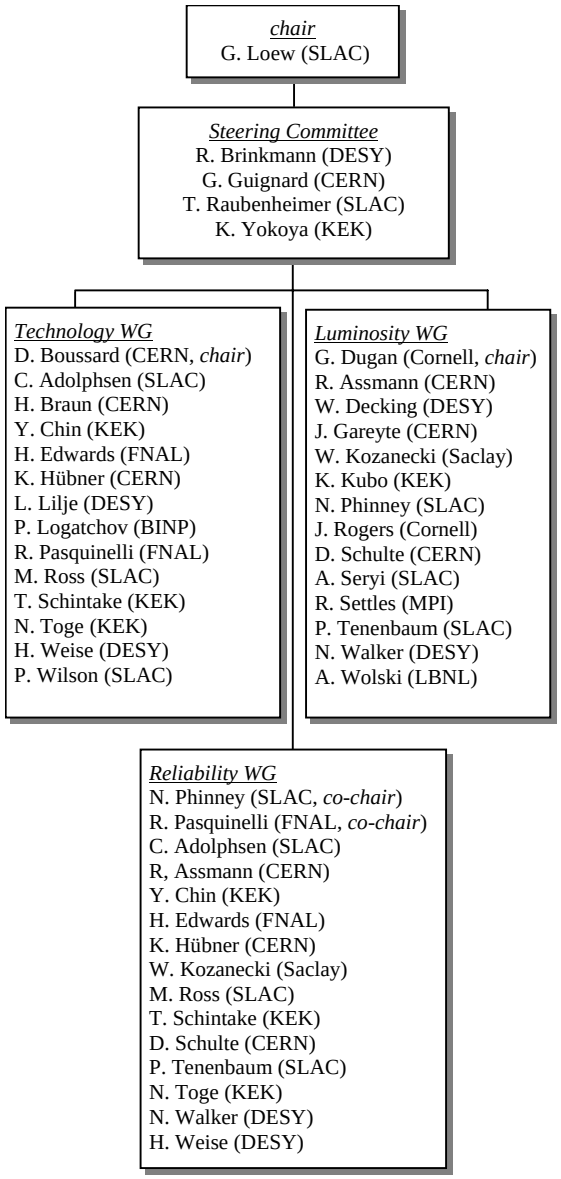

Figure 1: Structure of the second ILC-TRC.

The goals was to (where possible) produce results using the same software simulations across all the designs, and in doing so established benchmarked tools. In this respect, the ILC-TRC was much more than just a review, and many new never before attempted simulations were made. Particularly for the damping rings and the so-called low emittance transport (LET) systems (bunch compressor, main linac and beam delivery systems), the available software tools became more sophisticated, and new results were obtained as a direct result of the ILC-TRC process.

Of all the working groups, perhaps the reliability group had the hardest job. The first step was to attempt to tabulate reliability and availability numbers for existing machine designs. This in itself proved problematic, since different labs have different accounting procedures. The bottom line with respect to reliability is the total integrated luminosity at a specified centre-of mass energy within a given run period. To attempt to quantify this for the various machine designs, the particularly failure modes and their impact on luminosity first need to be accessed. Ultimately numbers such as mean time between failure (MTBF) are required, and in many instances these numbers are non-existent or based on such low statistics as to make their extrapolation to the quantities of components used in a linear collider questionable. Nevertheless, all agreed that such issues are of paramount importance when designing a new facility as complex as a linear collider.

THE FINDINGS: OVERALL CONCLUSIONS

After what is almost certainly over a total of a thousand man-years of linear collider R&D spread over a decade and a half, the first overall conclusion of the ILC-TRC was extremely positive: the report states that the ILC-TRC

> *"did not find any insurmountable obstacles to building TESLA, JLC-X/NLC, or JLC-C within the next few years and CLIC in a more distant future."*

In addition, the committee noted that for a 500 GeV c.m. machine, the TESLA design is the most mature. I believe this comment to be based purely on the linac technology, as it is hard to see how the TESLA damping ring design can be more mature than the NLC, for example.

Taken on its own, the above conclusion is enough for us to start lobbying the funding agencies. The opinion of the experts within the TRC was that we are ready to build a linear collider, and should move towards that realisation. However, by its nature, the ILC-TRC was a critical review, and true to its charge, it identified a total of 120 R&D items that should be addressed before the final construction phase of the machine. Of these items, 40 were common to all machines; the rest were distributed amongst the details of the individual designs. These items were ranked into four categories that will be dealt with in the next section.

Finally, the ILC-TRC took the opportunity in its overall assessment to point out that

- there is a severe lack of resources – both in terms of man-power and capital funds – to maintain parallel development of the four designs; and
- that several of the existing test facilities are effectively under used, either because of lack or resources, or because of the demands of other users.

As of writing, it is expected that a technology choice will be sometime in 2004; this decision will certainly help address the question of limited resources, but in my opinion, a rapid increase in the R&D money must appear soon after, if we are to realise construction of the machine within a few years. From this perspective, the

communities surrounding the machine designs will need to collaborate politically as well as technically.

THE FINDINGS: R&D RANKINGS

As I mentioned in the previous section, the ILC-TRC identified some 120 outstanding R&D items during the course of its studies. There are no doubt many more, but given the limited time and resources of the committee, identification of this many is already a significant contribution.

However, all R&D items are not born equal, and so during the DESY meeting in September 2002, it was decided that some sort of ranking or prioritisation was required. After much discussion, four rankings were agreed upon:

1. R&D needed for feasibility demonstration of the machine;
2. R&D needed to finalise design choices and ensure reliability of the machine;
3. R&D needed before starting production of systems and components;
4. R&D desirable for technical or cost optimisation.

Clearly the significance reduces down the list (although all of the items and many hundreds more must be dealt with before a machine can be built and operated successfully). The R1-4 (as they were to become known) were further divided into those pertaining to a 500 GeV c.m. machine, and those pertaining to an energy upgrade; this division reflected the charge given to the ILC-TRC by ICFA, although it might be argued[†] that the distinction is far from clear, particularly on the central issue of the linac structures and achievable gradient.

	TESLA		JLC-C	JLC-X/NLC		CLIC		com.
E_{cm}	500	800	500	500	1000	500	3000	
R1	0	1	1	2	0	3	0	0
R2	6	1	2	2	0	4	2	9
R3	13	5	2	13	2	5	2	26
R4	4	1	1	5	0	0	0	7

Table 3: Distribution of ranked R&D items. The c.m. energy is in GeV. com. refers to common items across all designs.

Table 3 shows the distribution of the ranked items across the machine designs and c.m. energies. Although it is almost inevitable, care should be taken in interpreting the 'score count', since I believe the numbers in the table hide much of subtle relevance behind each item. As an example, the absence of numbers for the upgraded c.m. energy generally reflect that the issues are faced 'up front' at the lower energy, and that there is no significant impact in going to higher energies. In that respect, it is beneficial to deal with each issue in its own right, and to understand its implications, especially with respect to any future decision on linac technology.

For the remainder of this section, I will briefly focus some of the more critical R1 and R2 issues.

TESLA R1

For TESLA, there is a single R1 item that refers to the 800 GeV upgrade capability:

- construction and test of a single cryomodule operating at a gradient of 35 MV/m, including measurements of quench rates, break-downs and dark current.

The report goes on to say that tests with electropolished cavities assembled in a cryomodule are foreseen in 2003. Unfortunately, due to lack of resources and budget problems at DESY, it is now very unlikely that such a complete test will be performed before 2005.

There is no equivalent TESLA R1 for 500 GeV c.m., since the committee felt that the demonstrations in the TESLA Test Facility (TTF) of gradients of the order of 23.4 MV/m where sufficient 'feasibility demonstration'. This finding provides the basic support leading to the statement concerning the 'maturity' of the TESLA technology for a 500 GeV c.m. machine. However 90-500 GeV c.m. is only the first phase of the project, and a clear (and cost effective) upgrade path to 800-1000 GeV c.m. is now mandatory. Therefore, it is the 35 MV/m goal that is important in showing that the TESLA technology can provide a viable solution for a future linear collider. Fortunately, despite the lack of a full cryomodule test in the near future as requested by the ILC-TRC, the high-gradient program continues to yield extremely promising results, some of which we will discuss in section below.

JLC-C R1

The ILC-TRC technology working group identified one 500 GeV c.m. R1 item for the JLC-C machine related to linac technology:

- High power tests of the proposed C-band choke-mode accelerating structures and pulse compression scheme.

The report also mentions that these tests are foreseen at the SPring-8 facility with the next few years.

JLC-X/NLC R1

For JLC-X/NLC there were two R1 items identified for 500 GeV c.m., both concerning the linac technology:

- Demonstration of the required unloaded gradient (65 MV/m) in a structure with the current baseline design parameters (including wakefield performance). Verification of RF breakdown rates.
- High-powered tests of the dual-moded SLED-II pulse compression system.

[†] and correctly so in my opinion.

Both these R1 issues are currently being aggressively addressed by the JLC-X/NLC collaboration, with tests scheduled for the end of 2003.

The JLC-X/NLC upgrade scenario is simply to build the linac longer (the tunnel will be constructed for 1 TeV c.m. but at the beginning will only be half full of linac). Consequently there are no additional R1 items for the energy upgrade.

CLIC R1

For CLIC, 3 items were identified:

- Tests of CLIC structures with full wakefield performance and the required unloaded gradient (172 MV/m) and pulse length (130 ns).
- Validation of the drive beam generation using a fully loaded linac.
- During an RF fault, a way must be found to turn off only a few structures within a drive beam unit (currently it is foreseen to turn the entire section off).

The first two issues are due to be tested in the CTF-3 experiment currently in preparation at CERN.

R2 items

As defined above, the 26 R2 items identified by the committee are not considered necessary for 'proof of principle', but are still a very high priority; in general they refer to topics which need to be resolved before the design of the machine can be finalised. Perhaps another way of looking at this is that these particular items raised some serious concerns over the *current* baseline designs amongst the working group members.

For TESLA, the R2 items can be briefly summarised as follows:

- A test of a complete linac unit (i.e. several cryomodules installed in an environment close to that foreseen for the final machine); such a facility would be used as a test bed for components. All foreseen components must be shown to be within their desired specifications, and that the linac performs at *the required gradient* and within tolerable breakdown and quench rates.
- Development of a fast (20 ns) damping ring kicker.
- For the damping rings, more systematic studies of the effects of multipoles (particularly from the wiggler fringe fields and errors) are required. The dynamic aperture of the positron ring must be improved over the current (TDR) lattice design.
- For the 800 GeV upgrade as proposed in the TDR calls for better damping ring performance[‡], which puts greater constraints on alignment tolerances and on the suppression of instabilities; these topics require further study.
- For the proposed head-on collision scheme at the interaction region, the beamstrahlung and disrupted beam stay-clear in the associated extraction line has been shown to be inadequate. The design must be re-evaluated, and in the event of no suitable solution, a crossing angle should be adopted (as proposed by the warm high-frequency machines).
- In terms of reliability, the single-tunnel solution for TESLA should be re-evaluated. The impact of frequent accesses to the linac housing for component repair – and particularly the damping rings – required further evaluation and detailed analysis.

The requirement of a *linac unit* test is a common theme that runs across all the machines. The first R2 requirement for the JLC-X/NLC – although worded slightly differently, and with more emphasis on the power source and distribution – is effectively the same requirement[§].

Perhaps most interesting from the point of view of potential collaboration is the list of common R2 items – all of which were identified by the luminosity and reliability working groups. The luminosity group identified several common items relating to damping rings and the low emittance transport beam dynamics:

damping rings

- Electron cloud effects: further work on theory, simulations and experiments in existing rings. Possible cures need to be experimentally tested.
- Fast ion instability: again more simulation/theoretical work, with tests in existing facilities such as the Accelerator Test Facility (ATF) at KEK.
- Extraction kicker stability ($<10^{-3}$) was identified as an important issue, and continued experiments were called for.
- More simulations of emittance correction algorithms, with enhanced (more complete) models of errors and 'environmental' effects (such as ground motion) are required.

low emittance transport

- As with the damping rings, more in depth studies (simulations) of static tuning and emittance control for the bunch compressor, main linac and beam delivery system is required. These simulations should be extended to include more 'real world ' effects; particular the effects of so-called *dynamic errors* (ground motion, vibration etc.).
- A rigorous R&D program to develop the most critical beam instrumentation (BPM development,

[‡] due to the proposed increase in luminosity at 800 GeV c.m.

[§] this apparently single requirement was divided into two separate items in the TRC, hence the 2 in table 3 for the JLC-X/NLC R2.

laser-based profile monitors, fast luminosity monitors) is mandatory.
- A sufficiently detailed prototype of a main linac girder/cryomodule (including a quadrupole) should be constructed to allow assessment of its vibration characteristics.

The reliability working group's common R2 items effectively summarised the working groups findings:

- A detailed evaluation of critical sub-system reliability is needed to demonstrate that adequate redundancy is provided and that the assumed failure rates (MTBF) for individual components has been achieved.
- The performance of beam-based alignment algorithms (for both magnets and structures) must be fully simulated including realistic errors (both static and dynamic).

The first point relates to long-term hardware tests of critical components to establish their failure rates (MTBF), and the need to perform a comprehensive Failure Mode and Error Analysis (FMEA) on what will be a complex system. The second point relates to the impact on the *integrated* luminosity of the various tuning algorithms foreseen, and clearly goes hand in hand with the emittance tuning simulation items for both the damping ring and the LET.

ADDED VALUE

During the course of the review, it was often said that the 'process was more important that the product'; by that we meant that the process of getting together as a single community to perform a single collaborative effort was probably more important than producing the report itself. As it stands, the ILC-TRC is an excellent example of what can be achieved by the various linear collider experts when they come together with a common goal: a proof of principle that we can all work together on a single design once the technology decision has been made.

Apart from the collaboration effort, there were other significant benefits. All the designs – and perhaps the TESLA design most of all – benefited from the intense critical review that they received. The report lists a number of 'design changes' or modifications that came about as a direct result of this process. In addition, we have already mentioned the significant advances made in the simulation software tools used during the luminosity performance working group's work (particularly for the LET and damping ring sub-groups). A considerable amount of new work was also performed on collimation system performance as part of the machine-detector interface sub-group. All of these cross-machine studies enabled the working group members to define benchmarks for making like comparisons of the different designs.

AFTER THE ILC-TRC: RECENT PROGRESS

As of writing it has been some six months since the publication of the committee's findings and recommendations. Since then there has been some significant progress, both on the R&D front, and on the world-wide political scene, with the formation of the International Linear Collider Steering Group (ILCSG), and its counterparts in the three global regions.

In this section, I will briefly mention the current status of the TESLA and JLC-X/NLC linac technology R&D.

TESLA

I have already mentioned that the 35 MV/m cryomodule test required for TESLA's R1 will certainly not be made before 2005 due to budget and resource problems. The test requires not only a full cryomodule with eight electropolished 35 MV/m cavities, but also a separate module test stand; this test stand has long been foreseen but has been delayed several times due to budget constraints. Despite this setback, there is still significant progress being made. The decision in January 2003 by the German government to finance the X-FEL part of the TESLA project is also positively significant for the linear collider. DESY – together with its European partners – will need to be in a position to start construction of a ~20 GeV linac based on this technology by 2006. Many of the R2-4 items pertaining to the linac technology and (in particular) operability and reliability will need to be aggressively addressed over the next two years. There is a naturally synergy between this effort and that needed for the construction of a linac for a linear collider.

But it is the high gradients needed for a linear collider which are the focus of attention. Despite a shift in emphasis to the X-FEL, the high-gradient program continues. Installation and commissioning of a new electropolishing facility at DESY is well underway. First results on single-cell cavities have all shown gradients in excess of 35 MV/m; the first full nine-cell DESY electropolished cavities are expected at the end of this year. While the TESLA R1 of a full 35 MV/m cryomodule test will now not happen before the technology decision, there is a current R&D program for long-term testing of a single 35 MV/m cavity in the horizontal test stand at DESY (CHECHIA[**]). As of writing, this cavity has run stably at a gradient of 35 MV/m for over 1000 hours at a pulse rate of 5 Hz, with no cavity our coupler events.

Another important milestone achieved is the test of the piezo-tuners, which are required at the high-gradient to compensate the so-called Lorentz detuning of the cavity. The system has recently been successfully operated at ~35 MV/m during the current CHECHIA tests.

Finally, the so-called TTF Phase II VUV-FEL is being installed at DESY. Three cryomodules with average

[**] this test cryostat can be thought of as 1/12th of a full TESLA cryomodule.

gradients of the order of ~25 MV/m are currently being tested with RF. Two more will be installed in September of this year, with beam commissioning in 2004. Operation of this linac will be an important (if not mandatory) step towards both the X-FEL and any future TESLA-based linear collider.

JLC-X/NLC

The focus of the X-band R&D is very much in achieving the two R1 items specified by the ILC-TRC, and in addition the linac unit test specified by the two R2 points. The aggressive goal of the collaboration is to demonstrate these hardware tests before the technology decision due in mid 2004.

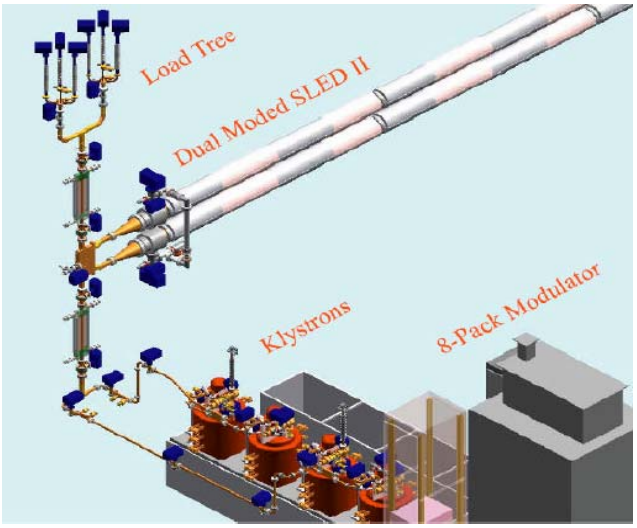

Figure 2: Schematic of the J/NLC 8-pack test.

The current R&D effort centres around two related goals: fabrication of short low group velocity structures which conform to the J/NLC specification, and the so-called 8-PACK test which is primarily a test of the multi-moded SLED-II pulse compression scheme and the full-spec solid state modulator (the 8-pack modulator). The final goal of the current program is to marry the two, by having the 8-pack system (shown schematically in figure 2) drive 8 J/NLC-spec structures in the NLC Test Accelerator (NLCTA); the structures in the NLCTA would effectively replace the load tree in figure 2. The current test set-up differs slightly from the baseline design for the linear collider, where two 75 MW PPM klystrons are foreseen. Due to availability and lead times, four 50 MW solenoid focus tubes will be used for the 8-pack test.

In the recent year, a structure has been operated at 90 MV/m[††] for several hundred hours and has shown acceptable breakdown rates. This structure is not, however, suitable for the J/NLC, since wakefield performance is not within the desired specifications. (The so-called T structures were only intended to demonstrate that a short 60 cm structure with a low group velocity would mitigate the structure damage problems first seen with the original 1.8 m structures in 2000). Tests of J/NLC ready structures (fabricated both at KEK and FNAL) are currently underway. Gradients at the required pulse lengths have been achieved, although the breakdown rates are currently still too high (factor of two at 65 MV/m).

R&D on the other important components of the 8-pack test – the solid state modulator, SLED-II system – is also on track for the proposed full system tests. The modulator has successfully driven four klystrons, although as of writing not at the full repetition rate. The SLED-II systems has generated the necessary high peak power (485 MW) but at a shorter pulse than required (150 ns). Although not foreseen for the 8-pack tests, a SLAC-built PPM klystron (the XP3-3) has been successfully tested at 75 MW peak power, 1.6 us pulse width at 120 Hz operation (a major milestone!)

Finally, the Damping Ring test facility at KEK (ATF), recently achieved a vertical emittance that is a factor of two smaller than required by the J/NLC.

FINAL REMARKS

The possibility of realising an e^+e^- linear collider has never looked better: on the one hand, we have the world HEP consensus on the need for such a machine to run concurrently with LHC; on the other we appear to have not one but two mature technologies with which to build it. There are only two remaining questions: how to decide which technology to adopt, and how to internationally fund such a project. The latter is beyond the scope of this report, but I would like to make some personal comments on the technology choice.

With respect to a technology decision, the ILC-TRC executive summary states:

> *Assuming that the above demonstrations of the TESLA and JLC-X/NLC subsystems are successful with the above schedule[‡‡], by the beginning of 2004 the two machines will be on an equal footing from the point of view their RF systems for the main linacs. If at that time the HEP community wanted to make a choice between these two, it would do so by weighing all the technical differences between the two machines and the challenges presented by the remaining R2 tasks.*

A decision on the technology to be used for the international linear collider is scheduled for mid-2004. It is now clear (and accepted) that the TESLA R1 will not have been demonstrated by that time. Although the JLC-X/NLC collaborations are still attempting to perform the R1 tests, it remains to be seen whether or not they will be successful before the decision is made. So it is very likely that the R1 issues will still be open, and some sort of

[††] the goal is 65 MV/m with some overhead.

[‡‡] this refers to the R1 linac technology demonstrations, which were at that time foreseen for both machines at the end of 2003.

extrapolation (leap of faith?) will be required by the decision makers.

I do not entirely agree with the TRC statement above. It is clear that technical issues (risks) must play a major role, but not exclusively. Other geo-political factors must be included: the potential for spin-off technology and 'synergy' with other fields is also important when selling a multi-billion dollar project to national funding agencies; considerations of potential international partners, host nations, etc., should also be considered. Only by considering the broader picture can we propose a machine that has a chance of being funded as part of a truly international project. With that said, I believe we are all looking forward to a decision in 2004! Exciting times lay ahead.

REFERENCES

[1] "International Linear Collider Technical Review Committee Second Report", SLAC-R-606, http://www.slac.stanford.edu/xorg/ilc-trc/2002/2002/report/03rep.htm, (2003).

[2] R. Brinkmann *et al*. (eds.), "TELSA Technical Design Report Part-II", DESY-2001-011, (2001).

[3] N. Toge, (ed). [JLC Design Study Group], "JLC Design Study", KEK-REPORT-91-1 (1997).

[4] N. Phinney, (ed) [NLC Collaboration], "2001 Report on the Next Linear Collider", a report submitted to Snowmass '01, SLAC-R-571 (2001).

[5] G. Guignard (ed) [CLIC Study Team], "A 3 TeV e^+e^- Linear Collider based on CLIC Technology", CERN 2000-008 (2000).

[6] "International Linear Colliders Technical Review Committee Report 1995", SLAC-R-471, http://www.slac.stanford.edu/xorg/ilc-trc/2002/1995/1995_report.htm, (1995).